UNIVERSITAT DE BARCELONA

Salt tectonics in contractional fold belts, the Kuqa foreland basin and thrust belt case (Tarim basin, China)

Oriol Pla de Casacuberta

Salt tectonics in contractional fold belts, the Kuqa foreland basin and thrust belt case (Tarim basin, China)

Oriol Pla de Casacuberta

Memòria de Tesi Doctoral
Març 2019

Institut de Recerca Geomodels
Grup de Recerca de Geodinàmica i Anàlisi de Conques
Departament de Dinàmica de la Terra i de l'Oceà
Universitat de Barcelona

Supervisors:
Dr. Eduard Roca
Dra. Esther Izquierdo-Llavall

The cover photograph shows the North-vergent Kuchetawu anticline (eastern Qiulitage) in the Kuche river cross section.

Institut de Recerca Geomodels

Grup de Recerca de Geodinàmica i Anàlisi de Conques

Departament de Dinàmica de la Terra i de l'Oceà

Universitat de Barcelona

Salt tectonics in contractional fold belts, the Kuqa foreland basin and thrust belt case (Tarim basin, China)

Memòria presentada per **Oriol Pla de Casacuberta** per optar al grau de Doctor en Ciències Geològiques per la Universitat de Barcelona.

Aquesta memòria s'ha realitzat dins del Programa de Doctorat de Ciències de la Terra (H0Z01 - HDK09), sota la direcció del **Dr. Eduard Roca Abella** i la **Dra. Esther Izquierdo-Llavall.**

Oriol Pla de Casacuberta

Barcelona, Març 2019

Dr. Eduard Roca Abella

Dra. Esther Izquierdo-Llavall

This PhD thesis has been realized within both, the Grup de Recerca de Geodinàmica i Anàlisi de conques (2014SGR467, funded by the Secretaria d'Universitats i Recerca del Departament d'Economia i Coneixement de la Generalitat de Catalunya and the Agènica de Gestió d'Ajuts Universitaris i de Recerca) and the Institut de Recerca Geomodels (funded by the Universtitat de Barcelona and the Fundació Bosch i Gimpera). Most of the work as PhD student has been carried out at the Departament de Dinàmica de la Terra i de l'Oceà (formerly Departament de Geodinàmica i Geofísica) of the Universitat de Barcelona.

The research project that has been financially supported by the project FBG308224 entitled "Salt Tectonics Modelling at Kuqa Foreland Fold and Thrust Belt, Tarim Oilfield" in which my supervisor, Dr. Eduard Roca, was the principal investigator. This project is a collaboration between the American-based company China National Petroleum Corporation (CNPC USA) and GEOMODELS Research Institute (via Fundació Bosch i Gimpera). The research project has also been funded by the projects SALTECRES (CGL2014-54118-C2-1-R-BTE) and SALTCONBELT (CGL2017-85532-P) from the Ministerio de Ciencia e Innovación of the Spanish Government.

The research project has been based in the first place on the interpretation of surface and subsurface structural data using academic software licenses of GoCad, Move and Kingdom Suite provided by Paradigm^{MT}, Midland Valley and HIS respectively, and secondly, it has been based on analog modelling. Sandbox experiments were carried out at the SIMGEO-Geomodels Analogue Modelling Laboratory. This laboratory was supported by a Scientific Infrastructures Project (UNBA08-4E-006) co-funded by Statoil and the European Regional Development Fund of the Ministerio de Ciencia e Innovación of the Spanish Government.

During the research project, Oriol Pla de Casacuberta benefited from two predoctoral contracts (FBG307451) from March 2014 to March 2015 and (FBG308984) from May to October 2018. Between both predoctoral contracts the research activities carried out by the PhD student have been financially supported by an APIF (Ajuts al Personal Investigador en Formació) predoctoral grant awarded from the Universitat de Barcelona.

A la Maria

AGRAÏMENTS

Sens dubte s'acaba una etapa que m'ha encantat viure, i per sobre de dot, això ha sigut així per les persones amb les que he compartit aquests anys de doctorat. És tanta la gent que d'una manera directa o indirecta ha contribuït en aquesta tesi que espero no deixar-me a ningú.

In the first place I want thank the financial support provided by China National Petroleum Corporation (CNPC) and Tarim Oilfield through the project FBG308224 "Salt Tectonics Modelling at Kuqa Foreland Fold and Thrust Belt, Tarim Oilfield". This thesis could not have been possible without their funding. I also want to thank CNPC for the permission to publish the data used and the interpretations carried out in this thesis in journals and congresses. Many thanks to CNPC and Tarim Oilfield staff for their help during the field campaigns. I also take this chance to thank all the "Kuqa team", I have learned a lot from them. Special thanks to Josep Antón Muñoz and Mark Rowan for their help beyond the PhD. Finally, I want to thank Neng Yuan for being a perfect host and for his friendship during these years.

Gràcies al Departament de Dinàmica de la Terra i de l'Oceà i al seu equip administratiu, així com el de la Facultat de Geologia, i el del Institut de Recerca Geomodels. En especial vull agrair a la Teresa Beamud Amorós per solucionar els problemes sempre amb un somriure.

Agrair especialment al meu tutor i director Eduard Roca la oportunitat de treballar en el projecte de Kuqa, fer camp a la província de Xinjiang és possiblement una de les millors experiències que he viscut. Agrair-li també, la seva dedicació des del dia que va acceptar dirigir-me el treball de fi de màster fins ara que estic finalitzant la tesi. Al teu costat he après moltíssimes coses, però el més important ha estat tenir sempre la teva confiança.

Muchas gracias a mi codirectora Esther Izquierdo, hacer buena parte de este doctorado a tu lado ha sido un lujo a todos los niveles. Guardaré con especial cariño el tiempo que pasamos juntos durante las campañas de campo en China.

Agrair a l'Oriol Ferrer i a l'Òscar Gratacós per dedicar part del seu temps a formar-me. Sempre heu estat disposats a donar un cop de ma en tot el que he necessitat. Amb vosaltres ha sigut més fàcil i sobretot, més divertit. Us trobaré a faltar parella! Gracias Pablo Granado por tus consejos sobre todo, geología, comida, cine y procrastinación. Agrair a la Mireia Butillé per

dedicar el temps que no tenia en dirigir-me el treball de fi de màster. Gràcies Frederic Oriol Escosa, vam començar a l'hora el doctorat sense tenir molt clar on ens ficàvem i tenir-te de company de promoció ha sigut un plaer.

Moltes gràcies a la resta de companys de la 226, Pau Arbués, Marco Snidero, Jordi Miró, Núria Carrera, Marco de Matteis, Patricia Cabello, Estefanía Górriz, Joana Mencos, Pablo Santolaria, Daniel Bello, Marina Nebot, Rodolfo Uranga, Lluís Valero i Elisabeth Wilson, perquè d'alguna manera o altre m'heu ajudat durant aquests anys.

Gràcies al meu amic David Cruset per la seva ajuda durant els anys de carrera, de màster, i per acompanyar-me al camp en la meva primera campanya a Artesa de Segre. Gondwana.

Com ja he dit, és el final d'una etapa, i quan aquests dies miro endarrere i faig memòria del camí recorregut et veig a tu, Maria, a cada revolt, cuidant-me i estimant-me. Gràcies per ser-hi, per fer el camí junts. En aquest sentit, també vull agrair a la meva família, i en especial als meus pares i germà, per ajudar-me, com sempre, en tot el que he necessitat.

TABLE OF CONTENTS

PREFACE AND THESIS DESCRIPTION

The thesis presented here spins off from the 2-year oil-industry project entitled "Salt Tectonics Modelling at Kuqa Foreland Fold and Thrust Belt, Tarim Oilfield" that was a collaboration between the American-based company China Petroleum Corporation (CNPC USA) and GEOMODELS Research Institute (via Fundació Bosch i Gimpera). This research project stems from the need to understand the structural character and evolution of the Kuqa fold-and-thrust belt (NW Xina) in order to identify exploration targets at the Mesozoic subsalt level. Specifically, the aim of the study was to identify exploration targets at the Paleogene subsalt structural level of the Kuqa foreland basin and adjoining fold and thrust belt, in particular beneath the Qiulitage fold-and-thrust system. In this scenario, the project research was focused on the definition and understanding of the different salt structures, their relationship with the geodynamic context and the different types of related hydrocarbon traps.

To achieve these objectives, it was agreed to carry out six regional cross-sections, three of them balanced and restored as well as eleven balanced cross-sections of the Qiulitage fold-and-thrust system, three of them restored. In addition, regional structural maps were produced showing the salt and subsalt structures as well as their relationships with salt distribution and thickness. This line of research has been complemented with the realization of eight numerical discrete-element models and eight scaled sandbox analogue models of tectonic wedges incorporating variations in the rheology of a weak layer and in the syn-kinematic sedimentary rate.

In order to accomplish these tasks, the company provided around 1500 km of 2D seismic lines and geophysical logs from numerous wells drilled in the area. In addition, two field campaigns were organized between June (15 days) and September 2015 (21 days) where structural data were collected to recognize the surface structure of the Kuqa fold-and-thrust belt. Moreover, several transects were realized during these field campaigns to recognize the surface expression of interpreted structures in the seismic lines.

In this context, this thesis deals only with the results obtained from the structural analysis based on surface and subsurface data and analogue modelling. These results are presented in this manuscript which includes the following chapters.

CHAPTER 1 that provides a summary of the thesis.

CHAPTER 2 which provides a general introduction to the geology and the kinematic evolution of the Tian Shan intraplate range. Then, the chapter focuses in the southern frontal structure of the central Tian Shan Range, the Kuqa fold-and-thrust belt, describing both the stratigraphy and the main features of its structure. Finally, the main objectives of this thesis are presented.

CHAPTER 3 that deals with the structural analysis carried out in the Kuqa fold-and-thrust belt with the field and subsurface data. The chapter shows the input data and the interpretation of both surface and subsurface data. The chapter describes the obtained results of three regional cross-sections as well as the regional structural maps of salt distribution and thickness. In addition, the chapter provides a kinematic evolution of the Kuqa fold-and-thrust belt and discusses the main parameters controlling it.

CHAPTER 4 that describes the data, methodology, procedure and results obtained in the analogue modelling experiments. These experiments where designed to analyze the influence of the rheological properties of two superimposed décollement layers but mainly the one of the syn-tectonic sedimentation. So, after a brief introduction to the purpose of the experimental program and the methodology used, this chapter describes the experimental results separating them according to the applied syn-kinematic sedimentary rate. Then, the obtained results are compared and discussed mainly focusing on: the influence of the mechanical properties of a weak layer; the syn-kinematic sedimentary rate in the geometry and kinematics of brittle-viscous tectonic wedges; as well as the interaction between sub-salt and salt-detached structures.

CHAPTER 5 which compares the experimental results with the structure and kinematic of the Kuqa fold-and-thrust belt defined from our structural field and subsurface analyses that is described in the Chapter 3.

CHAPTER 6 which depicts the main conclusions of this thesis.

CHAPTER 7 formed by the references mentioned throughout the text.

CHAPTER 1. ABSTRACT

The Kuqa fold-and-thrust belt, in the southern foreland of the central Tian Shan Range (NW China) was contractionally deformed during Late Mesozoic and Cenozoic times as recorded by well-preserved syntectonic continental sequences. In addition, its structural evolution was strongly controlled by synorogenic salt (Eocene-Oligocene in age) and presalt décollements with varying spatial distribution. In this scenario, we present a set of six balanced cross-sections, three of them are subsequentially restored across the Kuqa fold-and-thrust belt that provides a new interpretation of the structure beneath the evaporites, in which Paleozoic and Mesozoic strata are deformed by a thrust stack involving **(i)** a thin-skinned thrust system detached on Triassic-Jurassic coal/mudstone units, and **(ii)** an ensemble of south-directed basement thrusts. The latter formed from the inversion of Mesozoic extensional faults such as those preserved both in the Tarim Basin and beneath the frontal part of the Kuqa fold-and-thrust belt. Regional cross sections also show a total shortening (from Oligocene to the present-day) ranging from 30.5 km to the West to 24 km to the East (29 km in the central part) that was mostly accommodated from late Miocene to Pleistocene times. Total shortening in the Kuqa fold-and-thrust system decreases progressively eastwards, accordingly to the eastwards shortening decrease in the Tian Shan Range. The regional restorations depict a three-stage evolution for the Kuqa fold-and-thrust belt: **i)** minor Mesozoic extension; **ii)** an early compressional stage (Late Cretaceous to early Miocene) with low shortening and syntectonic sedimentary rates; and **iii)** a later compressional stage (late Pliocene-Pleistocene) characterized by a greater and progressively increasing shortening rate and rapid deposition.

To gain further insights about the influence of synkinematic sedimentation rate, décollement rheology, and the interaction between décollements on the deformation style in foreland areas of fold-and-thrust belts we present an experimental study including four 3D sandbox models inspired by the Kuqa fold-and-thrust belt. These experiments contain two décollements with different areal extents: a weak synorogenic salt layer; and a deeper, preorogenic and frictionless décollement (i.e., coal or mudstone). They show along strike variations of thickness and lithology which affect their rheology and mechanical behavior. The experimental results show that increasing synkinematic sedimentary rate: **(i)** generates a progressive change from distributed to localized deformation and, **(ii)** delays the development of frontal contractional structures detached on the salt, favoring the formation and reactivation of more hinterland thrusts and backthrusts. With respect to the rheology, our study reveals that as the viscosity of the prekinematic décollement increases: **(i)** the deformation propagates more slowly towards the foreland and, **(ii)** the underlying thrust stack becomes broader and lower and has a gentler thrust taper angle. The rheology of the

prekinematic décollement defines the distribution and geometry of the structures detached on it that in turn influence the development of overlying, salt-detached structures. Subsalt structures can: **(i)** determine the areal extent of the salt and therefore of any fold-and-thrust system detached on it and, **(ii)** hamper or even prevent the progressive foreland propagation of deformation above the salt. In addition, internal deformation of the salt highlights that there is a balance between salt flow related to the thrust emplacement and salt evacuation below the piggy-back basins.

The integration of surface data, seismic interpretation, and analogue modelling permitted us to a better understanding of the geometry and kinematic evolution of the Kuqa fold-and-thrust belt, as well as provided valuable insights on contractional deformation in the outer parts of fold-and-thrust belts including syntectonic sediments and multiple décollements.

CHAPTER 2. GENERAL INTRODUCTION AND OBJECTIVES

2.1. INTRODUCTION TO THE TIAN SHAN RANGE

The Tian Shan Range is part of the southern Central Asian Orogenic Belt (CAOB in **Fig. 2.1**) which is one of the world's largest, most complex, and long-lasting accretionary orogens that extends from the Uralides to the Pacific and from the Angara and Russian cratons to the North China and Tarim cratons (Wilde, 2015) (**Fig. 2.1**). In this setting, The Tian Shan is a thick-skinned fold-and-thrust belt that reaches 7400 m high and extends for more than 2500 km long from western China to Kazakhstan and Kyrgyzstan (Loury et al., 2015a; Loury et al., 2015b; Yu et al., 2014) (**Fig. 2.2B**)

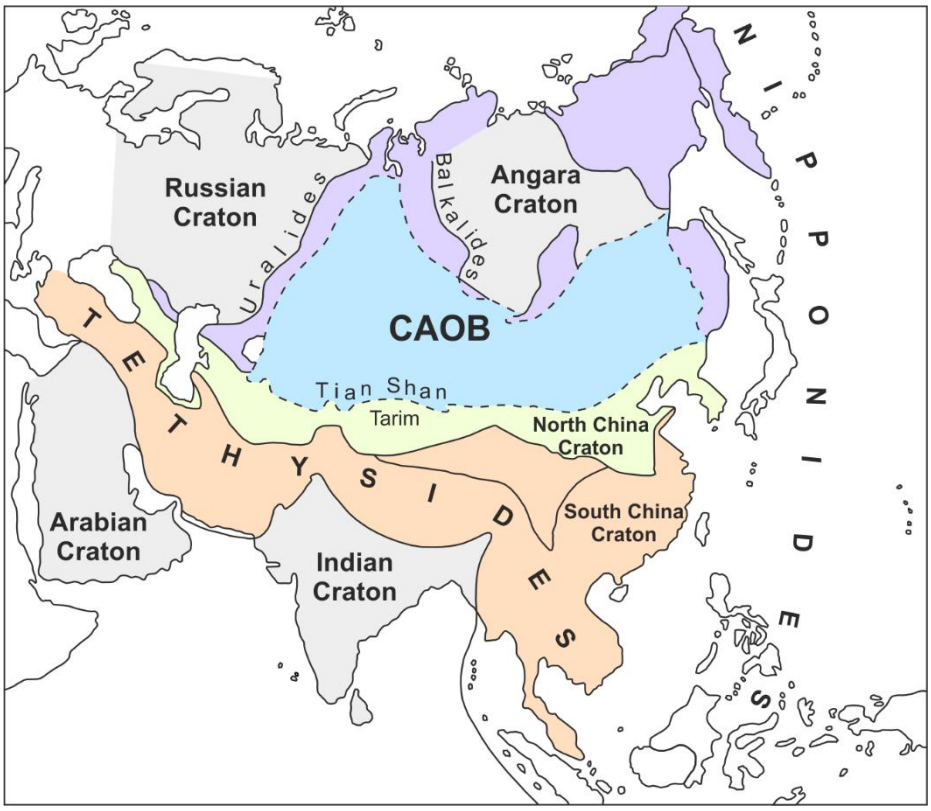

FIGURE 2.1. Map of the continental Asia showing the main paleotectonic units as interpreted by Sengör and Natal'in (1996). Note the location of the Tian Shan and Tarim Basin at the southern boundary of the Central Asian Orogenic Belt (CAOB), Modified by Wilde, 2015.

2.1.1. Structure

The Tian Shan is a doubly verging intraplate range, cored by Proterozoic to Carboniferous basements units that are unconformably overlain by Permian to Mesozoic sedimentary sequences (Charvet et al., 2011; Jolivet et al., 2010; Jolivet et al., 2013). This range is usually divided into three main tectonic units: The North Tian Shan and the Yili Block, the

Central Tian Shan, and the South Tian Shan (Allen et al., 1992; Hendrix et al., 1994; Windley et al., 1990) (**Fig. 2.2**). The present boundaries among these units are characterized by intensely

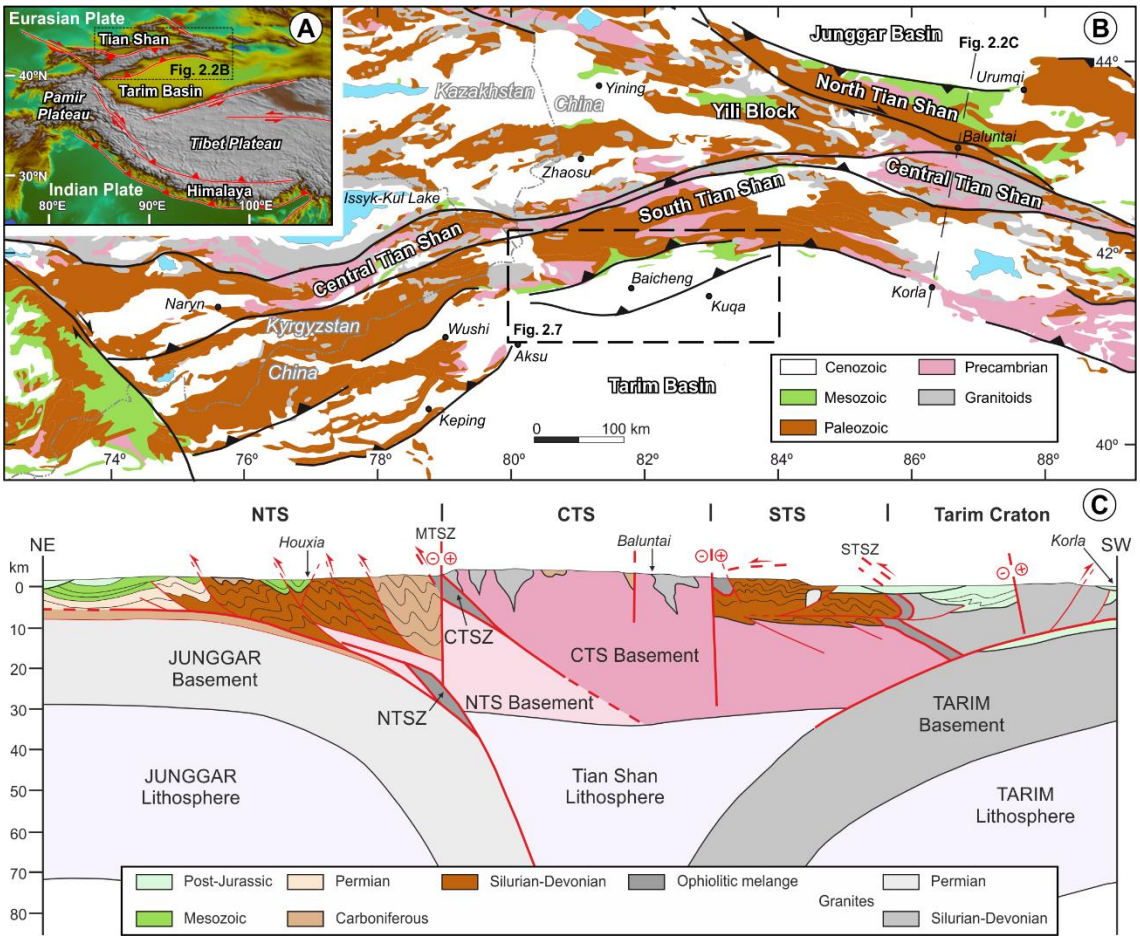

FIGURE 2.2. A: Tectonic sketch of central Asia with location of the Tian Shan and the Tarim Basin. **B:** Schematic geological map of Tian Shan Range. Black dashed rectangle shows the location of the Kuqa fold-and-thrust belt. **C:** Simplified lithosphere-scale cross-section of the Tian Shan, see location in **Fig**. 2.2B. CTS: Central Tian Shan; CTSZ: Central Tian Shan Suture Zone; MTSZ: Main Tian Shan Shear Zone; NTS: North Tian Shan; NTSZ: North Tian Shan Suture Zone; STS: South Tian Shan; STSZ: South Tian Shan Suture Zone. Modified from Charvet et al., 2011.

deformed suture zones where ophiolitic mélange crop out (Charvet et al., 2011). The North Tian Shan and the Yili Block are formed by Upper Devonian and Carboniferous sedimentary sequences and abundant calcalkaline volcanic and plutonic rocks (Carroll et al., 1995). These sedimentary sequences are deformed through upright to North-vergent folds that are subsequently faulted by a North-directed thrust system (**Fig. 2.2C**). To the south, the Central Tian Shan is characterized by a Proterozoic basement, Silurian-Devonian granitic gneisses and metasandstones and Silurian turbidites (Coleman, 1989). Devonian plutonic rocks and granites are abundant. Further south, the South Tian Shan is divided in two domains: the South Tian Shan and the basement of the Tarim Craton. The South Tian Shan is constituted by Silurian-

Devonian metamorphic rocks unconformably overlain by lower Carboniferous conglomerates (He et al., 2009). The basement of the Tarim Craton consists of Neoproterozoic to Ordovician platform sedimentary rocks (limestones and shales) with interbedded volcanic rocks (**Fig. 2.2C**). They are overlain by Silurian conglomerates and intruded by Upper Devonian-lower Carboniferous plutonic rocks (Cai and Lü, 20015). This sequence is unconformably covered by lower Carboniferous to lower Permian fluvial and marine sediments (Zhou et al., 2001).

During the Mesozoic, the Tian Shan was already an intraplate range characterized by an axial zone consisting of rocks deformed by previous Paleozoic orogenic systems and two adjacent foreland basins: the Tarim Basin to the north and the Junggar Basin to the south (Allen et al., 2002; Brunet et al., 2017). During the Eocene to the present day, renewed intraplate deformation produces right-lateral faulting, thrusting, and strong vertical uplift in the axial zone of the Tian Shan Range, whereas the northern Tarim and the southern Junggar basins registered a progressive, forward propagation of the deformation and were partly incorporated into the external domains of this range (Coleman, 1989) (**Fig. 2.2B**). The width of deformed domains in both foreland basins changes along-strike depending on the depth and lithology of weak décollements interbedded in the stratigraphic sequence. The fold-and-thrust system in the southern Junggar Basin is in general terms narrower, dominated by basement-involved and Mesozoic-detached north-directed thrusts (Deng et al., 2000). In the northern Tarim Basin, two main fold-and-thrust belts developed, the Kepintage and the Kuqa fold-and-thrust belts (Lu et al., 2010).

2.1.2. Geodynamic evolution

The present-day geometry of the Tian Shan Range is the result of the long and complex tectonic evolution. It developed over the western margin of the Central Asian Orogenic Belt that was initially built in late Paleozoic times through the amalgamation of continental blocks during two main collisional stages (Gao et al., 2011; He et al., 2016; Wilde, 2015): (i) the progressive accretion of continental blocks and island arcs to the southern margin of the Angara Craton that gave rise to the complex closure of the Paleo-Asian Ocean (Asiatic in **Fig. 2.3**) from Late Devonian to Early Carboniferous times (Zhou et al., 2001) and (ii) the collision of these accreted units with the Tarim Craton to the west and with the North China Craton to the east, from Late Carboniferous to Early Permian (Jolivet et al., 2010) (**Figs. 2.3 and 2.4**).

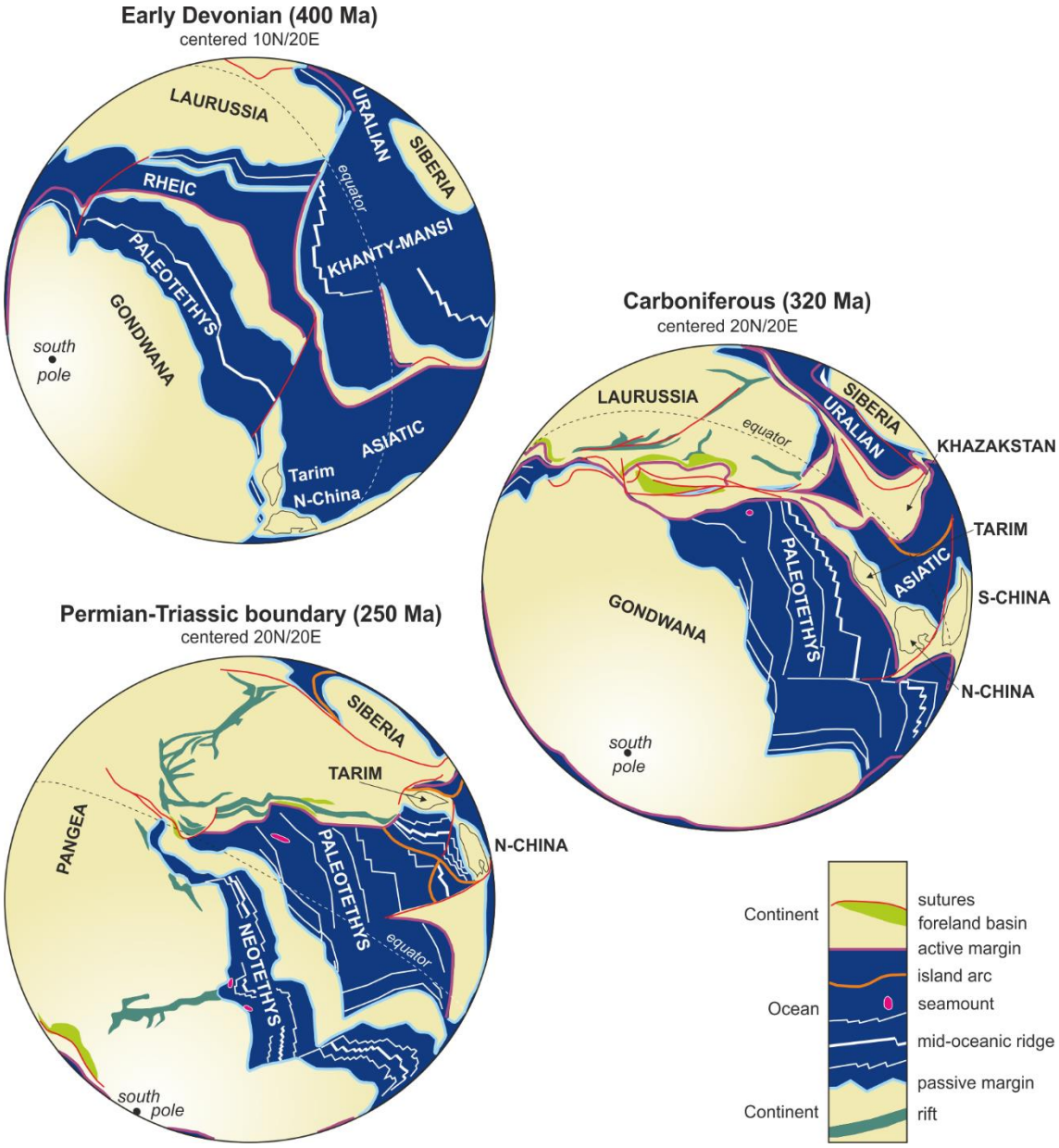

FIGURE 2.3. Plate tectonic evolution from Devonian to Early Triassic. Modified from Stampfli and Borel, 2002.

In the western CAOB, four main blocks were accreted during these stages: the Tarim Craton to the south, the Central Tian Shan and the Kazakhstan-Yili-North Tian Shan blocks in the central part, and the Junggar Block to the north (**Fig. 2.4A**) (Loury et al., 2015a). They were separated by oceanic domains (in blue in **Fig. 2.4**) and back-arc basins that were progressively closed forming E-trending suture zones with ophiolitic mélanges and HP metamorphic rocks (Charvet et al., 2011) (**Fig. 2.4**). These sutures zones started to form in the south and were progressively younger towards the north. Thus, the ones located between the southern and central blocks formed during Late Devonian whereas the North Tian Shan suture zone

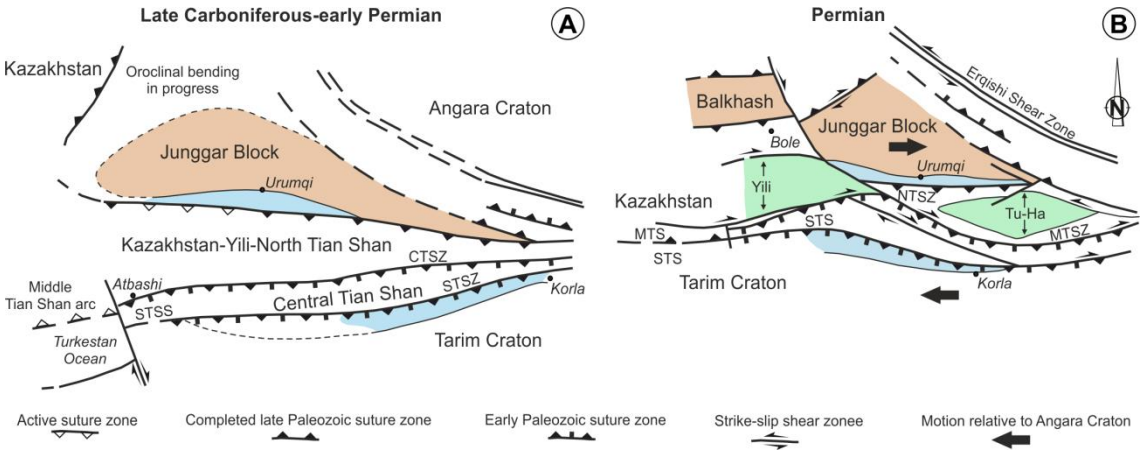

FIGURE 2.4. Map-view sketch showing the evolution of the main blocks and suture zones in the Tian Shan area during **A:** late Carboniferous-early Permian and **B:** Permian times. CTSZ: Central Tian Shan Suture Zone; STSZ: South Tian Shan Suture Zone; STSS: South Tian Shan Suture; MTSZ: Main Tian Shan Shear Zone; NTSZ: North Tian Shan Suture Zone; MTS: Middle Tian Shan; STS: South Tian Shan. Modified from Charvet et al., 2011.

(between the Junggar and the Kazakhstan-Yili-North Tian Shan blocks) developed during late Carboniferous-early Permian times. After the formation of this last suture the likely to represent the last oceanic closure in the CAOB (Charvet et al., 2011), the amalgamated units were subsequently affected by a middle-late Permian major dextral wrenching, in the Tian Shan that produced the opening of roughly E-W-trending pull-apart basins (in green in **Fig. 2.4B**).

The western part of the CAOB was contractionally reactivated during Mesozoic and Cenozoic times as the result of two different and time consecutive plate tectonic events (Coleman, 1989). The first one, Mesozoic in age, was dominated by the north directed subduction of the Paleotethys along the southern margin of Eurasia that led to the progressive accretion of three main blocks (Stampfli and Borel, 2002) (**Fig. 2.5**): the Qiantang, the Lhasa and the Pakistan blocks during the Latest Triassic, Latest Jurassic and Late Cretaceous respectively (Halim et al., 1998; Replumaz and Tapponnier, 2003, **Figs. 2.5 and 2.6**). The second tectonic event, Eocene to the present in age, resulted from the collision between the Indian subcontinent and the Eurasia plate (Avouac et al., 1993).

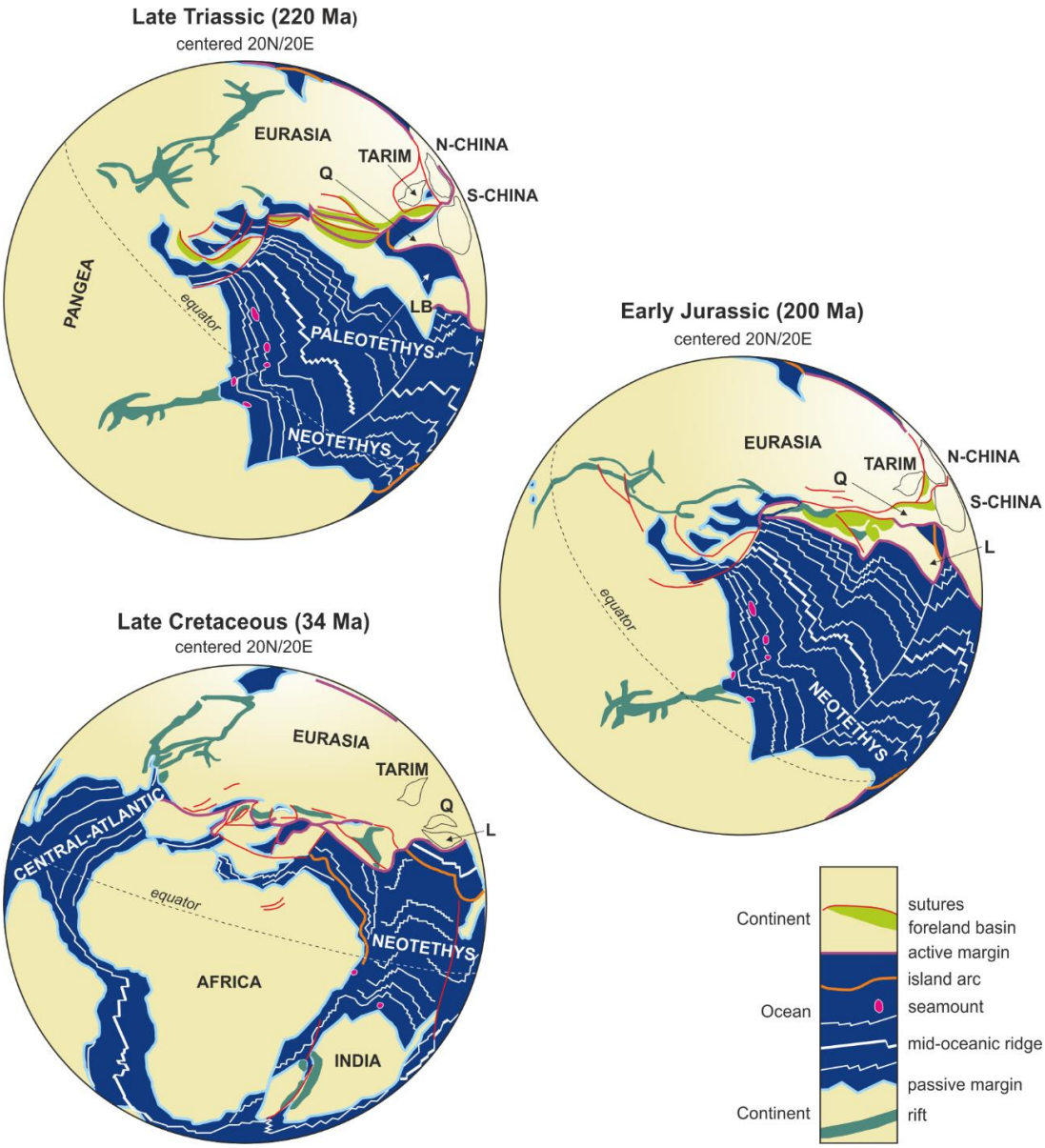

FIGURE 2.5. Plate tectonic evolution for the study area during the Mesozoic. Q: Qiantang Block; L: Lhasa Block. Modified from Stamplfi and Borel, 2002.

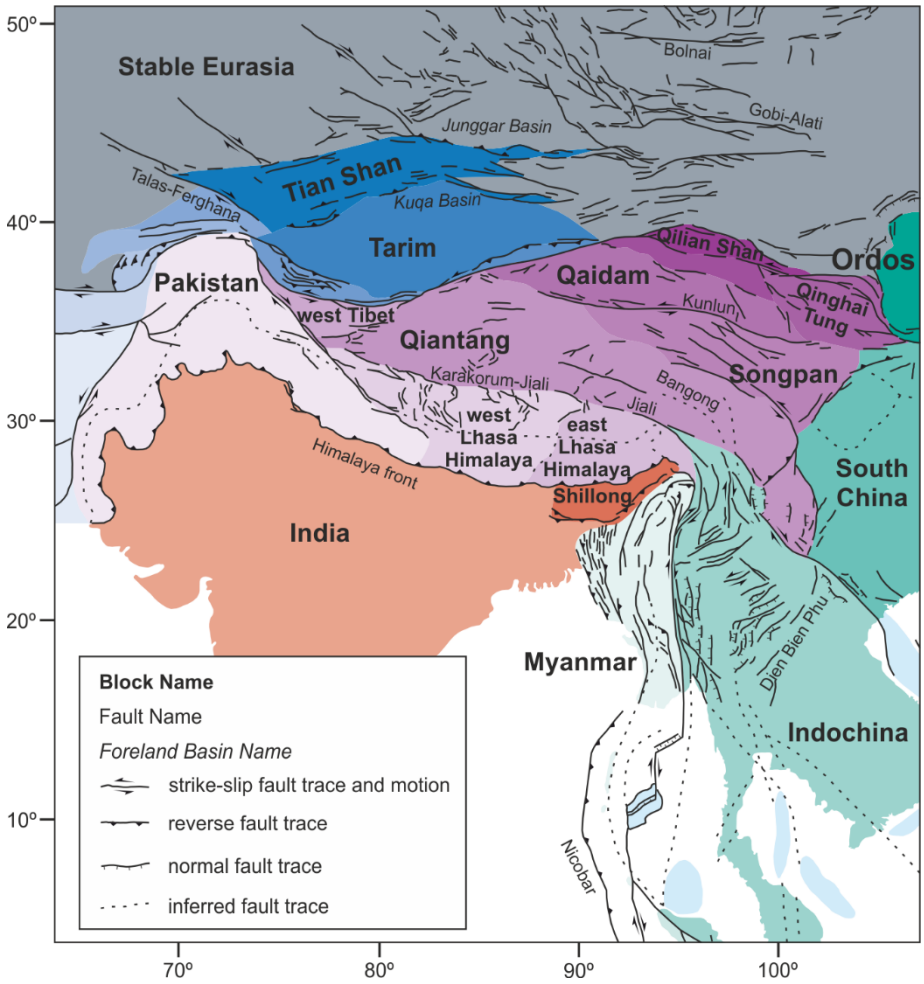

FIGURE 2.6. Block contours defined from active fault map of Asia (modified from Replumaz and Tapponnier, 2003).

2.2. INTRODUCTION TO THE KUQA FOLD-AND-THRUST BELT

The Kuqa fold-and-thrust belt represents the southern frontal structure of the central Tian Shan Range. It is a Cenozoic south-directed thin-skinned fold and thrust system developed as far-field effect of India-Asia collision and has been ongoing and accelerating since the latest Oligocene (Wang et al., 2011). The Kuqa fold-and-thrust belt extends more than 400 km-long and shows a meaningful along-strike width variation: it is about 80 km-wide in the central part but narrows both eastwards and westwards, describing an arcuate pattern in map view (**Fig. 2.7**) (Li et al., 2014). Its regional-scale structure is largely controlled by the presence of syncontractional salt units (Eocene-Oligocene in age) of lacustrine origin. They behaved as the main décollement during the development of the fold-and-thrust belt, decoupling the suprasalt deformation from that of the Mesozoic and Paleozoic presalt sequences (Li et al., 2014) (**Fig. 2.8**).

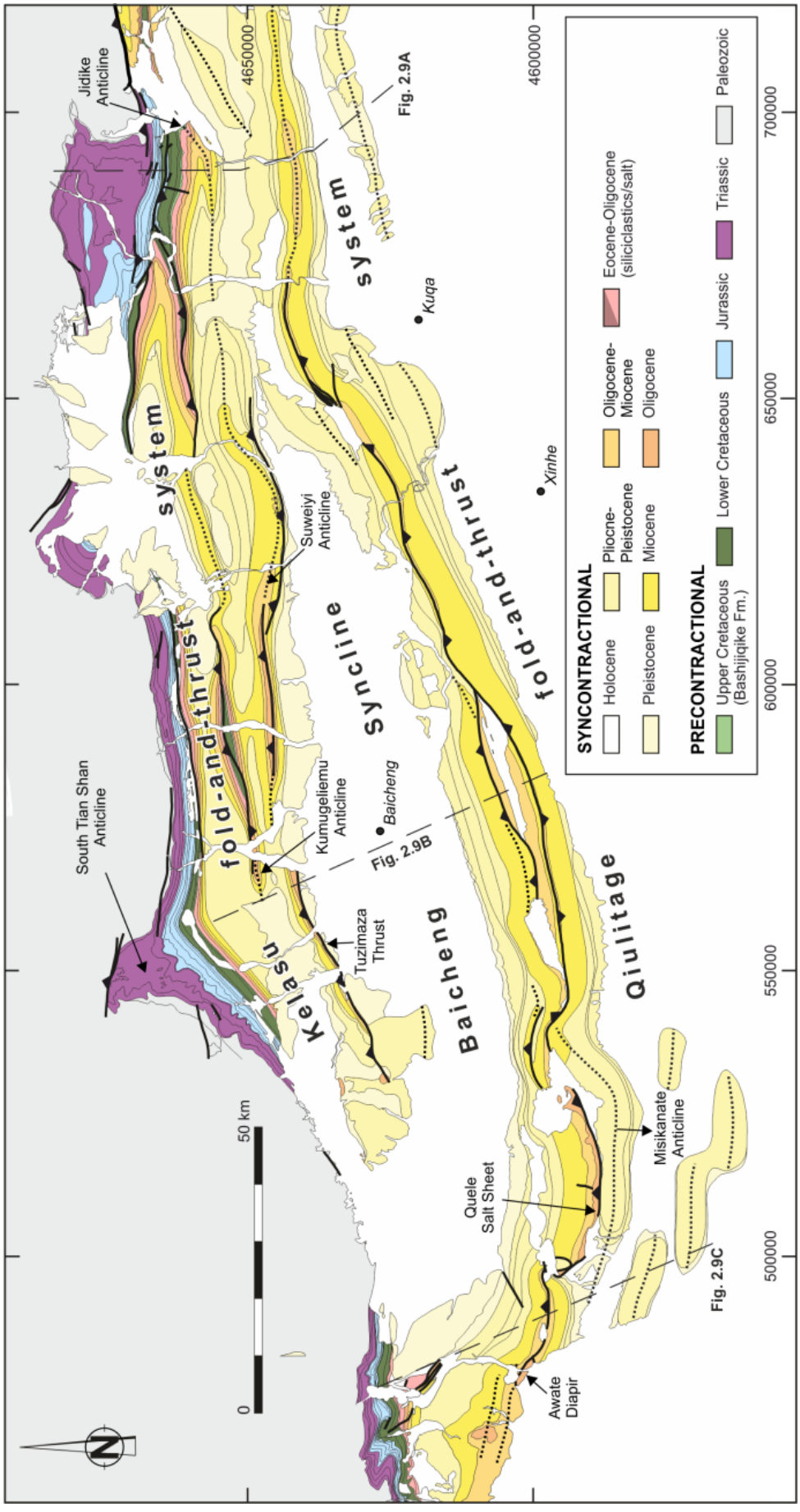

FIGURE 2.7. Geological map of the Kuqa fold-and-thrust belt. Coordinates are in meters in UTM, zone 44 northern hemisphere and datum WGS84.

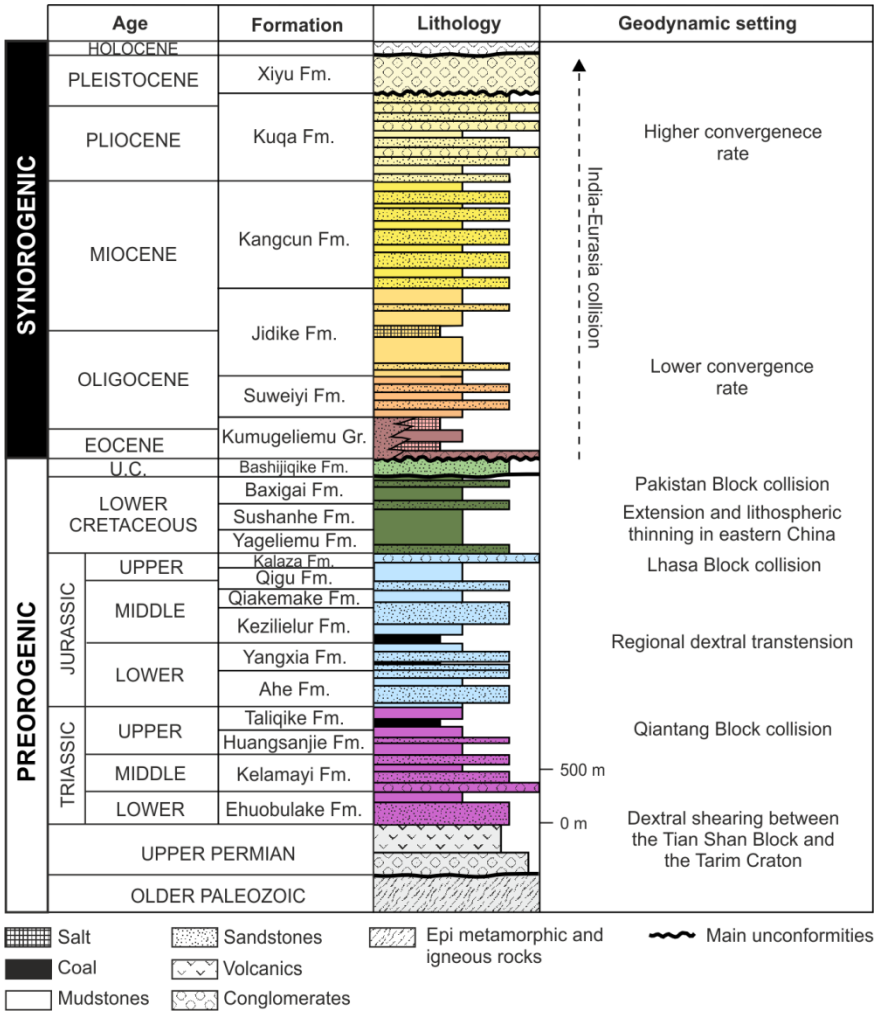

FIGURE 2.8. Synthetic stratigraphic column for the Kuqa fold-and-thrust belt in the inner Kelasu fold-and-thrust system with the geodynamic setting in which each unit was deposited. U.C.: Upper Cretaceous. Modified from Chen et al., 2004; Li et al., 2012; Li et al., 2014.

2.2.1. Stratigraphy of the Kuqa fold-and-thrust belt and underlying basement

The stratigraphy of the thin-skinned Kuqa fold-and-thrust belt involves Mesozoic-Cenozoic sedimentary successions (Guan, 2004). The underlying upper Permian basement is composed of continental purple sandy mudstones with interbedded gray conglomerates, sandstones, and black carbonaceous shales overlying lower Permian volcanics or the Carbonifereous limestones (Tang et al., 2004). The upper Permian is separated from older Paleozoic basement by a regional angular unconformity (He et al., 2016) (**Fig. 2.8**).

The Mesozoic-Cenozoic sedimentary succession involved in the Kuqa fold-and-thrust belt is formed entirely by continental detrital units with interbedded coal layers and evaporites. Considering the kinematic evolution of the Kuqa fold-and-thrust belt, a rough

distinction can be made between the Mesozoic, mostly predeformation sequence and the Cenozoic syndeformation sequence.

The Mesozoic sequence displays scarce internal unconformities, and its thickness progressively increases northward (toward the hinterland), where it reaches a maximum preserved thickness of about 5.700 m (Wang et al., 2011). It consists mainly of alternating shales, siltstones, sandstones, and conglomerates (Deng et al., 2000; Hendrix et al., 1992; Wang et al., 2011) that represent meandering fluvial systems with local lacustrine influence and development of stable coal-bearing depositional environments during Late Triassic (Taliqike Fm; see **Fig. 2.8**) and Early-Middle Jurassic times (Yangxia and Kezilienur Fms; see **Fig. 2.8**). Magnetostratigraphic profiles reveal that the Cretaceous sequence is time continuous except for its uppermost part, where the stratigraphic surface separating the Baxigai and Bashijiqike Fms represents a time gap of about 50 Myr (Peng et al., 2006).

The Cenozoic sequence displays common growth-strata geometries and cross-cutting relationships and attains a maximum thickness of 7.000 m in the Baicheng Syncline. It comprises basal evaporites (Eocene-Oligocene in age; Zhang et al., 2015, 2016) overlain by fluvial and alluvial detrital sequences. The basal evapoites (Kumugeliemu Group) consist of halite, gypsum, and anhydrite with interbedded dolostone and mudstone layers (**Fig. 2.8**). They grade northward to conglomerates and southward and eastward to fine-grain sandstones, siltstones, and shales (Wang et al., 2011). Conglomerates overlie Mesozoic units (either conformably or with a low-angle unconformity) in the northernmost outcrops of the Kelasu fold-and-thrust system. Overlying units coarse upward from red and gray shales with interbedded gypsum, siltstones, and medium-grains sandstones (Suweiyi and Jidike Fms of Eocene-early Oligocene and Oligocene-Miocene age, respectively; Zhang et al., 2015, 2016; although younger ages are given for the Suweiyi Fm by Huang et al., 2006) to sandstones with interlayered siltstones and conglomerates (Kangcun and Kuqa Fms, late Miocene and Pliocene in age; Charreau et al., 2009; Huang et al., 2006; Lin et al., 2002; Sun et al., 2009; Ye and Huang, 1990; Yin et al., 1998; Zhang et al., 2014, 2015, 2016) and to dark gray conglomerates (Xiyu Fm, essentially Pleistocene in age; Huang et al., 2006; Sun et al., 2009) (**Fig. 2.8**).

2.2.2. Structure of the Kuqa fold-and-thrust belt

The Kuqa fold-and-thrust belt is an ENE trending system that displays an arcuate shape in map view. Its structural style is dominated by tight anticlines that extend along-strike for

tens or even hundreds of kilometers and are separated by wide, open synclines. Anticlines involve Paleozoic and Mesozoic units to the north but are manifested by Cenozoic sequences to the south.

The Kuqa fold-and-thrust belt has classically been divided, from north to south, into three main units: the Kelasu fold-and-thrust system, the Baicheng Syncline and the Qiulitage fold-and-thrust system (**Fig. 2.7**).

The Kelasu fold-and-thrust system is bounded to the north by the basement-involved South Tian Shan Anticline (see location in **Fig. 2.7**) and consists of **s**everal E to ENE-striking tight and doubly plunging anticlines separated by narrow synclines. Folds change vergence along-strike and are commonly truncated by long thrusts that display kilometric hanging-wall flats along Mesozoic and Cenozoic units. The latter dominate in the frontalmost structure of the Kelasu fold-and-thrust system which is underlain by thick accumulations of salt (Wang et al., 2011) (**Fig. 2.7**).

South of the Kelasu fold-and-thrust system there is a major 200 km-long syncline that is wider (about 35km) in the central and western parts of the Kuqa fold-and-thrust belt than in the eastern one, where it narrows dramatically (about 7 km) (**Fig. 2.7**). This syncline, named Baicheng Syncline, is an open, symmetric fold containing a maximum thickness of 7 km of syn-contractional Cenozoic succession overlying a thin Mesozoic succession (Wang et al., 2011).

The Qiulitage fold-and-thrust system is the southern frontal structure of the Kuqa fold-and-thrust belt. It is a major antiformal structure on which its eastern and southern terminations are flanked to the south by upright gentle folds. In map view, the Qiulitage fold-and-thrust system shows an arcuate shape composed of E- and NE-striking tight anticlines and thrusts that involve only Cenozoic rocks at surface. As in the Kelasu fold-and-thrust system, long flats characterize thrusts and back-thrusts detached along Miocene and Oligocene layers (**Fig. 2.7**).

2.3. PROBLEM APPROACH

The Kuqa fold-and-thrust belt is one of the main hydrocarbon-producing areas of the Tarim Basin. It contains significant gas condensate resources, as well as small amount of black oil (Zou et al., 2006). The potential hydrocarbon source rocks consist of lacustrine

shales/mudstones and thin coal seams deposited in fluvial-deltaic and lacustrine environment (Taliqike Fm, Upper Triassic in age), and the coal beds of swamp-lacustrine origin (Yangxia and Kezilielur Fms, Lower-Middle Jurassic in age) (Loury et al., 2015b; Tang et al., 2014). The main reservoirs are sandstones (Bashijiqike Fm, Upper Cretaceous in age) and the regional cap rock are evaporites (Kumugeliemu Group, Eocene- Oligocene in age) (**Fig. 2.8**). Therefore, the petroleum system of the Kuqa fold-and-thrust belt is located beneath syncontractional salt units (Eocene-Oligocene in age). These units largely control the regional-scale structure behaving as the main décollement during the development of the fold-and-thrust belt, decoupling the deformation of the suprasalt Cenozoic sequences and the subsalt Mesozoic and Paleozoic rocks (Li et al., 2014; Zou et al., 2006).

Several structural studies (Guo et al., 2016; Jin et al., 2008; Qiu et al., 2012; Shi et al., 2012; Tang et al., 2014; Yu et al., 2014 among others) have been undertaken in the Kuqa fold-and-thrust belt during the past decade because of the great interest of the oil industry. They were mainly focused on the structure and kinematic evolution of synorogenic suprasalt units as well as of active salt structures (Chen et al., 2004; Li et al., 2012; Li et al., 2014; Tang et al., 2004; Wang et al., 2011 among others) that are widely exposed at surface and well imaged along seismic lines. However, despite the interest of the oil industry, the characterization of Mesozoic and Paleozoic units beneath the salt has been little discussed due to seismic data are usually of poor quality and the structural control from surface outcrops is limited.

The lack of conclusive data has led to very different interpretations of subsalt structure (**Fig. 2.9**). Some authors (Tang et al., 2004; Yu et al., 2014; Li et al., 2012) suggest that the Kuqa fold-and-thrust belt is a contractional system formed solely by thick-skinned thrusts (**Fig. 2.9B**). Yet others (Chen et al., 2004; Zhong and Xia, 1998) indicate that it is a contractional system consisting of thin-skinned thrusts detached on the Mesozoic. Or instead, authors (Qi et al., 2009) that propose that the Kuqa fold-and-thrust belt is a contractional system mainly constituted by high angle inverted faults that previously act as extensional faults. Finally, some other authors (Tang et al., 2007; Wang et al., 2011; Wang et al., 2017) that suggest that it is a combination of previous options (**Fig. 2.9A and C**).

Furthermore, it is also not clear the kinematic evolution of the Kuqa fold-and-thrust belt. Some authors (Li et al., 2012) suggested that the growth of the Qiulitage fold-and-thrust system was controlled by the location of the foreland salt pinchout but disregarded the

influence of subsalt faulting beneath the frontal structure, as pointed out on cross sections of previous authors (Chen et al., 2004; Tang et al., 2004, 2007; Wang et al., 2011) (**Fig. 2.9**).

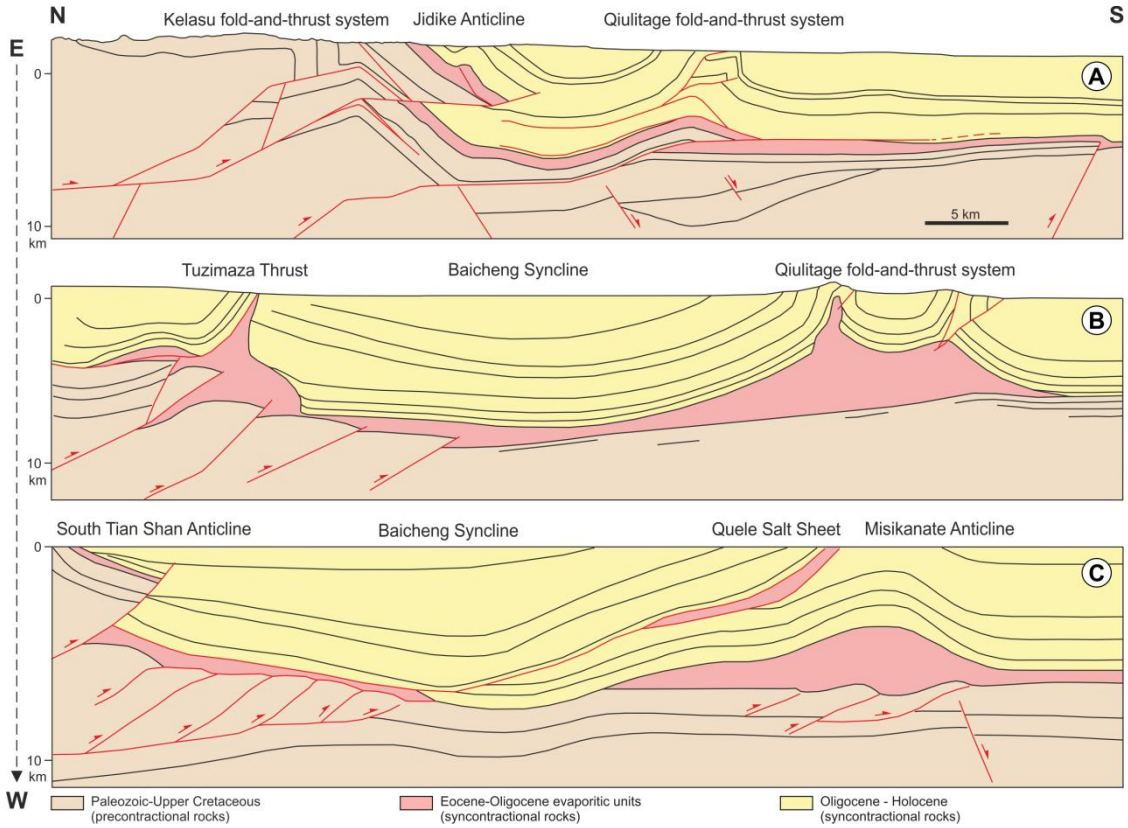

FIGURE 2.9. Proposed deformational styles for the subsalt at the Kuqa fold-and-thrust belt: seismic-based cross-sections along the Kuqa fold-and-thrust belt (see location in **Fig. 2.7**) redrawn from Wang et al., 2011 (cross-section A), Li et al., 2012 (cross-section B) and Tang et al., 2007 (cross-section C).

In this scenario, at the beginning of this thesis, there were some unanswered questions about the structure and kinematic evolution of the Kuqa fold-and-thrust belt. The most noteworthy of these questions were:

- What is the real structure beneath the salt? The characterization of the suprasalt structures is undertaken in several previous works (Chen et al., 2004; Li et al., 2012; Li et al., 2014; Tang et al., 2004, 2007; Wang et al., 2011), but subsalt geometry remains unclear.

- Which factors are controlling along- and across strike variations in the Kuqa fold and thrust belt structure?

- What is the origin of the diapiric salt structures and which parameters are controlling the distribution of the deformed salt in the Kuqa fold-and-thrust belt?

- How sediment-décollement interaction affects the geometry and kinematic evolution of the Kuqa fold-and-thrust belt? Some studies have quantified syntectonic sediment-accumulation rates (Charreau et al., 2006; Huang et al., 2006), but have not explored its impact on the structuring of the fold-and-thrust belt.

- What is the interplay between both sub- and suprasalt structures through time? Geometry and kinematic evolution is discussed in several works (Chen et al., 2004; Li et al., 2012; Tang et al., 2004; Wang et al., 2011), but detailed characterization of the early deformation stages coeval with the salt basin development is absent.

- Do inherited structures condition the locus of most of the basement deformation and the position of the salt pinchout? The presence of these early faults has been pointed out on cross sections of previous authors (Chen et al., 2004; Tang et al., 2004), but their influence on the geometry and the structural evolution of the Kelasu fold-and-thrust system as well as their relationship with salt-detached deformation remains unsolved.

2.4. OBJECTIVES

According to the state of the art, this thesis pursues the following objectives:

1. Provide a new structural and kinematic model for the Kuqa fold-and-thrust belt through the integrated understanding of the geometry of both supra and subsalt structures and the interaction between them over time.

2. Determine the influence of the syncontractional sedimentary rate and décollement rheology on the Kuqa fold-and-thrust belt deformation style.

Beyond pursuing specific objectives, this thesis pretends to contribute to the better understanding of other fold-and-thrust systems involving multiple décollement*s*. In this sense, the obtained results should not be only exceedingly useful to researchers in fold and thrust tectonics but also to industry geoscientists whose efforts are focussed on hydrocarbon exploration and production in subsalt contractional environments.

2.5. METHODOLOGICAL APPROACH TO THE PROBLEM

To undertake these objectives, regional balanced cross sections have been constructed across the Kuqa fold-and-thrust belt, extending from the Paleozoic outcrops along the southern boundary of the Tian Shan Range to the undeformed, northern Tarim foreland basin. These cross-sections are based on 2D seismic lines incorporates well data and newly acquired field data. Palinspastic sequential restorations of three cross sections have been carried out to validate the structural interpretation from both geometric and kinematic perspectives. These restorations consider recent salt tectonics concepts (Hudec and Jackson 2007; Hudec et al., 2011; Rowan and Ratliff, 2012) and consider the contribution of inherited faults and syntectonic sedimentation.

In addition, to complete the study of the Kuqa fold-and-thrust belt, and taking into account previous scaled sandbox analogue models, an experimental program inspired in this thrust belt has been designed. It consists of a set of tectonic wedges involving two décollements: an upper décollement representing a weak (salt) synorogenic salt layer and a lower one that is preorogenic and is made up by a higher viscosity material simulating coals and shales in the Kuqa fold-and-thrust belt. This lower décollement incorporates along-strike rheology changes.

CHAPTER 3. STRUCTURE OF THE KUQA FOLD-AND-THRUST BELT

3.1. DATA AND METHODOLOGY

To understand the structure and the evolution of the Kuqa fold-and-thrust belt, six regional and seismic-based geological cross sections were constructed (see location in **Fig. 3.1**). Additionally, sequential, palinspastic restorations of the western, central and eastern sections (see location in **Fig. 3.1**) have been carried out.

3.1.1. Input data

The cross sections are anchored to 2D depth-converted seismic profiles (section 3.1.3.; blue lines in **Fig. 3.2**) and integrate new and previously published field data (section 3.1.2.; Li et al*.,* 2012; Wang et al*.*, 2011) in addition to well information (**Fig. 3.2**). Interpretation of seismic horizons across the presented cross sections and their correlation to well top data derive from a wide seismic (around 1500 km of both inlines and crosslines, in black, blue and pink in **Fig. 3.2**) and well (well top data from 36 wells) survey and was carried out using Petrel 2015 (Schlumberger). New detailed geological maps were produced based on field observations and freely available Google Earth, Bing Maps and Landsat imagery (see location in **Figs. 3.1** and **3.2**). These maps provided surface constraints on the subsurface structure, especially in the Qiulitage fold-and-thrust system and the northern part of the Kelasu fold-and-thrust system where seismic data are poor and absent, respectively. Cross section construction and sequential restorations were carried out in Move 2015 (Midland Valley) using the 2D unfolding and move-on-fault algorithms provided by the software. Area balancing for the salt layers was generally used except when out of plane salt flow was interpreted.

3.1.2. Surface data

In this section, the surface observations done in the field and those inferred from the aerial photographs of the study area are described (**Fig. 3.2**). The description is focused on the structure of the Kelasu and the Qiulitage fold-and-thrust systems to the North and South of the study area, respectively, and their along-strike variations.

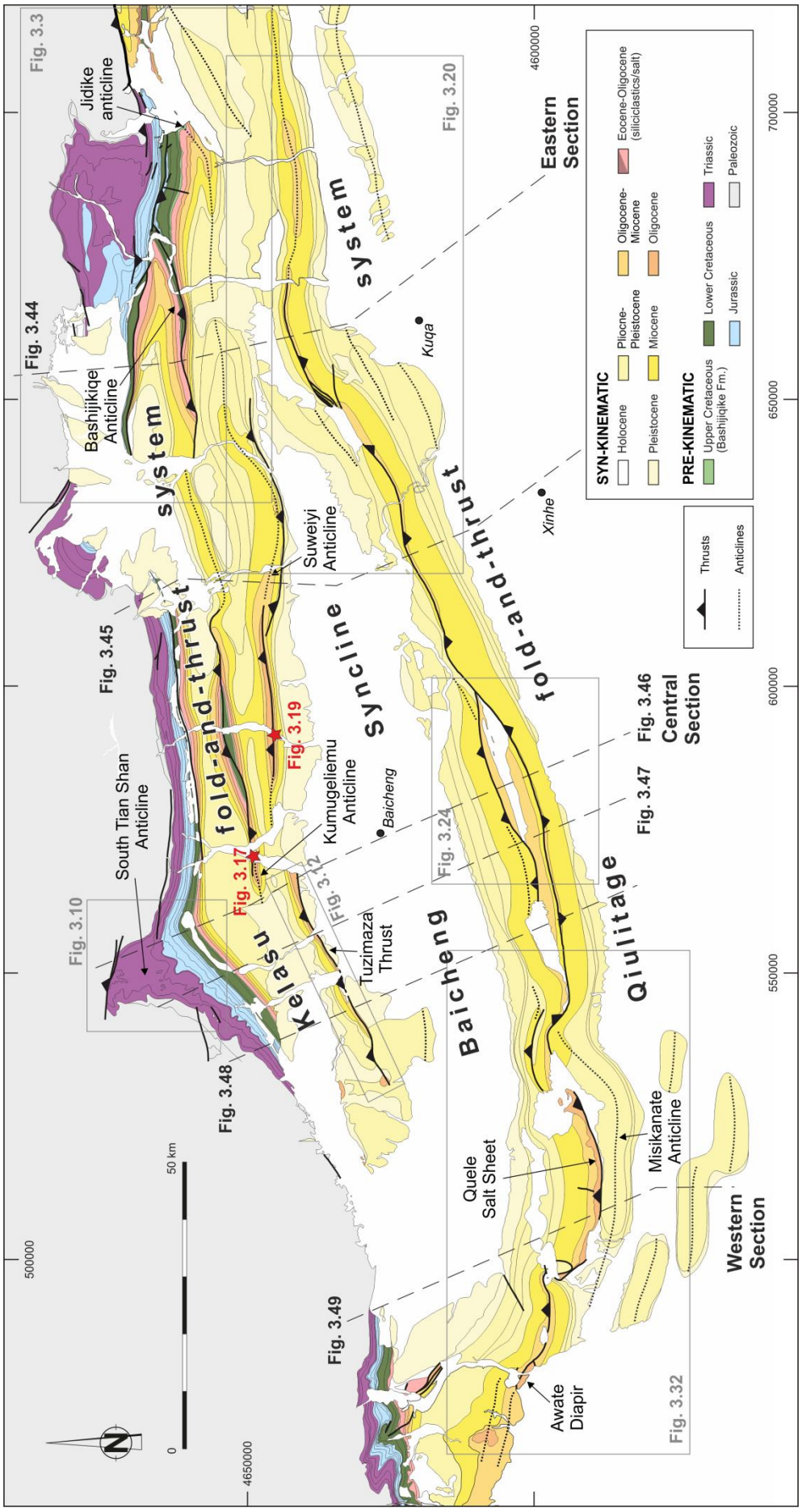

FIGURE 3.1. Geological map of the Kuqa fold-and-thrust belt (modified from Wang et al., 2011). Black dashed lines show the location of the six regional cross sections; the geological maps included in this section of the thesis are indicated by gray squares.

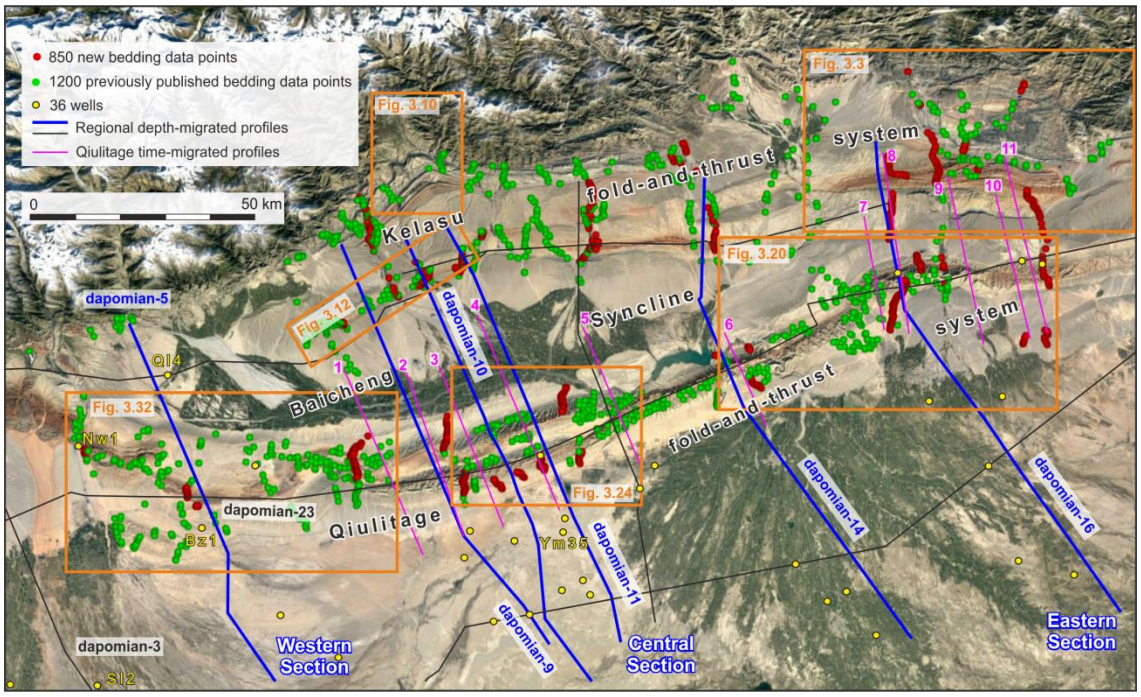

FIGURE 3.2. Aerial photograph of the study area showing: the new bedding data collected in the field (red dots) and the bedding data digitized from previous maps (green dots); the geological maps included in this section of the thesis are indicated by orange squares; the seismic survey (black, pink and blue lines) highlighting the three seismic lines used for describing the structure of the Kuqa fold-and-thrust belt (western, central, and eastern sections).

3.1.2.1. *The Kelasu fold-and-thrust system*

3.1.2.1.1. The eastern Kelasu fold-and-thrust system

Mesozoic units in the eastern Kelasu (**Fig. 3.3**) are unconformably lying on the Paleozoic units and roughly describe a kilometric-scale and basement-involved anticline with a subhorizontal to shallowly south-dipping backlimb and a steeply south-dipping forelimb. The structure has an overall, shallow westwards plunge (**Fig. 3.4**). The back-limb is deformed by open folds whereas the forelimb is cut by two main North-directed back-thrusts detached on Middle Jurassic and Upper Triassic units (**Fig. 3.3**). The latter back-thrust is E-W-striking and separates steeply South-dipping Triassic and Jurassic units in the hanging-wall from SSE-NNW-striking and shallowly SW-dipping Jurassic units in the foot-wall. It is characterized by a hangingwall flat geometry over a footwall ramp where a syncline developed (**Fig. 3.5**).

This surface structure points out that coal layers in the Triassic (and/or Jurassic) units behaved as an important décollement decoupling deformation in the Mesozoic sequences.

Similar structures are imaged at depth by seismic data (section 3.1.3.) and mapped at surface in the western Kelasu fold-and-thrust system (section 3.1.2.1.2.).

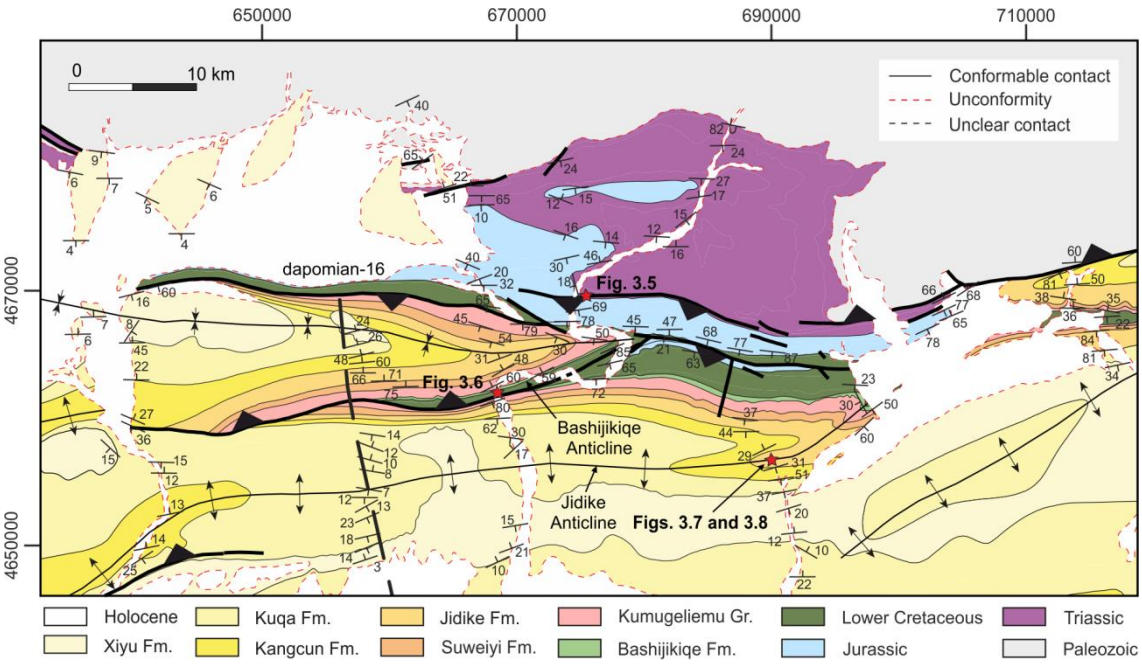

FIGURE 3.3. Geological map of the eastern Kelasu fold-and-thrust sytem (see location in **Figs. 3.1 and 3.2**).

To the South of the Mesozoic units forming the eastern Kelasu, two main structures are recognized, the Jidike and Bashijiqike anticlines, both deforming Cenozoic units at surface (see location in **Fig. 3.3**). The Bashijiqike Anticline is a South-verging anticline with steep limbs.

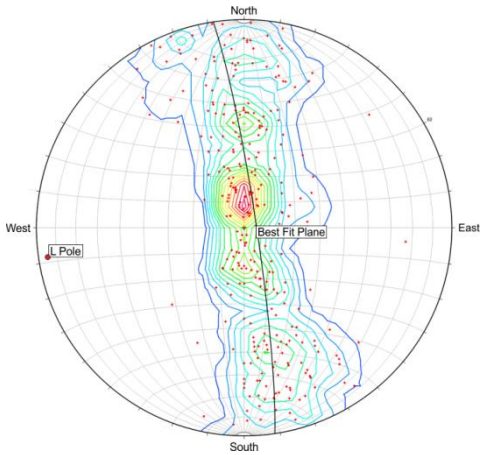

FIGURE 3.4. Stereoplot showing bedding orientation along the eastern Kelasu fold-and-thrust system.

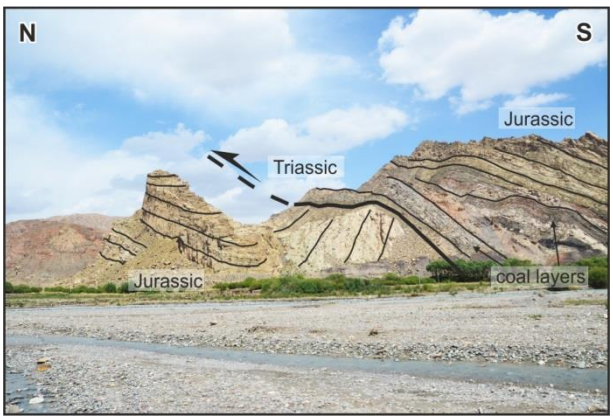

FIGURE 3.5. Field photograph of a back-thrust in the eastern Kelasu fold-and-thrust system (location in the geological map of **Fig. 3.3**).

Bedding in the southern limb is subvertical whereas bedding in the northern limb (Cretaceous units, Kumugeliemu and Suweiyi Fms.) is ENE-WSW-striking and steeply to intermediately North-dipping. The hinge zone of the anticline is cut by a steeply North-dipping thrust that shows an important flat along the Kumugeliemu Fm (**Fig. 3.6**).

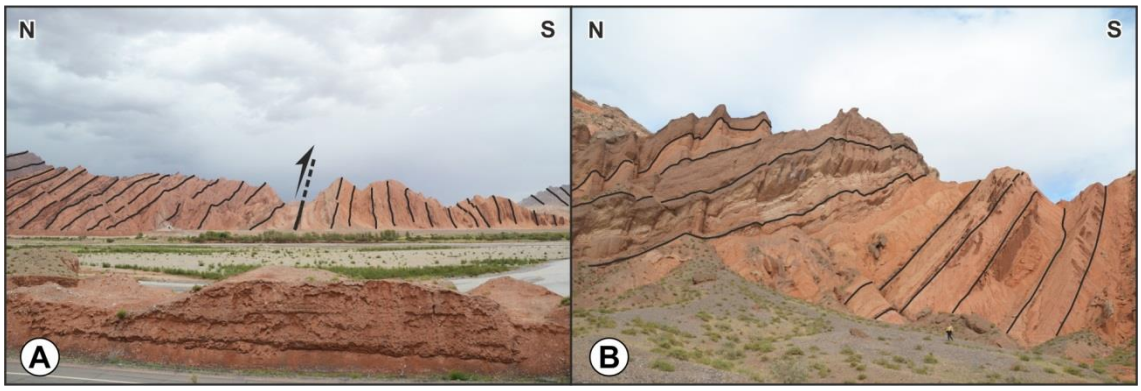

FIGURE 3.6. Field photographs of the eastern Kelasu fold-and-thrust system (location in the geological map of **Fig. 3.3**). **A:** Hinge zone of the Bashijiqike Anticline. **B:** North-dipping bedding in the northern limb of the anticline (Cretaceous units).

South of it, the Jidike Anticline (**Fig. 3.7**) is ENE-WSW-striking and slightly South-verging. The fold axis plunges shallowly to the WSW and the interlimb angle is about 100º. To the West, the Jidike Anticline becomes an open, up-right fold. Both its northern and southern limbs are shallowly dipping (maximum dips of 20-30º, **Fig. 3.8A**) and the interlimb angle increases up to 130º. Minor, North-verging folds were observed in the southern limb of the structure (**Fig. 3.8B**).

FIGURE 3.7. Field photograph of south-dipping bedding in the southern limb of the Jidike Anticline (top of the Jidike Fm.; location in the geological map of **Fig. 3.3**).

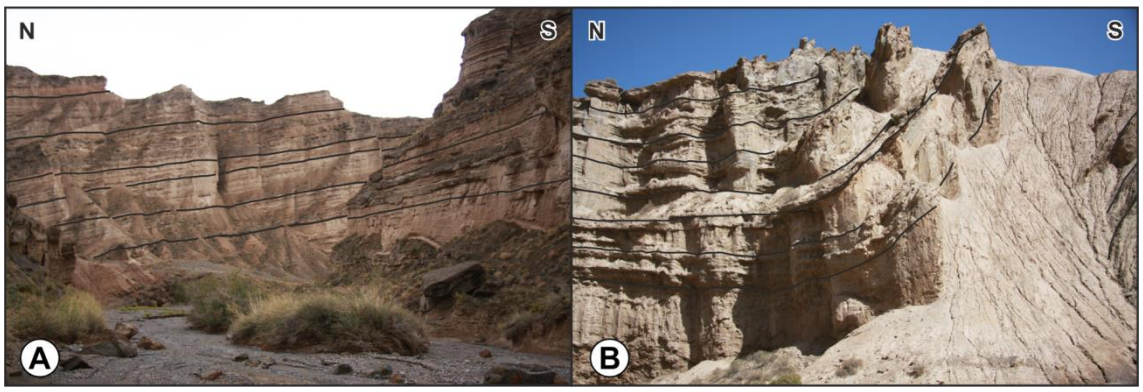

FIGURE 3.8. Field photographs of the eastern Kelasu fold-and-thrsut system (location in the geological map of **Fig. 3.3**). **A:** Shallowly North-dipping bedding in the northern limb of the Jidike Anticline. **B:** Minor North-vergent syncline deforming the southern limb of the Jidike Anticline.

3.1.2.1.2. The western Kelasu fold-and-thrust system

The western Kelasu fold-and-thrust system consists of a northern, basement-involved anticline (the South Tian Shan Anticline in **Figs. 3.1 and 3.9**) and a southern thrust-related anticline (the Tuzimaza-Suweiyi structure) separated by a wider syncline (see locations in **Fig. 3.1**). The central syncline is eastwards deformed by the Kumugeliemu Anticline, that laterally connects to the Bashijiqike Anticline in the eastern Kelasu, whereas the Tuzimaza-Suweiyi structure is eastwards relayed by the Jidike Anticline.

The South Tian Shan Anticline, with a kilometric wavelength, has an overall, shallow eastwards plunge (**Fig. 3.10**) and deforms the whole stratigraphic sequence, from the Paleozoic basement to the youngest Cenozoic units. It is characterized by a subhorizontal to shallowly South-dipping back-limb and an intermediately South-dipping forelimb. Although the regional-scale structure of Mesozoic units in this area is relatively simple, some minor-scale structures can be observed and provide essential information for (1) the proper reconstruction of cross sections in the northern boundary of the Kuqa fold-and-thrust belt, where seismic information is not available and (2) the definition of the Mesozoic structure at surface (Mesozoic units only crop out in the Kelasu fold-and-thrust system) that will help on its interpretation at depth, beneath the salt, where seismic data are poor. For these reasons, a new geological map was produced for this area (**Fig. 3.9**).

The structure in this area is probably controlled by a thrust reentrant at depth. The trend of the Mesozoic units changes from ESE-WNW strikes eastward to NE-SW strikes

westward (**Fig. 3.9**). The Paleozoic rocks and the lower part of the Mesozoic sequence are deformed by a series of minor-scale, south-verging folds. They strike NW-SE and die out southward in the footwall of North-directed back-thrusts that are detached along the Lower Jurassic coal units (**Fig. 3.11**). Mesozoic and Cenozoic units in the hanging-wall of the back-thrusts display a constant southwards dip.

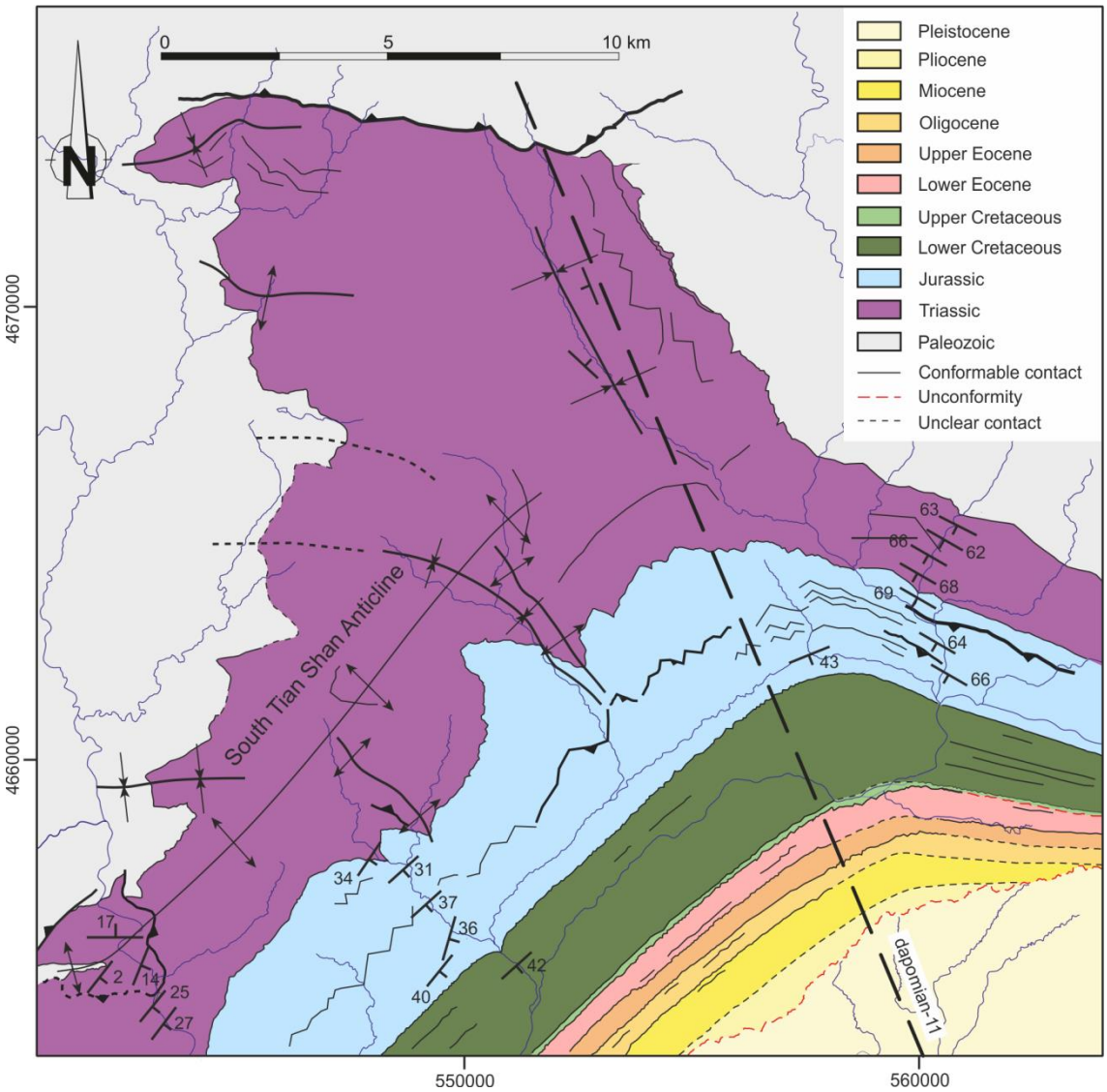

FIGURE 3.9. Geological map of the northern part of the western Kelasu fold-and-thrust system (see location in **Fig. 3.1 and 3.2**).

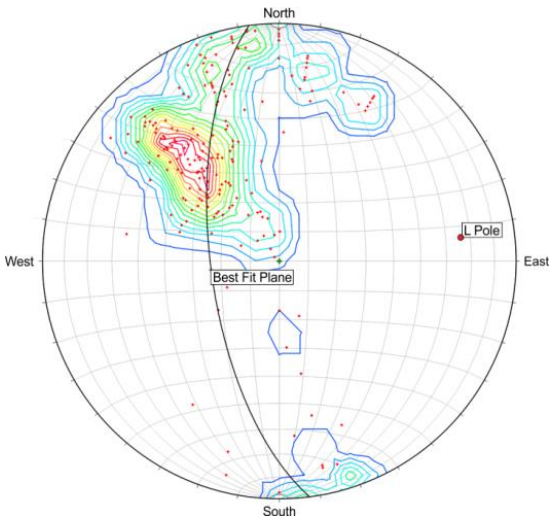

FIGURE 3.10. Stereoplot showing bedding orientation along the western Kelasu fold-and-thrust system.

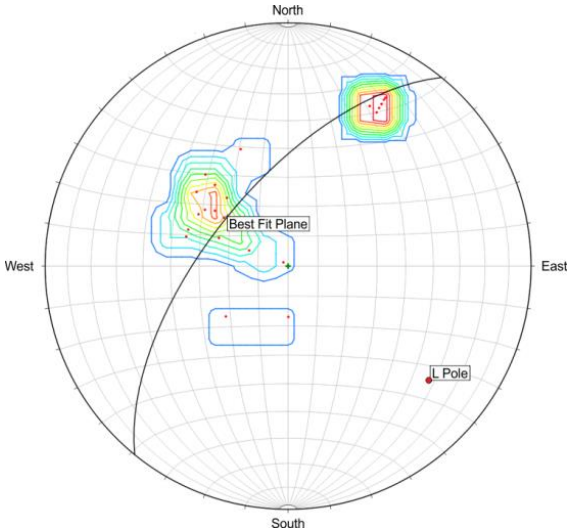

FIGURE 3.11. Stereoplot showing bedding orientation along the southern limb of the South Tian Shan Anticline.

To the South of the South Tian Shan Anticline, the Tuzimaza Thrust (**Fig. 3.12**) crops out. It is a 40-km-long, N110ºE-trending thrust that superposes the red shales and gypsum layers of the Suweiyi Fm. on the conglomerates of the Xiyu Fm. and the sandstones of the Kuqa unit (**Fig. 3.13A and B**). In the hangingwall of the structure, Cenozoic units (Suweiyi to Xiyu Fms.) dip to the North, the dip angle decreasing progressively towards younger units (**Fig. 3.14A**). To the East and West, truncated strata in the hanging wall indicate the presence of a minor anticline (**Fig. 3.14D**). In the footwall, the Xiyu conglomerates dip shallowly to the South although bedding planes are locally subvertical to overturned when approaching the thrust surface (**Fig. 3.14B and Fig. 3.15**).

One of the most striking features of this thrust is the presence of outcrops of Kumugeliemu Group evaporites in two diapirs along its trace. The diapirs are located 26 km apart; the diapir at the western edge of the structure has a rounded shape and a diameter of approximately 2 km whereas the diapir to the East is elongate parallel to the thrust with a major axis of 1.5 km (**Fig. 3.14C**). Eastward of the western diapir, a narrow strip, 100 m-wide, of Kumugeliemu evaporites extends for 7 km along the thrust trace, demonstrating the existence of a squeezed salt wall (**Fig. 3.12**, Li et al., 2014). The squeezed salt, the thrust connecting both diapirs and its eastward continuation (south-directed thrust featuring localized salt extrusions) are referred as the Tuzimaza Thrust (**Fig. 3.12**). It is flanked by growth

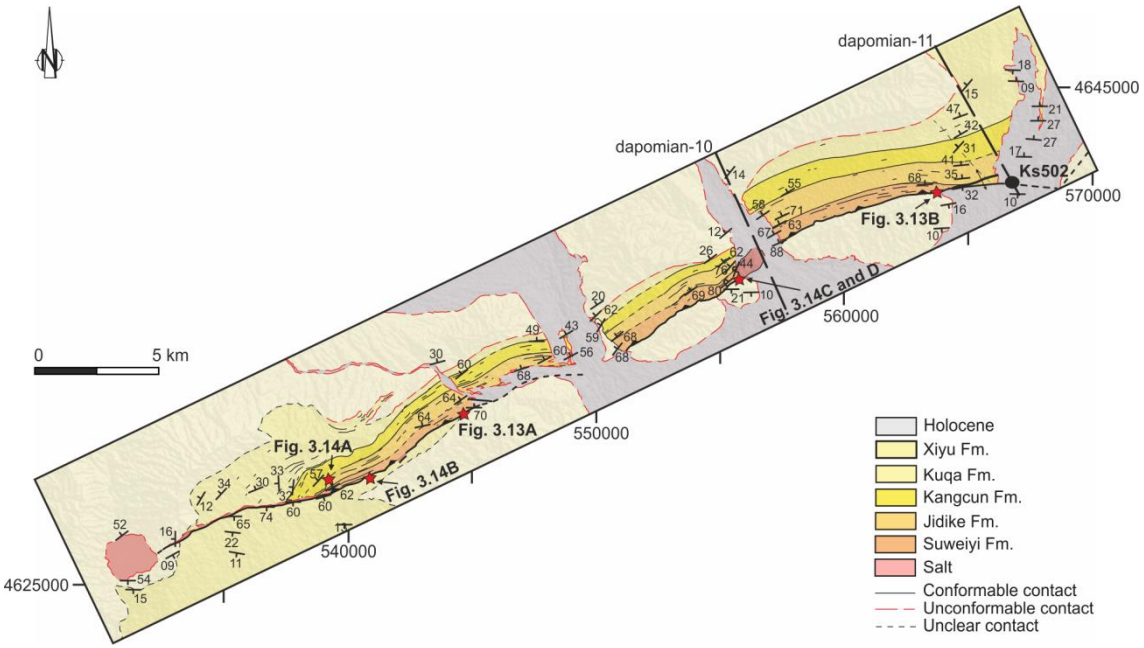

FIGURE 3.12. Geological map of the Tuzimaza Thrust (see location in **Figs. 3.1 and 3.2**).

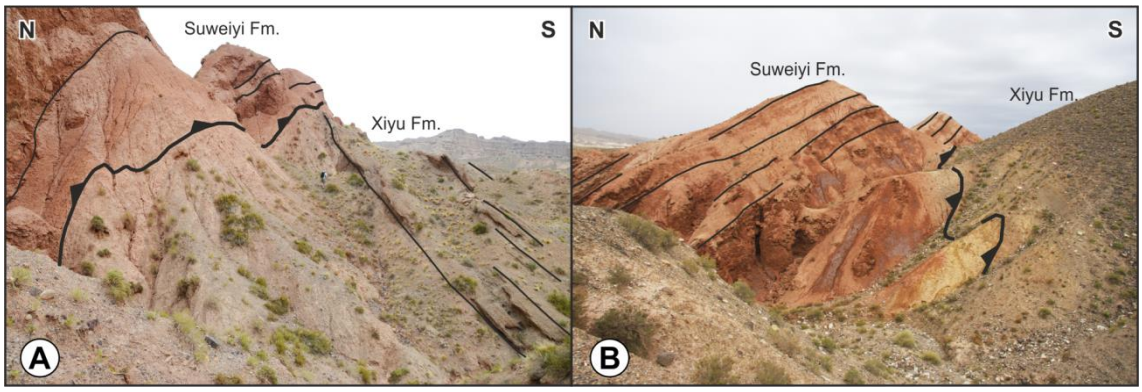

FIGURE 3.13. Field photographs of the Tuzimaza Thrust (see location in the geological map of **Fig. 3.12**). **A:** Western Tuzimaza Thrust. **B:** North-dipping bedding in the hanging-wall of the eastern Tuzimaza Thrust.

strata both in the northern (**Fig. 3.14A**) and southern limbs (**Fig. 3.14B**) that document growth from the Oligocene to Pleistocene. Besides, poorly consolidated conglomerates (probably Holocene in age) are uplifted and deformed on the top of the eastern diapir (**Fig. 3.14C**), suggesting recent activity in the eastern Tuzimaza Thrust salt structure (as defined in other active salt structures in the western Kuqa basin; Li et al., 2014). The Tuzimaza Thrust laterally branches to the East with the Suweiyi Anticline. The Suweiyi anticline is a 50 km-long, ENE-WSW-trending structure (**Fig. 3.16**). Across its central part, the northern limb of the anticline shows a constant dip (50ºN to 60ºN) whereas the southern limb is deformed by minor-scale folds and south-directed thrusts and bedding varies from subhorizontal to steeply South-

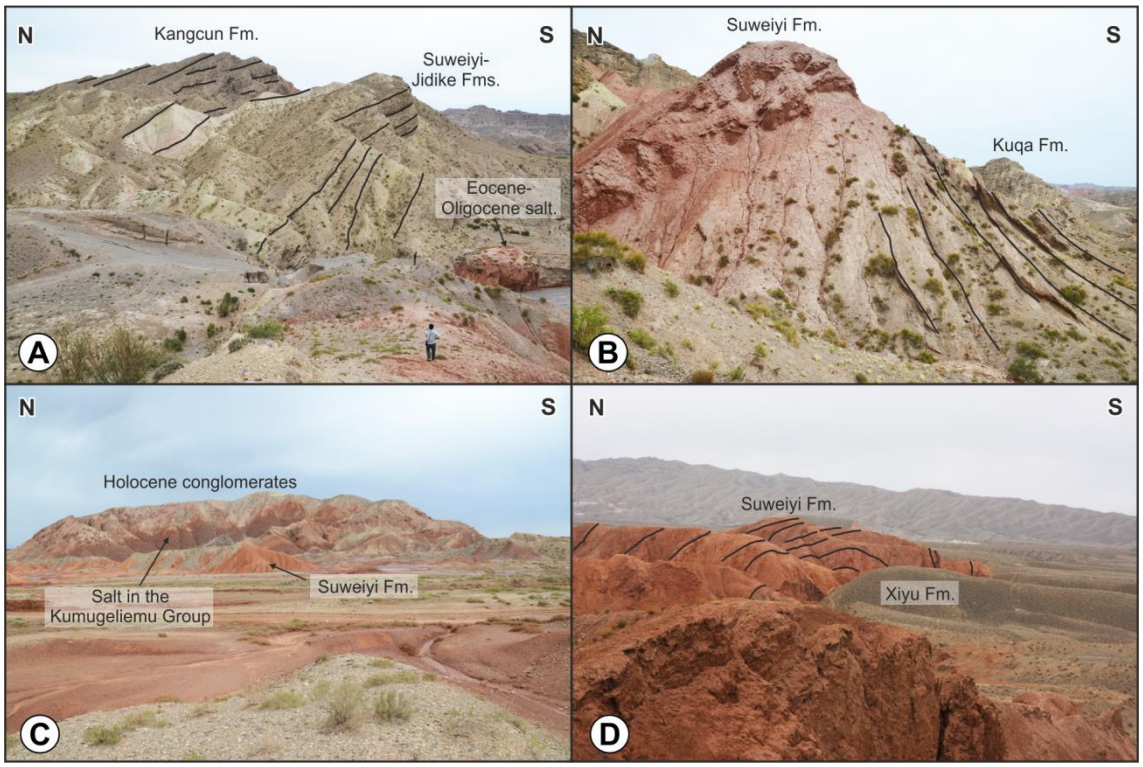

FIGURE 3.14. Field photographs of the Tuzimaza Thrust (see location in the geological map of **Fig. 3.12**). **A:** Oligocene to Miocene growth strata in the northern limb of the structure. **B:** Halokinetic sequences (Kuqa Fm.) in the southern limb. **C:** Holocene conglomerates uplifted and folded over the eastern diapir. **D:** Anticline deforming the Suweiyi Fm. in the eastern termination of the Tuzimaza Thrust.

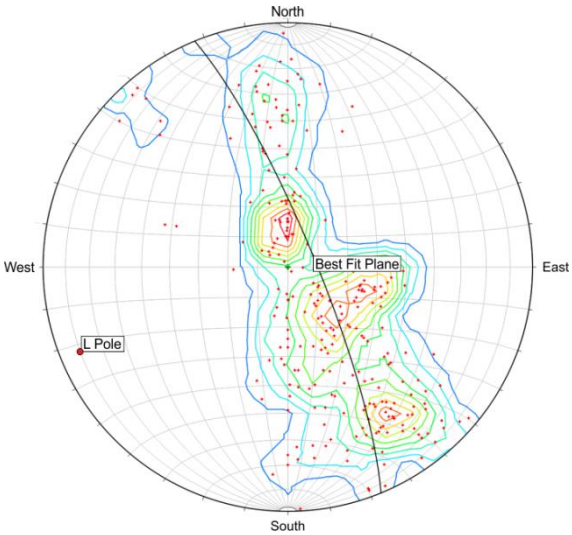

FIGURE 3.15. Stereoplot showing bedding orientation across the Tuzimaza Thrust.

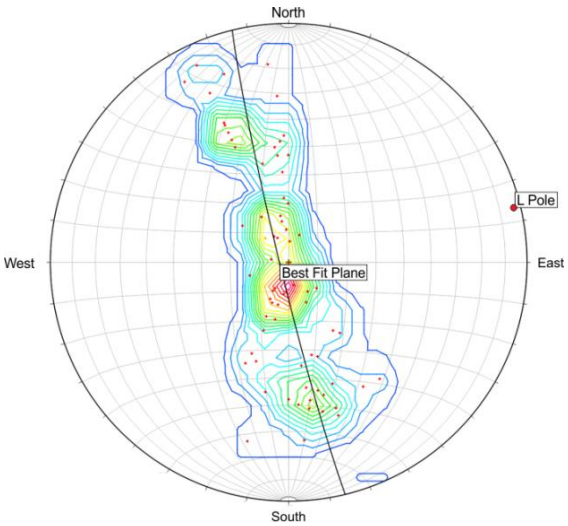

FIGURE 3.16. Stereoplot showing bedding orientation across the central part of the Suweiyi Anticline.

dipping (**Fig. 3.17**). North of it, the Kumugeliemu Anticline is a 40-km-long, ENE-WSW-trending fold (**Fig. 3.18**) that involves Cretaceous units in its core. The anticline is cut by a main thrust

that is South-directed in the central part of the structure but laterally evolves to a North-directed back-thrust involving salt units (Kumugeliemu group) in its hangingwall (**Fig. 3.19**). These evaporitic units represent the easternmost salt outcrop in the Kelasu fold-and-thrust system.

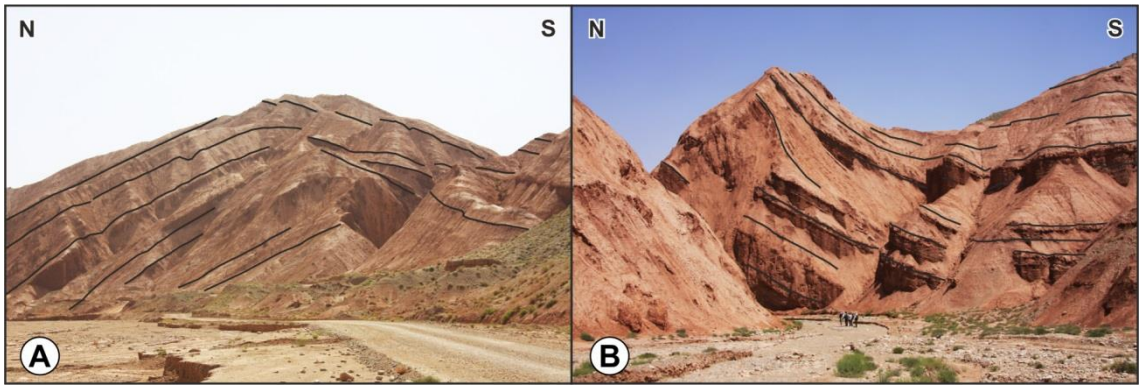

FIGURE 3.17. Field photographs of the Suweiyi Anticline (see location in the geological map of **Fig. 3.1**). **A:** Hinge zone of the Suweiyi Anticline. **B:** Bedding in the southern limb of the Suweiyi Anticline.

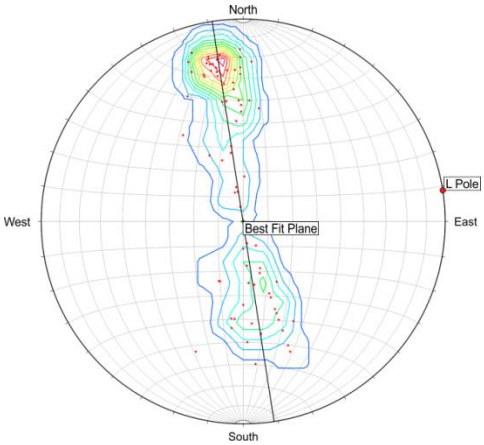

FIGURE 3.18. Stereoplot showing bedding orientation across the Kumugeliemu Anticline.

FIGURE 3.19. Back-thrust in the western termination of the Kumugeliemu Anticline (location in the geological map of **Fig. 3.1**).

3.1.2.2. *The Qiulitage fold-and-thrust system*

The Qiulitage fold-and-thrust system displays significant along-strike structural variations and can be splitted into an eastern, a central and a western segment (see location in **Fig. 3.1**).

3.1.2.2.1. The eastern Qiulitage fold-and-thrust system

The eastern Qiulitage fold-and-thrust system (traversed by seismic lines dapomian-14 and -16, see location in **Fig. 3.20**) is a NE-SW-trending and North-vergent anticline that is eastwards relayed by an E-W to ENE-WSW-trending and south-verging anticline. The structure runs 90 km along-strike and widens progressively to the East up to finally die out in an East-plunging pericline.

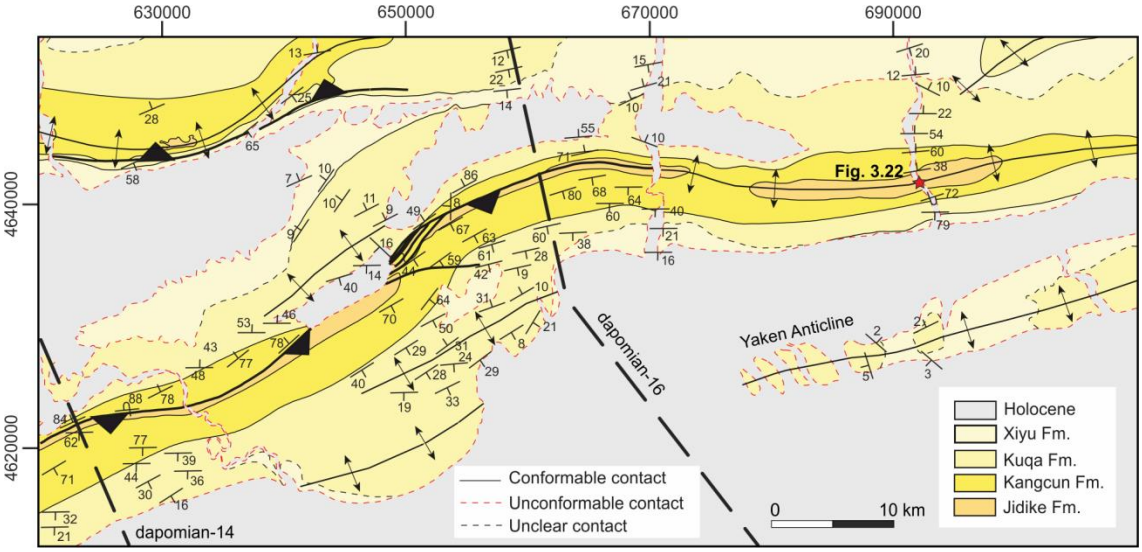

FIGURE 3.20. Geological map of the eastern Qiulitage fold-and-thrust system (see location in **Figs. 3.1 and 3.2**; redrawn from Wang et al., 2011).

The anticline to the East is characterized by a steeply South-dipping, subvertical or even overturned southern limb and a moderately North-dipping northern limb (**Fig. 3.21**): bedding dips 50-60º to the North in the Jidike, Kangcun and lower Kuqa Fms. although the dip angle decreases in the upper Kuqa and Xiyu Fms. (10-20ºN), the latter unconformably overlying older Cenozoic units.

The fold is cored by the Jidike Fm and a box fold geometry was observed in the hinge zone (**Fig. 3.22A**) which is affected by both north and south-directed thrusts with metric to decametric displacements (**Fig. 3.22B**).

The anticline to the West is characterized by a steeply North-dipping (Kuqa and Kangcun Fms.) to overturned (Jidike Fm) northern limb and a steeply to moderately South-dipping southern limb (**Fig. 3.23**), separated by a North-directed back-thrust cutting the hinge zone. Shallower dips are found in the Xiyu Fm conglomerates that unconformably overlay the

Kuqa Fm sandstones in the southern limb of the anticline (**Fig. 3.20**). To the South, two open anticlines developed, the southernmost probably connecting eastwards to the Yaken Anticline (see location in **Fig. 3.20**).

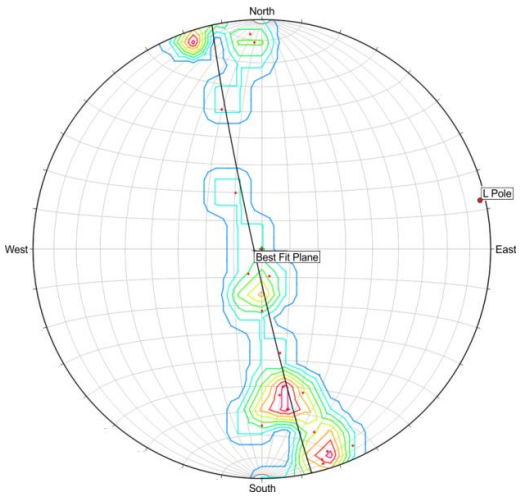

FIGURE 3.21. Stereoplot showing bedding orientation along the eastern part of the eastern Qiulitage fold-and-thrust system.

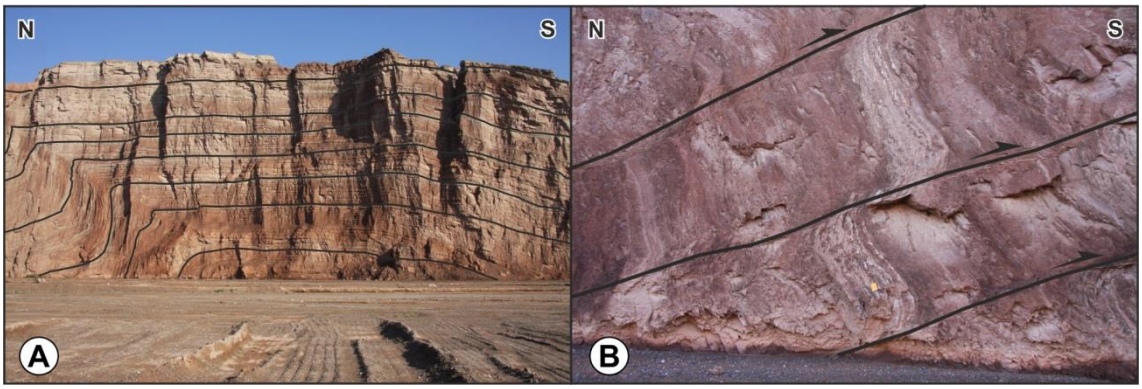

FIGURE 3.22. Field photographs of the eastern Qiulitage fold-and-thrust system (locations in the geological map of **Fig. 3.2**). **A:** Box fold geometry in the hinge zone of the eastern Qiulitage fold-and-thrust system. **B:** South-directed thrusts in the southern limb of the eastern Qiulitage fold-and-thrust system. Displacement of about 2.5 m (see yellow notebook for scale).

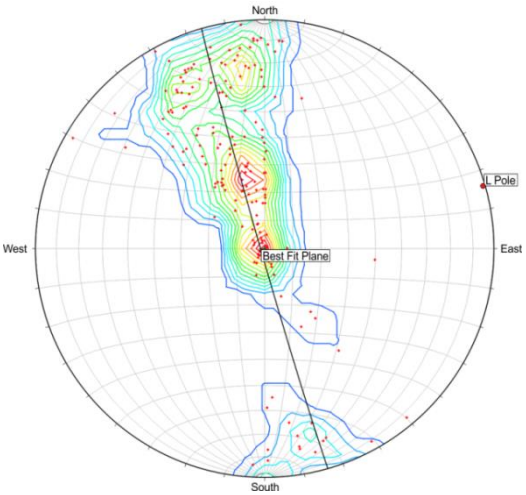

FIGURE 3.23. Stereoplot showing bedding orientation along the western part of the eastern Qiulitage fold-and-thrust system.

3.1.2.2.2. The central Qiulitage fold-and-thrust system

The central Qiulitage fold-and-thrust system is formed by two tight anticlines that are separated by a wider syncline (traversed by seismic lines dapomian 9, 10, 11, and 12, see location in **Fig. 3.2**). The anticlines are cored by the red shales and gypsum layers of the Jidike Fm. They show a curved shape in map view and branch towards the eastern (seismic line dapomian 14) and western margins of the central Qiulitage isolating the central syncline in the inner part of the structure.

A new geological map (**Fig. 3.24**) was produced along the central part of the structure. In this area, the northern anticline is characterized by a subvertical to overturned southern limb and by a northern limb that includes two NW-dipping domains: to the North, bedding is shallowly dipping (upper Kuqa and Xiyu Fms.) whereas steeply North-dipping bedding planes were recognized to the South (lower Kuqa, Kangcun and Jidike Fms., **Fig. 3.25A**). Bedding in the latter dip domain is deformed by shallowly North-directed back-thrusts (**Fig. 3.25B**) and box folds. The anticline is cut by a South-directed thrust that extends laterally for about 30 km (**Fig. 3.24**).

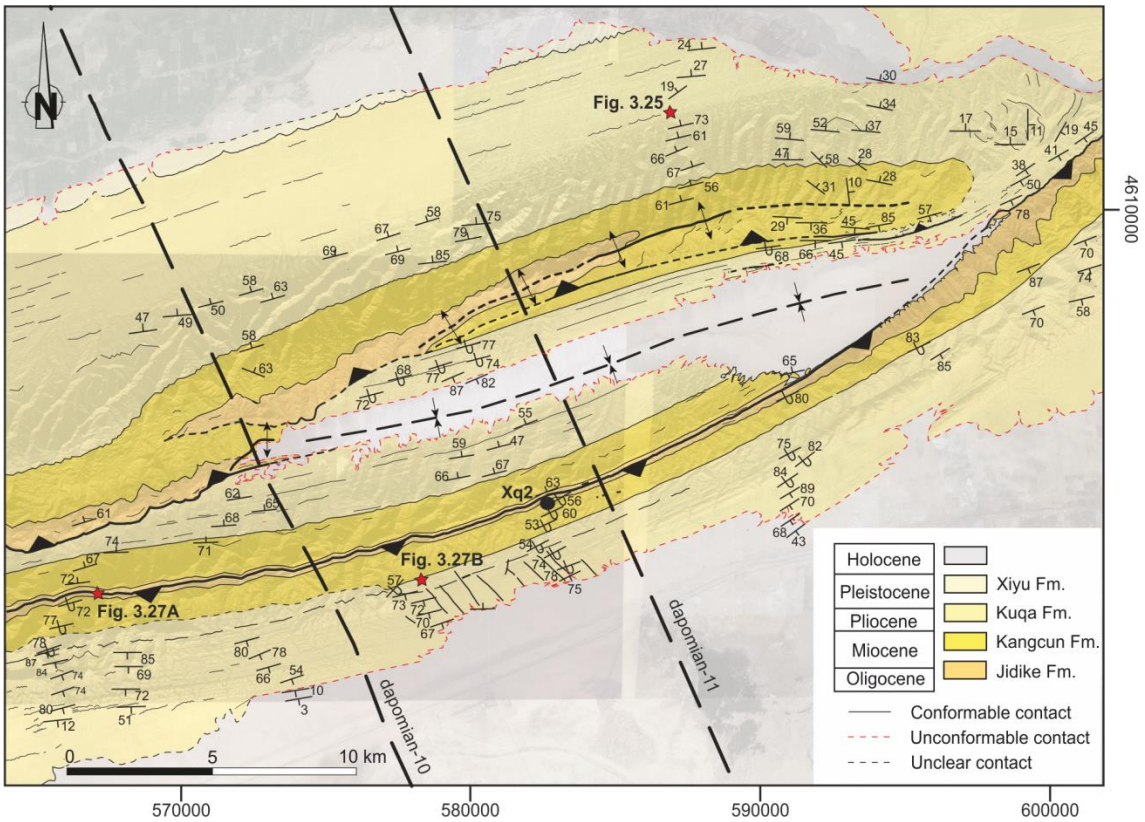

FIGURE 3.24. Geological map of the central Qiulitage fold-and-thrust system (see location in **Figs. 3.1 and 3.2**).

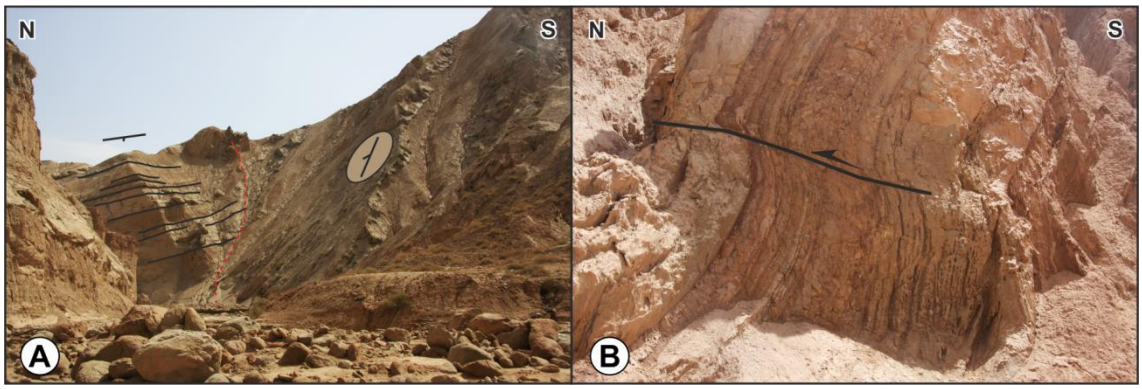

FIGURE 3.25. Field photographs of the central Qiulitage fold-and-thrust system (location in the geological map of **Fig. 3.24**). **A:** Two dip domains in the northern limb of the Qiulitage northern anticline (black dashed line shows the location of the axial trace). **B:** Minor North-directed back-thrust in the northern limb of the Qiulitage northern anticline.

The southern anticline shows an intermediately to steeply North dipping northern limb (70-55ºN) and a steeply South-dipping to overturned southern limb (**Fig. 3.26**). Dip values increase progressively from the outer limbs towards the fold core, describing a progressive unconformity. Its hinge zone is cut by a North-dipping, folded back-thrust (**Fig. 3.27A**). Besides, a kilometric-scale unconformity (located at the lower part of the Kuqa Fm.) was observed along the southern limb of the fold. This unconformity is folded, separates normal-polarity, South-dipping bedding from overturned-polarity, North-dipping bedding (**Fig. 3.27B**), although it laterally becomes a progressive unconformity.

The northern and southern Qiulitage anticlines branch both towards the West of the central Qiulitage fold-and-thrust system where the northern anticline splits into two south-verging anticlines (**Fig. 3.1**) that are cut or related to South-directed thrusts (**Fig. 3.28**).

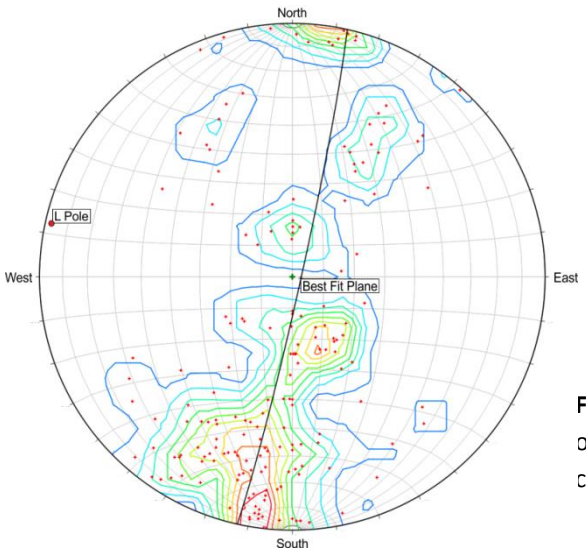

FIGURE 3.26. Stereoplot showing bedding orientation along the western termination of the central Qiulitage fold-and-thrust system.

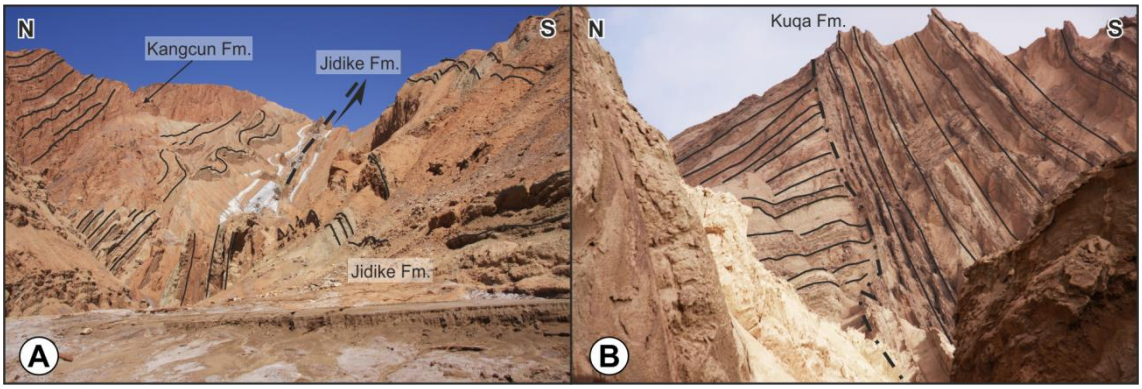

FIGURE 3.27. Field photographs of the central Qiulitage fold-and-thrust system (location in the geological map of **Fig. 3.4**). **A:** Folded backthrust across the hinge zone of the southern Qiulitage anticline. **B:** Angular unconformity in the southern limb of the southern Qiulitage anticline.

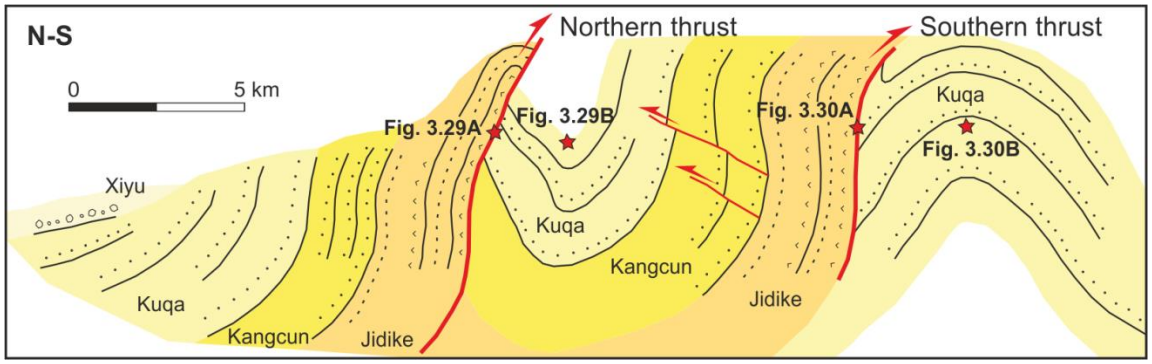

FIGURE 3.28. Schematic cross-section along the western termination of the central Qiulitage fold-and-thrust system.

The northern thrust cuts a South-vergent and west-plunging anticline located in its hanging-wall (**Fig. 3.29A**) whereas a tight syncline was observed in the footwall (**Fig. 3.29B**). The southern thrust (**Fig. 3.30A**) separates the Jidike Fm. in the hanging-wall from the Kuqa Fm. in the footwall, the latter deformed by a tight, minor syncline (cut to the East by the thrust) and an open anticline (**Fig. 3.30B**) that laterally connects with the southern Qiulitage anticline. The Kuqa Fm. in the southern limb of the anticline unconformably overlays older units (an angular unconformity is recognized in the aerial photographs).

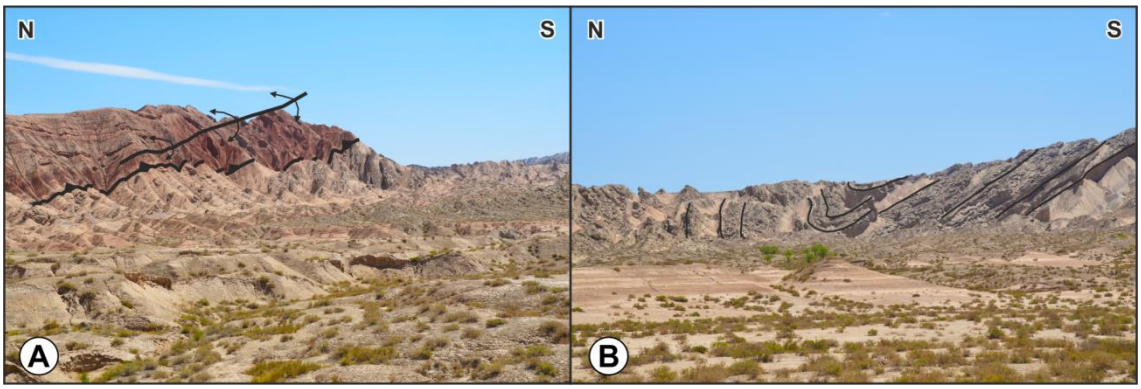

FIGURE 3.29. Field photographs of the central Qiulitage fold-and-thrust system. **A:** Northern, south-directed thrust in the western termination of the central Qiulitage fold-and-thrust system. **B:** Tight syncline in the foot-wall of the northern thrust.

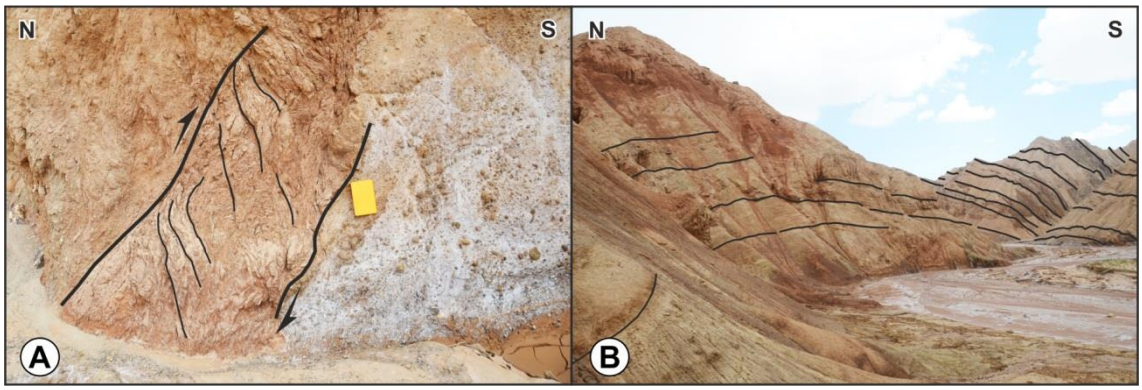

FIGURE 3.30. Field photographs of the central Qiulitage fold-and-thrust system. **A:** Sigmoidal foliations related to the southern thrust plane that is steeply dipping. **B:** Open anticline in the foot-wall of the southern thrust.

To the Eastern part of the central Qiulitage fold-and-thrust system, the northern and southern anticlines converge into a single north-verging anticline (**Fig. 3.1**) that is shallowly WSW-plunging (**Fig. 3.31**). It is cut by a NE-SW-striking back-thrust that extends laterally for tens of kilometers and probably corresponds to a later feature in the structuring of the study area (the Xiyu conglomerates in its hanging-wall conformably overlie the Kuqa Fm).

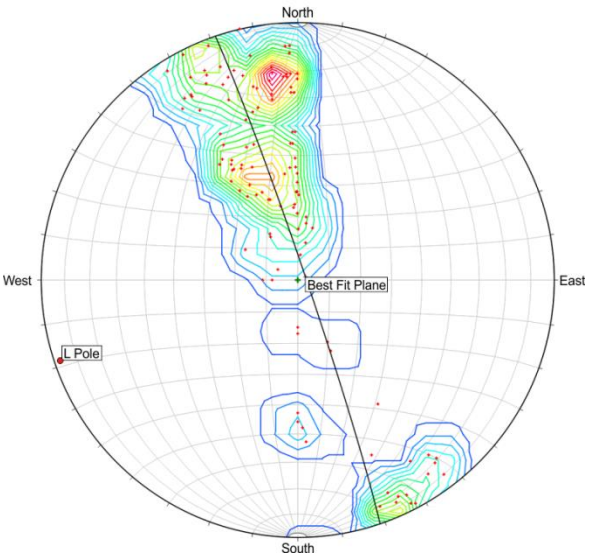

FIGURE 3.31. Stereoplot showing bedding orientation along the eastern termination of the central Qiulitage fold-and-thrust system.

3.1.2.2.3. The western Qiulitage fold-and-thrust system

Field observations in this area were mainly focused on the Quele Salt Sheet (traversed by seismic line dapomian-5, see location in **Fig. 3.32**). The Quele Salt Sheet is a North-dipping thrust characterized by a NW-SE to NE-SW-striking and intermediately to shallowly North-dipping (20 to 40ºN) hanging-wall (**Fig. 3.33**). The thrust cuts the northern limb of a south-vergent anticline, E-W-trending anticline: the so-called Misikantage Anticline (se location in **Fig. 3.32; Fig. 3.34**). This anticline changes strike to the East where it is NE-SW-trending and folds the eastern part of the Quele Salt Sheet and the earlier thrusts in the western termination of the central Qiulitage fold-and-thrust system (**Fig. 3.34**).

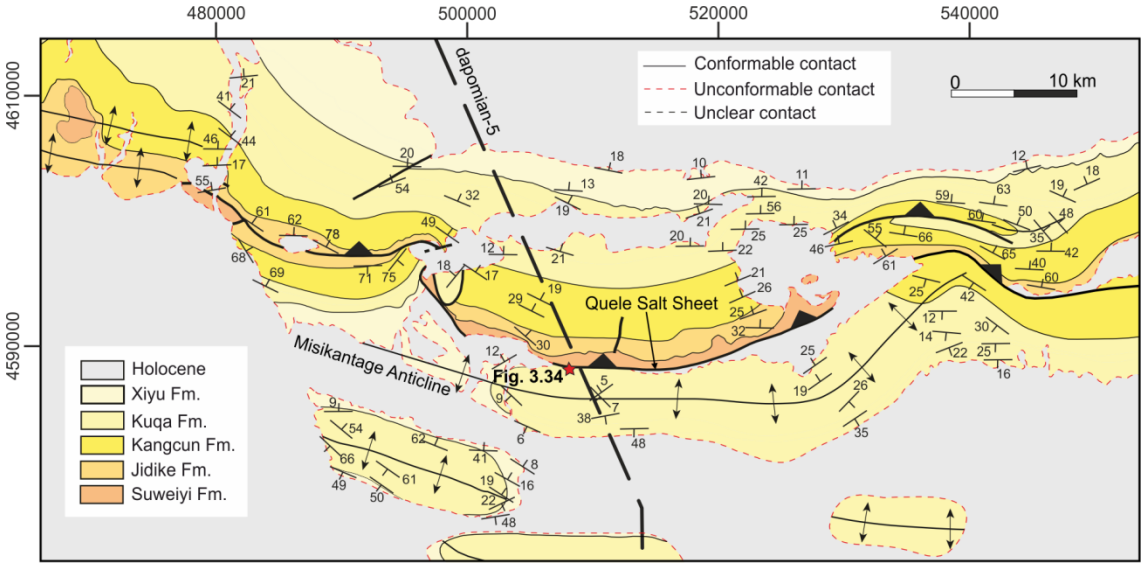

FIGURE 3.32. Geological map of the western Qiulitage fold-and-thrust system (see location in **Figs. 3.1 and 3.2**; redrawn from Wang et al., 2011).

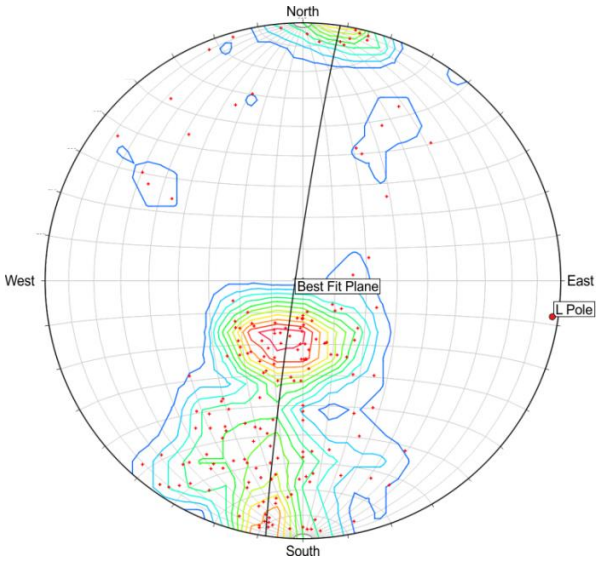

FIGURE 3.33. Stereoplot showing bedding orientation along the Quele Salt Sheet.

From the structures described across the Qiulitage fold-and-thrust system two significant observations derive:

(i) Folds are generally cut by thrusts (**Fig. 3.29A, Fig. 3.34B**) that are in turn steepened and tilted during latter folding (**Fig. 3.27**). Thus, the final architecture of the Kuqa fold-and-thrust system results from the superimposition of several folding and thrusting stages.

(ii) Progressive and angular unconformities are recognized at different levels of the stratigraphic sequence and are a valuable source of information for dating the diachronic growth of the different segments/structures forming the Qiulitage fold-and-thrust system.

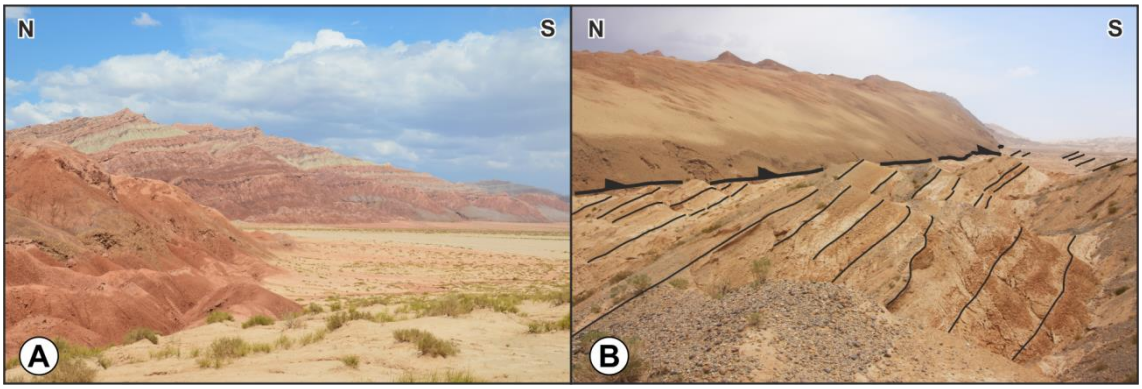

FIGURE 3.34. Field photographs of the western Qiulitage fold-and-thrust system (location in the geological map of **Fig. 3.32**). **A:** Salt units in the hanging-wall of the Quele Salt Sheet. **B:** Salt units thrusting upon the Kuqa Fm (north-dipping beds in the back-limb of the Misikantage Anticline).

3.1.3. Seismic interpretation

3.1.3.1. *Seismic facies characterization*

Seismic interpretation required the identification of seismic facies across the studied profiles. From well top data and their correlation trough seismic lines and to surface unit boundaries, four main seismic units are differentiated, from top to bottom: (1) the Oligocene-Pleistocene detrital sequence, (2) the Kumugeliemu Group, (3) the Mesozoic succession and (4) the Paleozoic basement (see numbering in **Fig. 3.35**). The upper unit is a highly reflective package with closely spaced and continuous reflectors. Across N-S-trending seismic profiles, it reaches its maximum thickness in the core of the Baicheng Syncline but thins sharply to the North (where cross-cutting relationships between reflectors are frequent) and progressively to the South (where reflectors are continuous and parallel). The upper part of the Oligocene-Pleistocene sequence is characterized by low amplitude reflectors whereas slightly thicker

reflectors are recognized towards the base of the unit, interbedded with semi-transparent bands that correspond to shaly packages in the Jidike and Suweiyi Fms (**Fig. 3.35**).

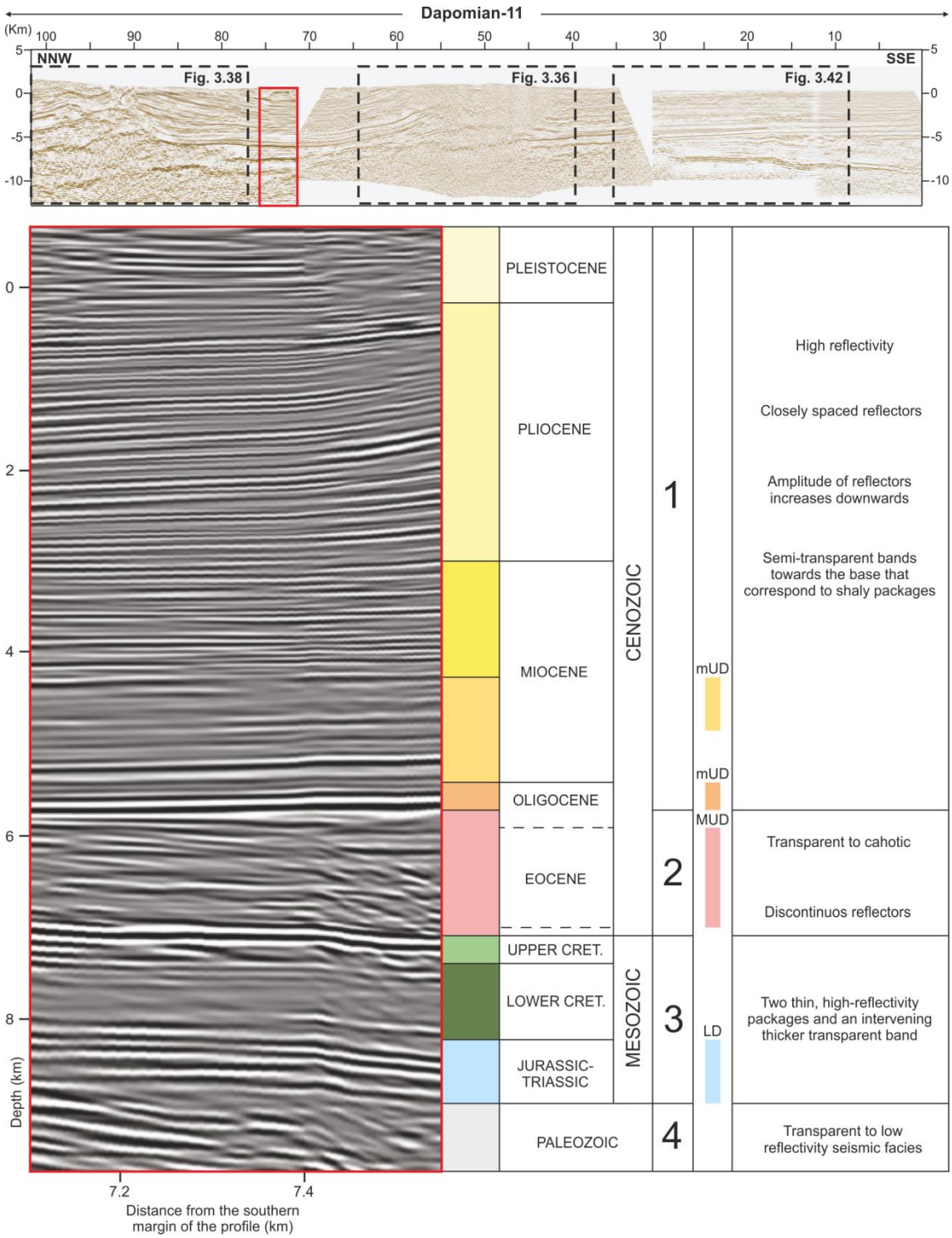

FIGURE 3.35. Reflectivity patterns observed in seismic lines across the Kuqa fold-and-thrust belt and their correlation with stratigraphic units derived from well ties (see position of dapomian-11 seismic line in **Fig. 3.2**). Four main units have been distinguished (see explanation in the text). Position of the décollements is indicated (LD, lower décollement; MUD, main upper décollement; mUD minor upper décollements) as well as the main characteristics of the seismic units.

The Kumugeliemu Group (Eocene-Oligocene in age) shows sharp thickness and seismic attribute changes. Northward, in the Kelasu fold-and-thrust system, it is represented by transparent facies. In the Baicheng Syncline and in the frontal structure of the Quilitage fold-and-thrust system, it corresponds to a package of discontinuous, transparent to chaotic seismic facies that indicate the presence of salt (**Fig. 3.35**). Internal higher-reflectivity reflections probably correspond to mudstone layers interlayered within the salt. The whole package attains its maximum thickness in the core of the Quilitage folds. South of this, the chaotic facies characteristic of the salt grades into a high-reflectivity sequence, with parallel and continuous reflectors, that thins progressively toward the foreland; the boundary between these two different seismic facies marks the southern limit of mobile Eocene-Oligocene salt (**Fig. 3.36**). Correlation between the position of the foreland salt pinch-out in different seismic lines (**Fig. 3.37**) allows defining the distribution of the salt and indicates this boundary runs obliquely to the main structures forming the frontal structure of the Qiulitage fold-and-thrust system. Beneath the Kumugeliemu Group, the Mesozoic sequence consists of two thin, high-reflectivity packages and an intervening thick transparent band. Correlation between surface, well and seismic data allowed us to determine that: (1) the upper high reflectivity sequence corresponds to the Bashijiqike Fm (Upper Cretaceous), (2) Lower Cretaceous units are mostly represented by the transparent sequence and (3) the lower high reflectivity package thus probably defines the Jurassic and Triassic units.

Jurassic and Triassic sequences unconformably overlie the Paleozoic units that, in the central part of the Kuqa fold-and-thrust belt, are characterized by transparent to low reflectivity seismic facies in the northern and central parts of the seismic lines and by continuous and high amplitude reflectors towards its southern boundary. The poor reflectivity zones are likely to correspond to igneous rocks whereas the reflective package is probably the expression of sedimentary units.

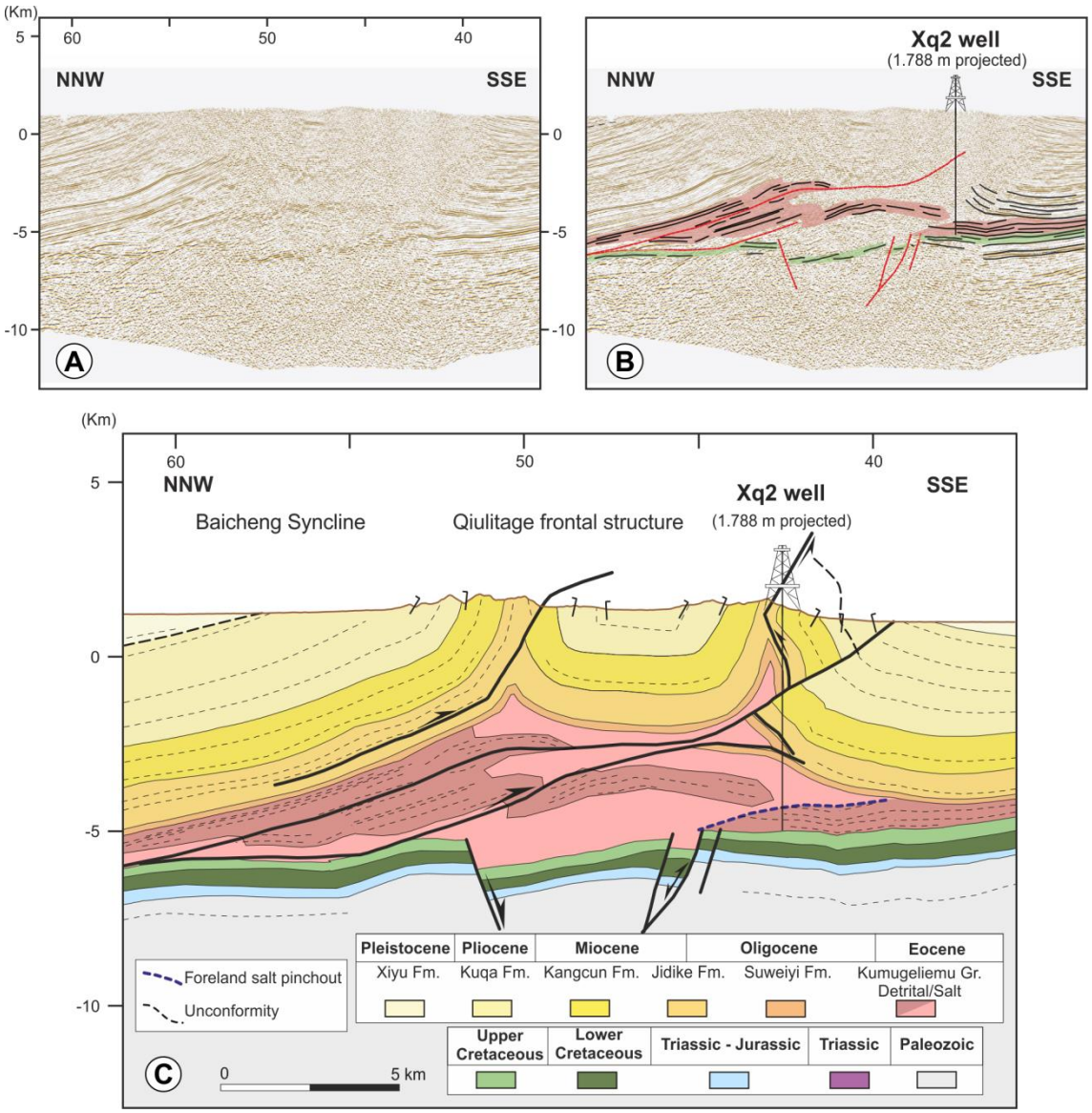

FIGURE 3.36. A: Enlarged seismic image of the central part of dapomian-11 (see location in **Fig. 3.35**) showing details of the Qiulitage fold-and-thrust system (no vertical exaggeration). **B:** Line drawing from the seismic image in **A** highlighting the detrital units in the Kumugeliemu Gr. and the structure beneath the salt. Projected distance of Xq2 well (see location in **Fig. 3.24**) is indicated. **C:** Cross section interpreted from the seismic in **A.**

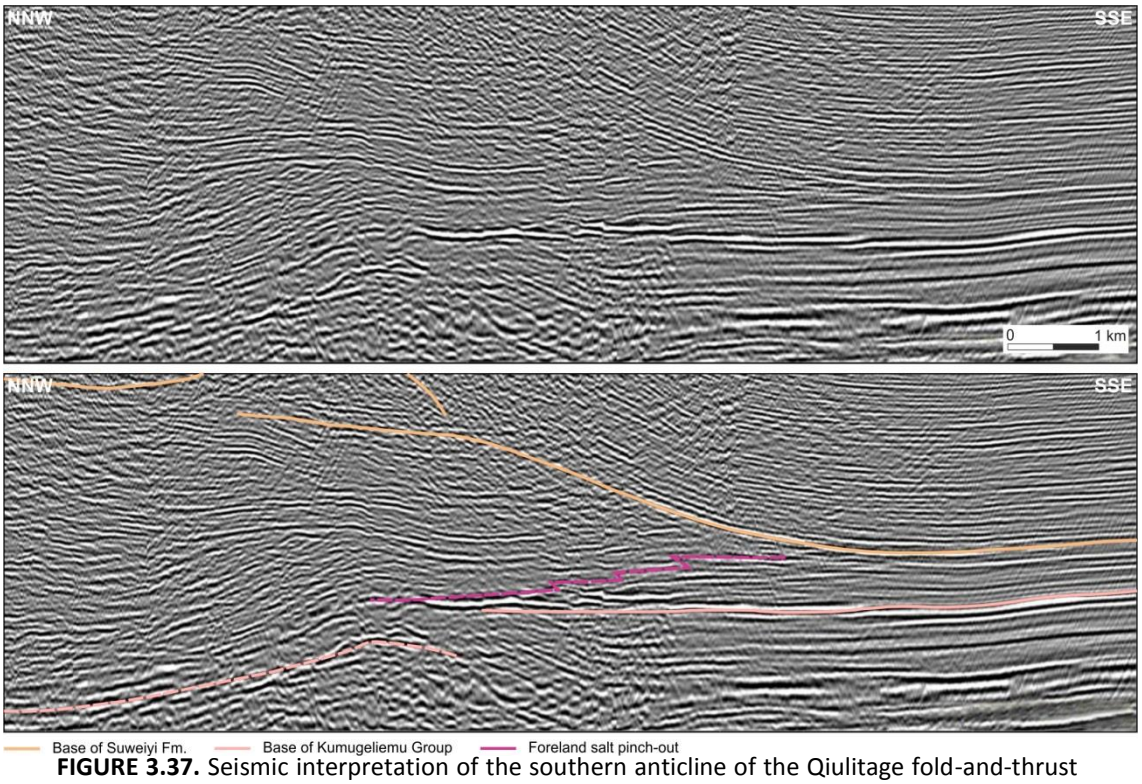

FIGURE 3.37. Seismic interpretation of the southern anticline of the Qiulitage fold-and-thrust system (seismic line 4; see location in **Fig. 3.2**, pink seismic survey).

3.1.3.2. *Key features derived from seismic interpretation*

This section includes a listing of some of the key features found in seismic lines that have allowed to reconstruct not only the structure at depth but also the kinematic evolution along the studied sections:

3.1.3.2.1. Kelasu fold-and-thrust system and Baicheng syncline

Seismic lines dapomian-11 and dapomian-10 (see location in **Fig. 3.2**) give a clearer image of the structure deforming presalt units underneath the Kelasu fold-and-thrust system. The top of the Mesozoic sequence (Bashijiqike Fm) is imaged by a high reflectivity, thin unit (as also observed beneath the Qiulitage fold-and-thrust system) that describes several, smaller wavelength anticlines. These anticlines are related to a thrust system detached along a relatively shallow décollement that is in the lower Mesozoic reflective unit (based on well data and surface observations, we propose it corresponds to Upper Triassic and/or Lower Jurassic coals). The whole thrust system is deformed by two higher wavelength anticlines that should be related to a deeper décollement. They have been interpreted as basement thrusts forming a thrust stack that partly post-dates thin-skinned thrusting along the intra-Mesozoic

décollement (**Fig. 3.38**). Reflectors in the Cenozoic units that overlie the frontal limb of the basement thrust stack image an anticline (**Fig. 3.38**). This fold is north-verging and develops in the hangingwall of a passive back-thrust. Deeper Cenozoic strata in this structure (the Suweiyi, Jidike and Kangcun Fms.) display a growth geometry (**Fig. 3.38**), thereby demonstrating an early growth of the fold during Oligo-Miocene times.

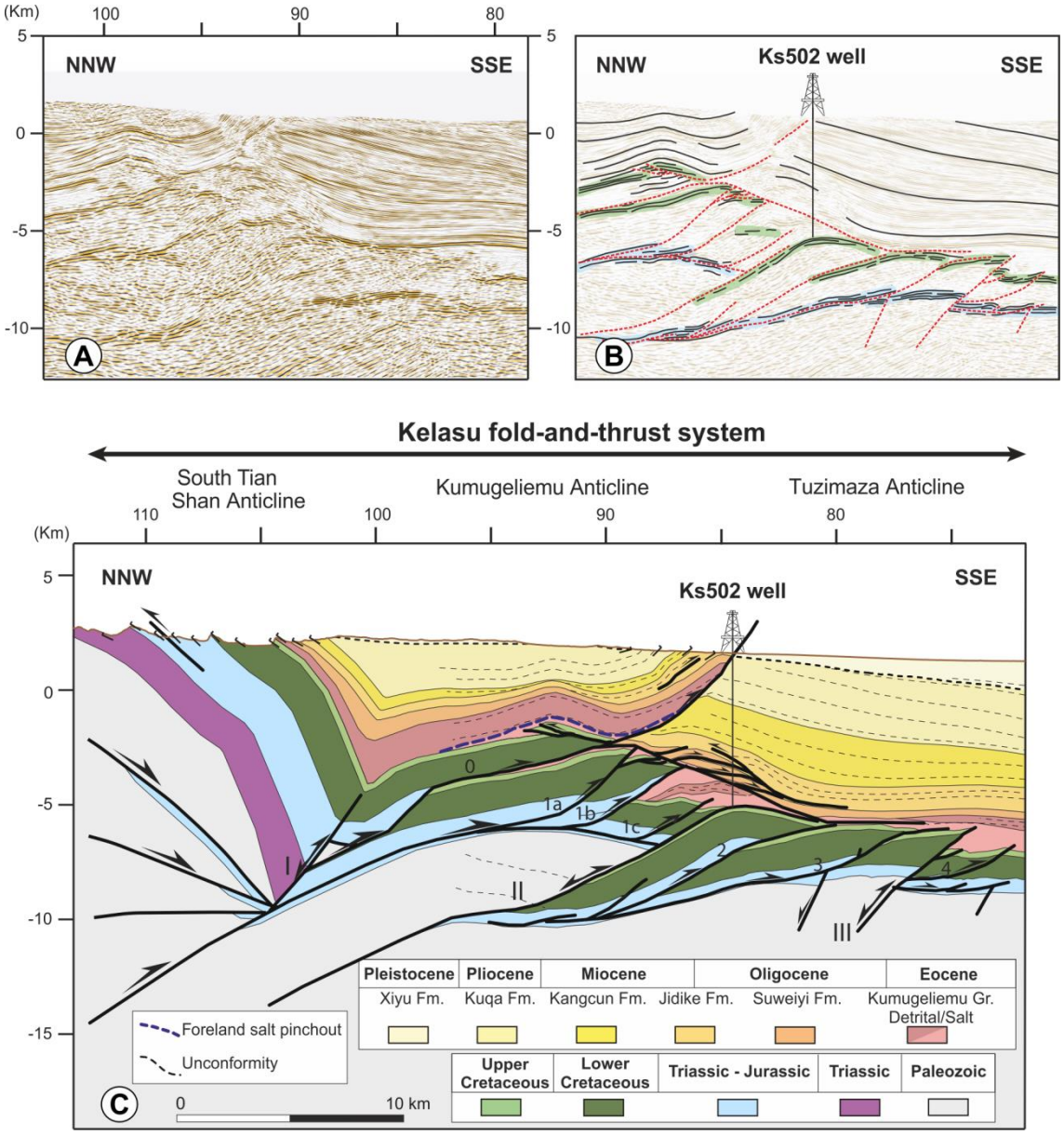

FIGURE 3.38. A: Enlarged seismic image of the northern part of dapomian-11 (see location in **Fig. 3.35**) showing details of the Kelasu fold-and-thrust system (no vertical exaggeration). **B:** Line drawing form the seismic in **A** highlighting the presence of a Mesozoic décollement. Position of Ks502 well (see location in **Fig. 3.12**) is indicated. **C**: Cross section interpreted from the seismic in **A**. Roman numbers refer to basement faults whereas Arabic numbers indicate thin-skinned thrusts detached along Triassic-Jurassic layers.

3.1.3.2.2. Qiulitage fold-and-thrust system

Seismic profiles show a clear structural decoupling above and beneath the Kumugeliemu salt that is represented by an almost 3-km thick package (**Fig. 3.36 and 3.37**). In supra-salt units, angular relationships between seismic reflectors point out to the presence of a secondary décollement along the Jidike Fm (**Fig. 3.39**): seismic reflectors corresponding to the Oligocene-Pleistocene sequence beneath the northern Qiulitage anticline display a divergence between a lower Cenozoic package that is continuous and folded and an upper Cenozoic sequence that shows a constant Northwards dip.

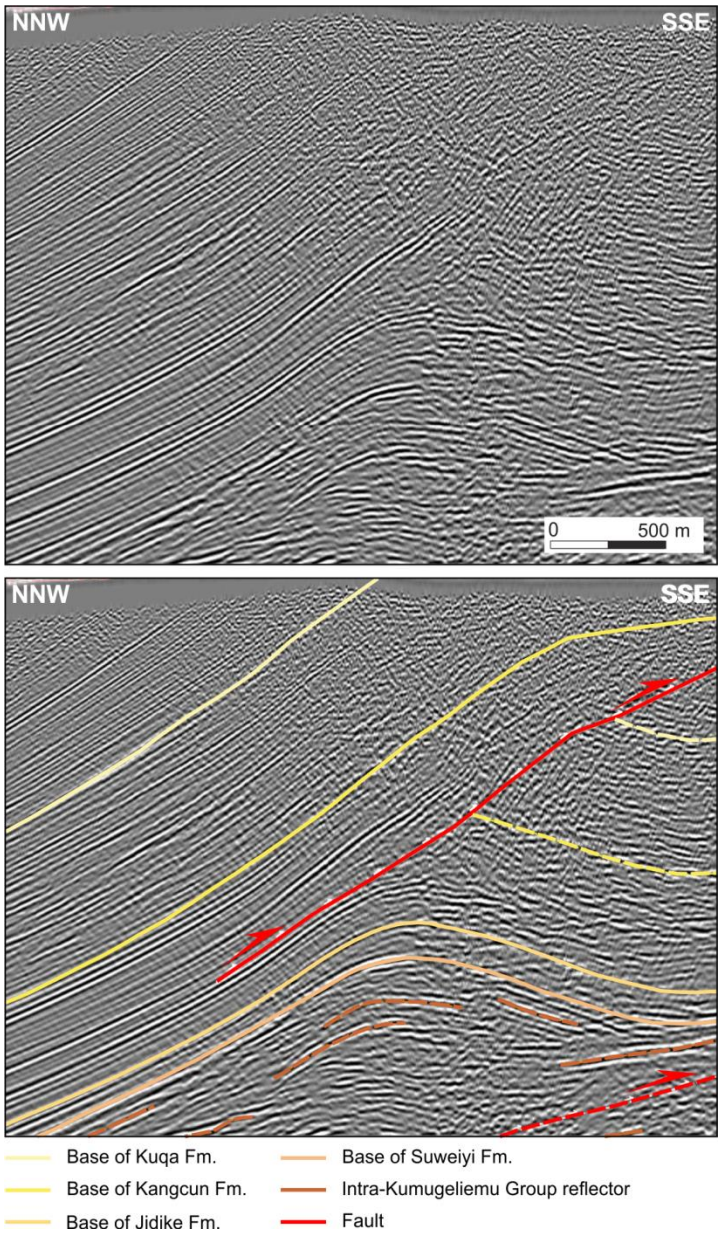

FIGURE 3.39. Seismic interpretation of the northern anticline of the Qiulitage fold-and-thrust system (seismic line 3; see location in **Fig. 3.2**, pink seismic survey).

This angular relationship has been interpreted as an intra-Cenozoic, South-directed thrust (**Fig. 3.39**) that is considered to detach along the Jidike Fm, accordingly to surface observations (i.e. long thrust flats along this unit, **Fig. 3.24**).

Regarding the presalt structure, and despite the poor quality of seismic images underneath the salt, we could track a reflective package corresponding to the Bashijiqike Fm. This package is broken in a way that allowed us to infer normal faulting in some areas beneath the Qiulitage fold-and-thrust system (**Fig. 3.40**) whereas high-angle reverse faults were interpreted in some others. These faults separate Mesozoic sequences displaying thickness variations that agree with their activity as extensional faults during Mesozoic times. Furthermore, intra-Mesozoic low angle unconformities are locally recognized in the footwall of the high angle faults beneath the Qiulitage frontal structure, consistently with footwall uplift during extensional faulting (**Fig. 3.41**).

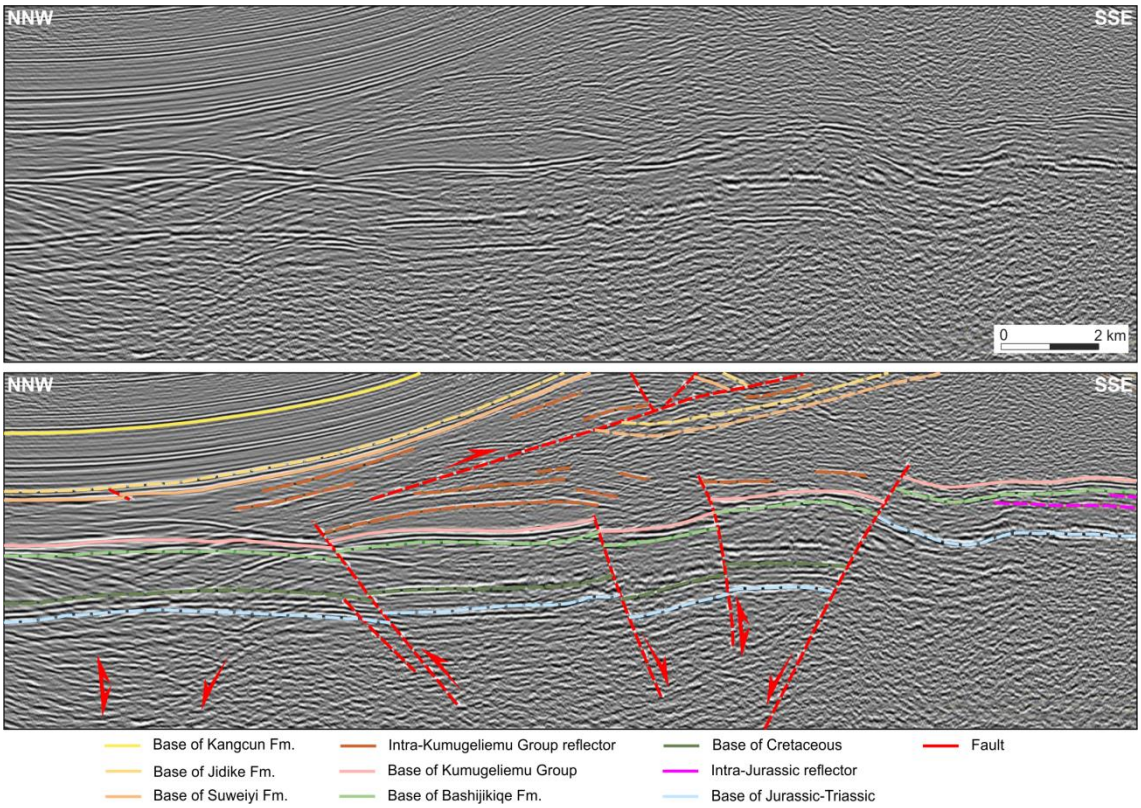

FIGURE 3.40. Seismic interpretation of Mesozoic units beneath the central Qiulitage fold and thrust system (seismic line 5; see location in **Fig. 3.2**, pink seismic survey).

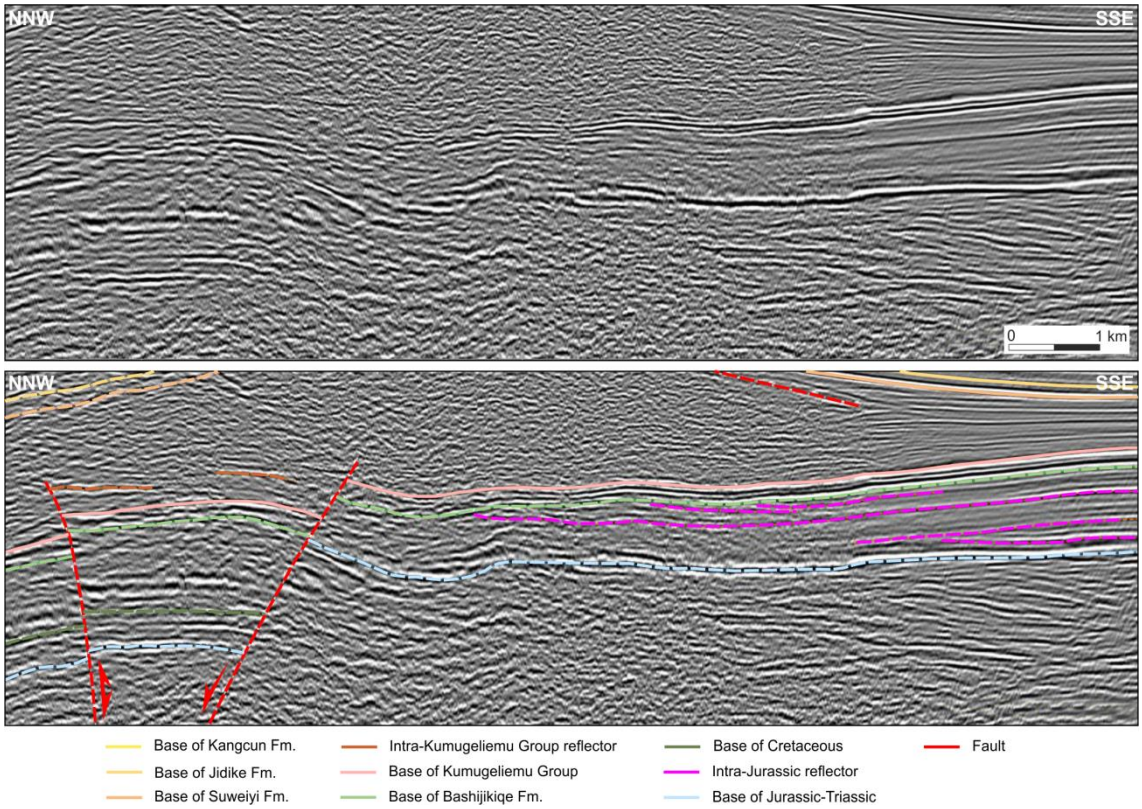

FIGURE 3.41. Seismic interpretation of Mesozoic units beneath the frontal structure of the central Qiulitage fold and thrust system (seismic line 5; see location in **Fig. 3.2**, pink seismic survey).

3.1.3.2.3. Northern Tarim Basin

To the South of the Qiulitage fold-and-thrust system, seismic profiles show that reflectors in the Mesozoic and Cenozoic units are almost undeformed except for a regional Northwards tilt and several open anticlines deforming the Cenozoic units (**Fig. 3.42**). These anticlines overlie basement antiforms that are overprinted by subvertical to high angle normal faults affecting not only the Paleozoic but also the Mesozoic units (**Fig. 3.43**). These structures are well-imaged in this part of the basin where bedding dips are shallower than to the North and salt is scarce or absent. They evidence that folds in the Cenozoic are intimately related to basement structures and that these basement structures are accommodating shortening to the South of the Qiulitage fold-and-thrust system (**Fig. 3.43**).

The structure in **Fig. 3.43** (seismic line dapomian-5 in the western part of the Kuqa fold-and-thrust belt) summarizes two of the key observations that allowed us to understand the evolution of the Kuqa fold-and-thrust belt through Mesozoic times: (1) The thickness of the Mesozoic sequence changes when the southern and northern limbs of the structure are

compared, suggesting this structure was already active during Mesozoic times, and (2) the Bashijiqike Fm uncomformably overlies older Mesozoic units indicating early compression took place during Cretaceous times.

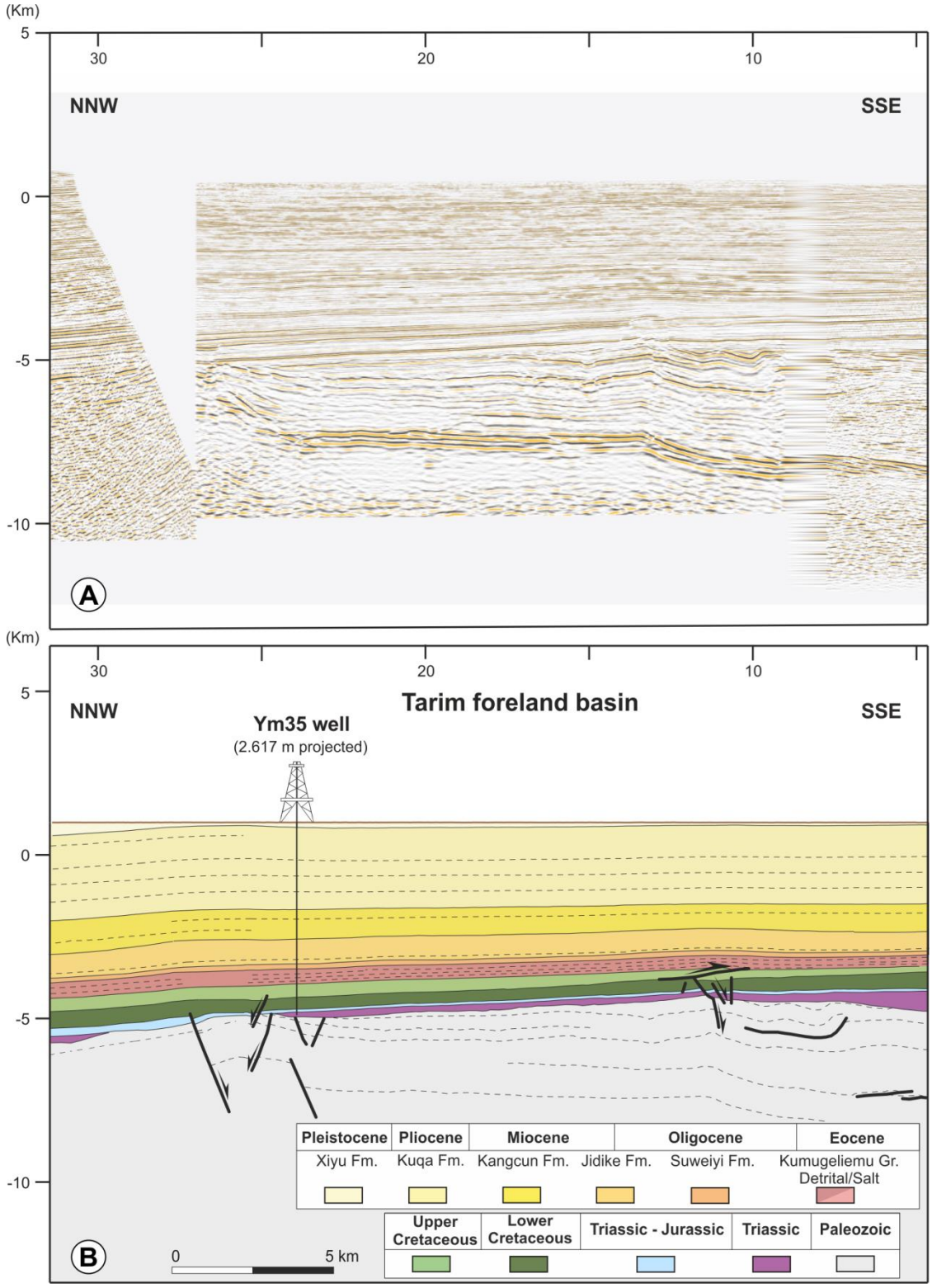

FIGURE 3.42. A: Enlarged seismic image of the southern part of dapomian-11 (see location in **Fig. 3.35**) showing details of the Tarim foreland basin (no vertical exaggeration). **B:** Cross section interpreted from the seismic in **A**. Projected distance of Ym35 well (see location in **Fig. 3.2**) is indicated.

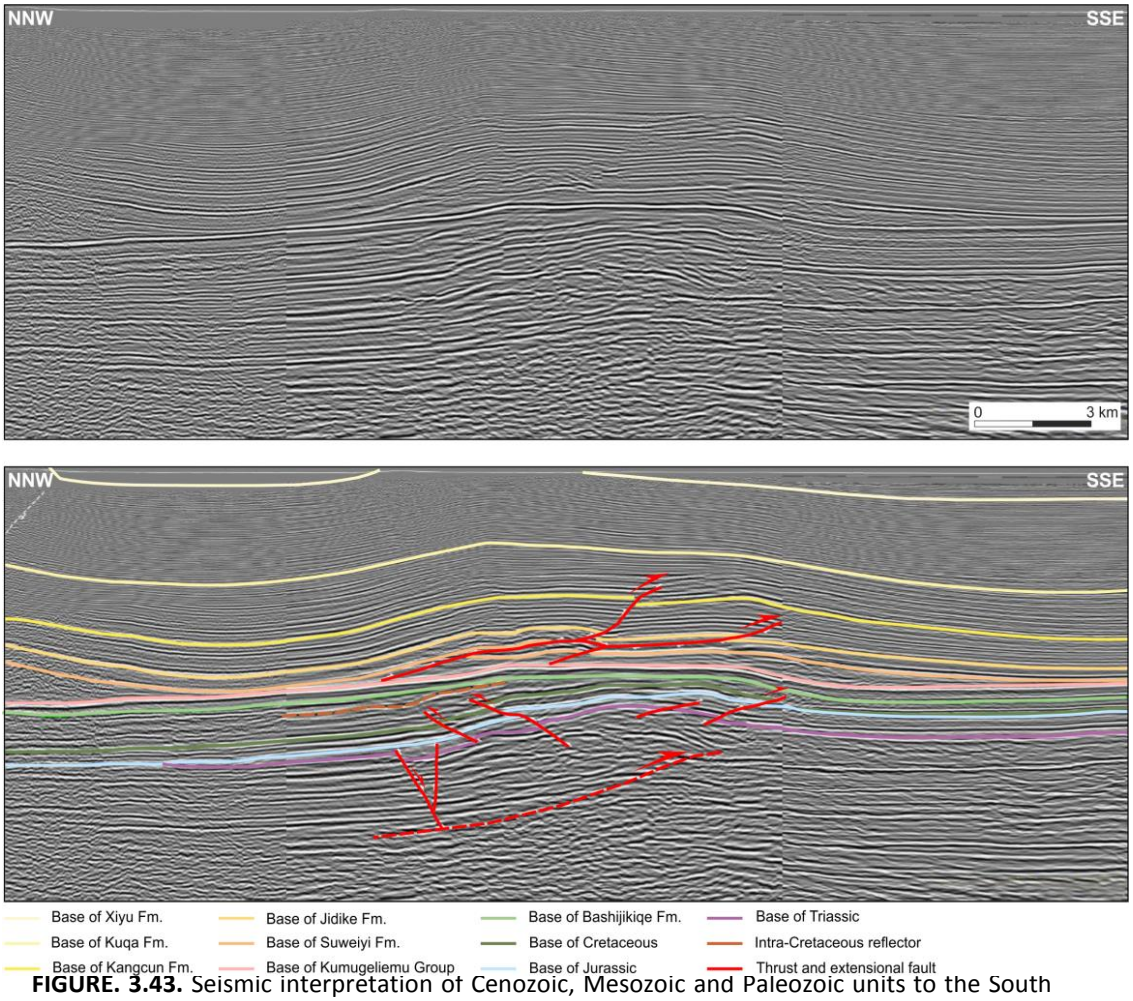

FIGURE. 3.43. Seismic interpretation of Cenozoic, Mesozoic and Paleozoic units to the South of the Qiulitage frontal structure, western part of the Kuqa fold-and-thrust belt (seismic line dapomian-5; see location in **Fig. 3.2**, pink seismic survey).

3.2. REGIONAL CROSS SECTIONS

As previously introduced, the study area extends from the southernmost outcrops of the Tian Shan Range to the northern part of the undeformed Tarim foreland basin (**Fig. 3.1**). Based on the stratigraphic position of the sole thrust, two structural domains can be distinguished: (i) a northern domain where the whole stratigraphic sequence, from the Paleozoic to the Cenozoic, is deformed and (ii) a southern domain where folds and thrusts are mainly detached along the Eocene-Oligocene salt. Hereinafter, we will refer to these domains as the Kelasu fold-and-thrust system and the Qiulitage fold-and-thrust system, respectively (see zone division in **Figs. 3.44, 3.45, 3.46, 3.47, 3.48**, and **3.49**). The extent and geometry of these domains varies along-strike as the depth, lithology and degree of overlap of the décollements does. In general terms, the Kelasu fold-and-thrust system keeps a constant width and the Qiulitage fold-and-thrust system narrows eastwards, where the sole thrust has been reported to climb into the Jidike Fm (Wang et al., 2011; Li et al., 2012).

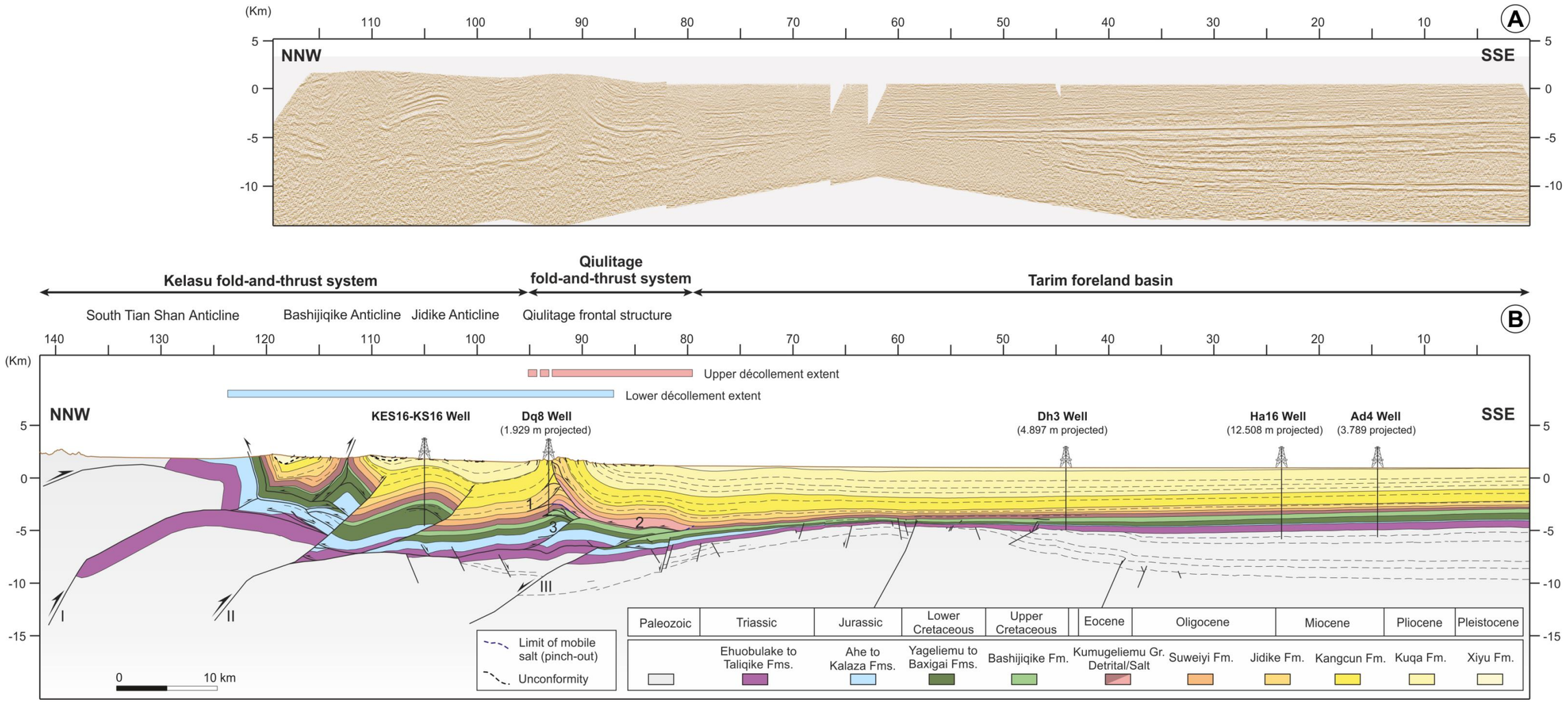

FIGURE 3.44. A: Depth-converted dapomian-16 seismic profile (see location in **Fig. 3.2**) across the eastern part of the Kuqa fold-and-thrust belt (no vertical exaggeration). **B:** Regional, seismic based across section (see location in **Fig. 3.1**) integrating new and previously published structural data and honoring new geological maps produced for this thesis. Seismic interpretation and cross section construction and balancing was completed in Petrel 2013 (Schlumberger) and Move 2015 (Midland Valley).

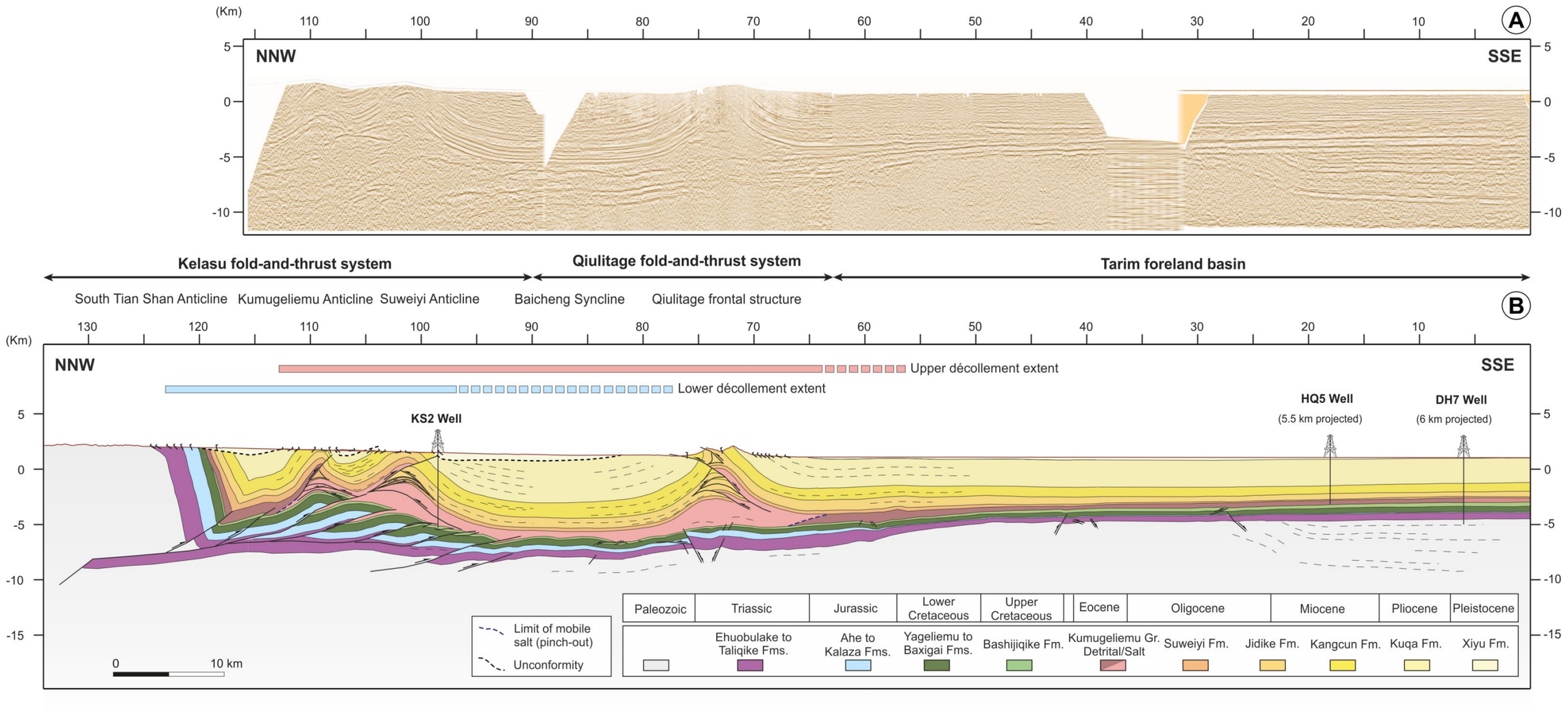

FIGURE 3.45. A: Depth-converted dapomian-14 seismic profile (see location in **Fig. 3.2**) across the eastern part of the Kuqa fold-and-thrust belt (no vertical exaggeration). **B:** Regional, seismic based cross section (see location in **Fig. 3.1**).

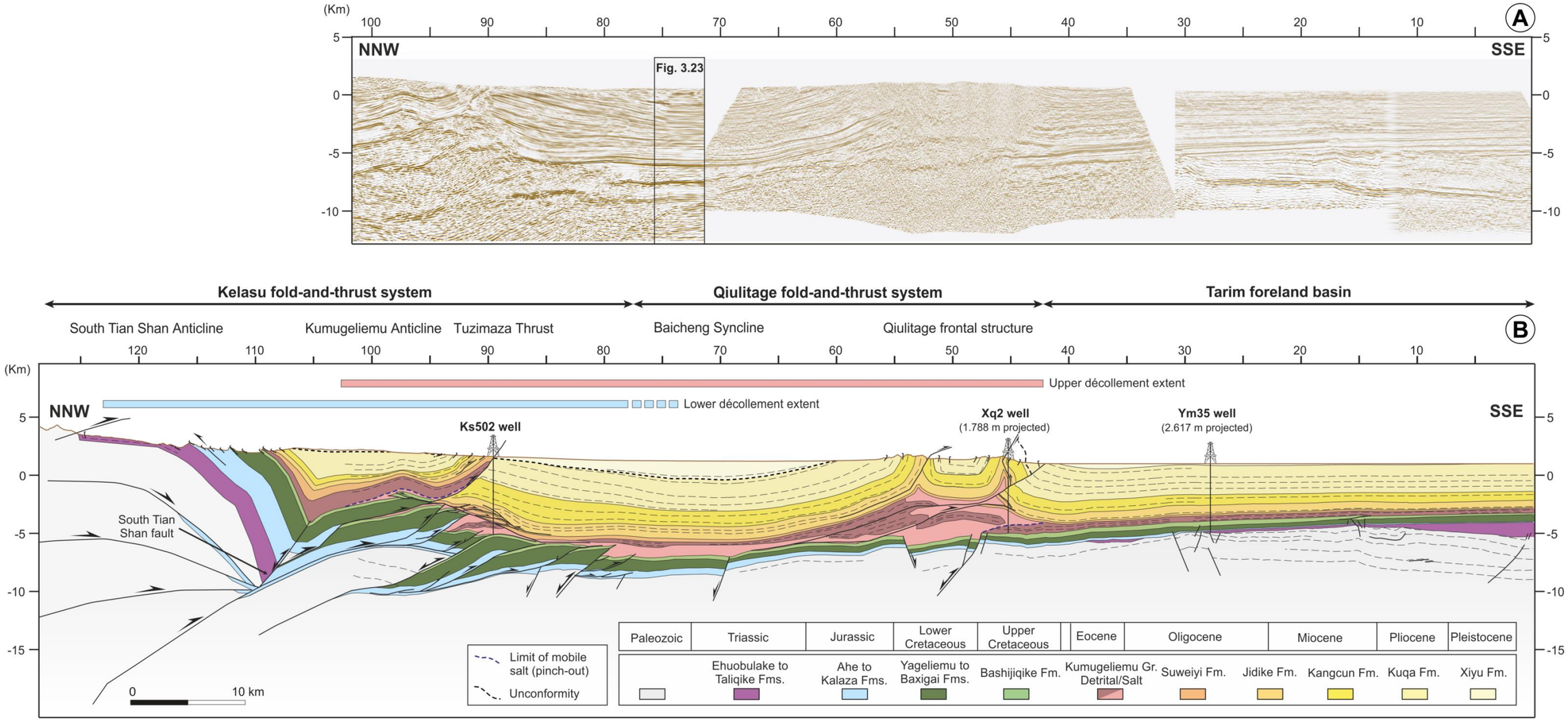

FIGURE 3.46. A: Depth-converted dapomian-11 seismic profile (see location in **Fig. 3.2**) across the central part of the Kuqa fold-and-thrust belt (no vertical exaggeration). **B:** Well top data in wells close to the seismic profile (left); stratigraphic sequence interpreted along the projection of the wells on the seismic line (right), resulting from the interpretation of a regional well and seismic survey and its integration with surface data. **C:** Regional, seismic based cross section (see location in **Fig 3.1**).

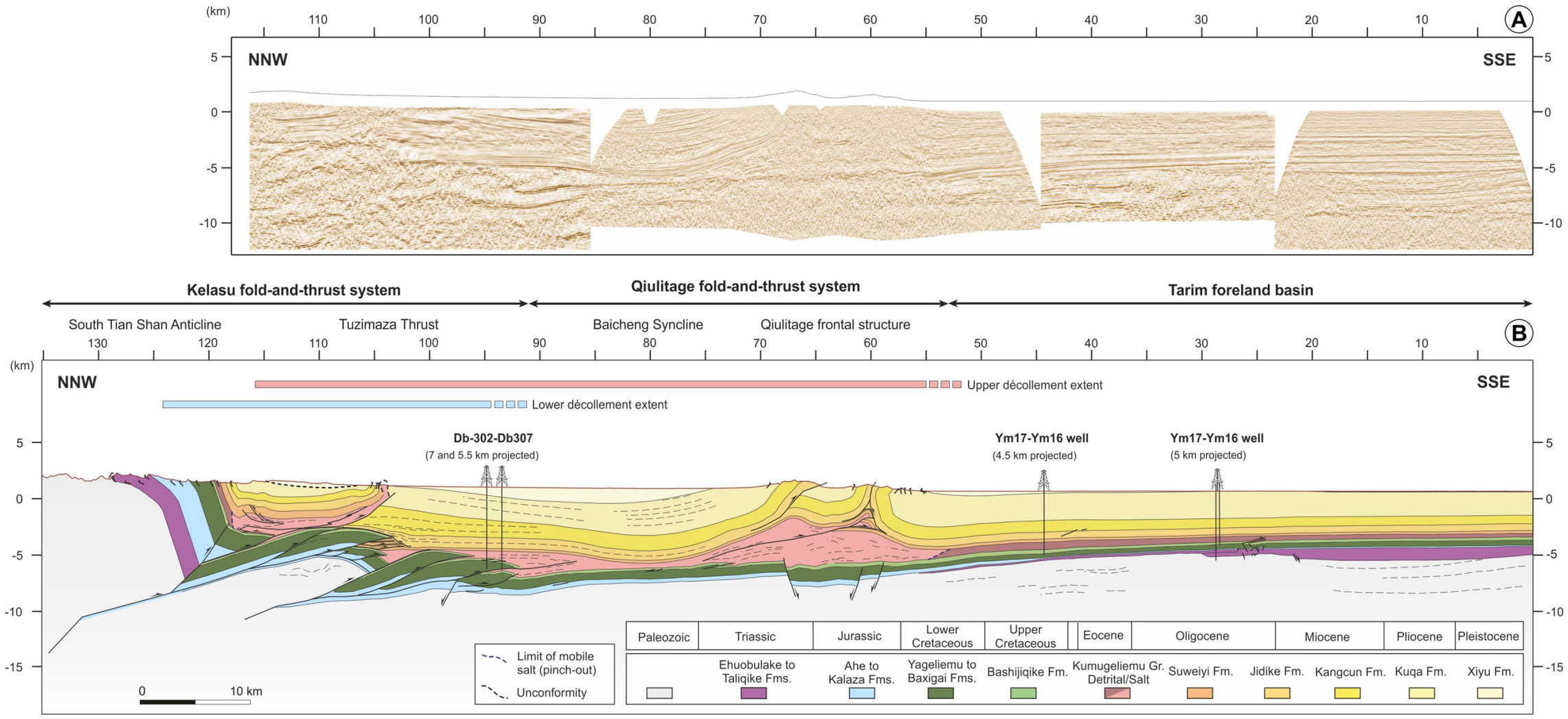

FIGURE 3.47. A: Depth-converted dapomian-10 seismic profile (see location in **Fig. 3.2**) across the central part of the Kuqa fold-and-thrust belt (no vertical exaggeration). **B:** Regional, seismic based cross section (see location in **Fig. 3.1**).

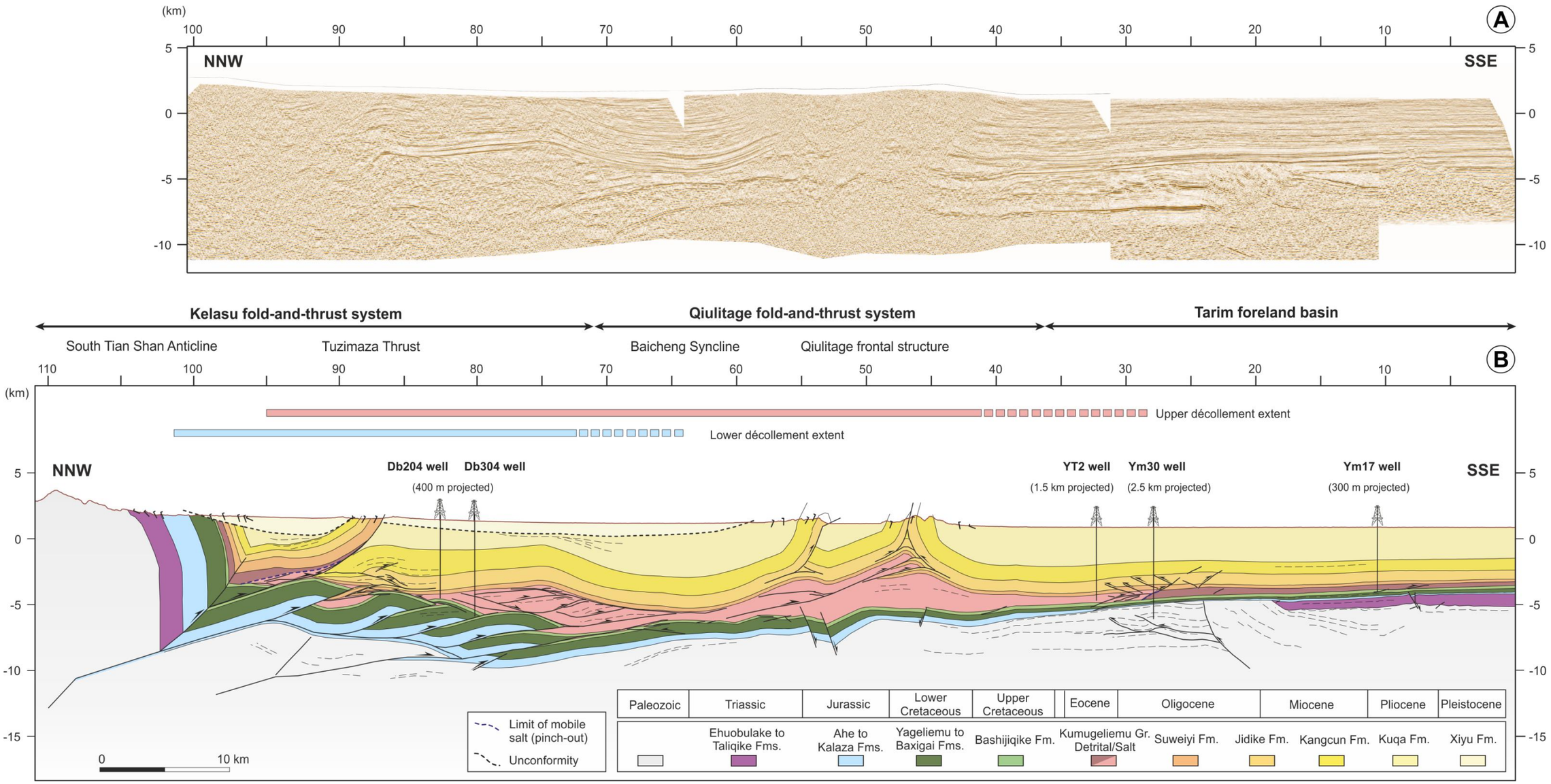

FIGURE 3.48. A: Depth-converted dapomian-9 seismic profile (see location in **Fig. 3.2**) across the central part of the Kuqa fold-and-thrust belt (no vertical exaggeration). **B:** Regional, seismic based cross section (see location in **Fig. 3.1**).

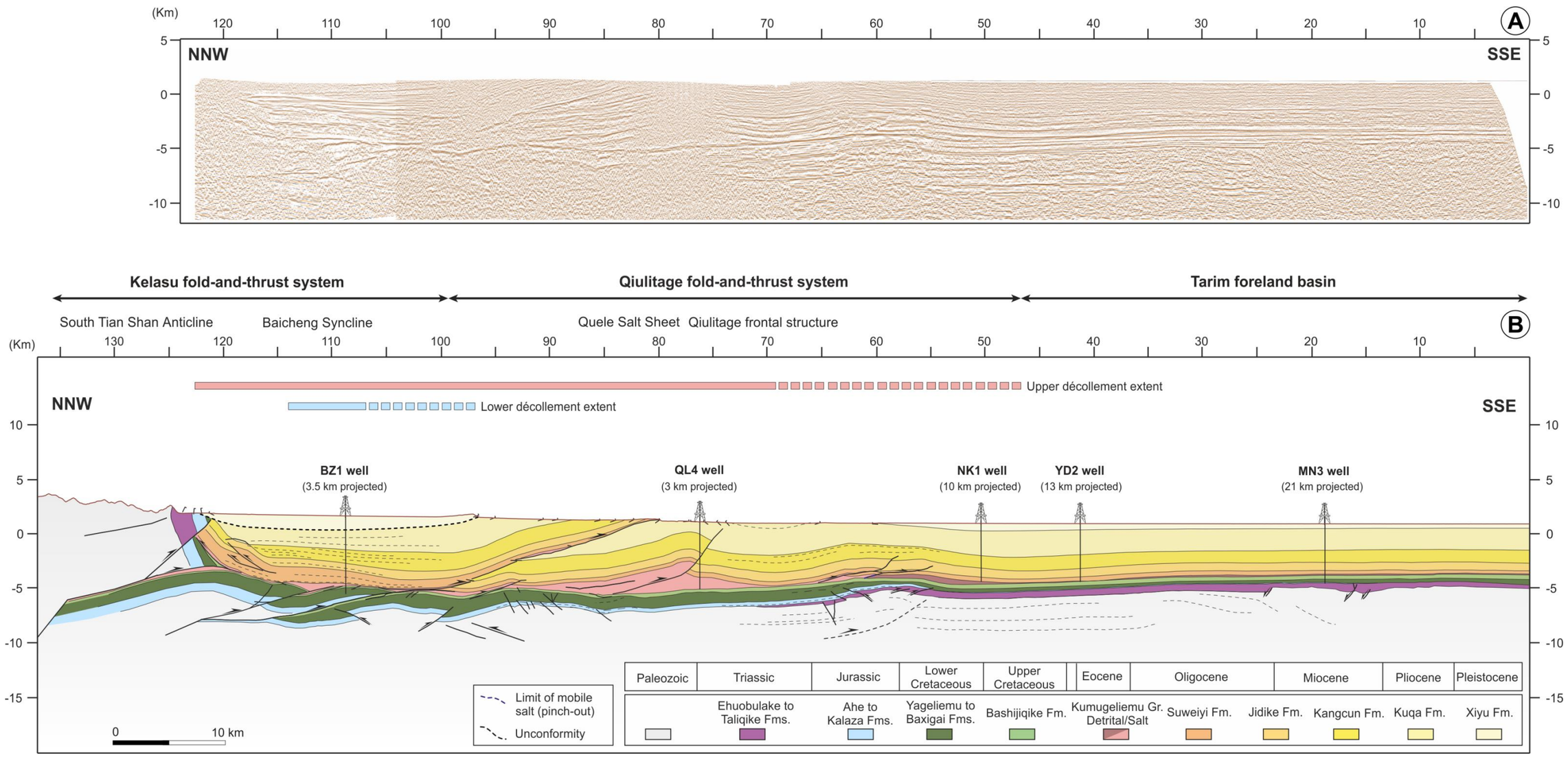

FIGURE 3.49. A: Depth-converted dapomian-5 seismic profile (see location in **Fig. 3.2**) across the western part of the Kuqa fold-and-thrust belt (no vertical exaggeration). **B:** Regional, seismic based cross section (see location in **Fig. 3.1**).

3.2.1. Central section dpm 11

For the central cross section (see location in **Fig. 3.1**), the first domain (Kelasu fold-and-thrust system) extends from the South Tian Shan Anticline to the hinge zone of the Baicheng Syncline whereas the second one encompasses the southern limb of the Baicheng Syncline and the Qiulitage frontal structure.

3.2.1.1. *The Kelasu fold-and-thrust system*

The northern domain is characterized by a major basement-involved fault (the South Tian Shan Fault) that connects southwards with a thrust system detached along a lower décollement in Mesozoic strata and an upper décollement at the Eocene-Oligocene evaporite level (**see Fig. 3.46**). The two décollements partly overlap, with the upper one shifted southwards with regard to the lower one (**Fig. 3.46**).

The South Tian Shan Anticline has a long wavelength and deforms the entire stratigraphic sequence from the Paleozoic basement to the youngest Cenozoic units. It is characterized by a subhorizontal to shallowly South-dipping northern limb and a moderately to steeply South-dipping southern limb (**Fig. 3.46** and see bedding data in **Fig. 3.10**). Mesozoic and Cenozoic units in the southern limb are conformable except for (i) a low-angle unconformity recognized at the base of the Kumugeliemu Group and (ii) an angular unconformity at the base of the Xiyu Fm (see **Fig. 3.10**). These geometries indicate moderate and progressive uplift of the South Tian Shan Anticline from Eocene to Pliocene times and more rapid uplift and forward tilt during the Pleistocene

The cross section runs parallel to the hinge of a NW-SE synform in map view that is probably related to a thrust reentrant at depth (**Fig. 3.10**). This reentrant is defined by the trend of Mesozoic units in the South Tian Shan Anticline (they change from E-W strikes eastward to NE-SW strikes westward; see **Fig. 3.10**) as well as by a series of oblique structures in the area mapped in **Fig. 3.10**. The Upper Paleozoic rocks and the lower part of the Mesozoic sequence in this area are folded by minor NW-SE trending folds which interfere with the South Tian Shan Anticline. As previously introduced, these folds die out southward in the footwall of North-directed back-thrusts that are detached along the Lower Jurassic coal units (**Fig. 3.10**). In addition, thrust flats along Triassic units have also been recognized (see **Fig. 3.10**). They are

deformed by basement-involved folds, suggesting thin-skinned thrusting partly predated basement deformation.

Along the central section, south of the South Tian Shan Anticline, the Kelasu fold and thrust system at surface is represented only by the Tuzimaza Thrust and a wide syncline in its hanging wall (**Figs. 3.38 and 3.46**). In map view, the thrust forms a 30 km-long apparent flat trending N65E along the Suweiyi Fm. (**Fig. 3.12**). To the East and West, truncated strata in the hanging wall indicate the presence of a minor anticline (**Fig. 3.12**).

Across the considered cross section, the Tuzimaza Thrust is represented by an E-W-striking thrust surface that cuts an ENE-WSW trending and South-verging anticline (**Fig. 3.12**). Bedding in the hangingwall is moderately North-dipping, sub-parallel to the thrust surface, whereas shallowly South-dipping bedding surfaces are recognized in the footwall. The subsurface geometry underneath the Tuzimaza Thrust and the syncline in its hanging wall has been nicely imaged by seismic data and constrained by existing exploratory wells (**Figs. 3.38 and 3.46**). A high reflectivity unit at the top of the Mesozoic sequence (the Bashijiqike Fm.) has been recognized and tracked in the seismic line and defines the main structural features (**Fig. 3.38**). This unit is folded by a series of South-verging anticlines that show wavelengths of a few kilometers and geometries (limb dips and flat-on-ramp and ramp-on-flat reflection patterns) that agree with fault-bend folds associated with south-directed thrusts (**Fig. 3.38**). In general, the structure defines a subsurface antiform decoupled from the surface deformation along the Kumugeliemu salt, as emphasized by the superimposed synclines and anticlines in the Tuzimaza Thrust (**Fig. 3.38**). The Mesozoic units form a duplex between this upper décollement and a lower décollement along Jurassic/Triassic coal units. This duplex comprises four main thrust sheets in the footwall of the South Tian Shan Fault, the northern one involving three closely-spaced thrusts (see numbering in **Fig. 3.38**). The spacing of these thrusts decreases toward the foreland as the thickness of the Mesozoic sequence also decreases, and they accommodate displacements that also diminish progressively towards the South. The floor thrust of the duplex branches off from the South Tian Shan Fault, whereas it is truncated and folded by two main basement–involved structures farther South (see roman numbering in **Fig. 3.38**). Basement folds display a wavelength of tens of kilometers and are related to North-dipping basement-involved faults. They accommodate displacements that diminish progressively to the South and cut a Triassic-Lower Cretaceous sequence that, along basement faults I and III, thins markedly in their footwalls. On the contrary, Upper Cretaceous layers (Bashijiqike Fm) are constant-thickness and locally overlie Lower Cretaceous rocks

unconformably. The basement anticline in the hangingwall of fault II displays a fault-bend geometry related to a thrust flat (and a potential décollement) at a depth of 4100 m from the top of the basement. Similar flat depths and hanging-wall geometries have been depicted for the basement stack (dashed line in **Fig. 3.46**) interpreted underneath the northern part of the cross section. These interpreted geometries agree with the late steepening and southwards tilt of the southern limb of the South Tian Shan Anticline, as registered by the angular unconformity mapped at the base of the Xiyu Fm (**Fig. 3.10**). To the east of the hinge area defining the thrust reentrant, the Tuzimaza Thrust is replaced by two structures: the Kumugeliemu Anticline to the north and the Suweiyi Anticline to the south (**Figs. 3.1 and 3.45**). The studied cross-section crosses the eastern end of the Tuzimaza Thrust but also intersects the western termination of the Kumugeliemu Anticline in its hanging wall. At the surface, the Kumugeliemu Anticline is an open fold deforming the Kuqa Fm, whose lower part shows a constant thickness but deeper strata (the Suweiyi, Jidike and Kangcun Fms.) display a growth geometry (**Fig. 3.38**).

Based on angular relationships among seismic reflectors (**Fig. 3.38**), this anticline has been interpreted to be related to two underlying minor backthrusts that accommodate a total displacement of about 1km. They are connected to the roof thrust of the duplex involving Mesozoic units suggesting that the hinterland pinch-out of the Eocene-Oligocene evaporites is located beneath the hinge or the backlimb of the Kumugeliemu Anticline (**Fig. 3.38**). Cenozoic units in the footwall of the Tuzimaza Thrust are also deformed by a North-verging anticline that is likely to be related to a main passive-roof backthrust along the Eocene-Oligocene salt. It is interpreted to be connected to a secondary backthrust at the base of the Jidike Fm. by a minor south-vergent duplex. This duplex can be recognized in the seismic line because of the presence of a reflective unit at the base of the Cenozoic sequence (Suweiyi Fm. according to **Fig. 3.35**) that slightly thickens in the footwall of the Tuzimaza Thrust. Seismic reflectors display angular relationships that prompt this thickening results from the stack of several, minor, south-directed thrusts (as shown in **Figs. 3.38 and 3.46**), although a thicker Suweiyi Fm has not been documented in well Ks502 (see location in **Fig. 3.12**). In this area, salt forms a small triangular body (**Fig. 3.38**) that was encountered by well Ks502, which cut 1065 m of halite and gypsum with interbedded mudstone layers.

3.2.1.2. *The Qiulitage fold-and-thrust system*

This domain is characterized by a sole thrust along the Eocene-Oligocene salt and includes both the southern limb of the Baicheng Syncline and the Qiulitage frontal structure (**Figs. 3.36 and 3.46**). The Baicheng Syncline is characterized by a shallow North-dipping southern limb (15 to 20º) and an 18 km-long, flat lying hinge zone (**Fig. 3.46**) that are underlain by 900-1200 m of salt. Beneath the salt, the Mesozoic sequence is mostly undeformed except for a 4º regional dip towards the North.

The Qiulitage frontal structure consists of two tight anticlines separated by a wider syncline with a 4 km-long, flat-lying hinge zone that is about 2 km above the regional elevation (**Fig. 3.36**).The southern Qiulitage anticline shows a moderately to steeply North-dipping northern limb (70-55ºN, Li et al*.,* 2012) and a steep to overturned southern limb, with dip values on both limbs (across the Kuqa Fm) progressively increasing towards the fold core and thus suggesting the anticline grew by limb rotation from Early Pliocene times. The anticline is cored by ~4 km of salt and its location is, at least in the central part of the Kuqa fold-and-thrust belt, intimately related to the position of the foreland pinch-out of the salt units in the Kumugeliemu Group. Three structures complicate the southern limb and hinge zone. First, an angular unconformity located in the lower part of the Kuqa Fm. separates a South-dipping stratigraphic panel with normal-polarity from a North-dipping overturned panel (**Fig. 3.27**). This unconformity is the key to understanding why the interpretation given in the present work for the southern Qiulitage anticline differs strongly from the one by Li et al*.* (2012). In the latter work, North-dipping beds in the southern limb of the southern Qiulitage anticline were considered as being right-side-up and consequently a tight, isoclinal fold deforming the Cenozoic suprasalt sequence was interpreted instead. Second, beds in the hinge zone are cut by a backthrust that shows a significant flat along the Jidike Fm. (**Figs. 3.24, 3.27, 3.36**). Third, the backthrust is folded and offset in the subsurface by a South-directed thrust detached in the Kumugeliemu salt unit (well Xq2 supports this interpretation, see location in **Fig. 3.46**).

The northern Qiulitage anticline is characterized by a subvertical to overturned southern limb (Li et al*.,* 2012) and a steeply to shallowly North-dipping northern limb. It is cored by ~3 km of salt and the forelimb is cut by a South-vergent thrust that is detached in the Jidike Fm and extends laterally for about 30 km (**Fig. 3.24**). Absence of preserved unconformities, thickness or clear dip variations in the lower part of the Kuqa Fm suggest the northern Qiulitage anticline initiated slightly latter than the southern one.

One of the key issues of the study area concerns the presalt geometry beneath the Qiulitage frontal structure and to what extent the geometry imaged in the seismic lines is real or apparent due to velocity artifacts resulting from the thickened salt body. Nonetheless, apparent thickness changes in the Mesozoic units underlying the Qiulitage frontal structure are interpreted to be real and suggest the existence of extensional faults with displacements of hundreds of meters. Along the studied transect, these high-angle normal faults bound a small graben centered beneath the Qiulitage fold-and-thrust system, with one of the faults having been inverted slightly (**Figs. 3.36 and 3.46**).

3.2.1.3. *Northern Tarim Basin*

To the South of the Qiulitage frontal structure, Mesozoic and Cenozoic units are almost undeformed except for a regional northwards tilt and two subtle anticlines in the Cenozoic (**Fig. 3.42**). The regional tilt varies between an average of 2.5º at the base of the Mesozoic and 0.5º at the base of the youngest Cenozoic unit (Xiyu Fm). The anticlines have a wavelength of close to 10 km and limb dips lower than 5º. They overlie basement anticlines that are cut by subvertical to high-angle normal faults that also affect the Mesozoic strata. The recognition of these basement faults underlying Cenozoic anticlines in the Tarim foreland basin (where bed dips are very shallow and seismic data are of good quality) supports our interpretation of the presalt geometry beneath the Qiulitage frontal structure.

3.2.2. Eastern section dpm 16

The Kuqa fold-and-thrust belt narrows progressively to the East reaching a minimum width of 60 km across the eastern section (see **Fig. 3.44**). In this domain, the Kelasu fold-and-thrust system (previously defined as the northern domain where the whole stratigraphic sequence, from the Paleozoic to the Cenozoic, is deformed by contractional structures) keeps the same width as in the central profile (about 50 km). The Eocene-Oligocene evaporites are limited to the southern part of the basin (beneath the Qiulitage frontal structure) and display a horizontal extent of less than 20 km. The southernmost basement thrust is located underneath the foreland salt pinch-out and climbs into the Jidike Fm. In general terms, the degree of decoupling between the Paleozoic-Mesozoic units and the Cenozoic sequence is significantly lower in this area than in the central sections, where the Eocene-Oligocene salt is wider and thicker.

3.2.2.1. *The Kelasu fold-and-thrust system*

At surface, the northern part of the Kelasu fold-and-thrust system is formed by a basement-involved structure (the South Tian Shan Anticline) to the North and the lateral continuation of the Kumugelimu and Tuzimaza-Suweiyi structure (Bashijiqike and Jidike anticlines respectively, see location in **Fig. 3.1**) to the South (see **Figs. 3.44, 3.45 and 3.46**).

The South Tian Shan Anticline is almost completely covered by Holocene units across the selected profile (dapomian-16, see location in **Fig. 3.2**), although it crops out few kilometers to the East. This anticline is characterized by a subhorizontal to shallowly South-dipping backlimb and a subvertical to overturned forelimb (**Fig. 3.44**). It has been interpreted to develop in the hangingwall of an underlying basement thrust with a long flat along Triassic units. As in the central cross section, this northern basement thrust connects southwards to a thin-skinned thrust system whose sole thrust is represented by Triassic-Jurassic coal layers. Nevertheless, it shows an overall geometry that significantly differs from that interpreted across the central Kuqa fold-and-thrust belt. Geometrical differences derive from lateral variations in the stratigraphic sequence being deformed: in the eastern section, (1) the northern boundary of the upper, Eocene-Oligocene décollement is about 25 km to the South of the northermost Mesozoic-detached structure (conversely to the central section, where they are overlapped; compare **Figs. 3.44 and 3.46**) and (2) intermediate décollements within Jurassic-Cretaceous units, probably represented by mudstone layers, are present in the northern part of the Kelasu fold-and-thrust system. The stratigraphic position of the décollements has been interpreted from both the correlation of stratigraphic horizons at surface and from well data. This interpretation is consistent with outcrop data since long thrust flats along Triassic, Jurassic and Cretaceous units are recognized along the structures immediately to the East of the studied profile (see **Fig. 3.3**). The thickness of the Mesozoic-detached thrust sheets is controlled by the vertical distance and horizontal offset between décollements and it varies across-strike: thrust sheet is thinner to the North (underneath the Bashijiqike Anticline), where Triassic, Jurassic and Cretaceous décollements are overlapped, but they thicken to the South (underneath Jidike Anticline) where the only décollement are the Triassic coals (see **Fig. 3.44**). The vergence of the thin-skinned thrust system also changes from North to South: doubly vergence thrusts to the North and forward directed thrusts to the South. The floor thrust of the thin-skinned thrust system is truncated and folded by a south-directed basement thrust (labelled as II in **Fig. 3.44**) whereas the whole system is transported

in the hangingwall of a south-directed basement thrust underneath the Qiulitage frontal structure (labelled as III in **Fig. 3.44**).

The Bashijiqike and Jidike anticlines are the surface expression of the Mesozoic-detached and basement-involved fold-and-thrust system in the northern Kelasu fold-and-thrust system. The Bashijiqike Anticline has been interpreted as a fault bend fold in the hangingwall of a Mesozoic-detached, North-directed back-thrust (**Figs. 3.3 and 3.44**). The Mesozoic and Cenozoic units coring this structure are affected by a fish-tail type structure consisting on a floor back-thrust with a ramp cutting Jurassic and Cretaceous units and a roof thrust that displays a long thrust flat along Cretaceous layers that traverses the hinge zone of the anticline (**Fig. 3.44**). At surface, bedding in the backlimb is steeply to intermediately North-dipping whereas in the forelimb, it is subvertical (**Fig. 3.6A**). At depth, Cenozoic units (from Suweiyi to Kangcun Fms.) in the backlimb are thickened with respect to the forelimb. Between the South Tian Shan anticline and the Bashijiqike Anticline a narrow syncline was developed. Mesozoic and Cenozoic units in the northern limb of this syncline are steeply south-dipping and conformable except for an angular unconformity at the base of the Xiyu Fm (see **Fig. 3.44**) whereas these units are intermediately North-dipping in the southern limb of the fold (see **Fig. 3.3**). To the south of the Bashijiqike Anticline, the Kelasu fold-and-thrust system is represented by the Jidike Anticline. Seismic data point out that this anticline is a fault bend fold in the hangingwall of a Mesozoic-detached South-directed thrust with a long ramp cutting Cenozoic materials up to Kangcun Fm. (see **Fig. 3.44**). The thickening of this unit in the backlimb with respect to the forelimb allows us to determine the kinematic evolution of the Jidike Anticline. At surface, the Jidike Anticline is an open up-right fold with both the backlimb and the forelimb dipping shallowly towards the North and South respectively (10-20º in **Fig. 3.3**) that evolves towards the east to a close anticline with steeper limbs (30-40º in **Figs. 3.3 and 3.7**).

The Mesozoic thicknesses interpretation (constrained by well data) reveal a thickening of the Cretaceous sequence in the hangingwall of the thrust underlying the Jidike Anticline. This thickening suggests that this thrust is an inherited, North-dipping, Cretaceous extensional fault that was later reactivated during the Cenozoic contraction.

3.2.2.2. *The Qiulitage fold-and-thrust system*

The Qiulitage fold-and-thrust system in the eastern cross-section consists of a narrow anticline. The main difference between the eastern and the central section is that the Mesozoic units underlying the salt are involved in the Qiulitage frontal structure (compare **Figs. 3.44 and 3.46**).

The Qiulitage frontal structre is cored at surface by Cenozoic units and its interpretation at depth indicates that there is a small decoupling between the structures deforming the underlying Mesozoic and the outcropping Cenozoic sequences. This decoupling is due to the presence of evaporites in the Kumugeliemu Group that grade into detrital units (hinterland salt pinch-out) immediately to the North of the anticline. Nevertheless, the degree of decoupling between the Mesozoic and the Cenozoic is lower than in the central section where the thickness and extent of the evaporites is higher (compare **Figs. 3.44 and 3.46**).

Cenozoic units are affected by a fish-tail structure consisting on a floor back-thrust (we will refer to this structure as back-thrust 1, labelled as 1 in **Fig. 3.44**) with a long flat in the Kumugeliemu evaporites and a roof thrust along the Jidike Fm. that branches into a triangle zone (**Fig. 3.44**). A later back-thrust (back-thrust 2, labelled as 2 in in **Fig. 3.44**) developed in this area, traversing and offsetting the complex previous structure.

Mesozoic units beneath the Qiulitage frontal structure are deformed by a basement thrust (labelled as III in **Fig. 3.44**) and by a South-directed thrust detached on Triassic coals (labelled as 3 in **Fig. 3.44**) that branches into the back-thrust 1 in the Cenozoic. The thickness variations in the Mesozoic between the hangingwall and the footwall of the basement thrust III point out that it is an inherited Permian-Triassic and/or Jurassic normal fault that was inverted and southwards transported during the Cenozoic compression. Shortening in the basement and in the Mesozoic was transferred to the Cenozoic cover units through the passive back-thrust 2 located in the hangingwall of the inverted basement thrust III.

3.2.2.3. *Northern Tarim Basin*

To the South of the Qiulitage frontal structure, the striking difference between the eastern and the central cross-sections is the presence of a basement uplift (compare **Figs. 3.42** and **4.44**). Intra-Paleozoic strata show a South-verging anticline that has a wavelength of close

to 70 km (**Fig. 3.44**). This anticline is overprinted by subvertical to high-angle normal faults affecting both the Paleozoic and the Mesozoic strata. These faults and are mostly localized along the hinge zone and the back-limb of the basement anticline. Mesozoic units unconformable overlay the Paleozoic anticline indicating that this basement structure was essentially active during Paleozoic times, but internal unconformities in the Mesozoic units suggest that there was a later, minor reactivation that took place during Mesozoic times. Slight folding in the lower part of the Cenozoic would agree with a second, contractional reactivation of this structure during Eocene-Miocene.

3.2.3. Western section dpm 5

The Kuqa fold-and-thrust belt also narrows to the West with respect to the central section with an extent of about 65 km across the western section (**Fig. 3.49**). However, there is a basement anticline located about 20 km to the South of the Qiulitage frontal structure deforming the whole stratigraphic sequence. In map view, this structure correlates with three doubly-plunging anticlines that laterally relay and disappear to the East (**Fig. 3.1**). In this section, Eocene-Oligocene evaporites display their maximum horizontal extent in the Kuqa fold-and-thrust belt (around 60 km). For this reason, the decoupling between the Paleozoic-Mesozoic units and the Cenozoic sequence is significantly higher in this area than in the eastern section (compare **Figs. 3.49** and **3.44**).

3.2.3.1. *The Kelasu fold-and-thrust system*

The Kelasu fold-and-thrust system is narrower in the western section (~35 km) than across the central and eastern sections. It consists of basement-involved structures decoupled from the overlying Cenozoic units located in the northern limb of the Baicheng Syncline (**Fig. 3.49**). Conversely to the central and eastern cross sections, the contribution of Mesozoic-detached thrusts in the structure of the Kelasu fold-and-thrust system is negligible and limited to the presence of local thrust flats along Triassic-Jurassic coal layers.

The northernmost structure is a fault-related basement-involved anticline (South Tian Shan anticline) whose forelimb is steeply South-dipping to overturned (**Fig. 3.49**). Few kilometers to the West of the presented profile, Jurassic units are covered by an incomplete Cretaceous sequence that is unconformably overlain by a lower, thin detrital unit (Eocene in age) and a thick, upper evaporitic unit (they both are coeval to the Kumugeliemu Group in the

central Kuqa fold-and-thrust belt). This unconformity is analogous to the low angle unconformity recognized at the base of the Kumugeliemu Group along the southern limb of the South Tian Shan anticline in the central cross section (**Figs. 3.10 and 3.46**). The South Tian Shan anticline grew during the Cenozoic as indicated by the presence of unconformities at the base of the Kumugeliemu Group and in the base of Xiyu Fm. (**Fig. 3.49**).

The southern limb of the South Tian Shan Anticline is traversed at depth by a basement thrust (resulting from the inversion of a Mesozoic normal fault) that branches southwards with a short-cut structurally analogous to the Tuzimaza Thrust (see **Figs. 3.47, 3.48 and 3.49**). Conversely to the central section, this structure is characterized by: (i) a thrust ramp in the Mesozoic sequence (no thrust flat was developed in the Cretaceous, as observed in the central section **Fig. 3.46**) and (ii) a north-directed passive back-thrust in the Eocene-Oligocene evaporites (instead of the south-directed thrust recognized in the central section **Fig. 3.46**). Considering the geometry of this structure in both the central and the western sections, the Tuzimaza Thrust would laterally change from a south-verging thrust to a north-directed back-thrust, probably due to the lateral variation in the presalt structure that conditioned the distribution and thickness of syntectonic units.

The overlying layers are affected by an open syncline (the Baicheng Syncline) that is 40 km wide and hosts about 8 km of Cenozoic sedimentary units in its hinge zone (similarly to the central cross section). The northern limb of the syncline was probably, passively thrusted onto the frontal limb of the underlying thrust stack (**Fig. 3.49**). Salt in the frontal limb of the basement stack was likely to migrate both laterally and southwards (several diapirs are recognized to the East, West and South and up to 1000 m of salt are still preserved in the hinge zone of the Baicheng Syncline in the central cross section, **Fig. 3.46**) since it is almost absent at present.

3.2.3.2. *The Qiulitage fold-and-thrust system*

To the South of the Kelasu fold-and-thrust system, two main salt-detached structures crop out. The northern one (the Quele Salt Sheet, **Figs. 3.32 and 3.49**) overlies basement faults cutting Jurassic and Cretaceous units, whereas the southern one (the Qiulitage frontal structure, **Fig. 3.49**) overlies flat-lying Mesozoic units displaying a regional tilt of 2º towards the North.

The Quele Salt Sheet is a South-directed thrust featuring important salt extrusions along its hangingwall (**Fig. 3.32**). It accommodates a total, minimum displacement of about 18 km and is detached along the Kumugeliemu salt although it probably involves evaporites from the overlying unit (the Suweiyi Fm). Bedding in the hangingwall of the thrust dips intermediately to the North. A south-verging fault-bend anticline was formed in the footwall of the Quele thrust, slightly deforming beds in the hangingwall (**Fig. 3.49**). It is related to a south-directed thrust characterized by a low angle ramp in the upper part of the Mesozoic sequence and the lower part of the Cenozoic.

The Qiulitage frontal structure is an E-W-striking and South-verging detachment anticline (that laterally branches to the southern Qiulitage anticline described in the central section **Figs. 3.46**) cored by about 2 km of the Kumugeliemu salt units. It is a gentle anticline characterized by a northern limb dipping 20 to 05º N and by a southern limb dipping 30 to 10º S (**Fig. 3.49**). This anticline is cut by a South-directed thrust showing a displacement of about 1000 m.

The kinematic evolution of salt-detached structures in both the western and the central section is quite similar. In the western section, bedding in the backlimb of the Qiulitage frontal structure is cut by the Quele thrust suggesting that the southern structure began to grow before than the northern one (**Fig. 3.49**). In the same way, in the central section, the southern Qiulitage anticline was developed earlier than the northern one (**Fig. 3.46**).

Mezozoic units underlying the Qiulitage have been interpreted based on: (i) the E-W seismic line dapomian-23 and (ii) the Nw1 well located about 20 km to the West of line dapomian-5 (**Fig. 3.50**). The Nw1 well found the Kumugeliemu unit directly overlying Permian units, with the top of the Permian at 4549 m. in depth. This well has been projected to seismic line dapomian-23 (**Fig. 3.50**) that images a progressively deepening of the top of the Paleozoic to the east: in the western part of the line, the Cenozoic unconformably overlies the Paleozoic units whereas to the east, the sequence between the base of the salt and the top of the basement thickens, likely related to the presence of Permian and Mesozoic units. These Mesozoic units are cut by wells along dapomian-5 (see wells Ql4 and Bz1 in **Fig. 3.49** that found Cretaceous units beneath the Kumugeliemu salt). Furthermore, dapomian-23 also images the location of the salt pinch-out in the western margin of the Kuqa fold-and-thrust belt: salt is absent to the West although it thickens progressively to the East reaching about 2000 m of vertical thickness at the intersection with seismic line dapomian-05 (**Fig. 3.50**).

Based on these observations, we have interpreted a Mesozoic sequence with maximum thickness of 1700 m beneath the salt-detached structures (**Fig. 3.49**). Mesozoic units are almost undeformed beneath the Qiulitage frontal structure although they are folded and faulted beneath the Quele Salt Sheet. On the one hand, a north-verging fault-bend anticline is deforming the Mesozoic beneath the footwall of the Quele thrust, probably related to a North-directed basement back-thrust (**Fig. 3.49**). On the other hand, a wide, symmetric, basement anticline is recognized beneath the hangingwall, the hinge of the anticline beneath the hinge of the Baicheng Syncline (**Fig. 3.49**). In this structure, the Bashijiqike Fm. unconformably overlies older Cretaceous units indicating there was a pre-Bashijiqike basement uplift that (i) would laterally connect to the one cut by the Nw1 well to the West and (ii) might be reinterpreted as with a slightly thinner although still present Mesozoic sequence.

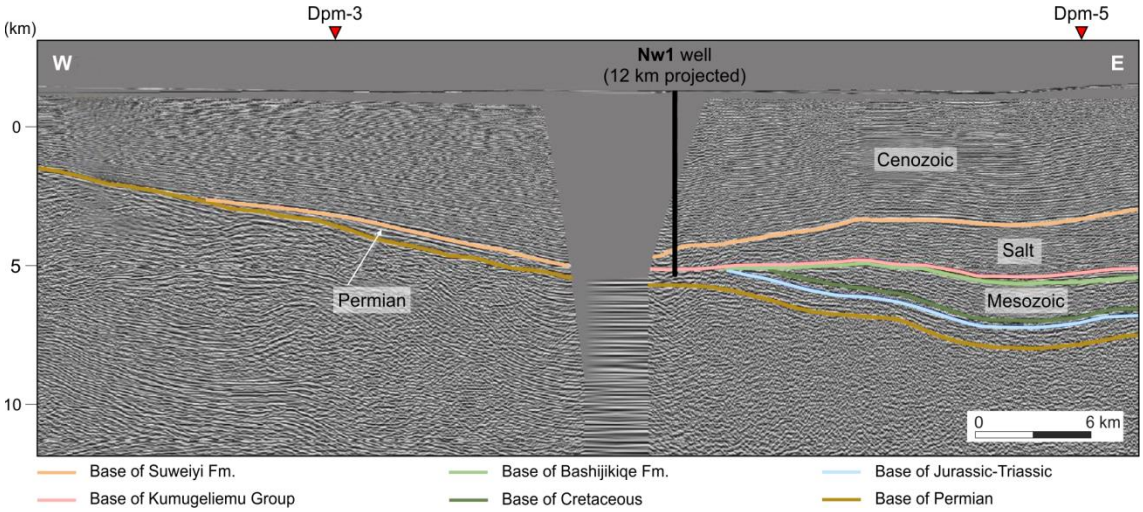

FIGURE 3.50. Seismic line dapomian-23 (see location in **Fig. 3.2**). To the West (dapomian-3; see location in **Fig. 3.2**), Cenozoic units overlie the Paleozoic basement, to the East (dapomian-5; see location in **Fig. 3.2**), two tapered units between the top of the basement and the base of the detrital Cenozoic are imaged: an upper one, coinciding with the Eocene-Oligocene salt, and a lower one, probably corresponding to the Mesozoic (we depicted the base of Jurassic, base of Cretaceous and base of Bashijikiqe horizons on their position at the intersection between dapomian-23 and dapomian-5). Cretaceous and Triassic units have been cut by wells to the South of dapomian-3 (well Sl2; see location in **Fig. 3.2**).

3.2.3.3. *Northern Tarim Basin*

To the South of the Qiulitage frontal structure, Mesozoic and Cenozoic units are almost undeformed except for a subtle North-verging Paleozoic anticline probably developed in the hangingwall of a basement thrust (**Fig. 3.49**). This thrust was active during Late Mesozoic: the Bashijiqike Fm. unconformably overlies older Mesozoic units in the hinge zone and in the northern limb of the basement anticline. Deformation in the Cenozoic sequences is decoupled

due to the presence of a thin, interbedded evaporitic unit (Kumugeliemu Group). Shortening was transferred to the Cenozoic through a series of South-directed thrusts that cut Suweiyi, Jidike and the lower part of the Kangcun Fm. The overlain units are constant-thickness except for the Kuqa Fm. that thins towards the hinge of the basement anticline indicating a second and late thrusting event that could laterally correlate to the slightly inverted faults found beneath the Qiulitage frontal structure across the central cross section (**Fig. 3.46**). Fault inversion during the Cenozoic is higher and probably earlier across the western profile and minor and later across the central one.

3.3. RESTORATIONS

We have carried out a sequential, palinspastic restoration of the eastern, central and western sections (**Figs. 3.51, 3.52 and 3.53** respectively) using a pin line to the South of the Qiulitage frontal structure, as deformation southwards of this line can be considered negligible. For each depicted time, the restoration was done in two steps: (1) unfaulting and unfolding of the selected horizon to the regional stratigraphic level (marked by the shallow northwards dipping horizons in the Tarim foreland basin) and (2) back-tilting of this regional level to the horizontal assuming a rotation axis at the southern edge of our cross sections. Most of the regional northwards tilt in the Cenozoic units of the Tarim basin probably results from the flexure produced by tectonic loading in the axial zone of the Tian Shan orogen.

Stepwise restorations of the sections indicate a total shortening ranging from 24 km to the East to 30.5 km to the West (29 km in the central part) that was mostly accommodated from Late Cretaceous to Pleistocene times. These values are higher than previously published values for the Kuqa fold-and-thrust belt (22-23 km of total shortening from the early Miocene to the present-day in both the central and western parts, Li et al*.,* 2012; 12 km of total shortening from late Oligocene to present-day in the eastern part, 16 km to 19 km in the central part, and 26 km in the western part, Wang et al., 2011) in part because they take into account a wider time span. Sequential restorations (**Figs. 3.51, 3.52 and 3.53**) present a complete picture of the evolving geometry of supra- and presalt units and their interplay through time. From them, two main stages can be differentiated in the kinematic development of the Kuqa fold-and-thrust belt: a first stage accommodating earlier (Late Cretaceous–early Miocene), relatively minor shortening and a later stage (late Miocene to Present) that was characterized by higher shortening rates (more than 80% of the total shortening occurred during this second stage).

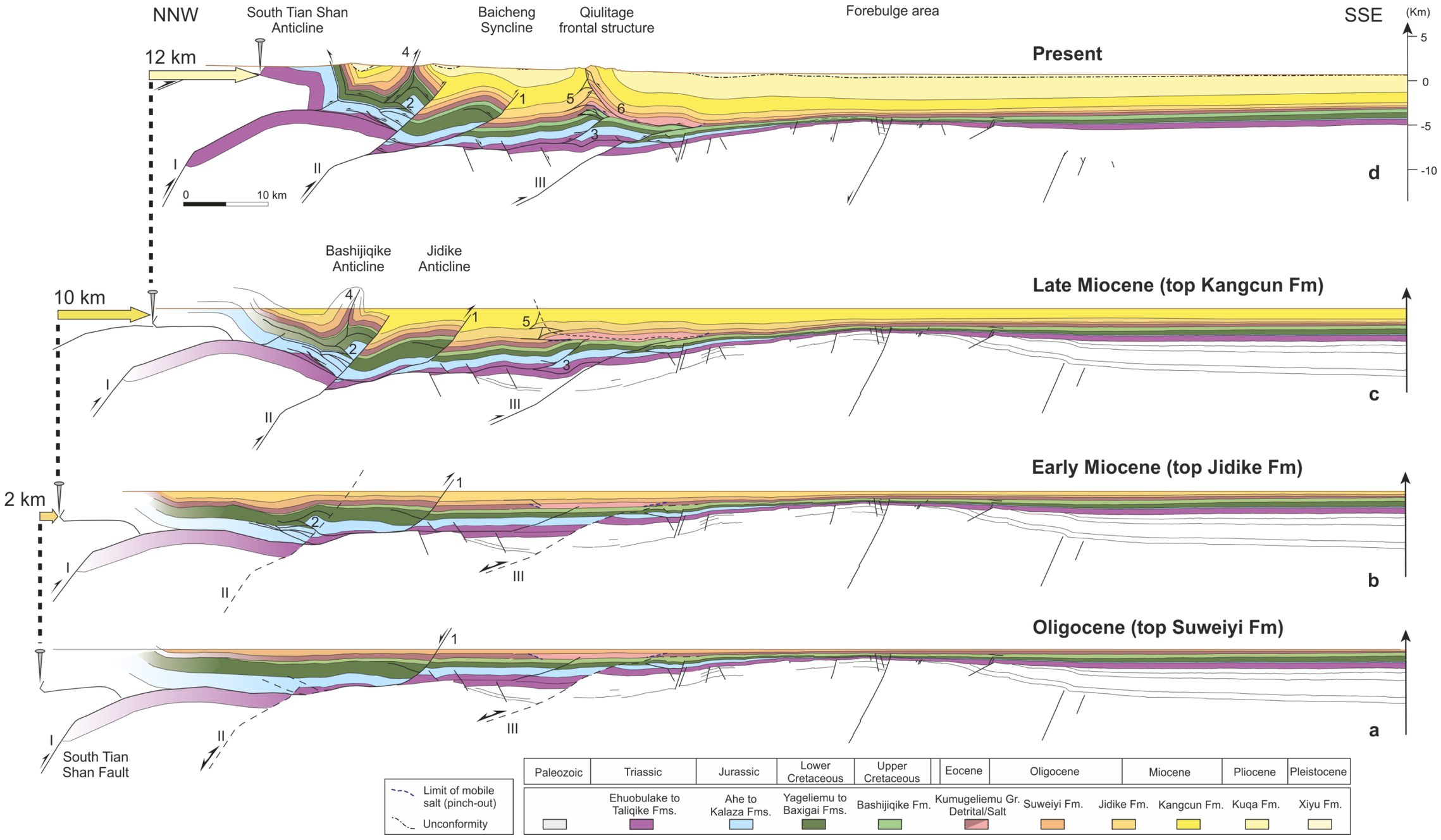

FIGURE 3.51. Sequential restoration of the regional cross section (based on seismic profile dapomian-16) across the eastern Kuqa fold-and-thrust belt.

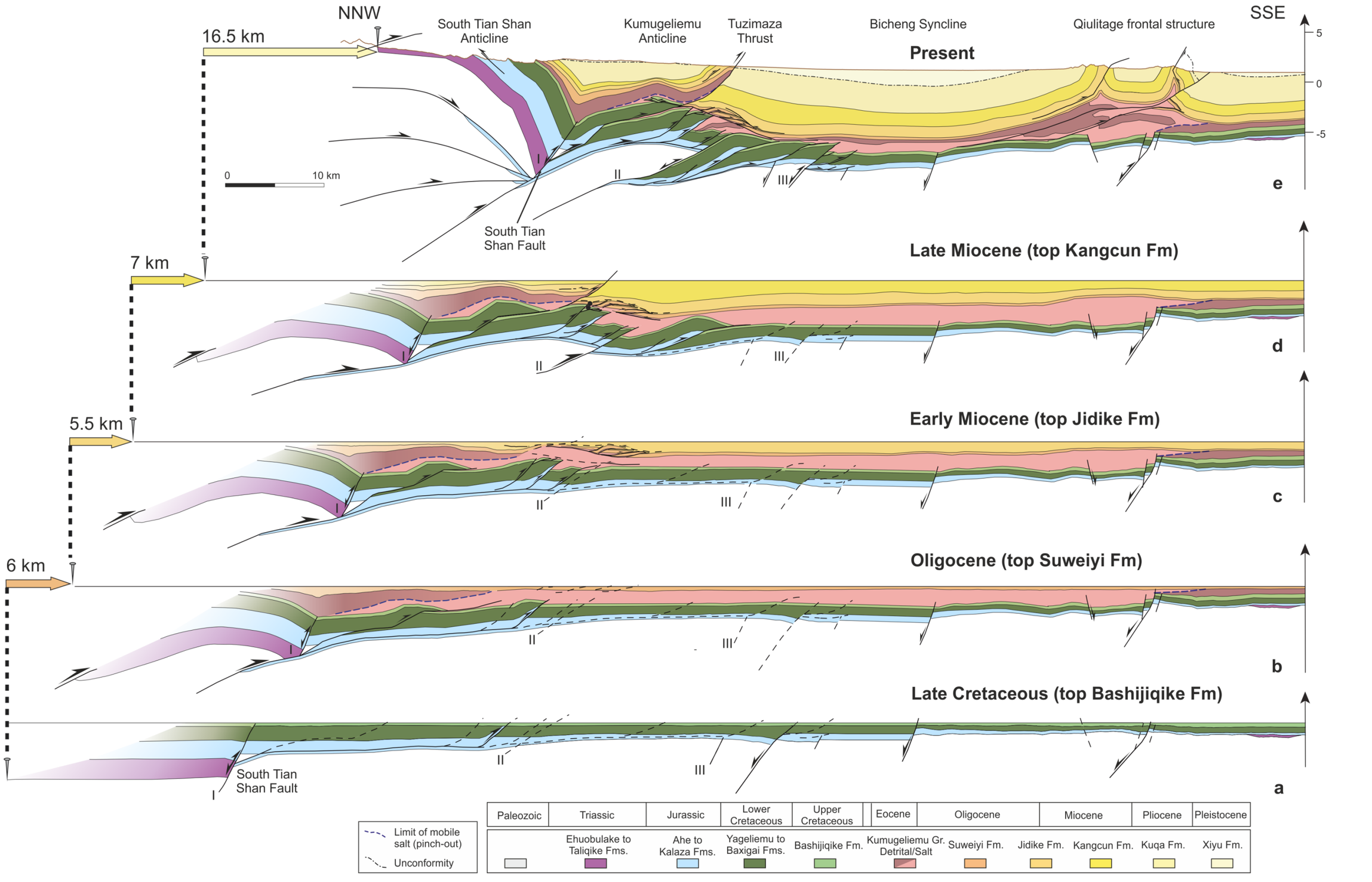

FIGURE 3.52. Sequential restoration of the regional cross section (based on seismic profile dapomian-11) across the central Kuqa fold-and-thrust belt.

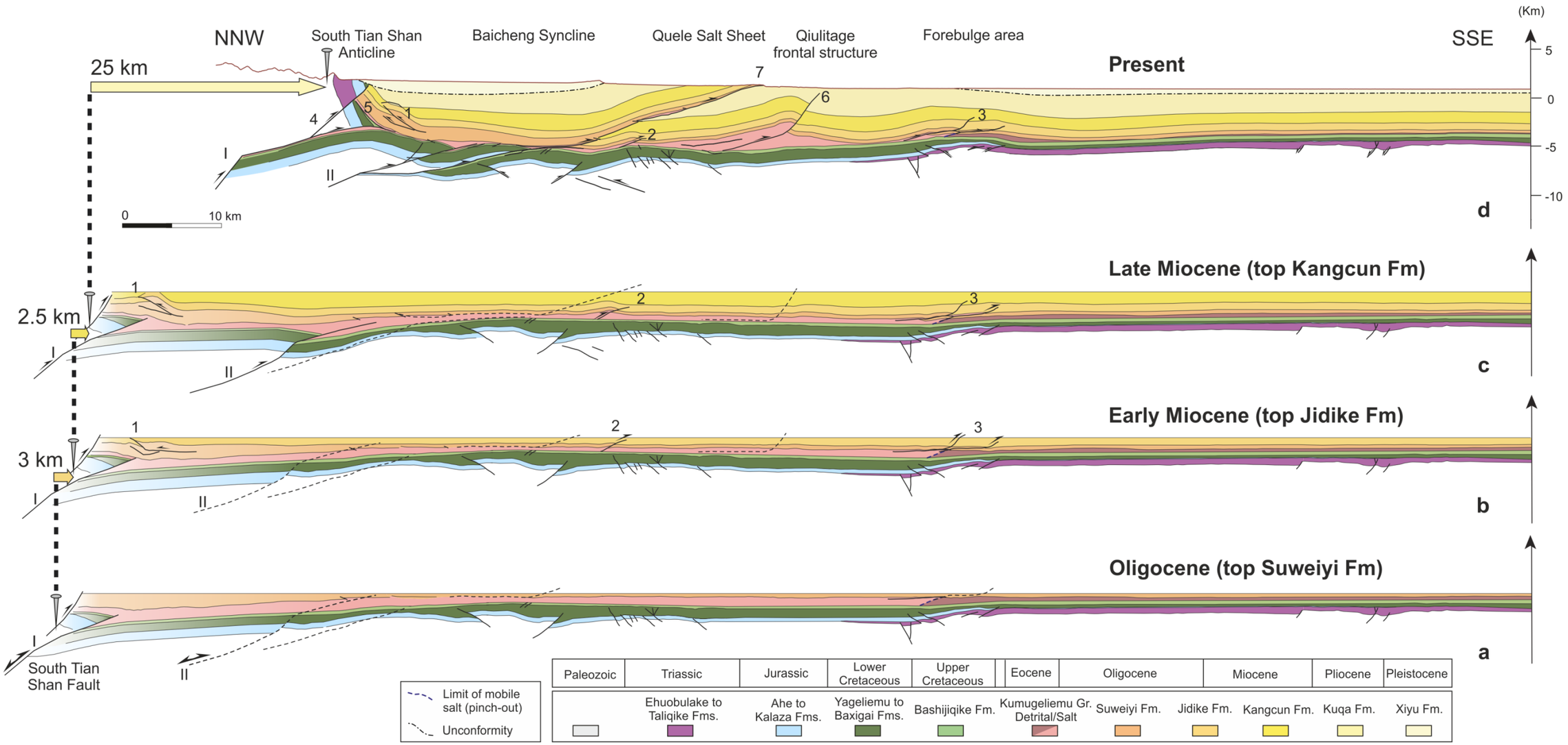

FIGURE 3.53. Sequential restoration of the regional cross section (based on seismic profile dapomian-5) across the western Kuqa fold-and-thrust belt.

3.3.1. Central section restoration

During the first stage (coeval to the sedimentation of the Kumugeliemu Group and the Suweiyi and Jidike Fms.; **Fig. 3.52a-c**), deformation was mainly localized in the northern part of the cross section: the South Tian Shan Fault was reactivated as a basement-involved reverse fault that transitioned to thin-skinned, Mesozoic-detached thrusting. The geometry of Eocene-Miocene units in the southern limb of the South Tian Shan Anticline (i.e., gradual northwards thinning without significant angular unconformities; **Fig. 3.10**) suggests low vertical-uplift rates for this structure during this stage, accordingly to the low angle thrust ramp and the shallow thrust flat we interpreted. Thin-skinned thrusts likely developed in a piggy-back sequence in the Kelasu fold and thrust system while coeval extensional faulting took place in the foreland located beneath the Qiulitage frontal structure. The coexistence of extensional southern structures and contractional northern ones is interpreted to represent local extension in the Eocene-Oligocene foreland-basin forebulge, as observed in many foreland basins elsewhere (see Tavani et al*.,* 2015 for a compilation). The assembly of structures that were active during the Eocene to early Oligocene produced an early basin topography that strongly influenced the spatial and thickness distribution of the syn-orogenic salt units of the Kumugeliemu Group (**Fig. 3.52b**): to the north, the hinterland salt pinch-out was located slightly southwards of the South Tian Shan anticline and it was deformed early by subsalt thrusting; to the south, the location of the foreland salt pinch-out was controlled by the position of the forebulge. Extensional faulting in the latter domain created a locally higher accommodation space that favored the sedimentation of thicker evaporitic sequences in the area presently located beneath the Qiulitage frontal structure.

Incipient postsalt deformation commenced during early Miocene times (**Fig. 3.52c**). This was localized close to the hinterland salt pinch-out and consisted of two open salt-cored anticlines (the Kumugeliemu Anticline and the Tuzimaza Thrust to the north and south, respectively) underlain by Mesozoic-detached thrusts. The presence of mobile evaporites resulted in decoupling between folds in pre- and suprasalt units, with the hinges of salt-cored folds located slightly to the south of those of presalt folds. In the southern (Tuzimaza Thrust) anticline, subsalt shortening was partly transferred to suprasalt units through the development of a backthrust along the Kumugeliemu Group and a duplex system deforming the overlying Suweiyi and Jidike Fms.

The second contractional stage (late Miocene to present; **Fig. 3.52d-e**) was coeval with sedimentation of the Kangcun, Kuqa and Xiyu Fms. During this stage, Mesozoic-detached thrusts propagated southwards and were subsequently cut by basement-involved faults II and III (see numbering in **Fig. 3.38**). In addition, basement underthrusting took place in the northern part of the Kelasu fold-and-thrust system, producing a pronounced forward rotation of the southern limb of the South Tian Shan anticline that was recorded by angular unconformities in the upper Pliocene-Pleistocene units. Presalt deformation in the Kelasu fold-and-thrust system (thrusting into the salt from below) promoted salt evacuation and local welding. In turn, welding (i) favored more coupled deformation and (ii) hindered the southwards transfer of presalt shortening, activating out-of-sequence suprasalt thrusting farther hinterland. Consequently, the Tuzimaza Thrust formed, cutting the previously developed anticline and likely reactivating the hinterland detrital/salt facies transition in the Kumugeliemu Group.

Late thrusting in the northern Kelasu fold-and-thrust system was coeval with the development of the Qiulitage frontal structure (**Fig. 3.52**). The southern Qiulitage anticline, located over the foreland pinch-out of the salt, initiated during late Miocene - early Pliocene times. We suggest it initially formed an open detachment fold (**Fig. 3.52d**) whose limbs progressively steepened during increasing shortening and syntectonic sedimentation (**Figs. 3.52d, 3.52e**). **Fig. 3.52e** also shows the incipient development of a fore- and backthrust pair (fishtail thrust) detached in the Kumugeliemu salt and the gypsum and shales of the Jidike Fm (**Fig. 3.36**). The backthrust was then offset by a larger forethrust and rotated to near-vertical to overturned (**Fig. 3.27A**) during fold tightening. The timing of backthrusting was probably registered by the angular unconformity on the southern limb of the south Qiulitage anticline, in the lower part of the Kuqa Fm (**Fig. 3.27B**). The northern Qiulitage anticline began to develop later but shares a common kinematic evolution, with early detachment folding and subsequent thrusting along the Jidike Fm. In late deformation stages, the whole Qiulitage fold-and-thrust system (i.e., the earlier southern anticline, the later northern anticline and the intervening syncline) was uplifted above the regional stratigraphic level. This late folding was probably due to a combination of two processes: (i) late inversion of the main basement normal faults that underlie the Qiulitage frontal structure and (ii) salt inflation generated by salt flow from beneath the Baicheng Syncline.

The distribution and thickness of syntectonic strata in the Baicheng Syncline was influenced by salt evacuation in addition to orogenic shortening. Basement-involved thrusting

gave rise to a progressive southward migration of depocenters through time (**Fig. 3.46**). Tectonic loading in the footwall of basement fault II generated an upper Miocene-Pliocene depocenter 5 km to the South of the Tuzimaza Thrust (**Fig. 3.52**). The accumulation of a thicker Cenozoic sequence at this part of the cross section was possibly accommodated in part by salt withdrawal from the basin axis towards peripheral areas, leading to the thick salt accumulations recognized by Li et al. (2012) in the footwall of the Tuzimaza Thrust, few kilometers to the East of the studied section. Whether any salt moved from the area of the cross section into the growing diapir located 10 km to the West is unknown.

The main depocenter shifted about 15 km to the south during late Pliocene times due to late reactivation along basement fault II (see **Fig. 3.52**) and subsequent thrusting along basement fault III (see **Figs. 3.38 and 3.52**), beneath the northern limb of the Baicheng Syncline.

3.3.2. Eastern section restoration

During the early contractional stage (coeval to the sedimentation of the Suweiyi and Jidike Fms.; **Fig. 3.51a-b**), deformation was mainly localized in the northern part of the cross section. The South Tian Shan Fault (basement thrust I, see numbering in **Fig. 3.51**) reactivated as a basement thrust that transferred shortening forwards to a thin-skinned, Mesozoic-detached thrust system. This thin-skinned thrust system detached along Triassic and Jurassic weak units that, as suggested in **Fig. 3.51**, were disrupted by previous extensional faults. Their lateral termination promoted the development of complex geometries consisting on abundant back-thrusts, reactivated normal faults (thrust 1 in **Fig. 3.51b**) and fish-tail structures that connected Triassic, Jurassic and Cretaceous decollements (**Fig. 3.51b**)

Contractional deformation in the northern part of the Tarim Basin and the axial zone of the Tian Shan produced a foreland flexure and the development of a prominent forebulge area (**Fig. 3.51**) in the central part of the eastern section that probably controlled the locus of the foreland salt pinch-out in the Kumugeliemu Group (**Fig. 3.51a**). In contrast with the central section, the presence of salt in the eastern Kuqa domain is more limited: to the north, the hinterland salt pinch-out is located at about 45 km from the south Tian Shan Fault (**Fig. 3.51a**); to the south, the location of the foreland salt pinch-out can be found immediately to the north of the forebulge. Incipient postsalt deformation commenced during early Miocene times (**Fig. 3.51b**). This was localized on the forelimb of the South Tian Shan anticline and consisted of (i)

an up-right fault bend fold developed in the hangingwall of the North-directed back-thrust 2 (**Fig. 3.51b**) and (ii) a drag fold developed in the hangingwall of the reactivated South-directed thrust 1 (**Fig. 3.51b**).

The second contractional stage (late Miocene to present; **Fig. 3.51c-d**) was coeval with the sedimentation of the Kangcun, Kuqa and Xiyu Fms. During this stage, Mesozoic-detached thrusts propagated southward (numbers 1 and 3 in **Fig. 3.51c**) and were subsequently cut by reactivated basement-involved faults (II and III in **Fig. 3.51c**). Coeval to that, the thrust cutting the hinge zone of the Bashijiqike Anticline (4 in **Fig. 3.51c**) developed. In addition, continued thrusting along basement thrust I (or basement underthrusting, as depicted in the central cross section) produced a pronounced uplift in the northern outcrops and forward rotation of the southern limb of the South Tian Shan Anticline that was recorded by angular unconformities in the upper Pliocene-Pleistocene units (**Fig. 3.51d**).

The Qiulitage frontal structure developed over the hinterland pinch-out of the salt (**Fig. 3.51c**) during the second contractional stage. We suggest it was initially formed as a fore- and backthrust pair (fishtail structure) detached in the Kumugeliemu salt and the gypsum and shales of the Jidike Fm (number 5 in **Fig. 3.51c**) when Mesozoic-detached thrust 3 or basement fault III transferred deformation to the Cenozoic units. Underneath the Mesozoic units deformation was centered on the reactivation of basement-involved thrust II producing a fault bend fold (Jidike Anticline in **Fig. 3.51c**). During Pliocene and Pleistocene times, the Qiulitage frontal structure continued to grow accommodating the shortening that was transferred from pre-salt structures. Consequently, a tight anticline was formed in the Cenozoic units, subsequently cut through the hinge zone by a backthrust detached over the foreland salt pinch-out (number 6 in **Fig. 3.51d**) and probably connected at depth to basement thrust III.

Compared to the central cross section, the presence of salt in the eastern section is reduced, therefore, the coupling increases and thick-skinned deformation predominates. In the central section the basement thrust II transferred deformation southwards through the salt, whereas in the eastern section it cut Mesozoic and Cenozoic units and previous Mesozoic-detached thrusts. This generated an uplift in relation to this structure (Jidike Anticline in **Fig. 3.51d**) that reduced the accommodation space. This, together with the fact that the Qiulitage frontal structure displays an arcuate shape in map view, and changes from a thrust to a backtrust from central to eastern sections cause that the Baicheng Syncline is narrower and thinner in this section.

3.3.3. Western section restoration

During the first shortening stage (coeval to the sedimentation of the Suweiyi and Jidike Fms.; **Fig. 3.53a-b**), shortening was mainly accommodated by the South Tian fault (basement-involved thrust I, see numbering in **Fig. 3.53**) that cut the Mesozoic units and transferred deformation to the Kumugeliemu salt. At this stage, our restoration suggests the development of two incipient backthrusts detached on the Suweiyi Fm. to the north (**Fig. 3.53b**) whereas minor, incipient folding could take place to the south, over the central part of the salt above its foreland pinch out (south-directed thrusts 2 and 3 in **Fig. 3.53b**).

This difference in the distribution of early, supra-salt deformation between this and the previously described sections is strongly related with the spatial distribution of the synorogenic salt units of the Kumugeliemu Group (**Fig. 3.53b**). The assembly of structures that were active during the Eocene to early Oligocene produced an early basin topography that allowed the deposition of the salt in a wider area than in the eastern and central sections: the hinterland pinch out of the salt was probably located to the north of the cross section boundary (salt units crop out at surface in the southern limb of the South Tian Shan Anticline) whereas the foreland salt pinch-out was controlled by the position of the forebulge. The wider depositional area of the salt in the West might result from the effect of the increasing westwards shortening in the inner zone of the Tian Shan, leading to a stronger flexure in its western foreland basin at the time salt was deposited.

During Late Miocene (coeval to the sedimentation of the Kangcun Fm; **Fig. 3.53c-d**) shortening in the basement and Mesozoic units was accommodated by the south Tian Shan structure and the reactivated basement-involved thrust II (see numbering in **Fig. 3.53**). Consequently, a fault bend fold was developed in the hangingwall of the thrust II. In the supra-salt units, additional shortening was basically transferred to the pre-existing structures (1, 2, and 3 in **Fig. 3.53c-d**).

Shortening mainly took place during Pliocene to the present day, coevally to sedimentation of the Kuqa and Xiyu Fms (**Fig. 3.53d**). During this stage, in the Kelasu fold-and-thrust system, the basement thrust I connects southwards with a short-cut and with a north-directed back-thrust (4 and 5 respectively in **Fig. 3.53d**). These structures produced respectively a pronounced forward rotation of the southern limb of the Tian Shan anticline,

and a backward rotation of the northern limb of the Baicheng Syncline that were recorded by an angular unconformity at the base of the Xiyu Fm.

Late thrusting in the northern Kelasu fold-and-thrust system was coeval with the development of the Qiulitage frontal structure (**Fig. 3.53d**). The Qiulitage frontal structure was located between the Quele Salt Sheet and the foreland pinch-out of the salt, it was initiated during Late Miocene as a detachment fold and its growth was probably due to salt flow from beneath the Baicheng Syncline. Furthermore, the forelimb of the Qiulitage frontal structure was cut by a South-directed thrust detached in the Kumugeliemu salt (6 in **Fig. 3.53d**). To the North of the Qiulitage frontal structre backlimb, the Quele thrust (**7 in Fig. 3.53d**) cut all the Cenozoic units. This South-directed thrust may developed on a primary weld that was probably caused by combination of two processes: (i) syn-kinematic sedimentation and (ii) salt flow towards the South to the Qiulitage frontal structure.

The kinematic evolution of the Baicheng Syncline was determined by salt evacuation in addition to orogenic shortening. As in the central section, basement-involved thrusting gave rise to a progressive southward migration of depocenters through time. During Pliocene and Pleistocene times (coeval to sedimentation of Kuqa and Xiyu Fms.), the depocenter shifted southwards over the fault bend of the Quele thrust.

3.4. REGIONAL MAPS

From the regional cross-sections presented in section 3.2 and the additional seismic information shown in **Fig. 3.2**, we have created regional maps indicating the correlation between basement features and the distribution of the two main décollements in the study area (**Fig. 3.54A**): the upper décollement corresponding to the lower Eocene-Oligocene salt, and the lower décollement located in the Upper Triassic-Lower Jurassic lacustrine mudstones and coals (Jia et al., 1998; Shuwei et al., 2010; Li et al., 2012; Ping et al., 2016) (**Fig. 3.54B**).

These two décollements have a different areal distribution. The Eocene-Oligocene salt shows a complex distribution (**Fig. 3.55A**) with a linear ENE-trending southern boundary and an E-trending northern boundary that, in the East, is suddenly shifted to the south by the expansion of lateral equivalent alluvial fans and lacustrine deltas causing a dramatic narrowing of the Kumugeliemu salt (Liu et al., 2008). The Upper Triassic-Lower Jurassic décollement is restricted to the Kelasu fold-and-thrust system and, in general terms, dies out to the western

Kuqa fold-and-thrust belt. Location of its northern and southern boundaries has been defined from the areal distribution of the thin-skinned, Mesozoic-detached thrusts: they are E-W-trending and the southernmost thrusts run broadly parallel to the trace of the Baicheng Syncline (**Fig. 3.55B**).

Triassic-Jurassic detached thrusts are abundant in the eastern and central domain of the Kuqa fold-and-thrust belt, but these thin-skinned structures disappear to the West. This along-strike structural variation is probably related to the lateral termination of the lower decollement or the diminution of its effectiveness as a décollement towards the west (Izquierdo-Llavall et al., 2018) (**Fig. 3.55B**). A decrease of the thickness of the coals and lacustrine mudstones (Li et al., 2004) or/and an increase of the maturation of the organic layers (Zhao et al., 2005) may explain this lateral variation.

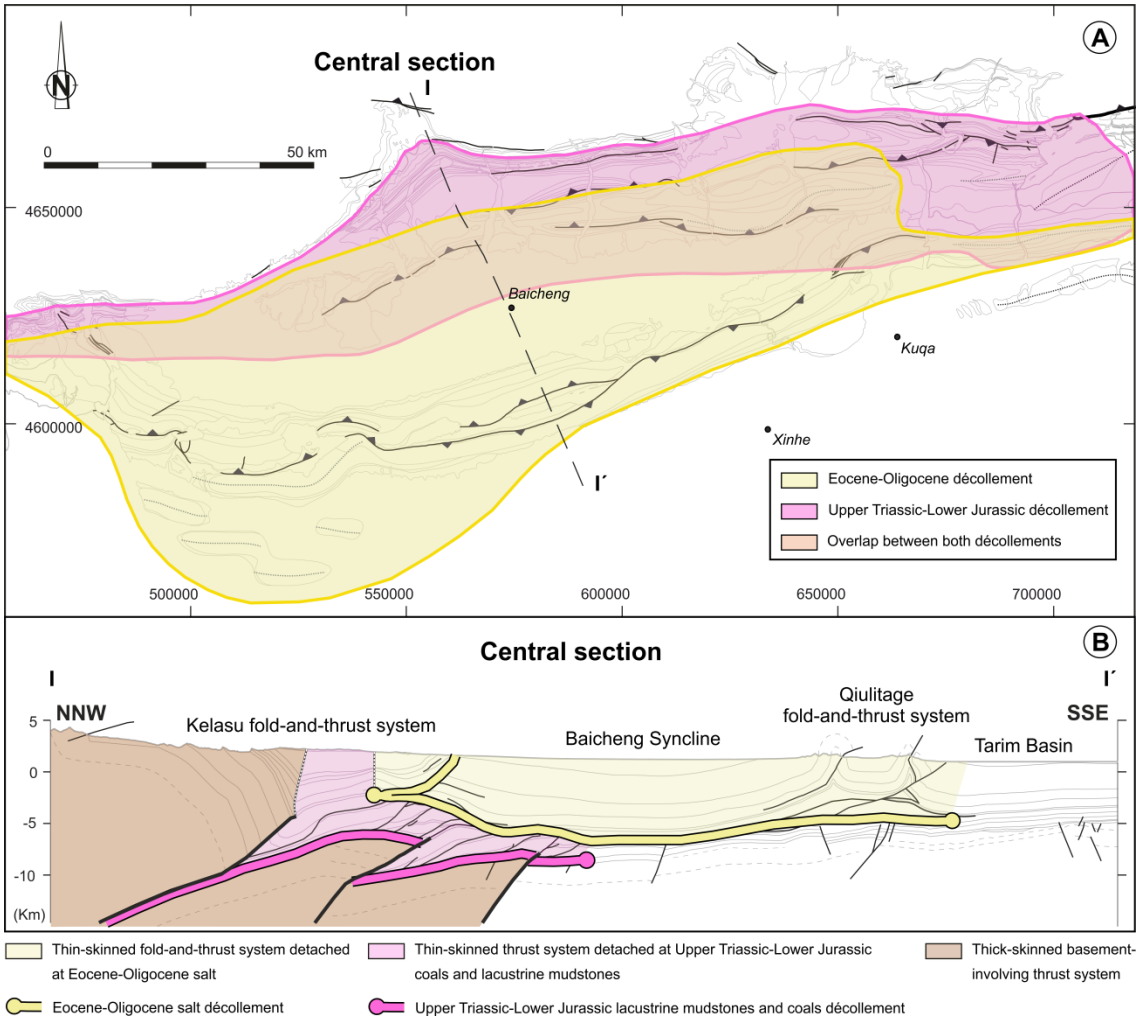

FIGURE 3.54. A: Structural map of the Kuqa fold-and-thrust belt showing the distribution of the Eocene-Oligocne and Upper Triassic-Lower Jurassic décollements. **B:** Central-section I-I' through the central Kuqa fold-and-thrust belt (see location in **Fig. 3.33A**) with the location of the décollements and related pinch-outs.

When the distribution of salt-detached structures (salt-cored anticlines and thrusts detached into this décollement*)* is compared to the distribution in map view of the Eocene-Oligocene salt, we observe that these structures are mainly concentrated on the salt boundaries, although they are also distributed throughout the inner part of the salt (**Fig. 3.55A**). However, regarding the thin-skinned thrust system detached in the lower décollement, thrusts are distributed throughout the décollement and show an approximately constant spacing. The number of trusts is higher in the central domain where the spacing among them is lower but decreases progressively to the East where the spacing among them is higher (**Fig. 3.55B**). The spacing increase results from the thickness increase in the stratigraphic sequence these thrusts deform.

Mesozoic-detached thrusts run approximately parallel to the strike inferred for the boundaries of the lower décollement. They are subparallel to salt-detached structures that are in turn sub-parallel to salt boundaries in the East but become oblique to the West, in the area where the salt pinch-out is shifted Southwards. At the western termination of the salt, they are at an angle of about 50º regarding the salt boundary (**Fig. 3.55C**).

Furthermore, the main basement structures in the different cross sections have been tentatively correlated throughout the study area. In general terms and based on the previously mentioned Mesozoic thickness variations in relation to basement faults, the basement thrust system mainly consists of previous (Mesozoic and/or Early Cenozoic) extensional faults that were partly or totally inverted during the Cenozoic compression. The basement-thrust system widens to the West and shows a tight correlation with the areal distribution of the Eocene-Oligocene upper décollement (**Fig. 3.55C**).

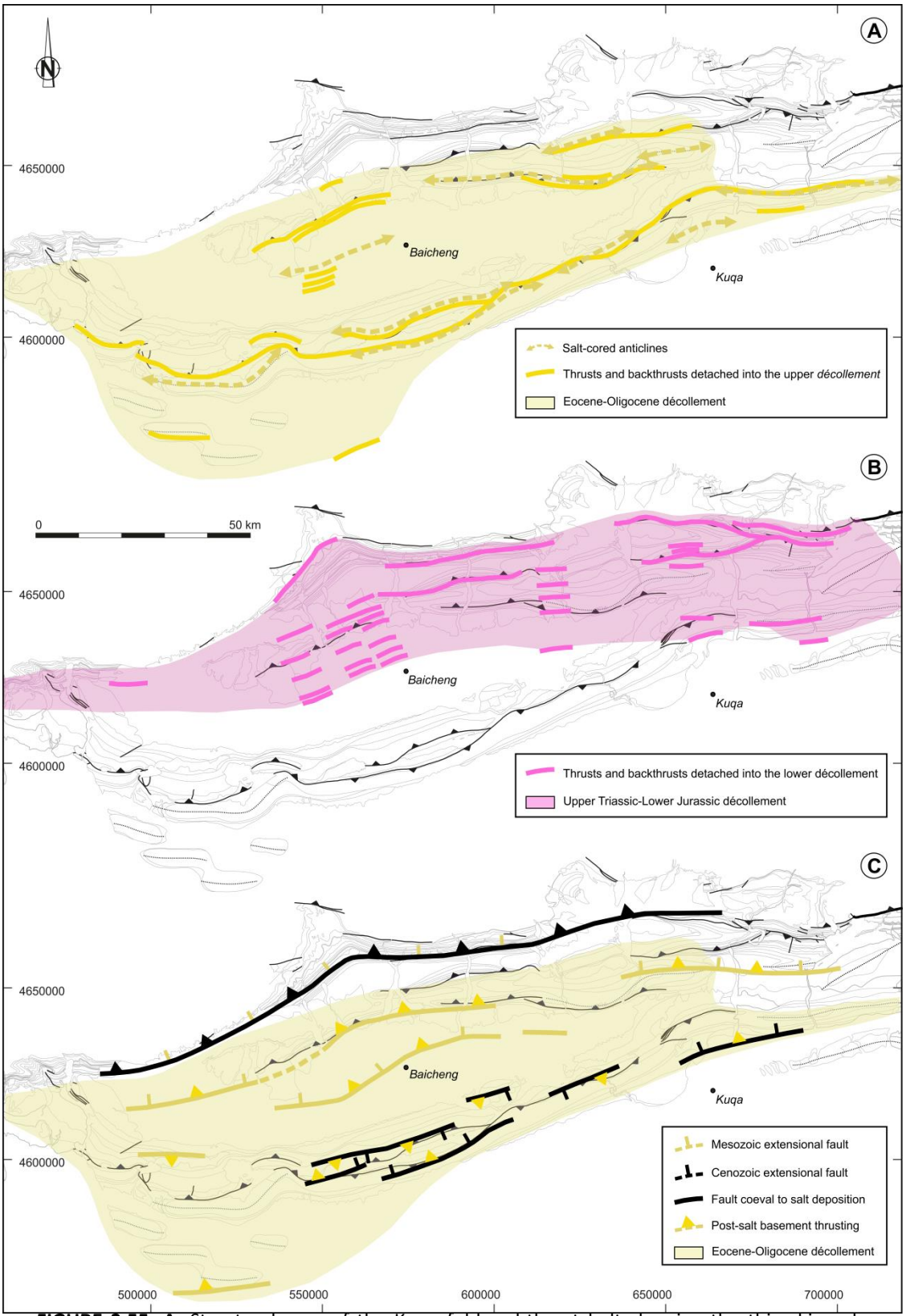

FIGURE 3.55. A: Structural map of the Kuqa fold-and-thrust belt showing the thin-skinned thrust system detached into the upper décollement (Eocene-Oligocene Kumugeliemu salt). **B:** Structural map of the Kuqa fold-and-thrust belt showing the extent of the thin-skinned thrust system detached into the lower décollement (Upper Triassic-Lower Jurassic coal). **C:** Structural map of the Kuqa fold-and-thrust belt showing the correlation between basement features and the distribution of the upper décollement.

3.5. KUQA FOLD-AND-THRUST BELT STRUCTURAL DISCUSSIONS

The sequentially restored cross sections emphasize that there are three primary factors controlling the geometry and kinematic evolution of the Kuqa fold-and-thrust belt: (1) the distribution of the two décollements within the Mesozoic-Cenozoic stratigraphic sequence (i.e., the Upper Triassic – Lower Jurassic shales and coal layers and the Eocene-Oligocene salt), (2) the syntectonic sedimentation, whose rate changed through time (as shortening rates also do) and (3) the reactivation of pre-contractional, inherited structures. The relative contribution and feedback between these factors is of key importance to the understanding of thrust systems that involve multiple décollements and variable syntectonic sedimentation rates.

3.5.1. Syntectonic sedimentation rates

Considering (i) the calculated shortening values in **Figs. 3.51, 3.52 and 3.53** (ii) the stratigraphic thicknesses of Cenozoic units in depocenters and (iii) the magnetostratigraphic ages (given by Zhang et al. (2015) and Zhang et al. (2016) for two profiles located about 30 km to the east of the central section, and by Charreau et al. (2006), Huang et al. (2006) and Sun et al. (2006) for additional magnetostratigraphic sections located about 30 km to the east of the eastern section), a clear distinction can be made between: an earlier contractional stage in the Kuqa fold-and-thrust belt (from top Cretaceous to early Miocene) that was dominated by lower shortening and sedimentation rates, and a later period (spanning the late Miocene to Pleistocene) characterized by higher rates of both processes (**Fig. 3.56**).

In the central section, the earlier stage had an average shortening velocity of about 0.2 mm/year and sediment-accumulation rates of 0.06 to 0.1 mm/year (**Fig. 3.56A**). However, the later stage was characterized by shortening rates of 1.5 and 3.2 mm/year and sediment-accumulation rates of 0.5 and 1 mm/year during the sedimentation of the Kangcun and the Kuqa and Xiyu Fms., respectively (**Fig. 3.56A**).

In the eastern section, the earlier stage had an average shortening velocity of about 0.04 mm/year and sediment-accumulation rates of 0.05 to 0.06 mm/year (**Fig. 3.56B**). In contrast, the later stage was characterized by shortening rates of 2 and 2.4 mm/year and a constant sediment-accumulation rate of 0.6 mm/year during the sedimentation of Kangcun, Kuqa and Xiyu Fms. (**Fig. 3.56B**).

In the western section, the earlier stage had an average shortening velocity of about 0.05 mm/year and sediment-accumulation rates of 0.09 to 0.07 mm/year (**Fig. 3.56C**). However, the later stage was characterized by shortening rates of 0.5 and 4.9 mm/year and sediment-accumulation rates of 0.2 to 0.6 mm/year during the sedimentation of the Kangcun Fm. and the Kuqa and Xiyu Fms., respectively (**Fig. 3.56C**).The obtained shortening velocities are in the range of previous values calculated for the central, western (Li et al*.,* 2012) and eastern (Wang et al*.,* 2011) Kuqa fold-and-thrust belt. If shortening rate values are compared along-strike, a westwards increase could be defined during the sedimentation of the Kuqa and Xiyu Formations. Nevertheless, this rate, would be lower and westwards decreasing during the sedimentation of the Kangcun Fm, accordingly with an eastward decrease in sediment-accumulation rates during this period.

The syntectonic sediment-accumulation rates are consistent with the values derived from magnetostratigraphic profiles for the Eocene-early Miocene period (average of 0.07 mm/year in the eastern continuation of the Kumugeliemu anticline, Huang et al*.,* 2006; compare with **Fig. 3.56**) but double or quadruple the rates calculated in growing structures during the late Miocene-Pleistocene (0.23 mm/year in the eastern Kelasu, Huang et al*.,* 2006; 0.5 mm/year in the eastern Qiulitage, Charreau et al*.,* 2006; compare with **Figs. 3.56A and B**).

In general terms, magnetostratigraphic profiles indicate a sudden increase in syntectonic sediment-accumulation rates during late Miocene (at 11 Ma in Charreau et al*.,* 2006; 7 Ma in Huang et al*.,* 2006) that is consistent with the increase in the shortening rate derived from the sequential restorations. The calculated syntectonic sediment-accumulation rates are comparable to those defined in other fold-and-thrust belts: the lower rates (Eocene-early Miocene) are similar to those in the Jura Mountains (Mugnier and Vialon, 1986) or the Canadian Rockies (Ollerenshaw, 1978) whereas the higher velocities (late Miocene-Pleistocene) are analogous to those registered in the Sub-Andean (Baby et al*.,* 1995) or Taiwan fold-and-thrust systems (Suppe, 1980).

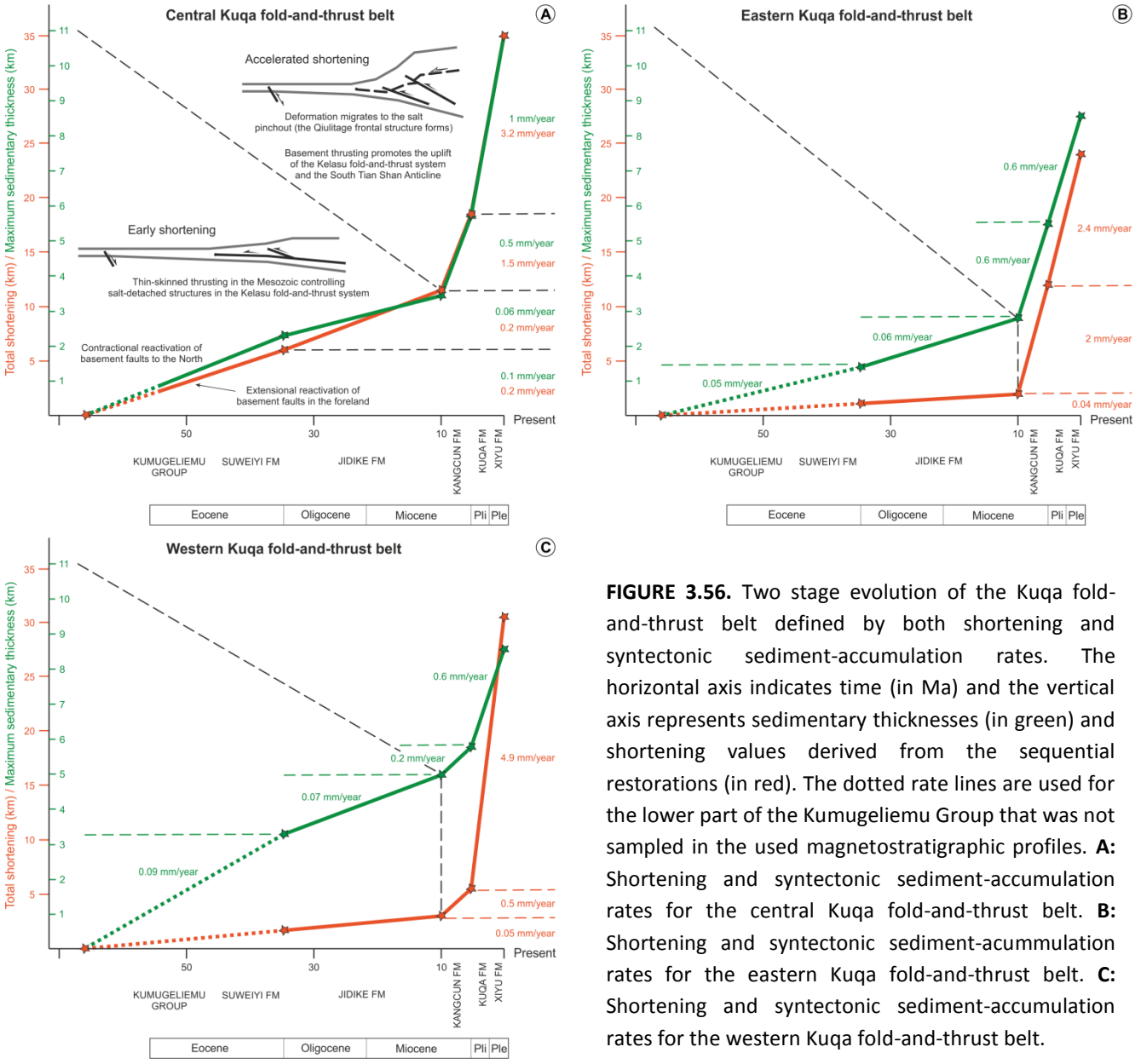

FIGURE 3.56. Two stage evolution of the Kuqa fold-and-thrust belt defined by both shortening and syntectonic sediment-accumulation rates. The horizontal axis indicates time (in Ma) and the vertical axis represents sedimentary thicknesses (in green) and shortening values derived from the sequential restorations (in red). The dotted rate lines are used for the lower part of the Kumugeliemu Group that was not sampled in the used magnetostratigraphic profiles. **A:** Shortening and syntectonic sediment-accumulation rates for the central Kuqa fold-and-thrust belt. **B:** Shortening and syntectonic sediment-acummulation rates for the eastern Kuqa fold-and-thrust belt. **C:** Shortening and syntectonic sediment-accumulation rates for the western Kuqa fold-and-thrust belt.

3.5.1.1. *Early shortening under low syntectonic sedimentation rates*

Interpretation of presalt deformation allowed us to expand the time period over which palinspastic restorations were carried out and thus enabled the characterization of early deformation geometries (Late Cretaceous to early Miocene) which are not considered in previous studies. Many authors (Hubert-Ferrari et al., 2007; Li et al., 2012; Tang et al., 2004; Wang et al., 2011) proposed that the onset of contraction took place by the end of the Pliocene or the early Miocene, whereas we document shortening as early as the Cretaceous (**Fig. 3.52a**). Early shortening stages are better explored in the central cross section where the

proposed restoration attains the top of the Cretaceous sequence (whereas the top of the Suweiyi Fm is the last restored horizon in the eastern and western sections).

During this early deformation stage, shortening in the central section, and to a lesser extent in the eastern one, was transferred to a thin-skinned thrust system detached in Triassic-Jurassic coal layers through a basement-involved thrust (the southern Tian Shan fault; **Fig. 3.52b, c and Fig. 3.51a, b**). Conversely in the western section, Triassic/Jurassic units did not behave as an effective décollement and basement shortening accommodated by the South Tian Shan Fault was instead transferred to the Eocene-Oligocene salt (**Fig. 3.53a, b**).

Early thin-skinned thrusting in the presalt sequence was balanced by the development of decoupled, salt-cored anticlines in the northern part of the central section (Kumugeliemu Anticline and Tuzimaza Thrust; **Fig. 3.52c**). The Kuqa fold-and-thrust belt grew as a wide thrust wedge, characterized by a low taper that was formed by numerous, closely-spaced structures displaying variable wavelengths beneath the salt but two longer-wavelength folds above the salt. It developed in a piggyback thrust sequence with both the upper and lower décollements being active, with partly decoupled deformation above and below the shallow salt detachment.

In the eastern section, thin-skinned, Mesozoic-detached thrusting is focused in two minor structures where the Bashijiqike and Jidike anticlines later developed (**Fig. 3.51b**). Early deformation in the Mesozoic and Cenozoic sequence is coupled and disconnected to the Kumugeliemu salt whose hinterland pinch-out is located few kilometers to the south of the Early Miocene deformation front. In addition to the presence/absence of salt, the geometry of the thin-skinned thrust system is controlled by areal distribution of the lower décollement. It is quite continuous in the central section, but it is disrupted, cut by extensional faults in the eastern section. As a result, the Kuqa fold-and-thrust belt during this stage was probably narrower in the East, the taper angle being lower than in the central section. On the contrary, the extension of the salt in the western section is the maximum in the Kuqa fold-and-thrust belt. Deformation was distributed from the northern part of the section to the foreland pinch out of the Kumugeliemu salt developing several incipient structures the southernmost located in the foreland pinch out of the salt (**Fig. 3.53b**). Consequently, the western Kuqa fold-and-thrust belt grew as a wide thrust wedge with a low taper angle.

These initial geometries resulted from the distribution of weak décollements that, under low sedimentation rates, efficiently propagated shortening towards the foreland and enabled the growth of the fold and thrust system through frontal accretion. The key role of syntectonic sedimentation on this process has been tested using both analogue (Duerto and McClay, 2009; Mugnier et al*.,* 1997; Storti and McClay, 1995) and numerical modelling techniques (Fillon et al*.,* 2013). Models show that lower sedimentation rates promote (i) a quicker propagation of thrusts towards the foreland and (ii) the development of thrust systems consisting of a higher number of shorter-lived structures, as we propose for the initial deformation stages in the presalt of the central Kuqa fold-and-thrust belt. Similar deformation styles are found in other thrust systems formed during low sedimentation rates such as the Canadian Rockies (Ollerenshaw, 1978), where folds and thrusts are numerous, have short wavelengths and developed with a consistent spacing.

The sequential restorations (**Fig. 3.52b, c**) suggest the salt-detached structures in the central section were initially located above coal-detached thrusts, with the hinges of supra- and presalt folds being slightly shifted. This structural style is common in contractional scenarios where salt thicknesses are comparable to those of the overlying suprasalt units (such as the Zagros (Fard et al*.,* 2011) and can be simulated in sand-silicone analogue models (see chapter 4). The geometries result from a combination of disharmonic folding and salt flow from above the hinges of presalt anticlines towards the cores of suprasalt anticlines, the latter locally evolving to thrusted folds and diapirs (Fard et al*.,* 2011). This mechanism could have played an important role in the formation of the Tuzimaza Thrust (**Fig. 3.52**), where salt flow from above the hinge zone of underlying presalt anticlines led to local salt welding and the activation of thrusting.

Early contractional deformation in the northern Kuqa fold-and-thrust belt was coeval to extensional faulting to the south in the forebulge. This controlled the location of the frontal Kumugeliemu salt pinch-out and created, in the central cross section, accommodation for locally thicker salt (**Figs. 3.51a, 3.52c, and 3.53b**). In turn, the location of the salt pinch-out controlled the locus of salt-detached structures formed during ongoing shortening (late Miocene to Pleistocene, see comments in the following section).

3.5.1.2. *Later contractional stage under accelerated shortening*

The increase in the syntectonic sedimentation rate during the Miocene (**Fig. 3.56**) was coincident with a change in the deformation style of the Kuqa fold-and-thrust belt, with basement-involved, thick-skinned thrusting dominating over thin-skinned thrusting along Jurassic coals and shales. Total shortening increases sharply in the later contractional stage in the Kuqa fold-and-thrust belt (**Fig. 3.56**), displaying a general increase to the West (compare **Figs. 3.51c, d; 3.52d, e and 3.53c, d**). To the west, shortening is mostly concentrated in the late Miocene to the present time interval (**Figs. 3.53c, d and 3.56**), whereas it is more gradual to the central and eastern sections (**Figs. 3.51c, d; 3.52d, e and 3.56**). The westwards shortening increase agrees with the regional structure of the Tian Shan that is wider and higher to the West but narrows and lows eastwards. The basement-involved, thick-skinned thrust system formed a thrust stack that uplifted the Kelasu fold-and-thrust system and strongly rotated the southern limb of the South Tian Shan Anticline.

As a result, the Kuqa fold-and-thrust belt evolved into a narrower and steeper thrust wedge (**Figs. 3.51d, 3.52e and 3.53d**). Analogue models (Duerto and McClay, 2009) have shown that rapid sedimentation at the front of an emerging thrust system enhances the stacking of thrust sheets, the narrowing of the thrust wedge and the rotation of the frontal limb of the stack, as observed in the Kuqa fold-and-thrust belt during its Miocene-Pliocene evolution. Thrust stacking produced an increase in the taper angle of the thrust wedge that, during late deformation stages, probably reached critical conditions and resulted in the late activation of the structures beneath the Qiulitage frontal structre (**Figs 3.51d and 3.52e**).

Shortening in basement was transferred via the salt to suprasalt folding and thrusting localized in a few structures that were separated from each other by the broad Baicheng Syncline (**Figs. 3.51d, 3.52e and 3.53d**). Analogue (Duerto and McClay, 2009, see chapter 4) and numerical models (Fillon et al*.,* 2013) demonstrate that localization of shortening in a few, long-lived and widely-spaced structures results from the increase in syntectonic sedimentary thicknesses (**Fig. 3.10b**). Similar geometries are found in other natural analogues such as the southern Central Pyrenees (Muñoz, 1992) that are characterized by a thick succession of syntectonic strata deformed by long thrusts and a wide wedge-shaped basin transported over an underlying décollement.

Modelling results also show that thrusts initiate at the point where the total work needed to slide on the décollement and to break through the overburden is minimal (Hardy et al., 1998; Fillon et al., 2013). This location could be either where the overlying strata have the minimum thickness (Fillon et al., 2013) or at the frontal termination of the weak décollement (see chapter 4). In the Kuqa fold-and-thrust belt, the foreland salt pinch-out controlled the locus of the frontalmost structures and the earlier development of the southern Qiulitage anticline in the eastern and central sections. In contrast, the frontal structures of the thrust system detached on Jurassic shales and coal emerged at the point where overlying syntectonic units tapered out (**Figs. 3.51c and 3.52d**). This observation suggests that the locus of presalt thin-skinned thrusts was probably more influenced by syntectonic sedimentary thicknesses than by the lateral termination of the coal or shales.

3.5.2. The role of the inherited Mesozoic structure

The restorations presented in this work depict a first picture of the Mesozoic structure predating the formation of the Kuqa fold-and-thrust belt. When considering the areal distribution of Mesozoic units, Triassic units display along strike variations: in the eastern section, they are present across the whole profile showing (i) a progressive thinning towards the Cenozoic forebulge area and (ii) sharp thickness variations to the North of the profile. Thickness variations in the North are related to inherited, North-dipping extensional faults. Triassic units in the central and western sections, crop out in the hangingwall of the South Tian Shan Fault but disappear in its footwall to be present again in the undeformed Tarim Basin domain, to the South. In contrast, Jurassic and Cretaceous sequences are continuous in the entire Kuqa fold-and-thrust belt and show both (i) a progressive southward thinning and (ii) local, sharp thickness variations related to North-dipping basement faults. The picture becomes more complicated in the western cross section where thickness variations and locally recognized unconformities in the Cretaceous point out to the existence of early contractional features, Mesozoic in age. The presence of these early faults had a first-order impact on the structural evolution of the Kuqa fold-and-thrust belt because they determined the locus of most of the basement thrusts acting during the Cenozoic and therefore the geometry of the thrust stack in the Kelasu fold-and-thrust system. Furthermore, in the eastern and central section, inherited basement faulting probably controlled the position of the Kumugeliemu salt pinch-out and contributed to the late-stage uplift of the Qiulitage fold-and-thrust system, showing a feedback relationship between basement-involved faults and salt-detached deformation. In this sense, our interpretation merges previous structural models that are

somewhat contradictory: Li et al*.,* (2012) suggested that the growth of the frontal structure was controlled by the location of the foreland salt pinch-out but disregarded the influence of subsalt faulting beneath the Qiulitage frontal structure, as pointed out on cross sections of previous authors (Chen et al., 2004; Tang et al., 2004).

Considering the plate tectonics scenario summarized in section 2.1., normal faulting during the Mesozoic took place mainly in a foreland basin context under regional compressional conditions (Halim et al*.,* 1998; Replumaz and Tapponier, 2003; Stampfli and Borel, 2002). This normal faulting was probably induced by flexural subsidence and tectonic loading in the contractionally reactivation of the Paleozoic Tian Shan and would be compatible with the early contractional features inferred in the western cross section.

3.5.3. Western termination of the Eocene-Oligocene salt

It is commonly assumed that new, salt-detached structures form at salt edges following their trend. However, in the western Kuqa fold-and-thrust belt, salt-detached structures are oblique regarding the salt boundary (**Fig. 3.55C**), similarly to what we observe in southern Central Pyrenees (**Fig. 3.57**). In previous publications (i.e. Cai and Lü, 2015), the structures developed at the salt edge in the western Kuqa fold-and-thrust belt were interpreted as en echelon folds of the cover on top of NW-SE-striking strike slip, basement faults. This clearly conflicts with our seismic interpretation along the seismic profile dapomian-23, where there is no remarkable shifting of the top basement that is instead affected by a progressive tilting to the East probably controlling the termination of the salt towards the West (**Fig. 3.50**). Based on previous analogue models, the obliquity between the salt boundary and the structures in the western Kuqa fold-and-thrust belt can be explained by the lateral termination of the salt with no need of basement strike-slip faulting underneath. Analogue models show that the orientation of the structures at salt edges depends on the angle between the salt pinch-out and the shortening direction. If the angle of the pinch out is either close to perpendicular to the shortening direction structures form parallel to the salt edges (Luján et al., 2003). However, if it is highly oblique, as in the Kuqa case study, most of structures will not follow the trend of the salt edges. They will be oblique to both the shortening direction and the salt edges (**Fig. 3.55C**). This is because structures developed above salt for a given time form further to the foreland and link as they progress with the adjacent structures formed on the frictional detachment. As a result, the salt boundary behaves as a shear zone with a displacement gradient which promotes vertical-axial rotation.

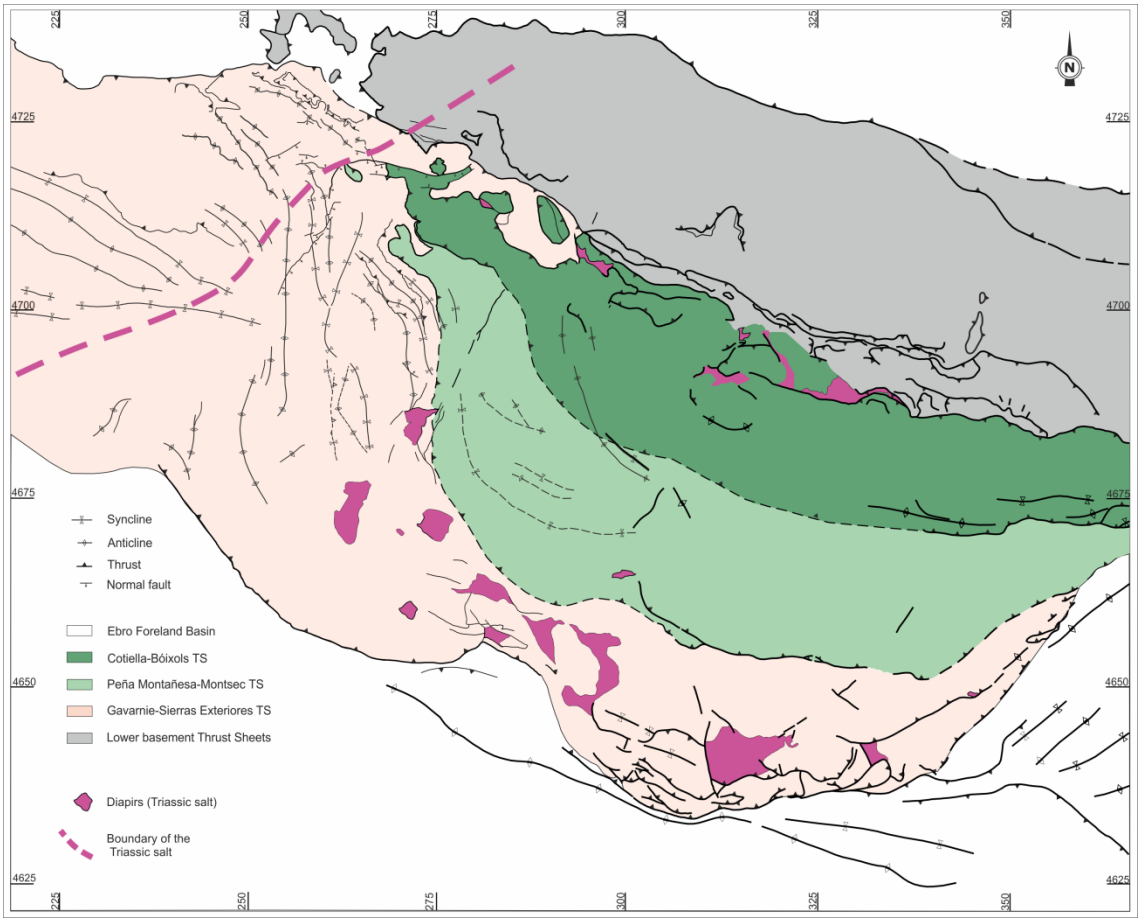

FIGURE 3.57. Geological map with the main structural units of the southern Central Pyrenees (Modified from Muñoz et al., 2013). Note that the structures are oblique with regard to the Triassic salt boundary (pink dashed line).

3.6. KUQA FOLD-AND-THRUST BELT STRUCTURAL CONCLUSIONS

Six regional cross sections have been constructed along the Kuqa fold-and-thrust belt that merge surface, well, and seismic data to provide a detailed structural model. Three sections have been restored, with gradually increasing shortening values that are balanced above and beneath the salt. From these results the following conclusions have been obtained.

With respect to the general structure of the Kuqa fold-and-thrust belt:

- The Kuqa fold-and-thrust belt is located over and on the front of the frontal basement thrust system of the southern Tian Shan Range and over the non-deformed basement of its southern foreland basin (Tarim Basin).
- The Kuqa fold-and-thrust belt is an ENE trending thin-skinned fold-and-thrust system characterized by folds, thrusts and backthrusts. Tight anticlines extend along-strike for

tens or even hundreds of kilometers and are separated by a wide, open syncline. Anticlines involve Paleozoic and Mesozoic units to the north but are manifested by Cenozoic sequences to the south.

- The structure of the thin-skinned Kuqa fold-and-thrust is controlled by two main décollements: One located in the syncontractional Eocene-Oligocene salt and the other, deeper and precontractional placed in the Upper Triassic-Lower Jurassic coal and lacustrine mudstones.

- Cross section balancing allowed us to estimate a total shortening (from Oligocene to the present-day) ranging from 30.5 km to the West to 24 km to the East (29 km in the central part) that was mostly accommodated from late Miocene to Pleistocene times.

With respect to the structure below the coal layers:

- The structure of the Kuqa fold-and-thrust belt below the lower décollement is characterized by north-dipping basement-involved thrust system forming a thrust stack. This thrust system cut and branches with the thin-skinned fold-and-thrust system detached on the coal layers.

With respect to the structure between the coal layers and the salt:

- Deformation in sub-salt units is strongly conditioned by the presence of coal layers that are interlayered within the Upper Triassic-Lower Jurassic sequence and behaved as a main décollement. In this sense, the thin-skinned fold-and-thrust system detached on the coal layers is well developed in the central and eastern part of the fold-and-thrust belt but dies out to the West.
- The geometry and width of the thin-skinned fold-and-thrust system detached on the coal layer vary along-strike depending on the thickness of the stratigraphic sequence the thrusts involve: the thrust system is wider and it is formed by a lower number of thrust sheets to the East where the deformed sequence is thicker but it is narrower and consists of a higher number of thrust sheets in the central part where the deformed sequence is thinner.

With respect to the structure above the salt:

- Three main structures deform the Cenozoic sequence from north to south: the northern structure comprises the Tuzimaza Thrust to the west, the Suweiyi Antricline in the central part, and the Jidike Anticline to the east, whereas the Qiulitage frontal anticline defines the southern structure. Both the northern and southern structures are detachment folds that were cut by thrusts and backthrusts detached along the Kumugeliemu salt and the Suweiyi and Jidike Fms. and are separated by the Baicheng Syncline.

With respect to the suprasalt/subsalt structural relationships

- The Tuzimaza Thrust, the Suweiyi Anticline and the eastern Qiulitage frontal structure developed along the hinterland pinch-out of the Kumugeliemu salt. Their evolution was markedly controlled by the interplay with sub-salt structures that yield to salt evacuation processes and salt welding. On the contrary, the central Qiulitage frontal structure is located along the foreland pinch-out of the Kumugeliemu salt and its geometry was almost not overprinted by sub-salt deformation except for a later episode of basement fault inversion that gave rise to the uplift of the structure.

With respect to the kinematic deformation

- Palinspastic restorations show extensional deformation during the Mesozoic characterized by noth-dipping extensional faults controlling local depocenters of Mesozoic units.

- The extensional faults inherited from Triassic to Late Cretaceous times were progressively inverted, from North to South during Cenozoic compression. These early extensional faults strongly control the facies distribution of Eocene-Oligocene evaporites which in turn governed the localization of Neogene deformation over the salt pinch-outs with the development of the Tuzimaza Thrust and the central and eastern Qiulitage frontal structure.

- The restorations results highlight a two-stage evolution in the kuqa fold-and-thrust belt during the Cenozoic. An earlier stage (Top Cretaceous-lower Miocene) with slow deformation (0.01-0.09 mm/year) and low syntectonin sedimentation rate (0.2-1

mm/year) and a later stage (Upper Miocene-Pleistocene) with rapid deformation (0.05-0.4 mm/year) and high syntectonic sedimentation rate (0.5-4.9 mm/year).

CHAPTER 4. ANALOGUE MODELLING

4.1. INTRODUCTION

The geometry and kinematics of contractional belts are controlled by the properties of the rocks (rheology, mechanical stratigraphy, preexisting weaknesses, friction of basal or interbedded décollements), the kinematics of convergence (obliquity and velocity), the flexural response to tectonic loading, the climate-dependent surface processes (erosion, transport and sedimentation), the fluxes within wedges (input and output), the inherited structure, or changes in confining pressure and temperature (Davis et al., 1983; Beaumont et al., 1992; Graveleau et al., 2012; Fillon et al., 2013). Each one of these factors has an impact on the contractional structure and dynamics that has been widely investigated in nature and explored through analogue and numerical models (Storti and McClay, 1995; Bonini, 2001; Soto et al., 2002; Ravaglia et al., 2004; Simpson, 2006; Stockmal et al., 2007; Bonnet et al., 2008; Graveleau and Dominguez, 2008; Konstantinovskaya and Malavieille, 2011; Ruh et al., 2012).

It is evident from these studies that the presence of weak frictionless layers (salt or overpressured shales) results in décollements above which the contractional belt shows a lower taper angle, a wider zone of deformation, and more symmetrical structures (Jaumé and Lillie, 1988). In these wedges, the precise external geometry and internal deformation, as well as the degree of decoupling, are determined by the strain rate, the viscosity and strength of the décollement, and the shape and depth of this weak layer (Bonini, 2003; Couzens-Schultz et al., 2003; Graveleau et al., 2012). In addition to these geometrical and mechanical factors, synkinematic erosion and sedimentation also impact the geometries because these two surface processes prevent the propagation of deformation toward the foreland and therefore reduce the width of the belt (Beaumont et al., 1992; Willett, 1999; Bonini, 2001; Simpson, 2006; Fillon et al., 2013). They also induce an increase of the dip and number of active thrusts (Storti and McClay, 1995; Persson et al., 2004; Bonnet et al., 2008). But these general patterns are subject to variations depending on the strength profile of the deforming rocks. For example, when this includes a viscous décollement, sedimentation can either promote or inhibit foreland propagation of the deformation and the growth of a large wedge (Bonini, 2001; Smit et al., 2010).

The way syntectonic sedimentation interacts with the mechanical stratigraphy of the deforming rocks has been analyzed in numerous analogue and numerical modeling studies. These studies have explored this interaction in fold-and-thrust systems with frictional homogeneous sequences (Bigi et al., 2010; Del Castello et al., 2004; Larroque et al., 1995;

Persson and Sokoutis, 2002; Persson et al., 2004; Storti and McClay, 1995; Storti et al., 2000; Wu and McClay, 2011), frictional sequences underlain by a weak basal décollement (Cobbold et al., 1993; Smit et al., 2010), and sequences incorporating a weak pre- or syncontractional interlayered décollement (Baby et al., 1995; Bonini, 2001; Bonnet et al., 2008; Duerto and McClay, 2009; Konstantinovskaya et al., 2009; Leturmy et al., 2000; Massoli et al., 2006; Mugnier et al., 1997; Wang et al., 2013; Wu et al., 2014).

However, the influence of syntectonic sedimentation in fold-and-thrust systems with two décollements has rarely been tested even though it is a common scenario in the outer parts of fold-and-thrust belts such the Apennines (Scisciani and Montefalcone, 2006), the Appalachians (Mount, 2014), the Pyrenees (Sans et al., 1996), the Zagros (Sherkati et al., 2006), or the Sub-Andean (Labaume and Moretti, 2001) and Kuqa fold-and-thrust belts (Izquierdo-Llavall et al., 2018). In all these cases, the deformational wedge includes syntectonic strata and two or more pre- or syntectonic décollements comprising salt, overpressured shales, or organic-rich shales and coals. Moreover, the few published studies on this subject are essentially focused on individual structures (Pichot and Nalpas, 2009; Driehaus et al., 2014; Darnault et al., 2016) and do not analyze sediment-décollement interaction at the regional fold-and-thrust belt scale.

In this context, the present study aims to understand how the rate of syncontractional sedimentation influences the deformation style in the foreland of fold-and-thrust belts involving multiple décollements; in particular, with a décollement placed in a very weak synorogenic salt layer and a deeper, preorogenic décollement comprising a less weak coal/shale lithology. To achieve this, we designed an analogue experimental program whose setup was inspired by the Kuqa fold-and-thrust belt (**Fig. 4.1A**). This setup incorporated two weak layers, each with its own areal distribution (see **Fig. 4.1B**) that was maintained in all experiments Moreover, the lower décollement was constructed with laterally varying strength. With these general features, four analogue experiments were carried out by applying the same amount of shortening but with different synkinematic sedimentary rates.

The experimental results allowed us to develop some basic guidelines to help understand how synkinematic sedimentation affects the deformation style of fold-and-thrust belts with multiple décollements. The results compare favorably with the geometries observed across the Kuqa fold-and-thrust belt and shed light on how known sedimentary rates controlled its kinematic evolution. Besides, the models can provide a powerful tool both to

help interpret the structure beneath the décollements that may be poorly imaged on seismic and to understand the kinematics and mechanics of fold-and-thrust belts which include more than one detachment level and sedimentary rates that potentially changed through time. In this sense, our results should be useful not only to researchers in fold-and-thrust belt tectonics but also to industry geoscientists whose efforts are focussed on hydrocarbon exploration and production in subsalt contractional environments.

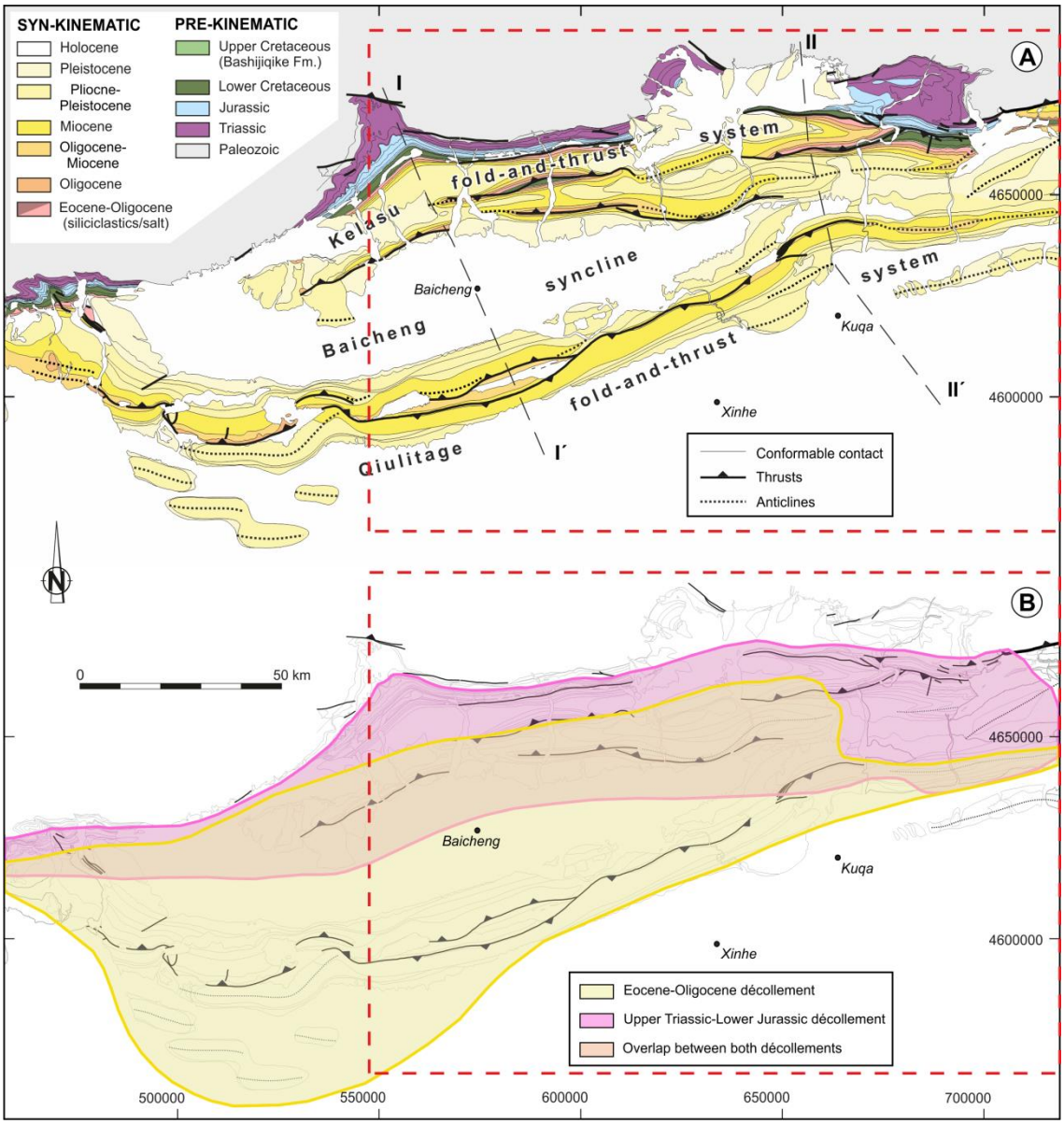

FIGURE 4.1. A: Geological map of the Kuqa fold-and-thrust belt. The red dashed rectangles show the modeled area in our experiments. **B:** Structural map of the Kuqa fold-and-thrust belt showing distribution of the Eocene-Oligocene and Upper Triassic-Lower Jurassic décollements. The red dashed rectangle shows the modeled area in our experiments. Coordinates are in meters in Universal Transverse Mercator, zone 44 northern hemisphere and datum WGS84.

4.2. EXPERIMENTAL METHODOLOGY

The model setup was based closely on the mechanical stratigraphy observed in the central part of the Kuqa fold-and-thrust belt (**Fig. 4.2**). The setup was the same in all models except for the synkinematic sedimentation rate which varied between the four 3D analogue models (**Table 4.1.**). All were carried out in a 112x90 cm glass-sided deformation rig whose base was a fixed Mylar sheet with glued sand. Below, we describe the materials used, the model scaling, the model setup, and the analysis methodology.

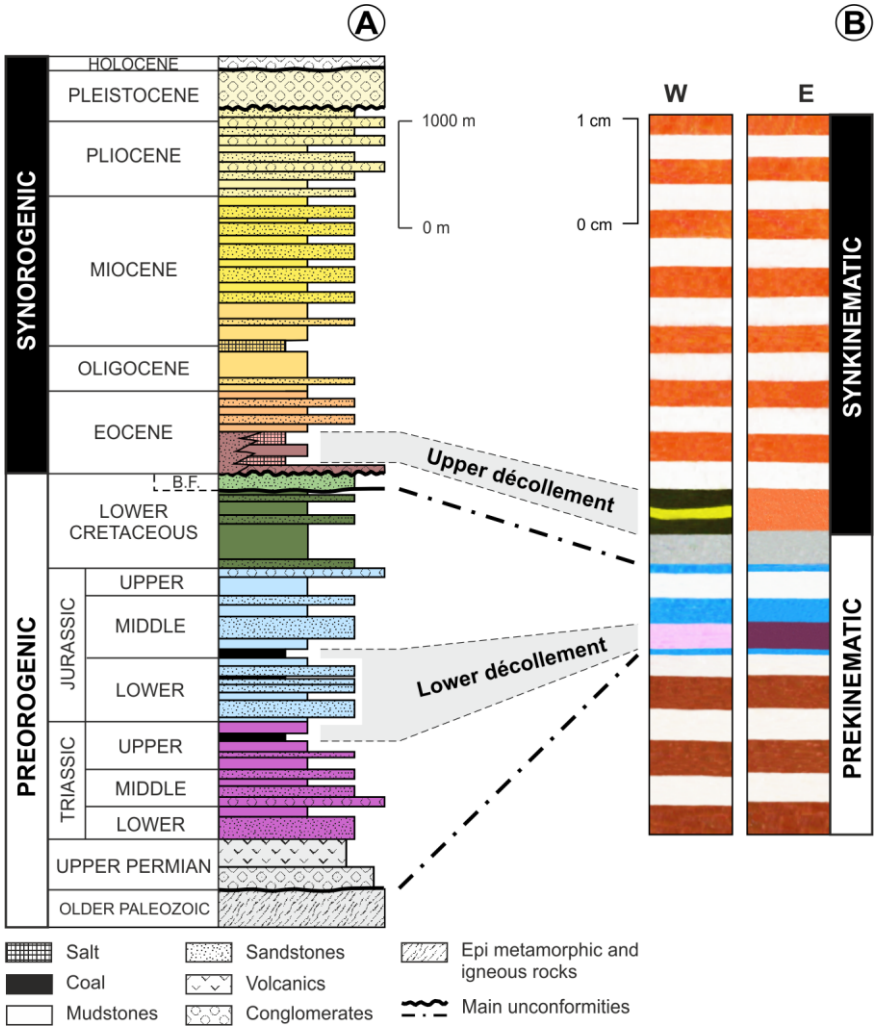

FIGURE 4.2. A: Stratigraphy of Kuqa fold-and-thrust belt in the inner Kelasu fold-and-thrust system (modified from Li et al., 2012). U.C.: Upper Cretaceous (Bashijikiqe Fm.). **B:** Stratigraphy of the analogue experiments at their central areas (equivalent to the Baicheng syncline area).

	Deposited unit (number of layers)	Model tilting applied before layer deposition	Accumulated tilting		Regional datum variation in each layer and erosive event			
					Model A	*Model B*	*Model C*	*Model D*
SYNKINEMATIC	Red and white sand (13)	0.2º	7.3º	3.3º	0	1 mm	2 mm	3 mm
	White sand layer (1)	0	4.7º		+3 mm			
	Silicone / Red sand (1)	0	4.7º		+4 mm			
	Yellow sand / Red sand (1)	0	4.7º		+1 mm			
	Silicone / Red sand (1)	0.7	4.7º		+7.5 mm			
PREKINEMATIC	Grey sand (1)	0	4º		+3 mm			
	Erosion							
	Model tilting		0.6º					
	White and blue sand (6)	0.1º	3.4º		+1.5 mm			
	Blue sand (1)	0	2.8º		+3 mm			
	White sand / mixtures of sand and pink polymer (1)	0	2.8º		+3 mm			
	Blue and white sand (3)	0.2º	2.8º		+0.5 mm			
	Erosion							
	Model tilting		2.2º					
	Brown and white sand (19)	0	0		+3 mm			

TABLE 4.1. Tilting and regional datum variations introduced during the set-up and posterior experiment running.

4.2.1. Mechanical properties of the analog materials

We used dry silica sand, silicone polymer, and mixtures of sand and silicone polymer to simulate the rocks of the Kuqa contractional wedge. We used a grainy basal sheet to increase the basal friction of the models (coefficient of friction of 0.5-0.6; Larroque et al., 1995), leading to the growth of an imbricate thrust system of short thrust sheets with a broad cross-sectional taper, similar to that observed in the modeled area (**Figs. 3.44 – 3.49**).

Frictional materials were simulated with dry silica sand, which is nearly pure silica (99%) and has an average grain size of 200 µm. This material has an angle of internal friction of about 30º and a cohesion of a few tens of Pascals, being an excellent analogue of brittle rocks in the upper continental crust (Krantz, 1991; Lohrmann et al., 2003; Schellart, 2000). In contrast, the two décollements were modeled using transparent polymer for salt and a mixture of pink polymer and white or black silica sand for the coal and lacustrine mudstones (**Fig. 4.2, Table 4.2**). The silicone polymer was silicone Rhodia Rhodosil GUM FM, from Bluestar Silicones (Dell'Ertole and Schellart, 2013; Ferrer et al., 2017), a transparent or pink, high-viscosity polydimethylsiloxane (PDMS) polymer. Within the range of strain rates used in all experiments, it behaves as a Newtonian fluid having a very low yield strength (Dell'Ertole and Schellart, 2013), as is the case for halite at geological time and space scales. The blend of sand and polymer was used to simulate a less effective décollement because it reproduces a

frictionless behavior but has a viscosity that is high enough to prevent its flow during the experiments. Following previous works (Callot et al., 2012; Cartwright et al., 2012; Ferrer et al., 2017), we used two mixtures with different weight proportions: 50% white silica sand and 50% pink polymer; and 30% black silica sand and 70% pink polymer (**Table 4.2**).

Nature			Experiment			Ratio	
Material	*Density*	*Viscosity*	*Material*	*Density*	*Viscosity*	*Density*	*Viscosity*
siliciclastics	2250-2750 kg m^{-3}*	—	pure silica sand	1400 kg m^{-3}	—	0.62-0.51	—
salt	2150-2350 kg m^{-3}*	5 x 10^{18} Pa s*	pure polymer (Rhodia Rhodosil GUM FM)	970 kg m^{-3}	0.74 x 10^{4} Pa s	0.45-0.41	1.5 x 10^{-15}
coals and lacustrine mudstones	1400-2250 kg m^{-3}**	Unknown	mixture of sand and polymer (50%/50% in weight)	1390 kg m^{-3}	1.80 x 10^{4} Pa s	0.99-0.62	Unknown
coal	1340-1400 kg m^{-3}**	Unknown	mixture of sand and polymer (70%/30% in weight)	1170 kg m^{-3}	1.05 x 10^{4} Pa s	0.87-0.84	Unknown

TABLE 4.2. Scaling parameters used in the experimental program. *Values from Guo et al., 2016. **Values from Lv et al., 2016.

4.2.2. Scaling

The material properties as well as the size of the models and the thickness of the deposited layers can be considered reasonably scaled compared to nature (Hubbert, 1937; Goncharov, 2010). Our model-to-nature size scaling ratios (**Table 4.2**) are similar to those used in other experiments analyzing the mechanical behavior of upper crustal rocks with interlayered weak layers (Cotton and Koyi, 2000; Costa and Vendeville, 2002; Ferrer et al., 2017).

In relation to the experiment kinematics and mechanics, a model-to-prototype ratio for stress $\sigma^* = 2.7 \cdot 10^{-6} – 6.6 \cdot 10^{-6}$ is obtained from:

$$\sigma^* = \rho^* \cdot g^* \cdot L^*,$$

where ρ^*, g^*, and L^* are the scaling ratios for density, gravity acceleration, and length, respectively, with $\rho^* = 0.41\text{-}0.99$ (**Table 4.2**), $g^* = 1$, and $L^* = 6.67 \cdot 10^{-6}$. The density ratio ρ^* is the average of density ratios for the sand, the polymer and the blend of sand and polymer that range from 0.41 to 0.99, being slightly higher in the sand/silicone mixtures (**Table 4.2**).

From σ^* and the viscosity ratio of the pure polymer η^*, the strain-rate ratio $\dot{\varepsilon}^*$ can be calculated as:

$$\dot{\varepsilon}^* = \sigma^* / \eta^* = 2.1 \cdot 10^{9}.$$

The time ratio t*, which is the inverse of Ɛ*, is $4.76 \cdot 10^{-10}$, meaning that one hour in the experiments represents about 240,000 years in nature. Our experiments lasted 45 hours, which equals 10.8 My of geological time. Finally, considering the shortening-rate ratio, the scaling ratio for velocities V* is

$V^* = Ɛ^* \cdot L^* = 13.8 \cdot 10^3$.

The shortening rate in our models was 0.6 cm/h, equivalent to 3.8 mm/y in nature, and the total shortening was 27 cm (40.5 km in nature).

4.2.3 Setup and procedure

The deformation rig was progressively filled by a prekinematic sand wedge with three packages separated by angular unconformities (**Figs. 4.2 and 4.3**). The lower package simulated the Paleozoic basement rocks. It consisted of a wedge with a taper angle of 2.2º formed by 3 mm-thick white and brown silica sand layers (**Fig. 4.2**) that were tilted 2.2º towards the mobile wall and leveled by a horizontal erosive surface (**Table 4.1** and lateral views of **Fig. 4.3**).

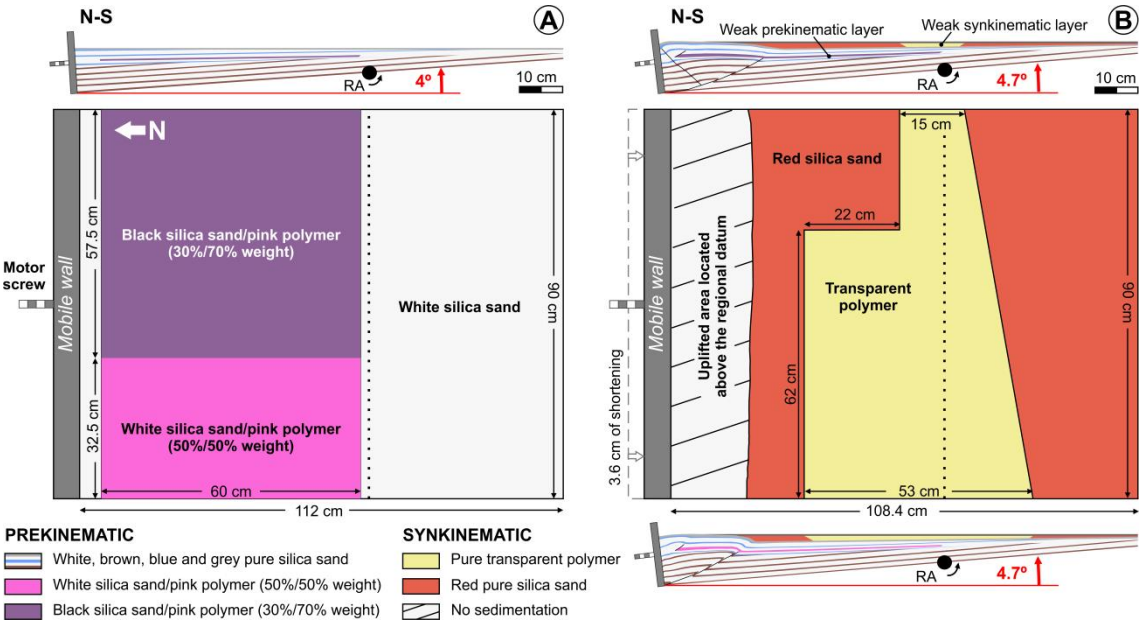

FIGURE 4.3. A: Lateral view of the entire prekinematic set-up configuration and top view of the prekinematic weak layer configuration (lacustrine mudstones and coal analogue). **B:** Lateral views and top view of the experiment at the end of the deposition of the first synkinematic layer (salt analogue). RA and black dotted line: location of the baseboard rotation axis; Red arrows and texts: sense and amount of baseboard rotation.

Overlying this surface, the intermediate package mimics the gradual northward thickening of the Permian-Mesozoic rocks in the Kuqa belt with leveled blue and white sand layers (**Figs. 4.2 and 4.3, Table 4.1**). The exception layer, with a constant 3 mm thickness, was located in the lower part of the package and simulated the Upper Triassic-Lower Jurassic décollement (coal and lacustrine mudstones) and its lateral coarser-grained detrital equivalent. They were modelled by mixed colored silica sand and polymer and white silica sand, respectively. The decollement was 60 cm wide and was separated by 5 cm from the mobile wall (**Fig. 4.3A, Table 4.1**). The proportion of silica sand and polymer changed laterally from a wider, eastern portion with 70% polymer to a narrower, western portion with only 50% polymer (**Fig. 4.3A**). The increase of sand in the blend produces an increase in the viscosity of the analogue material that simulates the westwards decrease in the effectiveness of the Triassic-Jurassic décollement in the Kuqa fold-and-thrust belt (see comments in section 3.4).

After the construction of the intermediate package, the models were tilted 0.6º northwards and leveled (**Table 4.1**), producing a low angle unconformity similar to the one observed at the base of the Lower Cretaceous Bashijiqike Fm. in the Kuqa fold-and-thrust belt (**Fig. 4.2**). This was covered by a constant thickness (3 mm thick) layer of pure grey sand representing the uppermost prekinematic package (Bashijiqike Fm.).

Once the prekinematic wedge was built, the four models were shortened by pushing the northern wall of the rig with a motor-driven worm screw (**Fig. 4.3**). The wall moved to the south a total of 270 mm at a constant velocity of 6 mm/h and shortening was accompanied by tilting of the models in the opposite direction (i.e. to the North) to reproduce foreland flexure of the foredeep. The taper angle of the synkinematic succession in the Kuqa fold-and-thrust belt is about 2.5-4.5º (**Fig. 3.46**); the equivalent tilting was 3.3º in our experiments (**Table 4.1**), which entailed a tilting rate of 0.2º for each 18 mm of shortening.

Shortening and coeval tilting were accompanied by the deposition of synkinematic layers. The first syn-kinematic layer, simulating the Eocene-Oligocene salt and detrital lateral equivalents, was added after 3.6 cm of shortening, when the model topography and equivalent shortening were similar to those inferred at the time the salt was deposited in the Kuqa fold-and-thrust belt (Izquierdo-Llavall et al., 2018). Salt and its detrital equivalents were modeled by transparent polymer and red silica sand respectively. The polymer distribution was polygonal to mimic the areal extent of the salt in the Kuqa Basin (**Figs. 4.1B and 4.3**), with the sand around it representing the laterally equivalent siliciclastic rocks. The polymer body

included an interbedded 1 mm-thick yellow silica sand layer, located 0.4 cm beneath the top, to reproduce the real stratigraphy of the Kuqa evaporite sequence (**Fig. 4.2**). Once the surface of the polymer was totally horizontal, it was covered by a 3 mm thick layer of white sand (**Fig. 4.2 and Table 4.1**).

In model A, no more sand was added after this white sand layer just above the silicone. In the other three models, this layer was totally or partially covered by 13 layers of red and white silica sand whose thickness varied in the different models. They were added after each 1.8 cm of shortening (0.2º tilting) until the end of the experiment. These layers simulated continuous synkinematic deposition and their thickness was determined by the wedge deformation, the progressive baseboard tilting, and the position of the regional datum. A different datum rise value was used to define the top of each synkinematic layer (+1, +2 and +3 mm for models B, C, and D, respectively; **Table 4.1**), generating an increasing regional sedimentation rate from model A to D. Finally, the models were covered by postkinematic dry sand, preserved, and sliced into closely spaced vertical serial sections (3 mm thick).

4.2.4. Model analysis procedure

The evolution of the experiments was documented and subsequently analyzed by means of lateral, oblique, and overhead time-lapse photographs taken every 2 minutes. In addition, scans of the model topography using a submillimeter resolution white light scanner (SidioPro from Nub3D) were performed after construction of the prekinematic wedge and subsequently after every 1.8 cm of shortening, prior and after deposition of each synkinematic layer.

In order to reconstruct and analyze the final structure of the model, the vertical sections cut at the end of each experiment were also photographed using high-resolution digital cameras. These photographs were used to reconstruct 3D virtual volumes of the experiments and the generation of key horizons (i.e., base and top of the weak layers) with Move 2015.2 software from Midland Valley.

4.3. EXPERIMENTAL RESULTS

In all four experiments, the contractional deformation was similar up to deposition of the first syn-kinematic layer after 3.6 cm of shortening. After an initial horizontal porosity

reduction of the sand by layer-parallel shortening, the prekinematic package was deformed by one or two 23-26º dipping forethrusts pinned at the base of the mobile wall and subsequently by a steeper minor backthrust that branched off the lower forethrust (upper lateral view of **Fig. 4.3B**). During displacement of the deep thrusts, the overburden of the prekinematic weak layer was deformed by fault-propagation folds above the thrust pin lines and smaller forethrusts and detachment anticlines at the hinterland and foreland weak layer pinch-outs (**Figs. 4.3 and 4.4**).

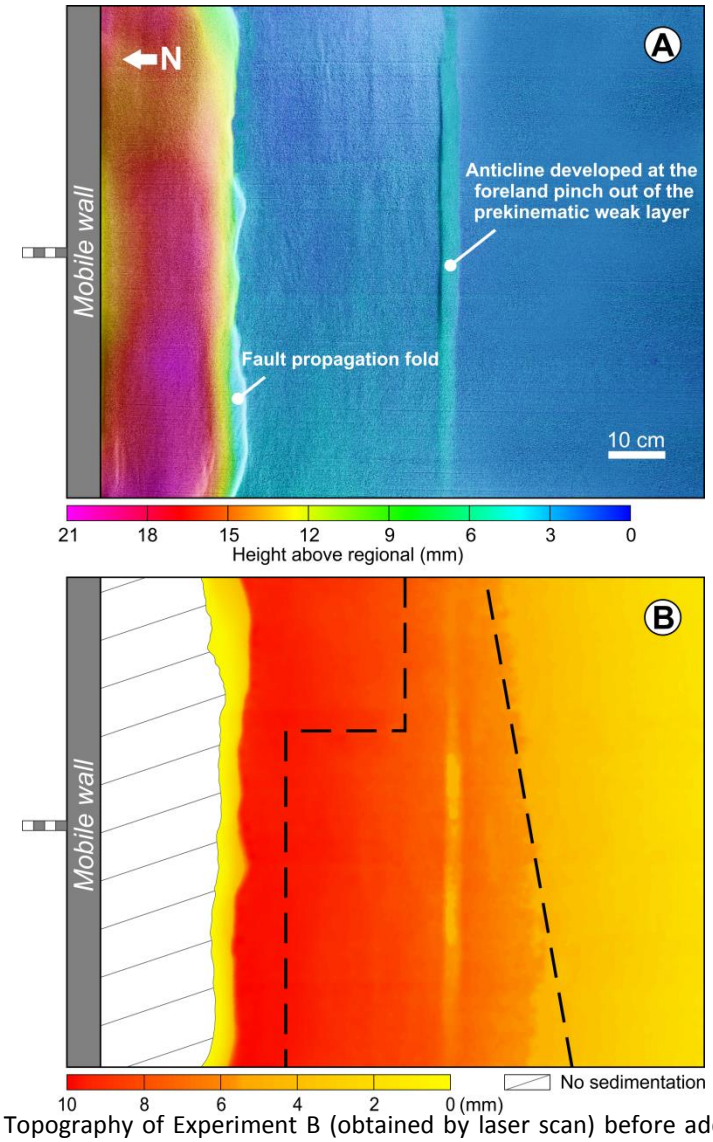

FIGURE 4.4. A: Topography of Experiment B (obtained by laser scan) before addition of the first synkinematic layer. **B:** Isopach map of the first synkinematic layer with the boundaries of the pure polymer body (black dashed lines).

During this stage, the lateral changes in the mechanical stratigraphy (composition) of the weak layer did not appear to affect significantly the deformation. The structures were consistent along the length of the experiments, except that the height of the anticline formed

at the foreland pinch-out was slightly lower above the sand/polymer mixture with a larger proportion of sand (western part of the experiments; **Fig. 4.4A**).

The initial contractional wedge structure was partially covered by the first synkinematic layer (**Fig. 4.4B**). Afterwards, in all four experiments, ongoing shortening resulted in the growth of a contractional wedge with: an inner, thick-skinned domain where the entire package thickened by thrusts detached on the experiment baseboard; and an outer, thin-skinned domain in which the contractional deformation was restricted to a fold-and-thrust system detached on the polymer layers (**Figs. 4.5, 4.6, 4.7**). Thus, they generated a structural zonation similar to that observed in any orogen with cover décollements (Zagros, southern Canadian Rockies, Pyrenees, eastern Alps, and of course the Kuqa Basin), in which there is a hinterland stack of basement-involved thrusts and a foreland system of folds and thrusts detached on syn- or prekinematic décollements over undeformed basement (Bally et al., 1966; Muñoz, 1992; Molinaro et al., 2005; Lammerer et al., 2008; Vergés et al., 2011; Wang et al., 2011). Having said that, the geometry and kinematics of the inner and outer domains were not equal in the four experiments, which showed some significant differences that are outlined below.

4.3.1. Experiment without additional synkinematic sedimentation (Experiment A)

INNER THICK-SKINNED DOMAIN

The inner thick-skinned wedge formed by the stacking of several thrusts dipping 14-26º towards the hinterland. They were detached on the baseboard of the experimental apparatus. Where the prekinematic layer was weaker (east), a duplex formed with a roof in the weak layer; in contrast, where this layer was a less effective décollement (west), the thrusts cut the prekinematic weak layer (**Fig. 4.5B**).

The lateral change in weak-layer effectiveness also influenced the number and maximum displacements of the thrusts. In particular, more thrusts with smaller individual displacement developed where the prekinematic weak layer had a higher polymer proportion and was thus more effective as a décollement (**Figs. 4.5 and 4.8**). Correspondingly, the inner-domain taper was broader, lower, and gentler where the prekinematic layer was stronger: taking the top of the pre-kinematic package as reference level, the forelimb of the thrust stack dipped 32º in this area but 40º where the layer was weaker (**Fig. 4.5B**).

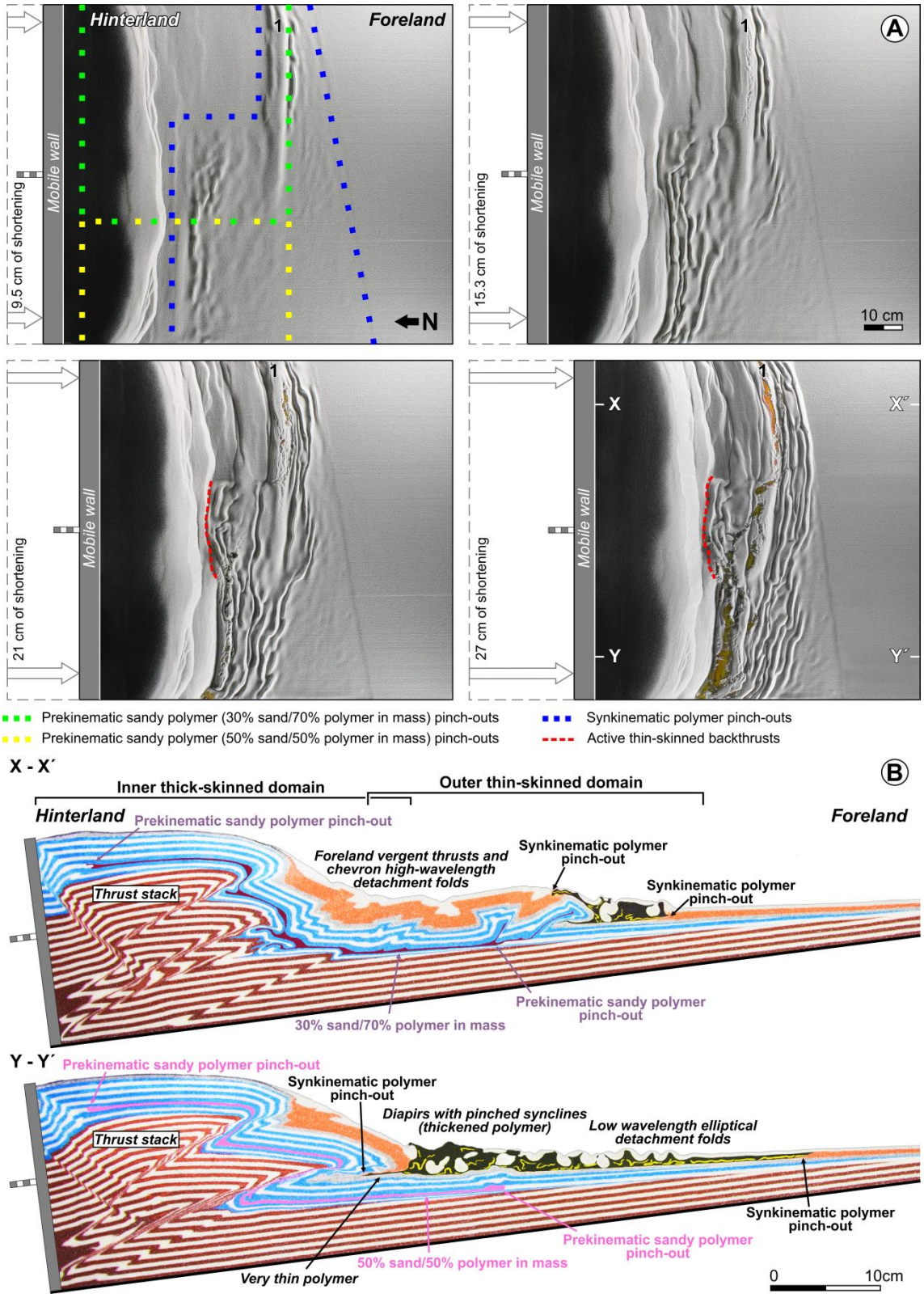

FIGURE 4.5. A: Sequential top views of Experiment A showing the locations of the boundaries of both décollements and the active thin-skinned thrusts and folds. **B:** Cross-sections of

Experiment A at the end of compression (27 cm shortening), see locations in the equivalent top view in **Fig. 4.5A**.

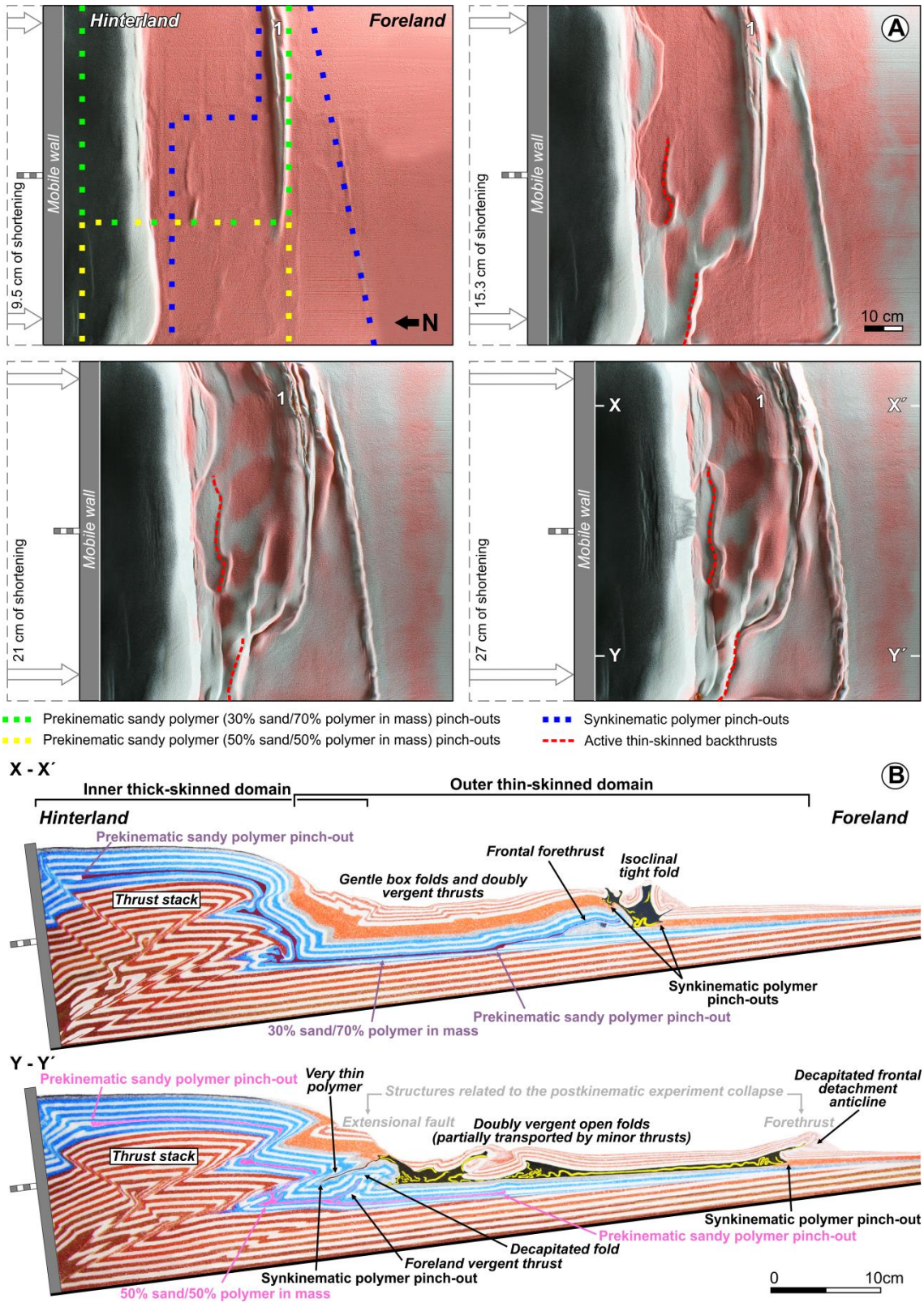

FIGURE 4.6. A: Sequential top views of Experiment B showing the locations of the boundaries of both décollements and the active thin-skinned thrusts and folds. **B:** Cross-sections of

Experiment B at the end of compression (27 cm shortening), see locations in the equivalent top view in **Fig. 4.6A**.

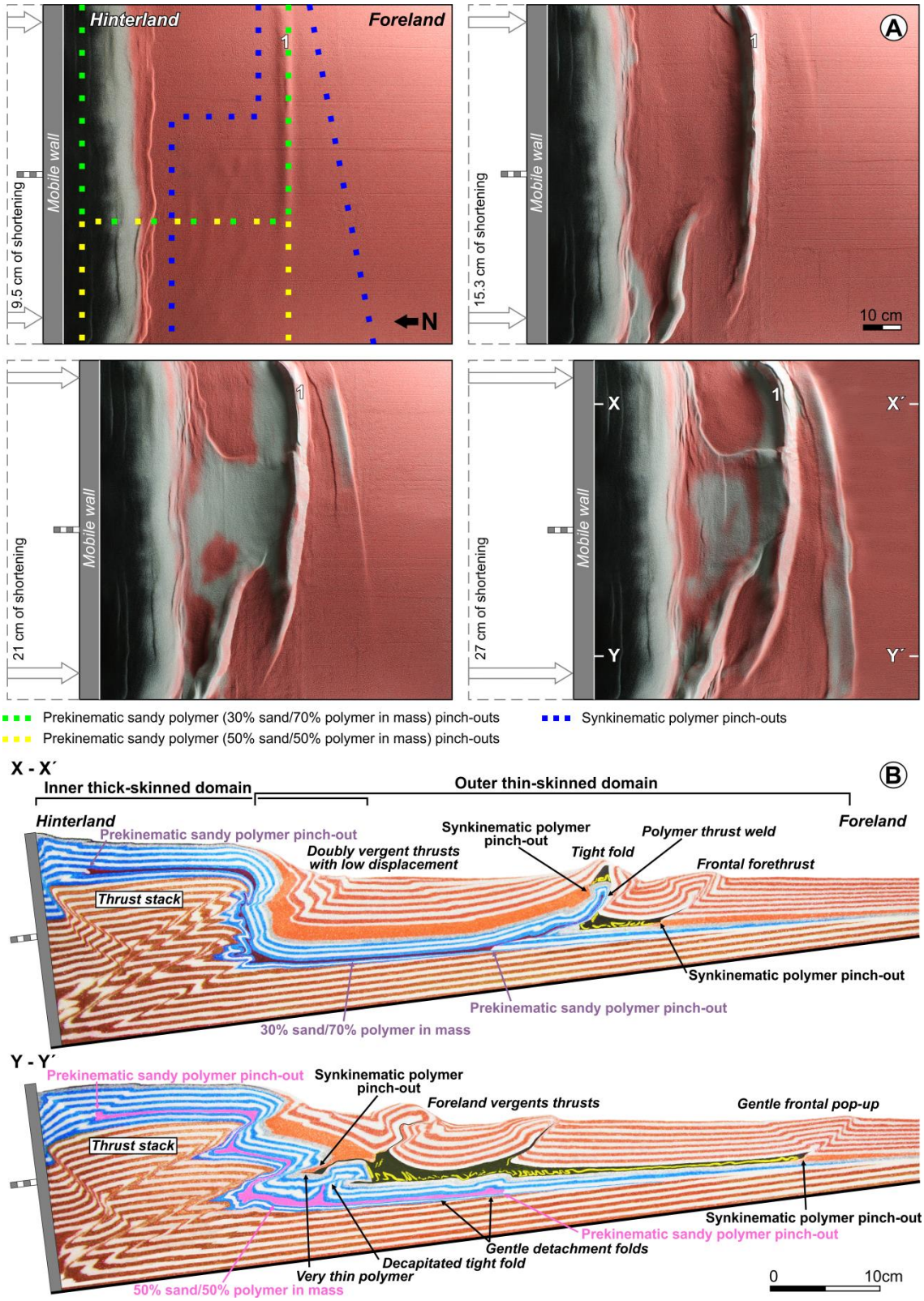

FIGURE 4.7. A: Sequential top views of Experiment D showing the locations of the boundaries of both décollements and the active thin-skinned thrusts and folds. **B:** Cross-sections of

Experiment D at the end of compression (27 cm shortening), see locations in the equivalent top view in **Fig. 4.7A**.

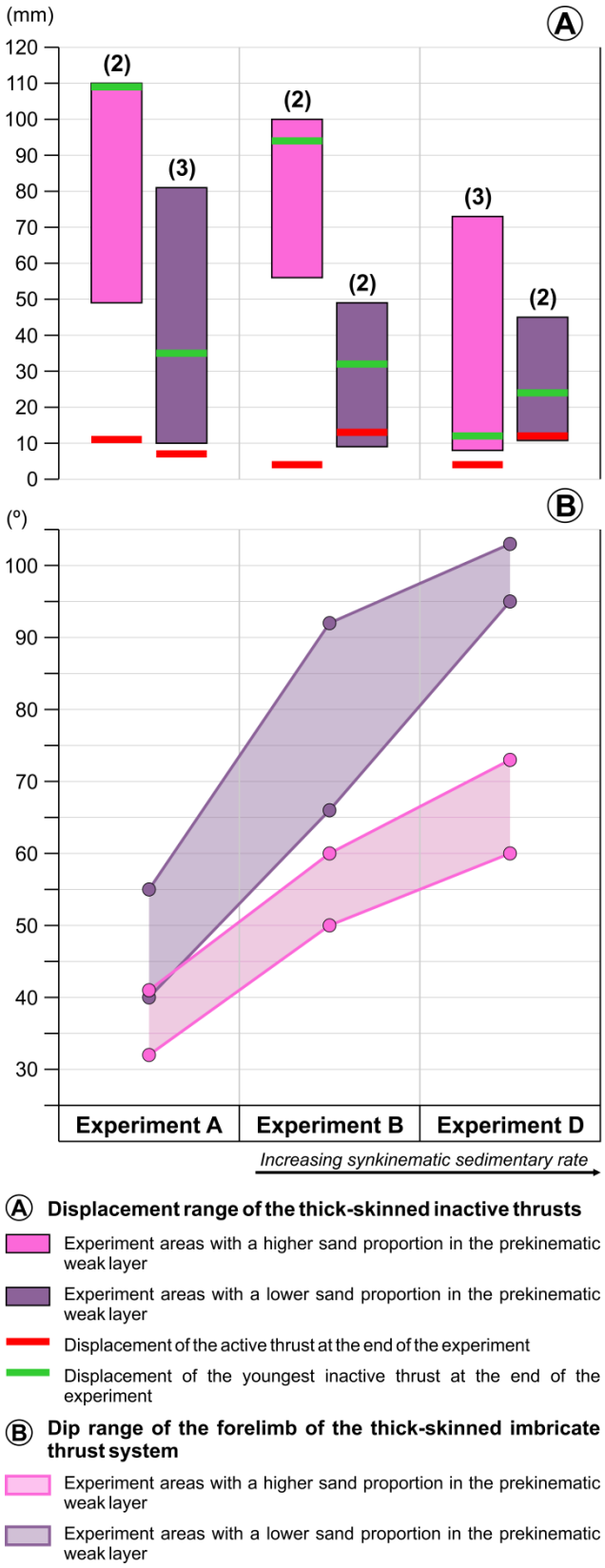

FIGURE 4.8. A: Displacement range of the thick-skinned inactive thrusts at the end of shortening. The horizontal axis indicates the model (A, B, and D) and the vertical axis

represents displacement (in mm). **B:** Dip range of the forelimb of the thick-skinned imbricate thrust system at the end of shortening. The horizontal axis indicates the model (A, B, and D) and the vertical axis represents dip range (in º).

The deformation kinematics of the inner domain was characterized by late-stage development of backthrusts branching off the forethrusts. These backthrusts cut and shifted the overlying thrusts (**Fig. 4.5B**), thereby indicating wedge growth by emplacement of the forethrusts in a piggy-back (foreland-propagating) sequence.

OUTER THIN-SKINNED DOMAIN

A fold-and-thrust system developed detached at the prekinematic sand/polymer mixture and/or the synkinematic pure polymer layer. The structure and kinematics of this thinner contractional wedge was controlled by: 1) the areal distribution of the weak layers; and 2) the lateral change in efficiency of the deeper layer (**Fig. 4.5A**). Only the areas in which the prekinematic weak layer had a higher polymer proportion did it continue to act as an effective décollement. Thus, the prekinematic sediments of the outer thin-skinned domain were only involved in the deformation in the eastern part of the thin-skinned fold-and-thrust system (**Fig. 4.5**, section X-X'); to the west, shortening was detached at the higher, synkinematic weak layer (**Fig. 4.5**, section Y-Y'). As a result, the style and kinematics of the contractional deformation above these two décollements was significantly different in each region.

To the east, where the prekinematic décollement was more effective, box folds and forethrusts detached on this layer. Box folds initially grew at or near the foreland pinch-out of the weak layer (**Fig. 4.5A**); as shortening progressed, they were cut and transported by forethrusts emanating from their cores. Motion on these thrusts was accompanied by the formation of thrusts and folds that grew in a break-back sequence. Deformation of the prekinematic sandy polymer and its overburden always took place in front of the toe of the active thick-skinned thrust system. Hindward thin-skinned structures became inactive as they were tilted/uplifted by the foreland-propagating thick-skinned thrusts, and no deformation was transferred to the hinterland pinch-out of the prekinematic weak layer (**Fig. 4.5B**).

Shortening developed over the synkinematic weak layer had a completely different style and was decoupled from any deeper structures. The synkinematic overburden formed symmetric upright detachment folds with smaller amplitude and wavelength than those above

the prekinematic weak layer. Most of these evolved through time into pinched synclines between diapirs where the polymer broke through anticline hinges (**Fig. 4.5B**, section Y-Y'). The amount of extruded polymer was controlled by the initial thickness of the source layer which, being thicker toward the hinterland, resulted in encasement of the pinched synclines.

Shortening above the synkinematic décollement started near its hinterland pinch-out and propagated toward the foreland. To the west, where the prekinematic layer was stronger, the frontal thick-skinned thrust merged upward with the hindward edge of the shallow décollement; to the east, however, it was the frontal thin-skinned thrust developed above the deeper weak level that merged upward with the shallow décollement (**Fig. 4.5B**). In the latter case, the frontal structure detached at the deep level folded the hindward portion of the shallow polymer layer, above which a backthrust developed at the hindward pinch-out (**Fig. 4.5B**, section X-X'). Eventually the deformation front reached the foreland pinch-out of the shallow polymer, after which the contractional front remained fixed.

The deformation kinematics did not develop similarly along the strike of the model. As stated before, the localization of the active deformation front (defined from the structures observed in sequential photographs) was strongly controlled by the degree of efficiency of the prekinematic weak layer as a décollement. Thus, it was located from the beginning in a more foreland position in the eastern part of the experiment, where the prekinematic weak layer was more effective (structure number 1 in **Fig. 4.5A**). Hence, the deformation front above the pure polymer layer was shifted gradually but significantly over the boundary between the two sand/polymer mixtures. As shortening increased and deformation stacked at the foreland pinch-out of the shallow décollement in the east, the lateral shift progressively diminished until it was negligible at the end of the experiment (**Fig. 4.5A**). During this evolution, the shifting of the deformation front was gradual along a soft transfer zone in which the folds detached at the prekinematic weak layer lost amplitude and eventually died out toward the west. The structures detached over the synkinematic décollement form perpendicular to the shortening direction until deformation reaches the foreland pinch-out (**Fig. 4.5A**). When this happens, the foreland pinch-out is activated and the frontal structure become parallel to the edge of the pure polymer.

It is worth mentioning the intra-polymer deformation recorded by the yellow sandy marker. In general, it was characterized by broken pieces with tight isoclinal folds without a dominant vergence. Moreover, it was slightly thickened in the anticline cores and close to the

thick-skinned thrust front, and thinned without apparent horizontal shearing in the synclines (**Fig. 4.5B**).

4.3.2. Experiments with continuous synkinematic sedimentation

Synkinematic sedimentation was incorporated into the next set of experiments, with the deposition rate increasing from experiments B to D. Only those with the lowest and highest rates (experiments B and D) will be described below. Experiment C will not be explained in this section since its results match those derived from analysis of the other two. However, it will be displayed in a later section because it best mimics the geometries seen in the Kuqa Basin.

4.3.2.1. *Low sedimentation rate (Experiment B)*

In this synorogenic depositional scenario, shortening triggered the formation of a contractional wedge similar to that of experiment A but with some differences in external shape and internal structure that were significantly greater in the outer than in the inner domain (**Fig. 4.6B**). Synkinematic sedimentation did not modify the deformation style and kinematics of the inner thick-skinned domain; instead, it produced only a decrease in the displacements of the middle and lower (younger) forethrusts and, as a result, a steepening of the dip of the thrust wedge forelimb (**Figs. 4.6B and 4.8**). Conversely, in the outer thin-skinned domain, synkinematic sedimentation not only modified the wedge shape and thrust displacements but also induced substantial changes in the distribution of structures and the deformation style above both the prekinematic and synkinematic weak layers.

Two changes are related to structures developed above the deeper, prekinematic décollement. First, there was more hinterland deformation to the west, where the layer was stronger, compared to what was observed in Experiment A. A new forethrust evolved from an asymmetric anticline detached at that level and was truncated by a near-horizontal splay of the overlying thick-skinned thrust (**Fig. 4.6B**, section Y-Y'). Thus, it was a relatively old structure that predated development of this thick-skinned thrust. Second, the distribution of structures also changed significantly to the east, where the décollement was weaker (**Fig. 4.6B**, section X-X'). Almost all shortening transferred to the forethrust developed at the foreland pinch-out and small amount of internal deformation occurred in the overburden of the prekinematic weak layer. Thus, most of the detachment folds and thrusts of experiment A did not develop.

Moreover, the displacement on this frontal thrust increased considerably from 2 to 9 cm (compare sections X-X' in **Figs. 4.5B and 4.6B**).

Deformation above the overlying synkinematic polymer layer was modified in a similar way by progressive synkinematic sedimentation. Contractional structures were concentrated at the pinch-outs of this décollement, resulting in a wide, flat-bottomed syncline (**Fig. 4.6**, top images and section Y-Y'). Moreover, the deformation front migrated very quickly to the foreland pinch-out of the pure polymer (**Fig. 4.6**, top images and section Y-Y'); in contrast, without synkinematic sedimentation deformation migrated slowly forwards and effectively never reached this location in the western part of the experiment (compare with **Fig. 4.5**, top images and section Y-Y').

Another difference is that in the western parts of the experiment, the detachment folds were no longer upright and isoclinal, with a roughly constant wavelength, as they were in Experiment A. Instead, they were larger but narrow open anticlines separated by broad flat-bottomed synclines, with the anticlines slightly truncated and partially transported by small thrusts directed predominantly toward the foreland (**Fig. 4.6B**, section Y-Y'). Conversely, the folds to the east, although still larger than in Experiment A, were tight and isoclinal with local development of passive diapirs (**Fig. 4.6B**, section X-X').

The western parts of the experiment were affected by late gravitational collapse induced by addition of the postkinematic sand package that commenced at the rear of the contractional wedge. This extensional collapse, detached at the pure polymer layer, led to the forwards translation of its overburden marked by the formation of an extensional fault located above the uplifted hinterland portion of the polymer and a forethrust at the foreland pinch-out (**Fig. 4.6B**, section Y-Y´). These two faults had practically the same slip (about 3 cm), suggesting that the entire overburden was passively transported without noticeable internal deformation. This allowed us to reconstruct reliably the geometry prior to the collapse and establish that the decoupling between supra- and subpolymer deformation was still significant but less than in experiment A.

The pure polymer was characterized by a general thickening towards its hinterland edge and a thinning beneath synclines (**Fig. 4.5B**). The intra-polymer sandy marker was generally broken into pieces close to the hinterland pinch-out but was practically continuous towards the foreland. Close-inclined and isoclinal-overturned folds with hinterland and

foreland vergence respectively were developed in the anticlines cores that bounded the wide syncline (**Fig. 4.6B**, section Y-Y').

4.3.2.2. H*igh sedimentation rate (Experiment D)*

In this model, with three times the aggradation rate of Experiment B, the structure of the thick-skinned domain did not vary substantially from that with lower sedimentation. The thick-skinned domain continued being a stack of 3-4 forethrusts with high-angle backthrusts branching off their hanging walls. There was a continuation of the changes seen between Experiments A and B: first, the average displacements of the middle to lower forethrusts further diminished until they were equal to or even lower than that of the uppermost (oldest) forethrust; and second, the dip of the thrust-stack forelimb consequently became near-vertical (**Figs. 4.7B and 4.8**).

Major changes in deformation style once again took place in the outer domain. For shortening above the prekinematic décollement, this was especially prominent to the west where there was a lower proportion of polymer (**Fig. 4.7B**, cross-section Y-Y'): 1) instead of the hinterland forethrust formed in experiment B, a tight detachment anticline formed and became decapitated; and 2) more gentle detachment folds formed, with that at the foreland pinch-out increasing its amplitude. These structural changes of decreasing fold amplitude suggest an increase in efficiency of the sandy polymer layer as a décollement. To the east, where the sandy polymer layer had a higher proportion of polymer, the box folds were replaced by foreland directed thrusts at the edge of the thick-skinned thrust stack (**Fig. 4.7B**, section X-X'). Toward the foreland, the overburden was passively transported above the frontal thrust without any significant internal deformation, with the thrust increasing its displacement from 9 to 10.5 cm. The geometry of this frontal thrust also changed: it had no upper flat at the base of the synkinematic polymer, as in previous experiments, but cut up through the overlying sands with a steeper ramp.

The substitution of detachment folds with thrusts also occurred above the synkinematic weak layer, with the exception of the detachment anticline near the eastern segment of its hinterland pinch-out (**Fig. 4.7**, section X-X´). This fold was still present in this experiment but with a lower interlimb angle and without a piercing diapir. Elsewhere, deformation above the shallow décollement was characterized by foreland directed thrusts locally linked with secondary backthrusts. These thrusts were more widely spaced that the

detachment folds of the previous experiments and their locations were controlled by the spatial distribution of both weak layers: one formed at the frontal pinch-out of the synkinematic décollement and another developed above the contractional structure formed at the foreland pinch-out of the underlying prekinematic weak layer (**Fig. 4.7**).

As already described, a frontal structure detached at the deep décollement developed only above the eastern, weaker portion of this layer (structure number 1 in **Fig. 4.5A-4.7A**). Its westward propagation into the area where the deep layer was stronger had a profound influence on the deformation above the shallow, synkinematic décollement that is best see in the top views: in Experiment A, a narrow soft transfer zone developed above the boundary between the stronger and weaker deep level (structure number 1 in **Fig. 4.5A**); in Experiment B, shallow structures trend highly obliquely in the soft transfer zone (structure number 1 in **Fig. 4.6A**); and in Experiment D, with a higher sedimentation rate, there was wide relay of two nearly parallel contractional structures in this area (structure number 1 in **Fig. 4.7A**).

The top views also depict differences in the evolution of the foreland propagation of deformation above the pure polymer. In Experiment A, deformation only reached the foreland pinch-out in the eastern part of the model whereas in Experiment B the frontal structure was already well developed at 15.3 cm of shortening (compare **Figs. 4.5A and 4.6A**). However, in experiment D, more rapid deposition hindered the foreland propagation of deformation above the pure polymer and reached the foreland pinch-out significantly later (compare **Figs. 4.6A and 4.7A** at 15.3 cm of shortening), and became well established across the entire model only by the end of the experiment (**Figs. 4.7A**).

The intra-polymer deformation was quite similar as described in the experiment B. However, it is worth noting that folds showed that there is hindward directed polymer flow in the internal part underneath a forward directed thrust with a displacement of almost 4 cm (**Fig. 4.7**, section Y-Y').

4.4. ANALOGUE MODELLING DISCUSSIONS

Analysis of the roles played by various parameters in fold-and-thrust belts with more than one décollement can be rather difficult. The complex structure and kinematics of these belts makes it difficult to identify systematic trends and patterns. Moreover, both physical experiments and the Kuqa example show that their structure and kinematics is strongly

controlled by the interaction of parameters that work simultaneously but in different ways above each décollement. Hence, before tackling a global analysis of belts with multiple weak horizons, we will discuss the roles played by weak-layer rheology and sedimentation rate in the deformation developed over a single décollement.

4.4.1. Influence of weak-layer rheology on thin- and thick-skinned deformation

As our experimental program shows and as is well known through previous studies (i.e., Bonini, 2003; Luján et al., 2003; Gradmann et al., 2009; Allen and Beaumont, 2012), the viscosity of the weak layer has a strong impact on the structure and kinematics of overlying thin-skinned deformation. Low-viscosity weak layers (i.e., salt in nature and the pure polymer in our experiments) serve as effective décollements with a high degree of decoupling between the underlying and overlying deformation (Bonini, 2003) (**Fig. 4.9**). They also promote the development of detachment folds without a consistent vergence (Davis and Engelder, 1985). Depending on several factors such as the thicknesses of the weak layer and its overburden, but also erosion of anticline crests (Darnault et al., 2016), they can evolve into salt walls as in our experiment A (**Fig. 4.5**).

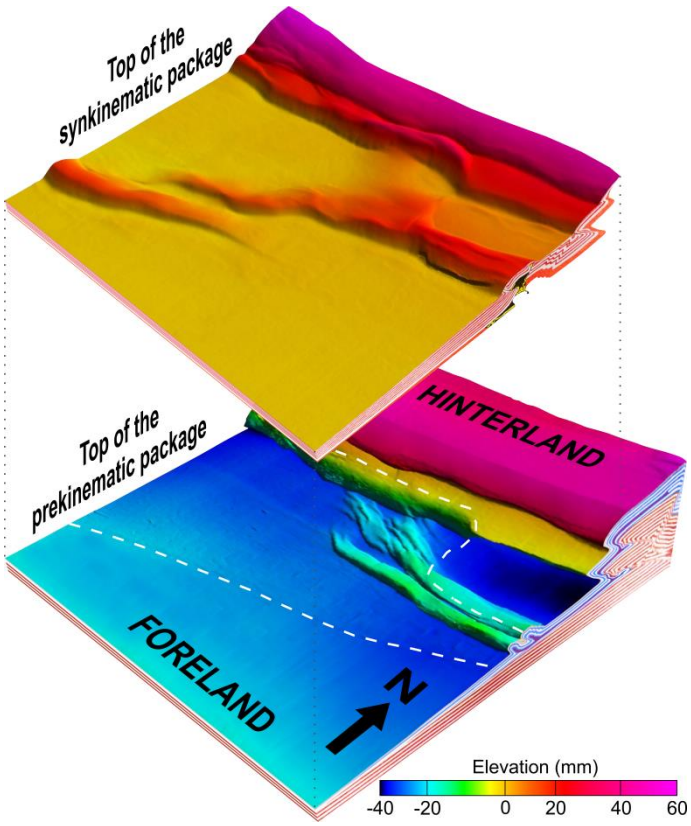

FIGURE 4.9. Oblique view of the top of the pre and synkinematic packages at the end of Experiment C. Note that the deep deformation curves and narrows toward the west, whereas the shallow deformation narrows toward the east. The white dashed line indicates the boundaries of the pure polymer.

This mechanical behavior of the deformation changes with increasing viscosity of the weak layer. As the viscosity increases, the weak layer become less effective as a décollement and the degree of decoupling between deformation of the under- and overlying layers decreases (Bonini, 2003). Thus, the higher-viscosity prekinematic layer (50% sand/50% polymer) was significantly less effective than the 30% sand/70% polymer mixture and even less effective than the pure polymer. Consequently, it manteined coupling much more than in the other two cases (compare sections X-X' and Y-Y' in **Fig. 4.5B**).

On the other hand, the increase of resistance to flow in higher viscosity weak layers means that: 1) it is more difficult to form both detachment folds and diapirs; and 2) the deformation propagates more slowly towards the foreland (Verschuren et al., 1996, Gradmann et al., 2009). For this reason, higher-viscosity décollements promote the formation of thin-skinned thrust systems with a major deformation front located more toward the hinterland than those with lower viscosity. A good example of this is the deformation above the prekinematic weak layer wich: 1) was characterized by foreland-directed thrusts (**Figs. 4.5B, 4.6B and 4.7B**); and 2) a major deformation front located over its foreland pinch-out when the polymer mixture is more effective (30% sand/70% polymer) and the deformation front was shifted towards the hinterland when its effectiveness decreases (50%sand/50% polymer; top of the prekinematic sandpack in **Fig. 4.9**).

Moreover, the prekinematic layer also influences the geometry of the inner thick-skinned domain when it is located above the thrust stack. The inner thick-skinned domain was characterized by an antiformal stack when the prekinematic layer has a low viscosity and becomes an imbricate thrust stack when the viscosity increases (**Fig. 4.10**). As a result, the inner thick-skinned wedge was broader and lower and had a gentler thrust taper angle when the thrust stack was overlain by the high-viscosity weak layer (50% sand/50% polymer; **Fig. 4.10**).

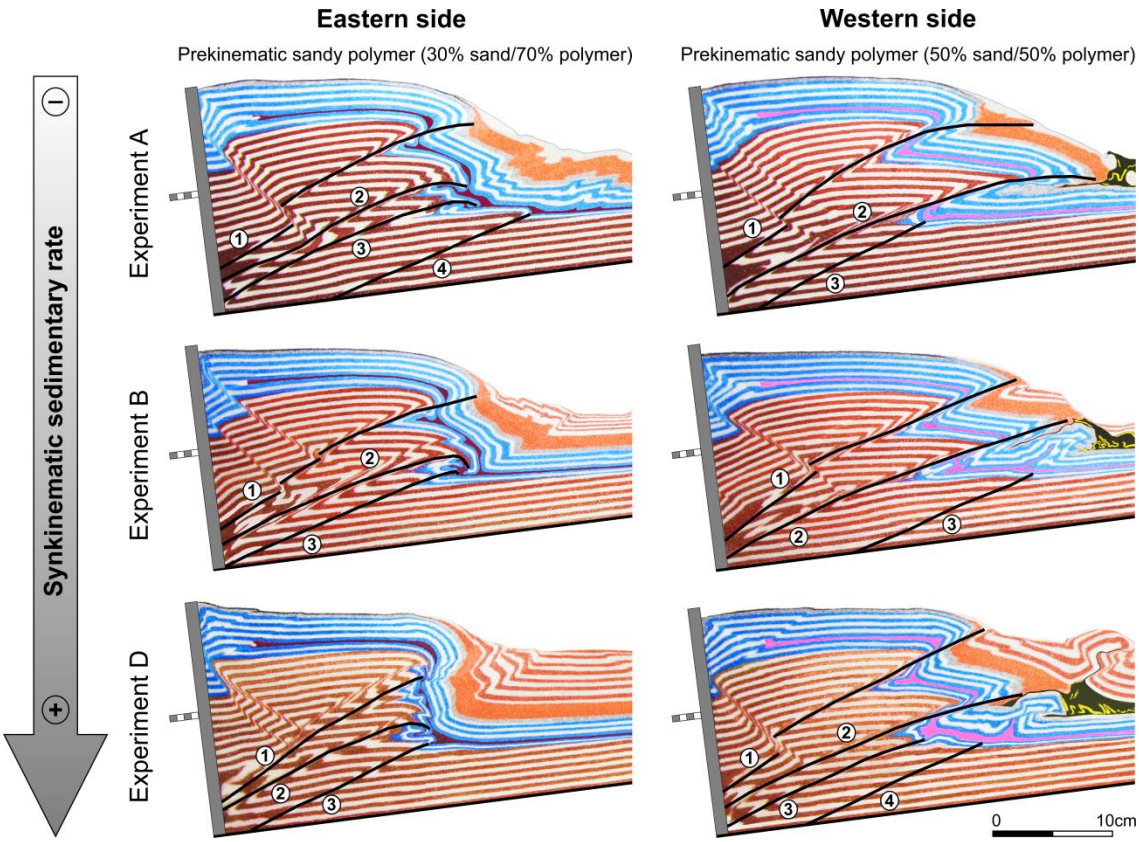

FIGURE 4.10. Geometry of the inner thick-skinned domain varying the syntectonic sedimentary rate. Numbers indicate the sequence of thrust development in each experiment.

4.4.2. Influence of synkinematic sedimentation rate on thin-skinned deformation

Our experimental program setup was designed in order to analyze the influence of the sedimentary load distribution on the structuring of the fold and thrust system when synkinematic sediments display a wedge-shaped geometry. The influence of this distribution on the deformation style and deformation kinematics is discussed below.

4.4.2.1. *Deformation style*

The total thickness of overburden above the décollements, whether pre- or synkinematic, determines the deformation mechanisms and therefore the structural style (Gutscher et al., 1996; Mugnier et al., 1997), including the geometry, size, number, and spacing of the resulting structures (Storti and McClay, 1995; Nalpas et al., 1999; Bonini, 2001; Pichot and Nalpas, 2009; Barrier et al., 2013). In experiments B-D, the overburden thickness was not constant: it was relatively thin and uniform during the early stages of shortening, then progressively increased over the outer thin-skinned contractional belt and adjoining

undeformed areas, but at different rates in each experiment. Consequently, the deformation style changed from one experiment to the next and also, albeit subtly, over time in each one. From this, two main general conclusions can be drawn about the influence of synkinematic sedimentation rate on the style of the deformation above a viscous décollement.

First, an increase in the sedimentation rate, and thus the resultant thicker overburden, leads to a decrease in the number of structures as well as an increase of their size. In particular, as shown in the final cross sections (**Figs. 4.5B, 4.6B and 4.7B**) and in previous studies (Storti and McClay, 1995; Bonnet et al., 2008; Fillon et al, 2013), folds have a longer wavelength and greater amplitude, thrusts sheets are thicker and wider, and both thrusts and folds are more widely spaced. Second, different types of structures develop. If the décollement is sufficiently thick and the overburden is relatively thin, shortening is accommodated by detachment folds (**Fig. 4.5B**). As the overburden thickens, however, deformation is progressively accommodated by thrusting rather than folding (**Fig. 4.7B**).

Both effects of varying synkinematic sedimentation rate described above influence the relationship between supra and subsalt/subpolymer deformation. As mentioned before, the location of the major subsalt deformation front (MSDF) was influenced by along-strike variations of the rheology of the prekinematic weak-layer. However, the relay zone of the MSDF and the deformation style of the overlying suprasalt structures is controlled by synkinematic sedimentation rate (**Fig.4.11**). Increasing synkinematic sedimentary rate there is a progressive change from a short relay zone where suprasalt structures formed parallel to the MSDF and can easily link each other to a long transfer zone where suprasalt structures mantein the same orientation but they are overlapped. In between these two extremes (experiment B), the relay zone showed an intermediate length and suprasalt structures become curved and oblique to the orientation of the MSDF (**Fig. 4.11**).

The geometry of individual folds and thrusts also evolves as the overburden thickens. First, the transition from one to the other is gradual, so that early detachment folds are often cut and transported by thrusts (**Figs. 4.6B and 4.7B**). Also, as shown in previous work (e.g., Baby et al. 1995; Nalpas et al., 1999; Bonnet et al., 2008; Graveleau et al., 2012; Barrier et al., 2013), folds tighten and thrusts become steeper with an increase of overburden thickness/synkinematic sedimentation rate. For example, the frontal thrust formed at the foreland pinch-out of the prekinematic décollement changed from a ramp-flat geometry under low sedimentation rates (**Fig. 4.6B**, section X-X') to a steeper ramp under high sedimentation

rates (**Fig. 4.7B**, section X-X'). Having made these distinctions about the influence of sedimentation rate on structural style, however, it should be kept in mind that similar changes are also influenced by the viscosity and thickness of the weak layer (see previous section).

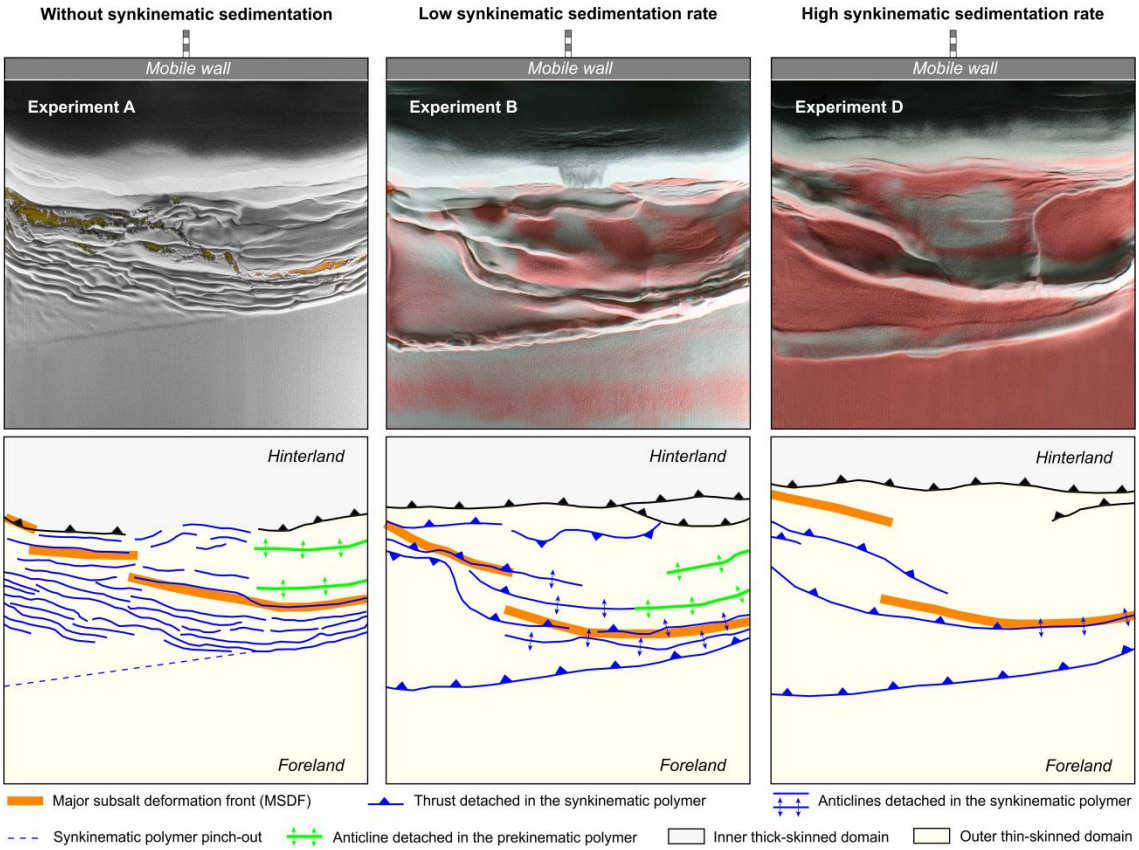

FIGURE 4.11. Plan-view comparison between experiments A, B and D at the end of shortening (top) and their respective structural interpretations showing the suprasalt deformation style in the relay zone of the major subsalt deformation front (bottom).

Even with a similar overburden thickness, thick or thin weak layers favor the development of detachment folds or thrust faults, respectively (Steward, 1996; Nalpas et al., 1999; Costa and Vendeville, 2002).

4.4.2.2. *Deformation kinematics*

The overburden thickness generated by the synkinematic sedimentation rate also determines the deformation kinematics and, in particular, the sequence in which structures develop (Baby et al., 1995; Storti et al., 2000; Bonini, 2001; Stockmal et al., 2007; Bigi et al., 2010; Fillon et al., 2013). In our models, the increase of synkinematic sedimentation rate/overburden thickness results in a modification of the deformation kinematics above the synkinematic weak layer/salt similar to that described in previous works (Beaumont et al.,

1992; Willett, 1999; Simpson, 2006; Fillon et al., 2013): formation of short-wavelength folds progresses slowly towards the foreland when the overburden is thin and the sedimentation rate is negligible (**Figs. 4.5 and 4.12**) but propagates rapidly as the overburden thickens by an increase of sedimentation rate (**Figs. 4.6 and 4.12**). Interestingly, high synkinematic sedimentary rate prevents further growth of these frontal structures and more hinterland structures may be reactivated (**Figs. 4.7B and 4.12**).

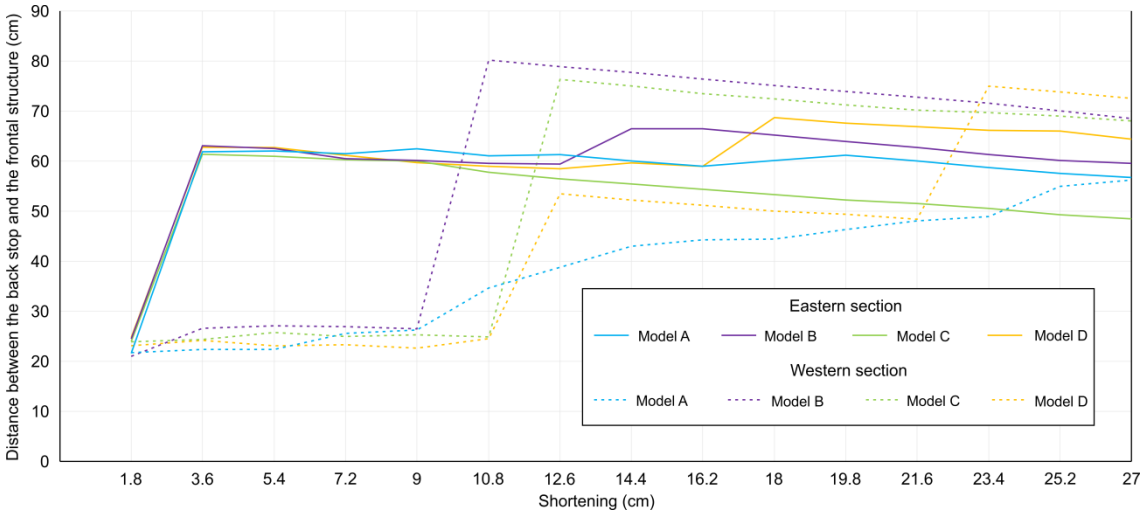

FIGURE 4.12. Frontal structure migration during the experiments. The horizontal axis indicates shortening (in cm) and vertical axis the distance between the backstop and the frontal structure (in cm). Values always taken from the same sections (**Figs. 4.5A – 4.7A and 5.2A, sections X-X' and Y-Y'**).

The geometry and kinematics of contractional wedges developed above weak layers are also influenced by the progressive tilting of the models toward the hinterland. Without synkinematic sedimentation, this tilting results in shorter, thicker, and steeper contractional wedges whose deformation front migrates very slowly forwards (Koyi and Vendeville, 2003). However, synkinematic sedimentation thickens the hinterland wedge, thereby increasing the taper angle in this area and enhancing the forward propagation of the tip of the thrust wedge and thus the deformation front (Smit et al., 2003; Wu et al., 2014). In this sense, the lack of wedge-shaped synkinematic sediments above the outer thin-skinned domain in experiment A would partially explain the slow foreland propagation of the deformation above the pure polymer (**Figs. 4.5 and 4.12**). This propagation was clearly faster in the experiments with synkinematic sedimentation (**Figs. 4.6, 4.7 and 4.12**).

In other words, the addition of synkinematic sediments promotes propagation of the deformation more quickly towards the foreland pinch-out of the salt. However, considering the same taper angle and wedge-shaped configuration for the synkinematic sandpack applied

in our experiments, we noticed that as synkinematic sedimentary rate increases, the vertical thickness gradient decreases and the development of frontal contractional structures is delayed (**Figs. 4.12 and 4.13**).

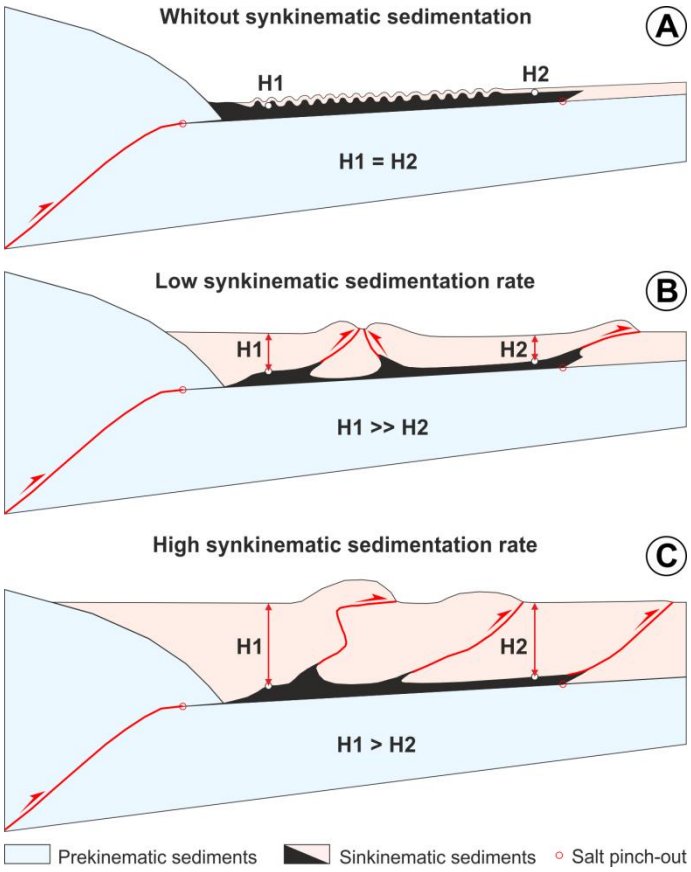

FIGURE 4.13. Relation between synkinematic load distribution and nucleation of thusts at the foreland pinch out of the salt. **A:** Isopach thin overburden does not promote the activation of the foreland salt pinch-out. **B:** Adding synkinematic sediments favours the activation of the frontal structure. **C:** Increasing synkinematic sedimentary rate decreases the pressure head gradient and delays the activation of the foreland salt pinch-out. H: vertical thickness.

4.4.3. Influence of synkinematic sedimentation rate on thick-skinned deformation

The total thickness of the overburden and consequently the synkinematic sedimentation rate also determines the kinematics and geometry of deformation in the pile of thick-skinned thrusts (**Fig. 4.10**). First, it reduces the critical taper angle of the wedge by onlapping its forelimb, and second, it hinders foreland propagation of the deformation because it affects the stress distribution by increasing the load in the foreland and piggy-back basins (Storti and McClay, 1995; Storti et al., 2000). Thus, synkinematic sedimentation slows down or even blocks the piggy-back propagation of thrusting, and new thrusts and backthrusts form ahead the leading frontal structure in order to compensate for the reduction of the taper

angle (Bonini, 2001; Duerto and McClay, 2009). Accordingly, in our experimental program, the higher the synkinematic sedimentation rate/thickness, the smaller the displacement of the younger, lower thick-skinned thrusts will be; as a result, using the top of the prekinematic package as a reference, the wedge of thick-skinned thrusts was narrower and had a steeper forelimb (**Figs. 4.8 and 4.10**).

4.4.4. Suprasalt/subsalt structural relationships

The influence of rheology and sedimentation rate/overburden thickness on the cover deformation is valid for both décollements modeled in our experiments as well as for those of the Kuqa fold-and-thrust belt. Consequently, the structural style and deformation kinematics associated with each is different since, among other factors, the rheology and thickness of the overlying rocks is not the same. In general, disharmonic structures develop, with the degree of decoupling of the two levels depending on several factors. The most common are the strain rate, the viscosity and thickness of each décollement, and the thickness of the overburden above each décollement (Couzens-Schultz et al., 2003; Gestain et al., 2004; Sherkati et al., 2006; Hudec and Jackson, 2011; Borderie et al., 2018).

In our experimental program and in the Kuqa fold-and-thrust belt, the synkinematic décollement is indeed a very effective decoupling layer that separates two frictional layers with different structures and deformation kinematics (**Fig. 4.9**). This might suggest that they work independently, but as shown in our study, the structures developed beneath the synkinematic décollement actually have a strong impact on those above this layer. First, the early-formed thrusts and folds formed above the weaker (eastern) prekinematic décollement controlled to some degree the areal extent of the synkinematic décollement and thus the fold-and-thrust system detached on it. Second, the same early structures generate topographic highs and thus areas of thinner synkinematic salt/polymer (**Fig. 4.4**); these hamper the foreland propagation of shallow deformation in that they act as a barriers that induce the formation of major thrusts and folds (**Fig. 4.7**, section X-X').

A similar effect is produced when the structures above the lower décollement form after sedimentation of the synkinematic salt/polymer. The geometry of these new thrusts in turn has a strong impact on deformation above the upper décollement. Where these thrusts form flats, deformation above the upper décollement consists of detachment folds and thrusts developed over both this flat and the frontal subsalt structure (**Figs. 4.5 and 4.6,** sections X-X').

If, however, they form simple ramps, all deformation above the upper weak layer is accommodated by the formation of a fault-propagation fold (**Fig. 4.7**, section X-X'). The development of subsalt ramps or flats is dependent not only on the rheology and effectiveness of the upper weak layer but also on the synkinematic sedimentation rate. Thus, low to medium synkinematic sedimentation rates promote the formation of sub-polymer staircase-shaped thrusts with an upper flat located in the upper weak layer (**Figs. 4.5 and 4.6**, sections X-X'), and high sedimentation rates favor the formation of higher-angle sub-polymer thrusts that cut the shallow décollement (**Fig. 4.7**, section X-X').

In all cases, the degree of decoupling is partly controlled by the synkinematic sedimentation rate because it is strongly dependent on the difference in thickness of the frictional successions located above and beneath the shallow décollement (Couzens-Schultz et al., 2003; Gestain et al., 2004; Sherkati et al., 2006; Hudec and Jackson, 2011; Borderie et al., 2018).

In the above analysis, the prekinematic décollement is regarded to be continuous, uniformly thick, and tilted slightly toward the hinterland prior to the onset of contractional deformation. In addition, there is no consideration of any preexisting structures. Therefore, the models and discussion address a simple scenario that does not match perfectly with most real cases (i.e, Zagros, Apennines, Pyrenees, and even the Tarim Basin). In this sense, it is evident that any departure from these assumptions would have a strong impact on the subsalt contractional deformation and consequently on the suprasalt structures (Callot et al., 2012; Graveleau et al., 2012; Lewis et al., 2013; Jackson and Hudec, 2017).

4.4.5. Internal deformation of the salt

Our experimental program setup includes a sand marker within the pure polymer/salt in order to examine the evolution of the internal structures. The experiments results show that variations in the synkinematic sedimentation rate/overburden thickness apparently do not induce significant changes in the deformation style of the internal structures. Regardless of what sedimentation rate was applied, the strong layer within the salt was always deformed by asymmetric inclined to recumbent folds of similar wavelength and amplitude (**Figs. 4.5B, 4.6B, 4.7B**). However, it was more disrupted in the experiment without synkinematic sedimentation in which the salt was deformed by detachment folds and diapirs (**Fig. 4.5B**).

Internal deformation of polymer/salt highlights there is salt evacuation underneath the piggy-back basins (**Figs. 4.6B and 4.7B**). Interestingly, there is hindward directed salt flow in the internal parts underneath forward directed thrusts (**Fig. 4.7B**, section Y-Y' and **Fig. 4.14**). In other words, there is a balance between salt flow related to the thrust emplacement and salt evacuation below the piggy-back basins. Contrary that to what was expected and according to the vergence of intrasalt folds in our experiments, salt flow could prevail over salt evacuation even though thrusts show displacements of several cm (3.7 cm) in our experiments which is equivalent to displacements of more than 5 km in the crust (**Fig.4.7B**, section Y-Y' and **Fig. 4.14**).

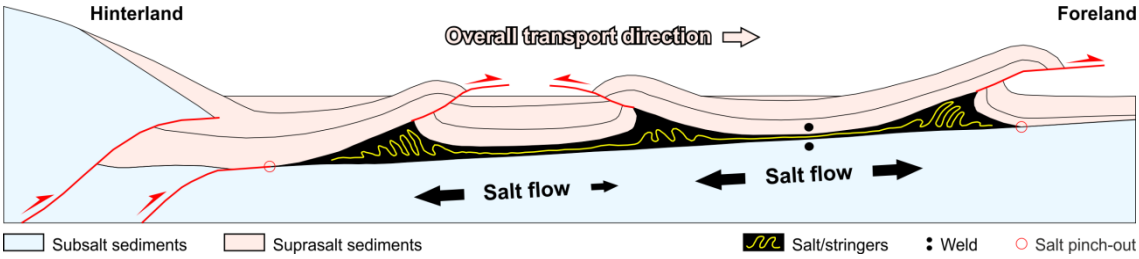

FIGURE 4.14. Conceptual sketch based on experiments B, C and D showing the internal deformation of the salt. Both hindward and foreland-directed salt flow underneath piggy back basins. Note that towards the hinterland salt pinch-out there is hindward directed salt flow below forward directed thrusts.

4.5. ANALOGUE MODELLING CONCLUSIONS

The four 3D experiments realized in this thesis have allowed us to obtain the following conclusions about the role of synkinematic sedimentation rate and décollement rheology in fold-and-thrust belts involving tow décollements: One synkinematic with low viscosity and another located in a deeper position, precinematic with high-viscosity.

With respect to the outer, thin-skinned domain, considering wedge shaped configuration for the synkinematic sandpack applied in our experiments we conclude that:

- Increasing synkinematic sedimentary rate there is a progressive change from distributed shortening with development of several small wavelength and closely spaced structures to fold-and-thrusts systems where deformation is localized into few, longer wavelength fault-related folds located over décollement boundaries.

- The addition of synkinematic sediments promotes propagation of the deformation more quickly towards the foreland pinchout of the salt. However, increasing synkinematic sedimentary rate delays the development of frontal contractional structures and favors the formation and reactivation of more hinterland thrusts and backthrusts.

In addition to influencing the thin-skinned part of the contractional wedge, synkinematic sedimentation and décollement rheology are also predominant factors controlling the shape and deformation style of the hinterland, thick-skinned thrust stack.

- The rheology of the deeper décollement influences the structuring of the inner, thick-skinned domain when the deeper décollement overlies the thrust stack. As viscosity increases, the geometry of the thrust stack changes from an antiformal stack to an imbricate thrust stack. As a result, the inner thick-skinned wedge becomes broader and lower and has a gentler thrust taper angle.

- Higher synkinematic sedimenatation rates and thicknesses result in smaller displacement of the younger (lower) thick-skinned thrusts.

In addition to the different deformation modes above each décollement, the interaction between them results in:

- The distribution of the deformation above the deeper décollement, controlled in part by its thickness and rheology, can generate structures that: first, determine the areal extent of the salt and therefore of any fold-and-thrust system detached on it; and second, hamper or even prevent the progressive foreland propagation of deformation above the salt.

- The degree of decoupling, which is partially dependent on the thickness difference between the overlying and underlying frictional sequences, changes through time as synkinematic sedimentation increases the thickness of the strata above the salt.

- The relay zone of the major subsalt deformation front (MSDF), controlled by synkinematic sedimentation and rheology, determine the geometry of the suprasalt

structures. Increasing the length of the relay zone, the suprasalt deformation change from structures formed parallel to the MSDF that easily link each other, then structures that become curved and oblique to the MSDF, and finally, overlapped structures that form again parallel to the MSDF.

Moreover, regarding the internal deformation of the polymer/salt we can conclude that:

- There is a balance between salt flow related to the thrust emplacement and salt evacuation below the piggy-back basins. Contrary that was expected, the second one could prevail over the first one even though thrusts show kilometric displacements.

CHAPTER 5. DISCUSSION

The experimental study presented in this thesis sheds some light on the influence of various parameters in the structuring of fold-and-thrust belts involving multiple décollements and developed under different synkinematic sedimentary rates. However, the analogue modelling technique present inherent limitations that do not allow a direct application in this regard. Therefore, to enable a better understanding of the processes involved in the structuring of the Kuqa fold-and-thrust belt an integrated analysis is needed. In this context, and considering inherent limitations, this section discusses firstly the structural similarities and differences between our sandbox experiments and the Kuqa fold-and-thrust belt. Then, the main factors controlling the contractional structure and dynamics of the Kuqa fold-and-thrust belt are pointed out, and finally, this section shows the applicability of an integrated structural model and its incidence on the petroleum system characterization.

5.1. COMPARISON WITH THE KUQA FOLD-AND-THRUST BELT

Comparison of our experimental results with the geometries observed in the central and eastern Kuqa fold-and-thrust belt reveal the strongest similarities with Experiment C, i.e., that with a rate of synkinematic sedimentation intermediate between those of Experiments B and D. Final synkinematic thicknesses in experiment C (3.3 cm over the rotation axis) are comparable to those recognized in the hinge zone of the Baicheng Syncline or in the Tarim Basin, to the South of the Qiulitage fold-and-thrust system (7.0 and 5.3 km that would be analogue to 4.6 and 3.5 cm in the models if the applied length scale factor is considered). Below, I discuss the similarities and differences as depicted in top/map and cross-sectional views (**Figs. 5.1 and 5.2**). Note that the western parts of our models correspond to the central part of the Kuqa fold-and-thrust belt, but I will call both the western areas.

There is a noteworthy similarity between the plan-view geometry and spatial arrangement of structures in the Kuqa fold-and-thrust belt and those in Experiment C (**Fig. 5.1**). In both cases, the zone of deformation in the east splits into two belts of structures in the west, with the intervening syncline widening to the west. Moreover, the change of position of the main deformation front, from above the foreland pinch-out of the prekinematic weak layer to that of the shallower weak layer, resulted in a frontal zone with arcuate structures and an overlapping relay.

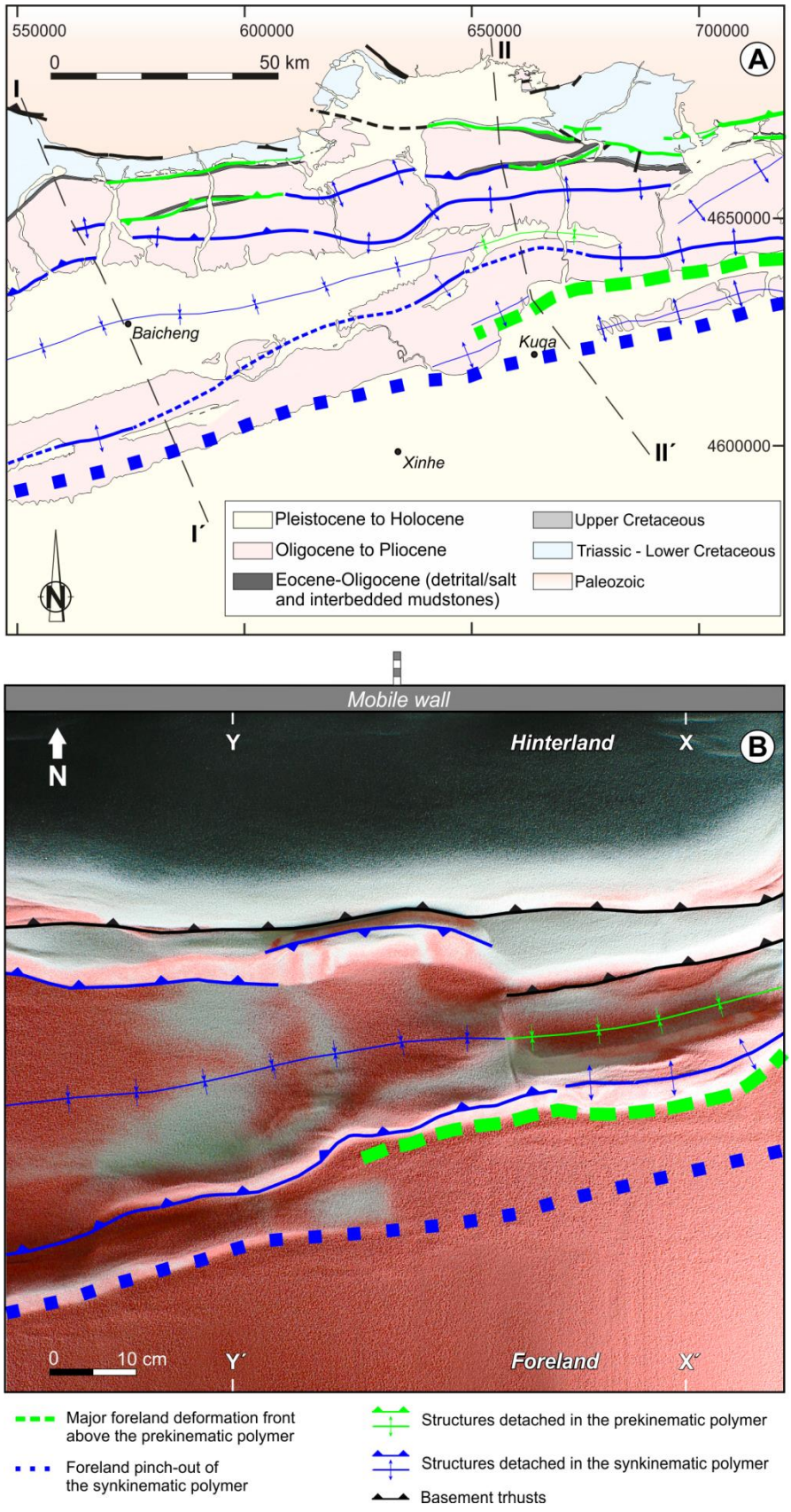

FIGURE 5.1. Plan-view comparison between: **A:** Geological map showing the main structures and deformation fronts of both décollements (modified from Wang et al., 2011; location in **Fig. 4.1**); and **B:** Experiment C at the end of shortening.

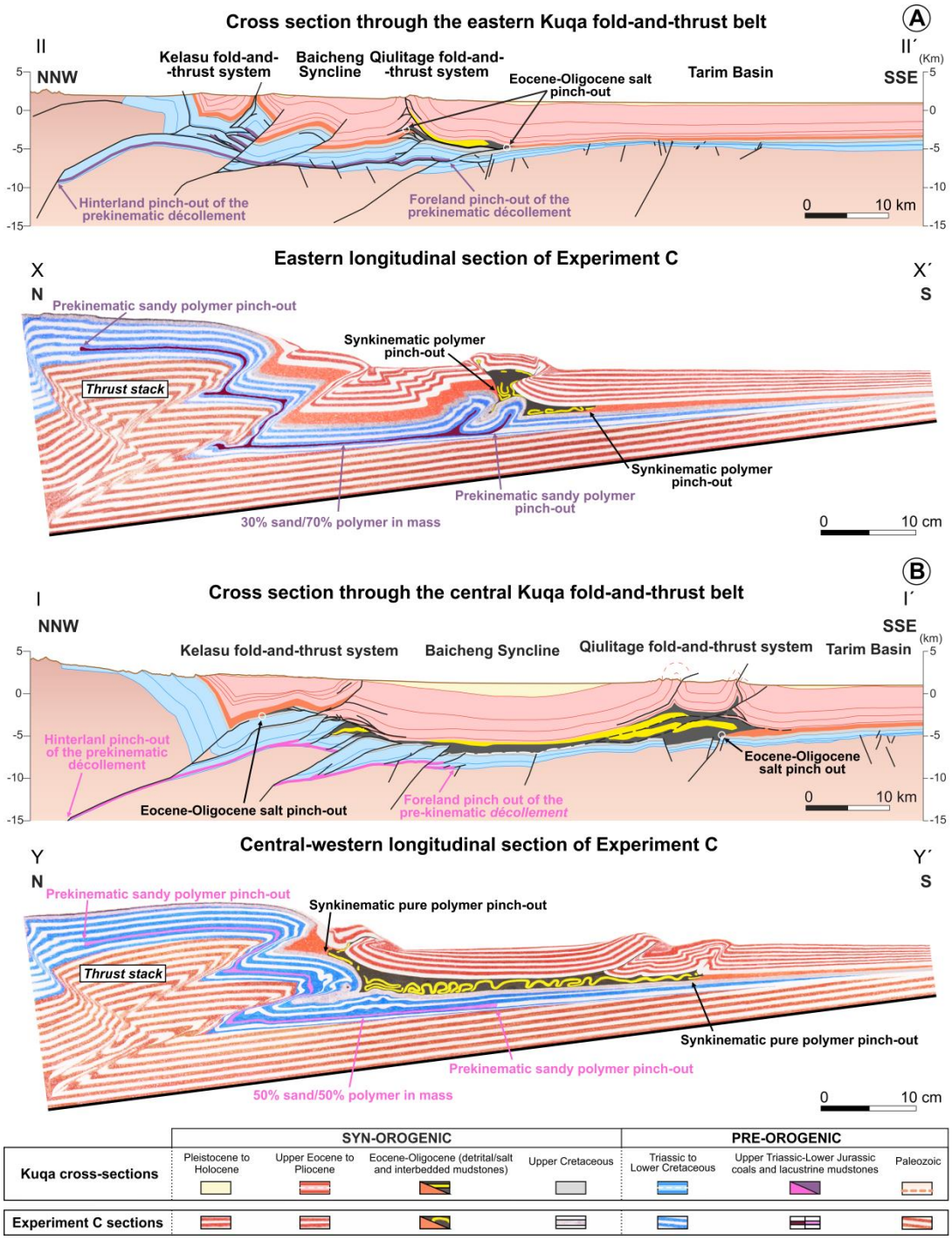

FIGURE 5.2. Comparison of seismic-based sections (top) and model sections of Experiment C (bottom). **A**: Eastern Kuqa fold-and-thrust belt and eastern part of model. **B:** Central Kuqa fold-and-thrust belt and western part of model. See locations in **Fig. 5.1**.

To the west, the salt-detached structures are dominantly vergent towards the foreland and are localized at both salt pinch-outs of the synkinematic layer, with a broad, flat-bottomed syncline in between, just as seen in the model (**Fig. 5.2B**). Beneath the hinterland parts of the salt layer, both the Kuqa fold-and-thrust belt and the model have one major thick-skinned

thrust that deforms the salt and its overlying structures; in its footwall there are minor thin-skinned thrusts detached in the lacustrine mudstones and coals of the prekinematic weak layer that are represented in the model by small folds. To the east, thin-skinned thrusts are better developed in both the coal-detached system and its model equivalent. Above the areally restricted Eocene-Oligocene salt horizon, most deformation is concentrated above the frontal coal-detached thrust (**Fig. 5.2A**).

Comparison of our experimental results with the Kuqa fold-and-trust belt also points out general differences in part related to nonmodeled parameters and sandbox experiments limitations. However, there also differences in geometry and spatial arrangement of structures in top/map and cross-sectional views.

In this sense, regarding the geometry of the inner thick-skinned domain in the Kuqa fold-and-thrust belt, it is constituted by south-directed basement-involved faults defining an antiformal stack (**Fig. 5.2**). These faults connect southwards with a thrust system detached along the lower décollement in Mesozoic strata. In contrast, in our experiments, the inner thick-skinned domain constitutes a thrust stack characterized by a north-directed backthrust and south-directed thrusts cutting the whole synkinematic sequence.

Furthermore, there are also differences in the thin-skinned thrust system detached on the Upper Triassic-Lower Jurassic coal layers. In the Kuqa fold-and-thrust belt, thrusts and backthrusts are generated rather than the detachment folds of our experiments, besides, the number of thrust imbricates is higher (**Fig. 5.2**). On the other hand, to the East of the Kuqa fold-and-thrust belt, deformation is transferred from the structure developed over the foreland pinch-out of the weak prekinematic layer to the foreland pinch-out of the weak synkinematic layer (**Fig. 5.2**) and shallow deformation can propagate southwards as observed in the eastern part of **Fig. 5.1.** In contrast, major thrusts and folds developed over the foreland pinch-out of the precinematic décollement in our experiments. These structures hamper the foreland propagation of shallow deformation acting as a barrier (**Figs 5.1 and 5.2**).

Finally, there are some differences regarding the Eocene-Oligocene salt layer. In the western Kuqa fold-and-thrust belt there is a depletion beneath the Baicheng Syncline and salt inflation in the western Qiulitage frontal structure that was not reproduced in our experiments (**Fig. 5.2**). To the east, the Qiulitage frontal structure is defined by a backthrust whereas in our experiments consist of a major uplifted fold (**Fig. 5.2**). Regarding intrasalt deformation, in the

Kuqa fold-and-thrust belt gentle folds and thrusts preferentially developed whereas intra-polymer deformation in the experiments is characterized by tight, short-wavelength buckle folds (**Fig 5.2**).

5.2. PARAMETERS CONTROLLING THE STRUCTURING OF THE KUQA-FOLD-AND-THRUST BELT

In this section, the observations in both the experiments and the natural analog are integrated and the main parameters controlling the structuring of the Kuqa fold-and-thrust belt are discussed.

5.2.1. Mechanical behavior of the lower décollement

The lower décollement in the Kuqa fold-and-thrust belt is made by coal and lacustrine mudstones within the Upper Triassic-Lower Jurassic sequence. This weak layer has a very high viscosity and very low friction and behaved as the primary décollement and sole thrust of a thin-skinned, piggyback thrust system. This weak layer shows a diminution of its effectiveness as a décollement towards the west due to a decrease of the thickness of the coals and lacustrine mudstones (Li et al., 2004) and/or an increase of the percentage of mudstones with respect to coals and/or an increase of the maturation of the organic layers (Zhao et al., 2005).

The viscosity of the prekinematic weak layer has a strong impact on the structure and kinematics of overlying thin-skinned deformation. The increase of resistance to flow in higher viscosity weak layers means that: 1) it is more difficult to form both detachment folds and diapirs; and 2) the deformation propagates more slowly towards the foreland (Verschuren et al., 1996, Gradmann et al., 2009) (compare models in **Fig. 5.2**). For this reason, higher-viscosity décollements promote the formation of thin-skinned thrust systems with a major deformation front located more toward the hinterland than those with lower viscosity (compare **Figs. 5.3G and 5.3H**). The behavior of the décollements and how they propagate deformation towards the foreland is also, partly controlled, by the thickness of synkinematic units. As shown in the analogue models presented in this thesis, the geometry of the structures detached in the lower décollements strongly depends on the synkinematic sedimentary rate (compare **Figs. 5.3G and 5.3F**).

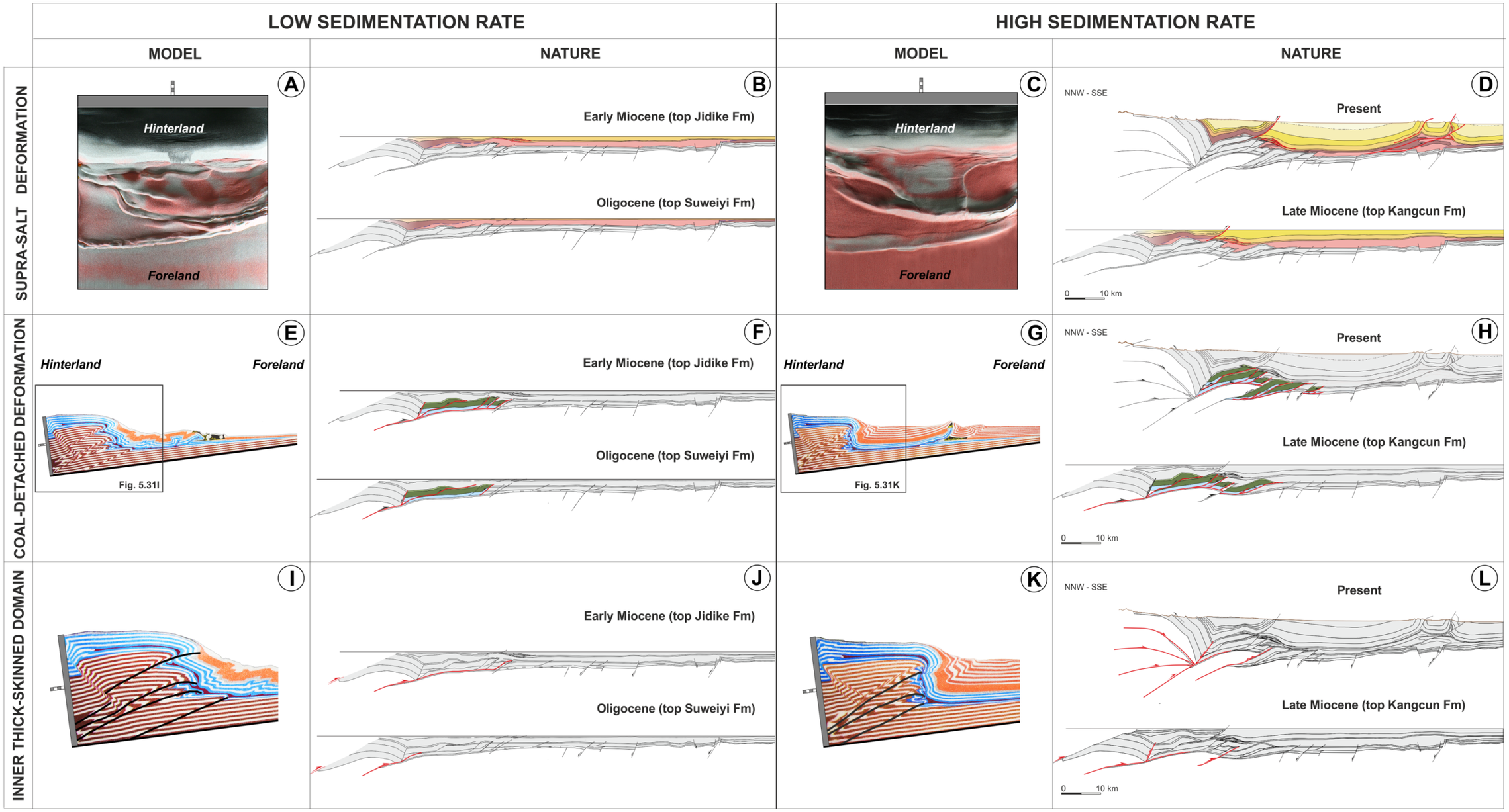

FIGURE 5.3. Summary of results integrating both the structural and the experimental studies. **A:** Top view of Experiment B at the end of shortening. **B:** Restorations at top of Suweiyi and Jidike Fms of the regional cross section (based on seismic profile dapomian-11) across the central Kuqa fold-and-thrust belt highlighting suprasalt deformation. **C:** Top view of Experiment D at the end of shortening. **D:** Restorations at top of Kangcun Fm and present-day of the regional cross section (based on seismic profile dapomian-11) across the central Kuqa fold-and-thrust belt highlighting suprasalt deformation. **E:** Cross-section of Experiment A at the end of shortening. **F:** Restoration at top of Suweiyi and Jidike Fms of the regional cross section (based on seismic profile dapomian-11) across the central Kuqa fold-and-thrust belt highlighting coal-detached deformation. **G:** Cross-section of Experiment D at the end of shortening. **H:** Restorations at top of Kangcun Fm and present-day of the regional cross section (based on seismic profile dapomian-11) across the central Kuqa fold-and-thrust belt highlighting coal-detached deformation. **I:** Enlargement of the inner thick-skinned domain (see location in **Fig. 5.3E**). **J:** Restorations at top of Suweiyi and Jidike Fms of the regional cross section (based on seismic profile dapomian-11) across the central Kuqa fold-and-thrust belt highlighting the inner thick-skinned domain. **K:** Enlargement of the inner thick-skinned domain (see location in **Fig. 5.3G**). **L:** Restoration at top of Kangcun Fm and present-day of the regional cross section (based on seismic profile dapomian-11) across the central Kuqa fold-and-thrust belt highlighting the inner thick-skinned domain.

Mismatches between model and Kuqa fold-and-thrust belt geometries could be partially related to the deformation-rate scaling, but there is no doubt that it is also controlled by a difference between the mechanical behavior of the Upper Triassic-Lower Jurassic lacustrine mudstones and coals and that of the analogue material used in the experimental program. The mudstones and coals are more viscous and, unlike the sand/polymer mixture, do not flow at upper crustal levels (Tang et al., 2007; Wang et al., 2011; Wang et al., 2017). Moreover, they may comprise multiple, discrete and thin detachment levels rather than the single thicker layer of sand/polymer mixtures. In any case, the results suggest that the coals and mudstones were more effective as a décollement than the experimental equivalent, therefore, a high viscosity and low basal friction weak layer could be more effective as a décollement than a lower viscosity weak layer.

5.2.2. Syncontractional sedimentation and erosion

Sedimentation rate in the Kuqa fold-and-thrust belt varies through time. A clear distinction can be made between: an earlier contractional stage (from top Cretaceous to early Miocene) that was dominated by lower shortening and sedimentation rates, and a later period (spanning the late Miocene to Pleistocene) characterized by higher rates of both processes.

During the early deformation stage, the Kuqa fold-and-thrust belt grew as a wide thrust wedge formed by a main basement thrust that transferred shortening to the overlying décollements (**Fig. 5.3J**). Deformation propagated slowly towards the foreland enabling the growth of the fold and thrust system through frontal accretion. Under these low sedimentation rates, shortening was distributed in several minor structures detached in the inner domain of both the upper evaporitic and the lower décollements (i.e. they are not localized over décollement boundaries; **Fig. 5.3B**). This feature is also recognized in the analogue models A and B where null/low synkinematic sedimentary rates favor the formation of multiple structures, more distributed over the décollements than in the models simulating higher sedimentary rates. In the natural case study, the lower sedimentary rate enhanced thin-skinned thrusting over the coal layers as recognized in the experiment A (**Fig. 5.3E**). Besides, dip similarities between the analogue models and the natural case study are found regarding the frontal limb of the thick-skinned thrust system: the dip of this limb is intermediate in models/shortening stages involving low sedimentary rates but steepens when these rates increase (both in the natural case study and the analogue models, compare **Figs. 5.3I and 5.3K**).

Syntectonic sedimentation rate increases in the Kuqa case study during the later deformation stages. This rate increase has a strong impact in its geometry that changes with respect to that depicted in the early stages. The Kuqa fold-and-thrust belt evolve into a narrower and steeper thrust wedge, coal-detached thrusts are less developed whereas basement thrusting played a major role. Besides, as predicted from the analogue models, shortening was localized in a few structures that are separated from each other by the broad Baicheng Syncline (**Fig. 5.3D**). As observed when experiments B and D are compared (**Figs. 5.3A and 5.3C**, respectively), high sedimentation rates lead to a decrease in the number of structures as well as an increase of their size. In particular, folds have a longer wavelength and greater amplitude, thrusts sheets are thicker and wider, and both thrusts and folds are more widely spaced. Regarding the thick-skinned domain, high sedimentary rates promoted the formation of steep frontal limbs in the analogue models, similarly to the steepening and forwards rotation inferred during late deformation stages for the frontal limb of the South Tian Shan Anticline (**Fig. 5.3L**).

Differences in suprasalt deformation between the Kuqa fold-and-thrust belt and sandbox models could be related to different parameters that remain constant or absent during the experiments. The sedimentation and the shortening rates as well as the accommodation space (tilting the baseplate) do not vary. In addition, differences in deformation above the synkinematic weak layer may be related in part to erosion, which is not modeled in our experimental program. Erosion enhances the effects of differential loading between areas of sediment accumulation and uplifted areas, helping drive migration of salt from beneath the synclines to the anticlines or thrust-fault hanging walls. Therefore, it could explain the coeval Eocene-Oligocene salt inflation in the frontal Qiulitage area and depletion beneath the Baicheng syncline that was not reproduced in our experiments (**Fig. 5.2B**). This effect may have been magnified by the greater density contrast between overburden and polymer (>1.4; **Table 2**) than the real contrast between overburden and salt, which can be less than 1 in the case of thin, young siliciclastics; this might have impeded any loading-induced polymer inflation in the structural highs.

5.2.3. Inherited structure

The Mesozoic structure predating the formation of the Kuqa fold-and-thrust belt is influenced by the presence of inherited, Paleozoic and/or Mesozoic North-dipping extensional faults. The presence of these early faults had a first-order impact on the structural evolution of the Kuqa fold-and-thrust belt because they determined the locus of most of the basement thrusts acting during the Cenozoic and therefore the geometry of the thrust stack in the Kelasu fold-and-thrust system. Furthermore, in the eastern and central section, inherited basement faulting probably controlled the position of the Kumugeliemu salt pinch-out and contributed to the late-stage uplift of the Qiulitage fold-and-thrust system. This indicates a feedback relationship between basement-involved faults and salt-detached deformation.

Differences in the geometry of the basement-involved thrust system between the Kuqa fold-and-thrust belt and our models largely result from the absence of basement anisotropies in the sandbox experiments. Thus, the models address a simple scenario that does not match perfectly with most real cases (i.e, Zagros, Apennines, Pyrenees, and even the Tarim Basin). In this sense, it is evident that in any departure model including structural inheritance, these inherited structures would have a strong impact on the subsalt contractional deformation and consequently on the suprasalt structures as shown by previous analogue modelling studies (Callot et al., 2012; Graveleau et al., 2012; Lewis et al., 2013; Jackson and Hudec, 2017).

5.3. APPLICABILITY

The integration of the structural and analogue model data for the Kuqa fold-and-thrust belt presented in this thesis, together with a better understanding of the main parameters that control the structuring of the thrust belt, provide new perspectives in terms of hydrocarbon exploration and production in subsalt contractional environments.

5.3.1. Implications for traps development

The cross sections constructed in this thesis point out several implications in the development of new traps. On the one hand, the recognition and characterization of a thin-skinned fold-and-thrust system detached along Upper Triassic-Lower Jurassic coal means (regarding previous interpretations) a higher compartmentalization of the reservoir unit

beneath the Kelasu fold-and-thrust system (represented by the Bashijiqike Formation) and a higher number of thrust imbricates. Hangingwall anticlines related to these thrusts are potential traps (**Fig 5.4**).

Furthermore, the interpretation of normal faults affecting the Mesozoic units that underline the central Qiulitage frontal structure also opens new possibilities regarding trap development in their footwalls (**Fig. 5.4**).

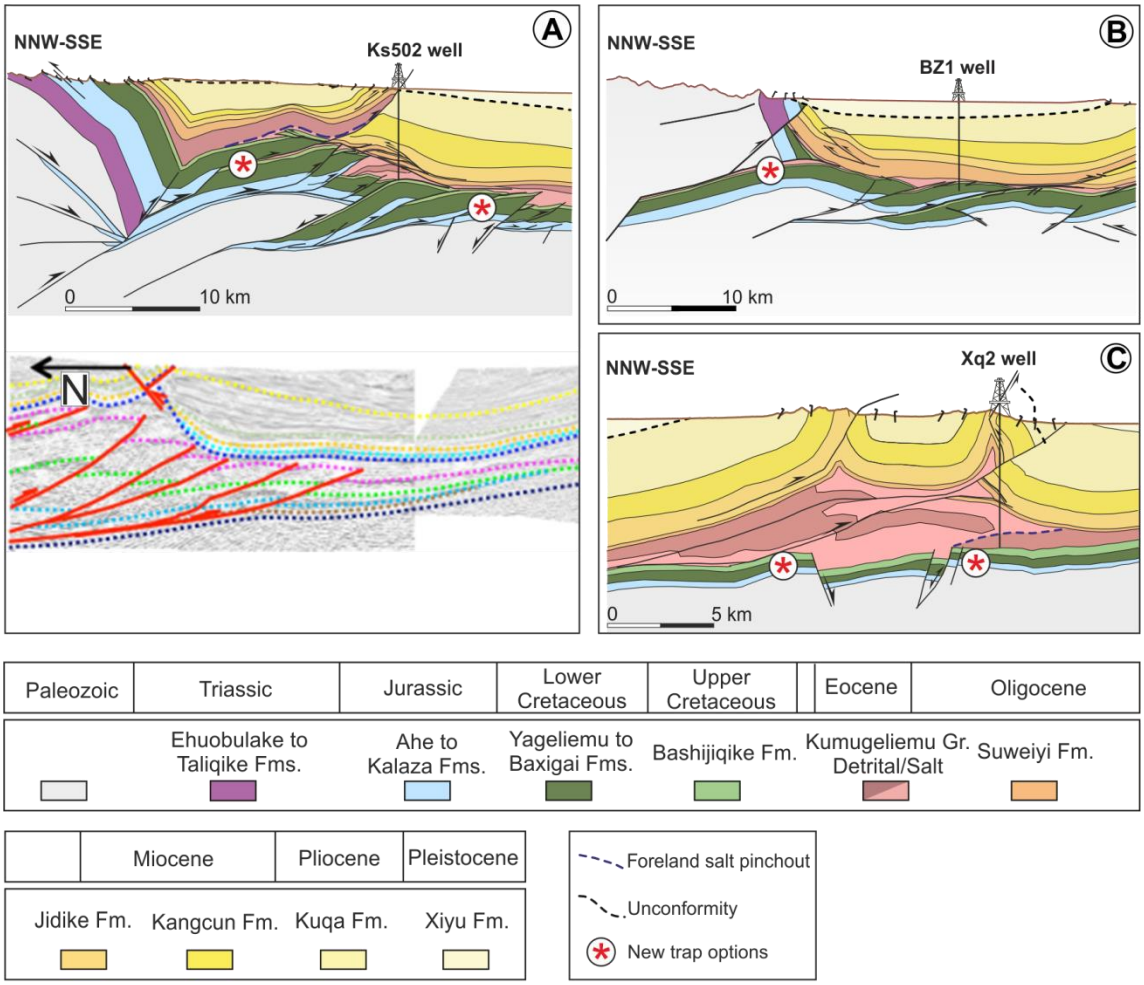

FIGURE 5.4. New potential traps in: **A:** the central Kelasu fold-and-thrust system. Note that in previous interpretations for the central Kelasu fold-and-thrust system the detachment level for the thin-skinned subsalt system is located at a lower stratigraphic position and the number of imbricates is lower. **B:** New sub-basement traps to North of the western Kelasu fold-and-thrust system**. C:** Extensional footwall traps in western Qiulitage.

5.3.2. Implications for source-rock distribution

The source rock in the Kuqa fold-and-thrust belt (Upper Triassic-Lower Jurassic coal layers) is coincident with the lower décollement. This correspondence gives us an additional constrain when mapping the areal distribution of the source rock: if thin-skinned Mesozoic-detached imbricates are recognized, the source rock will be present at that position. Mapping of the distribution of the thin-skinned thrust system shows an excellent match with the thickness of the source rock (**Fig. 5.5**, constructed from well data by Tarim Oilfield). This good correspondence evidences how a good understanding of the structure is a potential and powerful tool for the mapping of the source rock in the Kuqa fold-and-thrust belt and in other fold-and-thrust belts where source rocks behave as décollements.

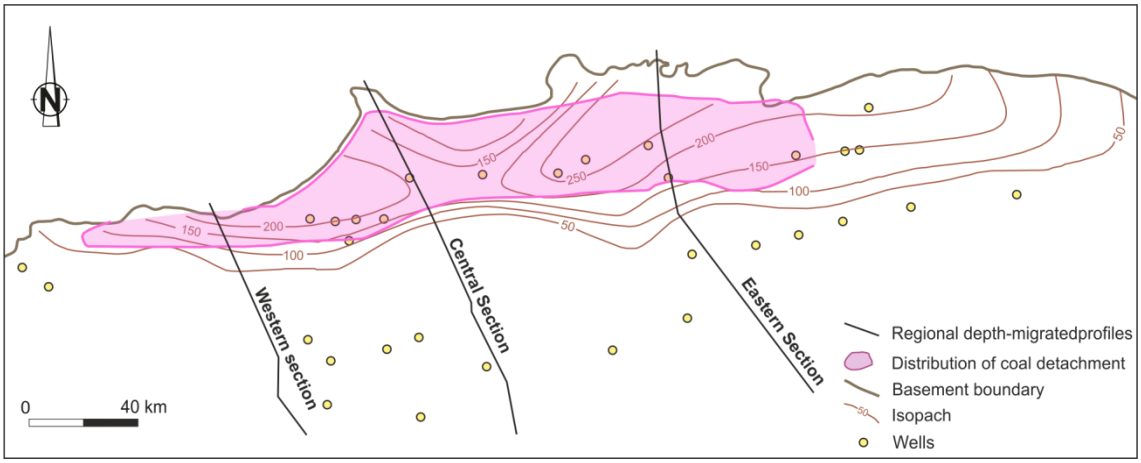

FIGURE 5.5. Correlation between the areal distribution of the coal-detached thin-skinned thrust system (obtained exclusively from the cross sections presented in this project, without well data) and the thickness map for the Lower Jurassic source rock (provided by Tarim Oilfield, based on well data).

5.3.3. Implications for reservoir charge and oil migration

The palinspastic restorations realized in this thesis point out to a late expulsion and migration of the hydrocarbons. This migration was probably coeval to the sedimentation of the Kuqa and Kangcun Fm., when the thin-skinned thrust system detached into Upper Triassic-Lower Jurassic coal layers was already developed (**Fig. 5.6**). Two different migration paths took probably place: (i) a short distance migration, charging the traps represented by the hangingwall anticlines in the thin-skinned subsalt thrust system and (ii) a long-distance migration path, updip from the northern part of the fold-and-thrust belt towards the foreland basin. The latter, long distance migration could have charged the potential fault-related traps beneath the Qiulitage frontal structure (**Fig. 5.6**).

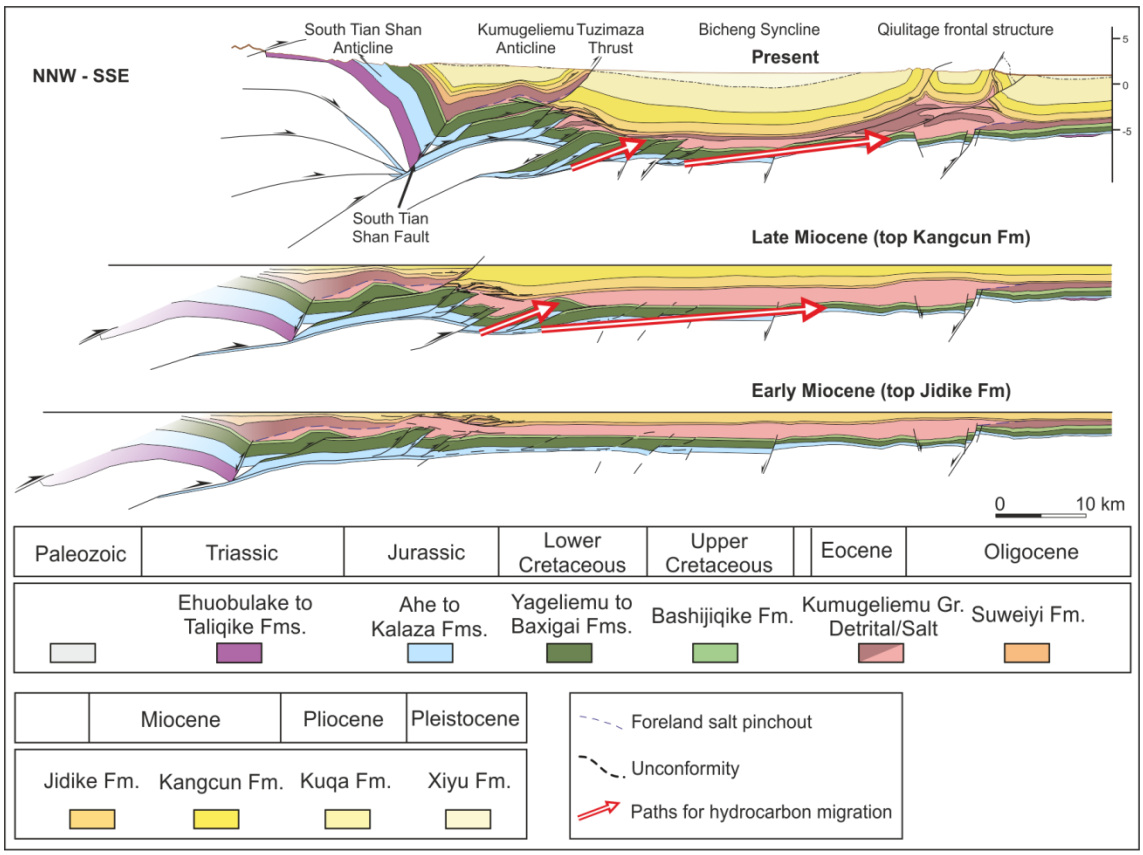

FIGURE 5.6. Timing and possible paths for oil migration in the Kuqa fold-and-thrust belt.

CHAPTER 6. CONCLUSIONS

The detailed conclusions of the structural analysis of the Kuqa fold-and-thrust belt as well as the ones obtained from the experimental study are shown in chapters 3 and 4, respectively. Here, a summary of these conclusions is pointed out together with the general conclusions obtained from the integration of both studies.

- The Kuqa fold-and-thrust belt is a thin-skinned thrust system that involves two main décollements: The syncontractional salt layer (Eocene-Oligocene in age) and a deeper, precontractional décollement comprising coal and lacustrine mudstones (Upper Triassic-Lower Jurassic in age).
- Deformation in sub-salt units is strongly controlled by along-strike effectiveness variation of the precontractional décollement and synkinematic sedimentation. In this sense, analogue models validate seismic interpretation and confirm the roles of décollement distribution/rheology and sedimentation rate.
- The Kuqa fold-and-thrust belt present two-stage evolution during the Cenozoic. The first stage (Top Cretaceous-lower Miocene) with slow deformation (0.01-0.09 mm/year) and low syntectonin sedimentation rate (0.2-1 mm/year) and a later stage (Upper Miocene-Pleistocene) with rapid deformation (0.05-0.4 mm/year) and high syntectonic sedimentation rate (0.5-4.9 mm/year).
- The presalt structure of the Kuqa fold-and-thrust belt is characterized by an inner-thick skinned domain formed by a basement-involved thrust stack that cut and branches with a thin-skinned fold-and-thrust system detached on the coal layers. Under low synkinematic sedimentation rate, this thrust stack presents a low taper angle and the dip of frontal limb is smaller. In contrast, when synkinematic sedimentation increases the basement thrust stacking produce forward rotation of the frontal limb and its dip is higher.
- The thin-skinned fold-and-thrust system detached on the prekinematic décollement is well developed in the central and eastern part of the Kuqa fold-and-thrust belt but dies out to the West. In addition, under low synkinematic sedimentation rate, this thrust system propagates southwards in a piggy back sequence whereas under high sedimentation rate the lower décollement becomes less effective and the propagation of the deformation towards the foreland is reduced.
- Suprasalt deformation is strongly influenced by synkinematic sedimentation rate. Increasing synkinematic sedimentation rate leads to a progressive change from distributed deformation to deformation localized in the pinch-outs of the salt. The number of structures is reduced but its size increases. In addition, increasing

synkinematic sedimentation rate promotes propagation of the deformation more quickly towards the foreland. However, when sedimentation rate is very high, it can slow down or even blocks the piggy-back propagation of thrusting, and new thrusts and backthrusts form towards the hinterland.

- Salt diapiric structures are mainly driven by erosion of the salt-cored anticlines and thrusts and high pression head gradients produced between these eroding structures and the adjacent synclines where thick synorogenic successions are deposited.

- Our results emphasize that the evolution of fold-and-thrust systems involving interbedded weak horizons should be understood in light of a continuous interplay between the reactivation of inherited features, the behavior and extent of the décollements, and the effects of systectonic deposition.

CHAPTER 7. REFERENCES

Abdrakhmatov, K.E., Aldazhanov, S.A., Hager, B.H., Hamburger, M.W., Herring, T.A., Kalabaev, K.B., Makarov, V.I., Molnar, P., Panasyuk, S.V., Prilepin, M.T., Reilinger, R.E., Sadybakasov, I.S., Souter, B.J., Trapeznikov, Yu. A., Tsurkov, V.E., Zubovich, A.V., 1996. Relatively recent construction of the Tian Shan inferred from GPS measurements of present-day crustal deformation rates. *Nature*, **384**, 450-453.

Allen, M. B., Windley, B.F., Zhang, C., 1992. Paleozoic collisional tectonics and magmatism of the Chinese Tien Shan, Central Asia. *Tectonophysics*, **220**, 89-115.

Avouac, J.P., Tapponnier, P., 1993. Kinematic model of active deformation in central Asia. *Geophysical Research Letters*, **20**, 895-898.

Avouac, J.P., Tapponnier, P., Bai, M., You, H., Wang, G., 1993. Active thrusting and folding along the northern Tien Shan and late Cenozoic rotation of the Tarim relative to Dzungaria and Kazakhstan. *Journal of Geophysical Research: Solid Earth*, **98**, 6755-6804.

Baby, P., Moretti, I., Guillier, B., Limachi, R., Mendez, E., Oller, J., Specht, M., 1995. Petroleum system of the northern and central Bolivian sub-Andean zone. In A.J. Tankard, R. Suarez, H.J. Welsink (Eds.), *Petroleum Basins of South America*. *American Association of Petroleum Geologist* Memoir, **62**, 445-458

Bally, A.W., Gordy, P.L., Stewart, G.A., 1966. Structure, seismic data, and orogenic evolution of southern Canadian Rocky Mountains. *Bulletin of Canadian Petroleum Geology*, **14(3)**, 337-381.

Barrier, L., Nalpas, T., Gapais, D., Proust, J.N., 2013. Impact of synkinematic sedimentation on the geometry and dynamics of compressive growth structures: Insights from analogue modelling. *Tectonophysics*, **608**, 737-752.

Beaumont, C., Fullsack, P., Hamilton, J., 1992. Erosional control of active compressional orogens. In K.R. McClay (Ed.), *Thrust Tectonics*. Chapman & Hall, London, pp. 1–18.

Bigi, S., Di Paolo, L., Vadacca, L., Gambardella, G., 2010. Load and unload as interference factor son cyclical behavior and kinematics of Coulomb wedges: insights from sandbox experiments. *Journal of Structural Geology*, **32(2)**, 28-44.

Bonini, M., 2001. Passive roof thrusting and forelandward fold propagation in scaled brittle-ductile physical models of thrust wedges. *Journal of Geophysical Research*, **106(B2)**, 2291-2311.

Bonini, M., 2003. Detachment folding fold amplification, and diapirism in thrust wedge experiments. *Tectonics*, **22(6)**, 1065, doi: 10.1029/2002tc001458.

Bonnet, C., Malavieille, J., Mosar, J., 2008. Surface processes versus kinematics of thrust belts: impact on rates of erosion, sedimentation, and exhumation-insights from analogue models. *Bulletin de la Société Géologique de France*. **179(3)**, 179-192.

Borderie, S., Graveleau, F., Witt, C., Vendeville, B., 2018. Impact of an interbedded viscous décollement on the structural and kinematic coupling in fold-and-thrust belts: Insights from analogue modeling. *Tectonophyiscs*, **722**, 118-137.

Brunet, M.F., Sobel, E.R., McCan, T., 2017. Geological evolution of Central Asian Basins and the western Tien Shan Range. *Geological Society of London Special Publications*, **427**, Doi: 10.1144/SP427.17.

Cai, J., Lü, X., 2015. Substratum transverse faults in Kuqa Foreland Basin, northwest China and their significance in petroleum geology. *Journal of Asian Earth Sciences*, **107**, 72-82.

Callot, J.-P., Trocmé, V., Letouzey, J., Albouy, E., Jahani, S., Sherkati, S., 2012. Pre-existing salt structures and the folding of the Zagros Mountains. In G.I. Alsop, S.G. Archer, A.J. Hartley, N.T. Grant, R. Hodgkinson (Eds.), *Salt tectonics, sediments and prospectivity*. Geological Society of London Special Publications, **363**, 545-561.

Canerot, J., Qu, G., 1998. La Cuenca Jurásica del Tarim suroccidental, provincia de Xinjiang (República Popular de China). Relación con el Tethys nororiental y evolución durante el ciclo himalayense. *Cuadernos de Geología Ibérica*, **24**, 311-331.

Carrol, A.R., Graham, S.A., Hendrix, M.S., Ying, D., Zhou, D., 1995. Late Paleozoic tectonics amalgamation of northern China-sedimentary record of the northern Tarim, nortwestern Turpan, and southern Junggar basins. *Geological Society of American Bulletin*, **107**, 571-594.

Cartwright, J., Jackson, M.P., Dooley, T., Higgins, S., 2012. Strain partitioning in gravity-driven shortening of a thick, multilayered evaporate sequence. In G.I. Alsop, S.G. Archer, A.J. Hartley, N.T. Grant, R. Hodgkinson (Eds.), *Salt tectonics, sediments and prospectivity*. Geological Society of London Special Publications, **363**, 449-470.

Charreau, J., Gilder, S., Chen, Y., Dominguez, S., Avouac, J. P., Sen, S., Jolivet, M., Li, Y., Wang, W., 2006. Magnetostratigraphy of the Yaha section, Tarim Basin (China): 11 Ma acceleration in erosion and uplift of the Tian Shan mountains. *Geology*, **34(3)**, 181-184.

Charvet, J., Shu, L., Laurent-Charvet, S., Wang, B., Faure, M., Cluzel, D., Chen, Y., De Jong, K., 2011. Palaeozoic tectonic evolution of the Tianshan belt, NW China. *China Earth Sciences*, **54(2)**, 166-184.

Chen, J., Lu, H., Wang, S., Shang, Y., 2005. Geometric tests and their application to fault-related folds in Kuqa. *Journal of Asian Earth Sciences*, **25**, 473-480.

Chen, S., Tang, L., Jin, Z., Jia, C., Pi, X., 2004. Thrust and fold tectonics and the role of evaporites in deformation in the Western Kuqa Foreland of Tarim Basin, Northwest China. *Marine and Petroleum Geology*, **21**, 1027-1042.

Cobbold, P.R., Davy, P., Gapais, D., Rossello, E.A., Sadybakasov, E., Thomas, J.C., Tondji Biyo, J.J., Urreiztieta, M., 1993. Sedimentary basins and crustal thickening. *Sedimentary Geology*, **86(1-2)**, 77-89.

Coleman, R. G., 1989. Continental growth of northwest China. *Tectonics*, **8**, 621-635.

Costa, E., Vendeville, B.C., 2002. Experimental insights on the geometry and kinematics of fold-and-thrust belts above weak, viscous evaporitic décollement. *Journal of Structural Geology*, **24(11)**, 1729-1739.

Cotton, J., Koyi, H.A., 2000. Modelling of thrust fronts above ductile and frictional décollements; examples from The Salt Range and Potwar Plateu, Pakistan. *Geological Society of America Bulletin*, **112**, 351-363.

Couzens-Schultz, B.A., Vendeville, B.C., Wiltschko, D.V., 2003. Duplex style and triangle zone formation: insights from physical modeling: *Journal of Structural Geology*, **25**, 1623-1644.

Darnault, R., Callot, J.P., Ballard, J.F., Fraisse, G., Mengus, J.M., Ringerbach, J.C., 2016. Control of syntectonic erosion and sedimentation on kinematic evolution of a multidecollement fold and thrust zone: Analogue modeling of folding in the southern subandean of Bolivia. *Journal of Structural Geology*, **89**, 30-43.

Davis, D.M., Suppe, J., Dahlen, F.A., 1983. Mechanics of fold-and-thrust belts and accretionary wedges. *Journal of Geophysical Research*, **88**, 377-378.

Davis, D.M., Engelder, T., 1985. The role of salt in fold and thrust belts. *Tectonophysics*, **119**, 67-68.

Del Castello, M., Pini G.A., McClay, K., 2004. Effect of unbalanced topography and overloading on Coulomb wedge kinematics: insights from sandbox modeling. *Journal of Geophysical Research*, **109**, B05405. Doi: 10.1029/2003JB002709.

Dell'Ertole, T., Schellart, W., 2013. The development of sheath folds in viscously stratified materials in simple shear conditions: An analogue approach. *Journal of Structural Geology*, **56**, 129-141.

Deng, Q.D., Feng, X.Y., Zhang, P.Z., Xu, X.W., Yang, X.P., Peng, S.Z., Li, J., 2000. Active Tectonics of the Chinese Tianshan Mountain. *Seismology Press Beijing*, 127-141

Driehaus, L., Nalpas, T., Ballard, J.F., 2014. Interaction between deformation and sedimentation in a multidecollment thrust zone: analogue modeling and application to the Sub-Andean thrust belt of Bolivia. *Journal of Structural Geology,* **65**, 59-68.

Duerto, L., McClay, K., 2009. The role of syntectonic sedimentation in the evolution of doubly vergent thrust wedges and foreland folds. *Marine and Petroleum Geology*, ***26*(7)**, 1051-1069.

Fard, I. A., Sepehr, M., Sherkati, S., 2011. Neogene salt in SW Iran and its interaction with Zagros folding. *Geological Magazine*, ***148*(5-6)**, 854-867.

Ferrer, O., Gratacós, O., Roca, E., Muñoz, J.A., 2017. Modeling the interaction between presalt seamounts and gravitational failure in salt-bearing passive margins: The Messinian case in the northwestern Mediterranean Basin. *Interpretation*, **5**, 99-117.

Fillon, C., Huismans, R. S., van der Beek, P., 2013. Syntectonic sedimentation effects on the growth of fold-and-thrust belts. *Geology*, **41(1)**, 83-86.

Gao, J., Klemd, R., Qian, Q., Zhang, X., Li, J., Jiang, T., Yant, Y., 2011. The collision between the Yili and Tarim blocks of the Southwestern Altaids: geochemical and age constraints of a leucogranite dike crosscutting the HP-LT metamorphic belt in the Chinese Tianshan Orogen. *Tectonophysics*, **499**, 118-131.

Gestain, V., Nalpas, T., Rouby, D., Barrier, L., 2004. Rôle des niveaux incompétents syn-cinemátiques sur l'évolution des zones chevauchantes-modélisations analogiques. *Bulletin de la Société Géologique de France,* **175 (4)**, 351-359.

Goncharov, M.A., 2010. Applicability of similarity conditions to analogue modelling of tectonic structures. *Geodynamics & Tectonophysics*, **1(2)**, 148-168.

Gradmann, S., Beaumont, C., Albertz, M., 2009. Factors controlling the evolution of the Perdido Fold Belt, northwestern Golf of Mexico, determined from numerical models. *Tectonics*, **28(2)**, doi: 10.1029/2008TC002326

Graveleau, F., Dominguez, S., 2008. Analogue modelling of the interactions between tectonics, erosion and sedimentation in foreland thrust belts. *Comptes Rendus Geoscience*, **340(5)**, 324-333.

Graveleau, F., Malavieille, J., Dominguez, S., 2012. Experimental modelling of orogenic wedges: a review. *Tectonophysics*, **538-540**, 1-66.

Guan, S.W., Wang, X., Yang, S.F., Zhao, W.D., Xu, F., Lei, G.L., 2003. The 3-D analysis to the Qiulitage fold belt of Kuqa in South Tian-Shan. *Geologic Review*, **49**, 464-473.

Guo, X., Liu, K., Jia, C., Song, Y., Zhao, M., Lu, X., 2016. Effects of early petroleum charge and overpressure on reservoir porosity preservation in the giant Kela-2 gas field, Kuqa depression, Tarim Basin, northwest China. *American Association of Petroleum Geologist Bulletin*, **100(2)**, 191-212.

Gutscher, M.A., Kukowski, N., Malavieille, J., Lallemand, S., 1996. Cyclical behavior of thrust wedges: insights from high basal friction sandbox experiments. *Geology*, **24(2)**, 135–138.

Halim, N., Cogné, J.P., Chen, Y., Atasiei, R., Besse, J., Courtillot, V., Gilder, S., Marcoux, J., Zhao, R. L., 1998. New Cretaceous and Early Tertiary paleomagnetic results from Xining-Lanzhou basin, Kunlun and Qiangtang blocks, China: Implications on the geodynamic evolution of Asia. *Journal of Geophysical Research: Solid Earth*, **103(B9)**, 21025-21045.

Hardy, S., Duncan, C., Masek, J., Brown, D., 1998. Minimum work, fault activity and the growth of critical wedges in fold and thrust belts. *Basin Research*, ***10*(3)**, 365-373.

He, D., Zhou, X., Yang, H., Lei, G., Ma, Y., 2009. Geological structure and its controls on giant oil and gas fields in Kuqa Depression, Tarim Basin: A clue from new shot seismic data. *Geotectonica et Metallogenia*, **33(1)**, 19-32.

He, B., Jiao, C., Xu, Z.., Cai, Z., Zhang, J., Liu, S., Yu, Z., 2016. The paleotectonic and paleogeography reconstructions of the Tarim Basin and its adjacent areas (NW China) during the late Early and Middle Paleozoic. *Gondwana Research*, **30**, 191-206.

Hendrix, M.S., Dumitru, T.A., Graham, S.A., 1994. Late Oligocene-Early Miocene unroofing in the Chinese Tian Shan: An early effect of the India-Asia collision. *Geology*, **22**, 487-490.

Hendrix, M.S., Graham, S.A., Carroll, A.R., Sobel, E. R., McKnight, C. L., Schulein, B. J., Wang, Z., 1992. Sedimentary record and climatic implications of recurrent deformation in the Tianshan: Evidence from Mesozoic strata of the north Tarim, south Junggar, and Turpan basins, northwest China. *Geological Society of America Bulletin*, **104**, 53-79.

Huang, B., Piper, J. D. A., Peng, S., Liu, T., Li, Z., Wang, Q., Zhu, R., 2006. Magnetostratigraphic study of the Kuche depression, Tarim Basin, and Cenozoic uplift of the Tian Shan Range, western China. *Earth and Planetary Science Letters*, **251**, 346-364.

Hubbert, M.K., 1937. Theory of scale models as applied to the study of geologic structures. *Geological Society of America Bulletin*, **48(10)**, 1459-1519.

Hubert-Ferrari, A., Suppe, J., Gonzalez-Mieres, R., Wang, W., 2007. Mechanisms of active folding of the landscape (southern Tian Shan, China). *Journal of Geophysical Research*, **112**, 39, B03S09, doi: doi:10.1029/2006JB004362.

Hudec, M. R., Jackson, M. P., 2007. Terra infirma: Understanding salt tectonics. *Earth-Science Reviews*, **82**, 1-28.

Hudec, M. R., Jackson, M. P., Vendeville, B. C., Schultz-Ela, D. D., Dooley, T. P., 2011. The salt mine: A digital atlas of salt tectonics. *Bureau of Economic Geology Udden Book Series* No. 5 and *American Association of Petroleum Geologists Memoir*, 99.

Izquierdo-Llavall, E., Roca, E., Xie, H., Pla, O., Muñoz, J.A., Rowan, M.G., Yuan, N., Huang, S., 2018. Influence of overlapping décollements, syn-tectonic sedimentation and structural inheritance in the evolution of a contractional system: The central Kuqa fold-and-thrust belt (Tian Shan Mountains, NW China). *Tectonics*, **37(8)**, 2608-2632, doi:10.1029/2017TC004928

Jackson, M., Hudec, M., 2017. Contractional Salt-Tectonic Systems. In *Salt Tectonics*: *Principles and Practice*, Cambridge University Press, Cambridge, pp. 304-335.

Jaumé, S.C., Lillie, R.J., 1988. Mechanics of the Salt Range-Potwar Plateau, Pakistan: a fold-and-thrust belt underlain by evaporites. *Tectonics*, **7(1)**, 57-71.

Jia, D., Lu, H., Cai, D., Wu, S., Shi, Y., Chen, C., 1998. Structural features of northern Tarim basin: implications for regional tectonics and petroleum traps. *American Association of Petroleum Geologists Bulletin*, **82(1)**, 147-159.

Jin, Z., Yang, M., Lu, X., Sun, D., Tang, X., Peng, G., Lei, G., 2008. The tectonics and petroleum system of the Qiulitagh fold and thrust belt, northern Tarim basin, NW China. *Marine and Petroleum Geology*, **25**, 767-777.

Jolivet, M., Dominguez, S., Charreau, J., Chen, Y., Li, Y., Wang, Q., 2010. Mesozoic and Cenozoic tectonic history of the central Chinese Tian Shan: Reactivated tectonic structures and active deformation. *Tectonics*, **29***,* 1-30*.*

Jolivet, M., Heilbronn, G., Robin, C., Barrier, L., Bourquin, S., Guo, Zh., Jia, Y., Guerit, L., Yang, W., Fu. B., 2013. Reconstructing the Late Paleozoic-Mesozoic topographic evolution of the Chinese Tian Shan: available data and remaining uncertainities. *Advances in Geosciences*, **37**, 7-18.

Konstantinovskaya, E.A., Malavieille, J., 2011. Thrust wedges with décollement levels and syntectonic erosion: A view from analog models. *Tectonophysics*, **502**, 336-350.

Konstantinosvskaya, E.A., Rodriguez, D., Kirkwood, D., Harris, L.B., Thériault, R., 2009. Effects of basement structure, sedimentation and erosion on thrust wedge geometry: an example from the Quebec Appalachians and analogue models. *Bulletin of Canadian Petroleum Geology*,

57(1), 34-62.

Koyi, H.A., Vendeville, B.C., 2003. The effect of décollement dip on geometry and kinematics of model accretionary wedges. *Journal of Structural Geology*, **25(9)**, 1445-1450.

Krantz, R.W., 1991. Measurements of friction coefficients and cohesion for faulting and fault reactivation in laboratory models using sand and sand mixtures. *Tectonophysics*, **188(1-2)**, 203-207.

Labaume, P., Moretti, I., 2001. Diagenesis-dependence of cataclastic thrust fault zone sealing in sandstones. Example from the Bolivian Sub-Andean Zone. *Journal of Structural Geology*, **21**, 1659-1675.

Lammerer, B., Gebrande, H., Lüschen, E., Veselá, P., 2008. A crustal-scale cross-section through the Tauern Window (eastern Alps). In S. Siegesmund, B. Fügenschuh, N. Froitzheim (Eds.), *Tectonic aspects of the Alpine-Dinaride-Carpathian System*. Geological Society of London Special Publications, **298**, 219-229.

Larroque, C., Calassou, S., Malavieille, J., Chanier, F., 1995. Experimental modelling of forearc basin development during accretionary wedge growth. *Basin Research*, **7(3)**, 255-268.

Leturmy, P., Mugnier, J.L., Vinour, P., Baby, P., Colletta, B., Chabron, E., 2000. Piggyback basin development above a thin-skinned thrust belt with two detachment levels as a function of interactions between tectonic and superficial mass transfer: the case of the Subandean Zone (Bolivia). *Tectonophysics*, **320 (1)**, 45-67.

Levashova, N.M., Mikolaichuk A.V., McCausland P.J.A., Bezhenov M.L., Van der Voo, R., 2007. Devonian paleomagnetism of the North Tien Shan: implications for the middle-Late Paleozoic paleogeography of Eurasia. *Earth and Planetary Science Letters*, **257**, 104-120.

Lewis, M.M., Jackson, C.A.L., Gawthorpe, R.L., 2013. Salt-influenced normal fault growth and forced folding: The Stavanger Fault System, North Sea. *Journal of Structural Geology* 54, 156-173.

Li, J., Webb, A.A.G., Mao, X., Eckhoff, I., Colón, C., Zhang, K., He, D., 2014. Active surface salt structures of the western Kuqa fold-thrust belt, northwestern China. *Geosphere*, **10**, 1219-1234.

Li, S., Wang, X., Suppe, J., 2012. Compressional salt tectonics and synkinematic strata of the western Kuqa foreland basin, southern Tian Shan, China. *Basin Research*, **24**, 475-497.

Li, Z., Song, W., Peng, S., Wang, D., Zhang, Z., 2004. Mesozoic–Cenozoic tectonic relationships between the Kuqa subbasin and Tian Shan, northwest China: constraints from depositional records. *Sedimentary Geology*, **172**, 223-249.

Lin, C., Liu, J., Zhang, Y., Xiao, J., Chen, J., Ji, Y., 2002. Depositional architecture of the Tertiary tectonic sequences and their response to foreland tectonism in the Kuqa despression, the Tarim Basin. *Science in China*, **45(3)**, 250-258.

Liu, J., Wang, Q., Lin, C., Zhang, L., Lei, Y., Hu. G., Hu, B., 2008. Sequence and systems tract of Paleogene Kumugeliemu Group in Western Kuqa Depression, Tarim Basin. *Petroleum Exploration and Development*, **35(6)**, 651-656.

Lohrmann, J., Kukowski, N., Adam, J., Oncken, O., 2003. The impact of analogue material properties on the geometry, kinematics, and dynamics of convergent sand wedges. *Journal of Structural Geology*, **25(10)**, 1691-1711.

Loury, C., Rolland, Y., Cenki-Tok, B., Lanari, P., Guillot, S., 2015a. Late Paleozoic evolution of the South Tien Shan: Insights from *P-T* estimates and allanite geochronology on retrogressed eclogites (Chatkal range, Kyrgyzstan). *Journal of* Geodynamics, **96**, 62-80, doi: 10.1016/j.jog.2015.06.005

Loury, C., Rolland, Y., Guillor, S., Mikolaichuk, A.V., Lanari, P., Brugueier, O., Bosch, D., 2015b. Crustal-scale structure of South Tien Shan: implications for subduction polarity and Cenozoic reactivation. In M.F. Brunet, T. McCann, E.R. Sobel (Eds.), *Geological Evolution of Central Asian and the Western Tien Shan Range.* Geological Society of London Special Publications, **427(1)**, 197-229.

Lu, H., Burbank, D.W., Li, Y., Liu, Y., 2010. Late Cenozoic structural and stratigraphic evolution of the northern Chinese Tian Shan foreland. *Basin Research,* **22(3)**, 249-269.

Luján, M., Storti, F., Balanyá, J-C., Crespo-Blanc, A., Rossetti, F., 2003. Role of décollement material with different rheological properties in the structure of the Aljibe thrust imbricate (Flysch Trough, Gibraltar Arc): an analogue modelling approach. *Journal of structural geology*, **25**, 867-881.

Lv, D., Liu, J., Wu, X., Yang, Q., Yong, P., 2016. *Qapqal coal characteristics analysis of Yinan coalfield in Xinjiang province, western China*. International Conference on Power, Energy Engineering and Management (PEEM 2016). ISBN: 978-1-60595-324-3.

Massoli, D., Koyi, H., Barchi, M., 2006. Structural evolution of a fold and thrust belt generated by multiple décollements: analogue models and natural examples from the Northern Apennines (Italy). *Journal of Structural Geology*, **28**, 185-199.

Molinaro, M., Leturmy, P., Guezou, J.C., Frizon de Lamotte, D., Eshraghi, S.A., 2005. The structure and kinematics of the southeastern Zagros fold-and-thrust belt, Iran: from thin-skinned to thick-skinned tectonics. *Tectonics*, **24(3)**, TC3007, 19 pp, doi:10.1029/2004TC001633.

Molnar, P., Tapponnier, P., 1975. Cenozoic tectonics of Asia: effects of a continental collision. *Science*, **189**, 419-426.

Mount, V. S., 2014. Structural style of the Appalachian Plateau fold belt, north-central Pennsylvania. *Journal of Structural Geology*, **69**, 284-303.

Mugnier, J. L., Vialon, P., 1986. Deformation and displacement of the Jura cover on its basement. *Journal of Structural Geology*, **8(3-4)**, 373-387.

Mugnier, J. L., Baby, P., Colletta, B., Vinour, P., Bale, P., Leturmy, P., 1997. Thrust geometry controlled by erosion and sedimentation: A view from analogue models. *Geology*, **25(5)**, 427-430.

Muñoz, J. A., 1992. Evolution of a continental collision belt: ECORS-Pyrenees crustal balanced cross-section. In K.R. McClay (Ed.), *Thrust Tectonics*. Chapman & Hall, London, pp. 235-246.

Muñoz, J.A., Beamud, E., Fernández, O., Arbués, P., Dinarès-Turell, J., Poblet, J., 2013. The Ainsa Fold and thrust oblique zone of the central Pyrenees: Kinematics of a curved contractional system from paleomagnetism and structural data. *Tectonics*, **32**, 1142-1175.

Nalpas, T., Györfy, I., Guillocheau, F., Lafont, F., Homewood, P., 1999. Influence de la charge sédimentaire sur le développement d'anticlinaux synsédimentaires. Modélisation analogique et exemple de terrain (bordure sud du bassin de Jaca). *Bulletin de la Société Géologique de France*, **170(5)**, 733–740.

Ollerenshaw, N.C., 1978. Calgary, Alberta–British Columbia: Canada, Geological Survey of Canada, Map 1457A, scale 1:250000, 2 sheets.

Peng, S., Li, Z., Huang, B., Liu, T., Wang, Q., 2006. Magnetostratigraphic study of Cretaceous depositional succession in the northern Kuqa Depression, Northwest China. *Chinese Science Bulletin*, **51**, 97-107.

Persson, K.S., Sokoutis, D., 2002. Analogue models of orogenic wedges controlled by erosion. *Tectonophysics*, **356(4)**, 323-336.

Persson, K.S., Garcia-Castellanos, D., Sokoutis, D., 2004. River transport effects on compressional belts: firsts results from an integrated analogue-numerical model. *Journal of Geophysical Research* 109, B01409, 11 pp, doi: 10.1029/2002JB002274.

Pichot, T., Nalpas, T., 2009. Influence of synkinematic sedimentation in a thrust system with two decollement levels; analogue modelling. *Tectonophysics*, **206(2-3)**, 371-388.

Ping, Y., Longde, S., Jiafu, Q., 2016. Key seismic exploration techniques for foreland thrust belt: a case from the complex deep subsalt structure of Kuqa, Tarim Basin, Western China. *Interpretation*, **4(3)**, T337-T346.

Qi, J., Lei, G., Li, M., Xie, H., Yang, S., 2009. Contractional structure model of the transition belt between Kuche Depression and South Tianshan uplift. *Earth Science Frontiers*, **16(3)**, 120-128.

Qiu, N., Chang, J., Zuo, Y., Wang, J., Li, H., 2012. Thermal evolution and maturation of lower Paleozoic source rocks in the Tarim Basin, northwest China. *American Association of Petroleum Geologists Bulletin*, **96(5)**, 789-821.

Ravaglia, A., Turrini, C., Seno, S., 2004. Mechanical stratigraphy as a factor controlling the development of a sandbox transfer zone: a three-dimensional analysis. *Journal of Structural Geology*, **26**, 2269-2283.

Replumaz, A., Tapponnier, P., 2003. Reconstruction of the deformed collision zone between India and Asia by backward motion of lithospheric blocks. *Journal of Geophysical Research: Solid Earth*, **108(B6)**, 2285, doi: 0.1029/2001JB000661

Rowan, M.G., Ratliff, R.A., 2012. Cross-section restoration of salt-related deformation: Best practices and potential pitfalls. *Journal of Structural Geology*, **41**, 24-37.

Ruh, J.B., Klaus, B.J.P., Burg, J-P., 2012. Numerical investigation of deformation mechanics in fold-and-thrust belts: Influence of rheology of single and multiple décollements. *Tectonics*, **31**, TC3005, doi: 10.1029/2011TC003047.

Sans, M., Muñoz, J.A., Vergés, J., 1996. Triangle zone and thrust wedge geometries related to evaporitic horizons (southern Pyrenees). *Canadian Petroleum Geology Bulletin*, **44(2)**, 375-384.

Schellart, W.P., 2000. Shear test results for cohesion and friction coefficients for different granular materials: scaling implications for their usage in analogue modelling. *Tectonophysics*, **324(1-2)**, 1-16.

Scisciani, V., Montefalcone, R., 2006. Coexistence of thin and thick-skinned tectonics: An example from the Central Apennines, Italy. In S. Mazzoli, R.H.W. Butler (Eds.), *Styles of continental contraction*: Geological Society of America Special Paper, **414**, pp. 33-54.

Sherkati, S., Letouzey, J., Frizon de Lamotte, D., 2006. Central Zagros fold-thrust belt (Iran): New insights from seismic data, field observations and sandbox modeling. *Tectonics*, **25**, TC4007, doi: 10.1029/2004TC001766.

Shi, P., Fu, B., Ninomiya, Y., Sun, J., Li, Y., 2012. Multispectral remote sensing mapping for hydrocarbon seepage-induced lithologic anomalies in the Kuqa foreland basin, south Tian Shan. *Journal of Asian Earth Sciences*, **46**, 70-77.

Shuwei, G., Zhuxin, C., Benliang, L., Chaojun, Z., 2010. Discussions on the character and interpretation model of Kelasu deep structures in the Kuqa area. *Petroleum Exploration and Development*, **37(5)**, 531-536.

Simpson, G.D.H., 2006. Modelling interactions between fold-thrust belt formation, foreland flexure and surface mass transport. *Basin Research*, **18**, 125-143.

Smit, J.H.W., Brun, J.-P., Soukoutis, D., 2003. Deformation of brittle-ductile thrust wedges in experiments and nature. *Journal of Geophysical Research*, **108(B10)**, 2480, doi:10.1029/2002JB002190.

Smit, J., Burg, J.-P., Dolati, A., Sokoutis, D., 2010. Effects of mass waste events on thrust wedges: analogue experiments and application to the Makran accretionary wedge. *Tectonics*, **29**, TC3003, doi:10.1029/2009TC002526.

Soto, R., Casas, A.M., Storti, F., Faccenna, C., 2002. Role of lateral thickness variations on the development of oblique structures at the Western end of the South Pyrenean Central Unit. *Tectonophysics*, **350**, 215-235.

Stampfli, G.M., Borel, G.D., 2002. A plate tectonic model for the Paleozoic and Mesozoic constrained by dynamic plate boundaries and restored synthetic oceanic isochrons. *Earth and Planetary Science Letters*, **196**, 1, 17-33.

Steward, S.A., 1996. Influence of detachment layer thickness on style of thin-skinned shortening. *Journal of Structural Geology*, **18(10)**, 1271-1274.

Stockmal, G.S., Beaumont, C., Nguyen, M., Lee, B., 2007. Mechanics of thin-skinned fold-and-thrust belts: Insights from numerical models. In J.W. Sears (Ed.), *Whence the Mountains? Inquiries into the Evolution of Orogenic Systems: A volume in Honor of Raymond A. Price.* Geological Society of America Special Paper, **433**, pp. 63-98.

Storti, F., McClay, K., 1995. Influence of syntectonic sedimentation on thrust wedges in analogue models. *Geology*, **23(11)**, 999-1002.

Storti, F., Salvini, F., McClay, K., 2000. Synchronous and velocity-partitioned thrusting and thrust polarity reversal in experimentally produced, doubly-vergent thrust wedges: implications for natural orogens. *Tectonics*, **19(2)**, 378-396.

Sun, J., Li, Y., Zhang, Z., Fu, B., 2009. Magnetostratigraphic data on Neogene growth folding in the foreland basin of the southern Tianshan Mountains. *Geology*, **37**, 1051-1054.

Suppe, J., 1980. Imbricated structure of western foothills belt, southcentral Taiwan. *Petrol. Geol. Taiwan*, **17**, 1-16.

Tang, L., Jia, C., Pi, X., Chen, S., Wang, Z., Xie, H., 2004. Salt-related structural styles of Kuqa foreland fold belt, northern Tarim basin. *Science in China Series D: Earth Sciences*, **47(10)**, 886-895.

Tang, L., Yu, Y., Jia, C., Jin, Z., 2007. Differential Deformed Salt-Related Tectonics of the Kuqa Foreland Fold-Thrust Belt, Tarim Basin, Northwest China. Paper presented at AAPG Annual Convention, Long Beach, California.

Tang, X., Yang, S., Hu, S., 2014. Thermal and maturation history of Jurassic source rocks in the Kuqa foreland depression of Tarim Basin, NW China. *Journal of Asian Earth Sciences*, **89**, 1-9.

Tavani, S., Storti, F., Lacombe, O., Corradetti, A., Muñoz, J. A., Mazzoli, S., 2015. A review of deformation pattern templates in foreland basin systems and fold-and-thrust belts: Implications for the state of stress in the frontal regions of thrust wedges. *Earth-Science Reviews*, **141**, 82-104.

Tang, L., Yu, Y., Jia, C., Jin, Z., 2007. *Differential Deformed Salt-Related Tectonics of the Kuqa Foreland Fold-Thrust Belt, Tarim Basin, Northwest China*. Paper presented at American Association of Petroleum Geologists Annual Convention, Long Beach, California.

Vergés, J., Saura, E., Casciello, E., Fernàndez, M., 2011. Crustal-scale cross-sections across the NW Zagros belt: implications for the Arabian margin reconstruction. *Geological Magazine*, **148(5-6)**, 739-761.

Verschuren, M., Nieuwland, D., Gast, J., 1996. Multiple detachment levels in thrust tectonics: sandbox experiments and palinspastic reconstruction. In P.G. Buchanan, D.A., Nieuwland (Eds.), *Modern developments in structural interpretation, validation and modelling*. Geological Society of London Special Publications, pp. 227–234.

Wang, B., Shu, L.S., Cluzel, D., Faure, M., Charvet, J., 2007. Geochemical constraints on Carboniferous volcanic rocks of the Yili block (Xinjiang, NW China): implications for the tectonic evolution of western Tianshan. *Journal of Asian Earth Sciences*, **29**, 148-159.

Wang, C., Chen, H., Cheng, X., Li, K., 2013. Evaluating the role of syn-thrusting sedimentation and interaction with frictional detachment in the structural evolution of the SW Tarim basin, NW China: Insights from analogue modeling. *Tectonophysics*, **608**, 642-652.

Wang, W., Yin, H., Jia, D., Li, C., 2017. A sub-salt structural model of the Kelasu structure in the Kuqa foreland basin, northwest China. *Marine and Petroleum Geology*, **88**, 115-126.

Wang, X., Suppe, J., Guan, S.W., Hubert-Ferrarri, A. Jia, C.Z., 2011. Cenozoic structure and tectonic evolution of the Kuqa foldbelt, southern Tianshan, China. In: McClay, K.R., Shaw, J., Supper, J. (Eds.), Thrust Fault- Related Folding. *American Association of Petroleum Geologists Memoir,* **94**, 215–243.

Wilde, S., Zhou, J.-B., 2015. The late Paleozoic to Mesozoic evolution of the eastern margin of the Central Asian Orogenic Belt in China. *Journal of Asian Earth Sciences*, **113(2)**, 909-921.

Windley, B.F., Alexeiev, D., Xiao, W., Kröner, A., Badarch, G., 2007. Tectonic models for accretion of the central Asian orogenic belt. *Journal of the Geological Society*, **164**, 1, 31-47.

Windley, B.F., Allen, M.B., Zhang, C., Zhao, Z.Y., Wang, G.R., 1990. Paleozoic accretion and Cenozoic re-deformation of the Chinese Tien Shan Range, Central Asia. *Geology*, **18**, 128-131.

Wu, J.E., McClay, K.R., 2011. Two-dimensional analog modeling of fold and thrust belts: dynamic interactions with syncontractional sedimentation and erosion. In K. McClay, J. Shaw, J., Suppe (Eds.), *Thrust fault-related folding*. American Association of Petroleum Geologists Memoir, **94**, pp. 301-333.

Wu, Z., Yin, H., Wang, X., Zhao, B., Jia, D., 2014. Characteristics and deformation mechanism of salt-related structures in the western Kuqa depression, Tarim basin: Insights from scaled sandbox modeling. *Tectonophysics*, **612-613**, 81-96.

Xu, C., Zhou, X, 2007. Seismic interpretation of the Kelasu triangle zone in the southern Tian Shan foothills, northwestern China. *American Association of Petroleum Geologists Bulletin*, **91(2)**, 161-171.

Ye, C. H., Huang, R. J., 1990. Tertiary stratigraphy of the Tarim Basin. In: Zhou, Z., and Chen, P. (Eds.), Stratigraphy of the Tarim Basin. Beijing, Sciences Press, 308–363.

Yin, A., Nie, S., Craig, P. Harrison, T.M., 1998. Late Cenozoic tectonic evolution of the southern Chinese Tian Shan. *Tectonics*, **17**, 1–27.

Yu, S., Chen, W., Evans, N.J., McInnes, B.I., Yin, J., Sun, J., Li, J., Zhang, B., 2014. Cenozoic uplift, exhumation and deformation in the north Kuqa Depression, China as constrained by (U-Th)/He thermochronometry. *Tectonophysics*, **630**, 166-182.

Zhang, T., Fang, X., Song, C., Appel, E., Wang, Y., 2014. Cenozoic tectonic deformation and uplift of the South Tian Shan: implications from magnetostratigraphy and balanced cross-section restoration of the Kuqa depression. *Tectonophysics*, **628**, 172-187.

Zhang, Z., Shen, Z., Sun, J., Wang, X., Tian, Z., Pan, X., Shi, L., 2015. Magnetostratigraphy of the Kelasu section in the Baicheng depression, Southern Tian Shan, northwestern China. *Journal of Asian Earth Sciences*, **111**, 492-504.

Zhang, Z., Sun, J., Tian, Z., & Gong, Z., 2016. Magnetostratigraphy of syntectonic growth strata and implications for the late Cenozoic deformation in the Baicheng Depression, Southern Tian Shan. *Journal of Asian Earth Sciences*, **118**, 111-124.

Zhao, W., Zhang, S., Wang, F., Cramer, B., Chen, J., Sun, Y., Zhang, B., Zhao, M., 2005. Gas systems in the Kuche Depression of the Tarim Basin: source rock distributions, generation kinetics and gas accumulation history. *Organic Geochemistry,* **36**, 1583-1601.

Zhong, D., Xia, W. S., 1998. The investigation report of Mesozoic–Cenozoic strata, structure, sedimentary faces, and petroleum potential of Kuche foreland basin outcrop area (with 1:100,000 Kuche foreland basin geologic map) (in Chinese with English abstract): Research report of Tarim Oilfield Company, Xinjiang, 462 p.

Zhou, D., Graham, S.A., Chang, E.Z., Wang, B., Hacker, B., 2001. Paleozoic tectonic amalgamation of the Chinese Tian Shan: Evidence from a transect along the Dushanzi-Kuqa Highway. *Geological Society of America Memoir*, **194**, 23-46.

Zou, Y.R., Zhao, C.Y., Wang, Y.P., Zhao, W.Z., Ping, P.A. Shuai, Y.H., 2006. Characteristics and origin of natural gases in the Kuqa depression of Tarim Basin, NW China. *Organic Geochemistry*, **37**, 280-290.